STUDIES ON PREPARATION AND CHARACTERIZATION OF SILK FIBROIN/PVA/ZnO NPs COMPOSITES FOR WOUND DRESSING APPLICATION

A THESIS SUBMITTED TO

D. Y. PATIL EDUCATION SOCIETY, KOLHAPUR

Deemed to be University

(Declared u/s 3 of the UGC Act. 1956)

FOR THE DEGREE OF

DOCTOR OF PHILOSOPHY IN

BIOTECHNOLOGY

UNDER THE FACULTY OF

INTERDISCIPLINARY STUDIES

BY

MS. PRIYANKA POPAT PATIL

M. Sc.

UNDER THE GUIDANCE OF

PROF. (DR.) S. G. NANAWARE

M. Sc., Ph. D.

FORMER DEAN, FACULTY OF INTERDISCIPLINARY STUDIES AND FORMER CO-ORDINATOR, STEM CELL AND REGENERATIVE MEDICINE, D. Y. PATIL EDUCATION SOCIETY, KOLHAPUR-416006 (M.S.) INDIA

AND,

PROF. (DR.) S. H. PAWAR Emeritus Scientist (CSIR)

M. Sc., Ph. D., F. I. C. C., F. M. A. Sc.

DISTINGUISHED PROFESSOR

D. Y. PATIL EDUCATION SOCIETY, KOLHAPUR – 416 006 (M.S.) INDIA AND DIRECTOR, CENTER FOR INNOVATIVE AND APPLIED RESEARCH, ANEKANT EDUCATION SOCIETY, BARAMATI – 413 102 (M.S.) INDIA

CENTRE FOR INTERDISCIPLINARY RESEARCH

D. Y. PATIL EDUCATION SOCIETY,

KOLHAPUR-416 006 (M.S.) INDIA

MARCH 2019

DECLARATION

I hereby declare that the work presented in this thesis entitled **"Studies on Preparation and Characterization of Silk Fibroin/PVA/ZnO NPs Composites for Wound Dressing Application"** is entirely original and was carried out by me independently in the D. Y. Patil Education Society (Deemed to be University), Kolhapur under the supervision of Prof. (Dr.) S. G. Nanaware, Former dean, Faculty of Interdisciplinary Studies and Former Coordinator, Stem cell & Regenerative Medicine, D. Y. Patil, Education Society, Kolhapur, and Prof. (Dr.) S. H. Pawar, Emeritus scientist (CSIR) and Distinguished Professor, D. Y. Patil Education Society, Kolhapur. I further declare that it has not formed the basis for the award of any degree, diploma, fellowship or associate ship or similar title of any University or Institution. The extent of information derived from the existing literature has been indicated in the body of the thesis at appropriate places giving the references.

Place: Kolhapur

Date: 30/03/2019

Research Student,
Ms. Priyanka Popat Patil
Center for Interdisciplinary Research
D. Y. Patil Education Society,
Kolhapur–416 006, (M.S.) India

CERTIFICATE

This is to certify that the thesis entitled **"Studies on Preparation and Characterization of Silk Fibroin/PVA/ZnO NPs Composites for Wound Dressing Application"** is submitted herewith for the degree of Doctor of Philosophy in Biotechnology to D. Y. Patil Education Society, Kolhapur by **Ms. Priyanka Popat Patil** is absolutely based upon her own work under my supervision. Neither this thesis nor any part of it has been submitted elsewhere for any degree/diploma or any other academic award anywhere before.

Date: 30|03|2019

Research Guides

Prof. (Dr.) S. G. Nanaware
Former Dean, Faculty of
Interdisciplinary Studies and
Former Coordinator, Stem cell
& Regenerative Medicine,
D. Y. Patil, Education Society,
Kolhapur - 416 006 (M.S.) India

Prof. (Dr.) S. H. Pawar
Emeritus Scientist (CSIR) &
Distinguished Professor, Center for
Interdisciplinary Research
D. Y. Patil Education Society,
Kolhapur - 416 006 (India) &
Director, Center for Innovative and
Applied Research, Anekant
Education Society, Baramati – 413
102 (M.S.) India

30/3/2019

Research Director and Dean
Center for Interdisciplinary Research
D. Y. Patil Education Society,
Kolhapur - 416 006 (M.S.) India

Acknowledgment

I wish to express my deep sense of gratitude and profound thanks to my supervisor's ***Prof. Dr. Shivdas G. Nanaware*** *Former Dean, Faculty of Interdisciplinary Studies and Former Coordinator, Stem cell & Regenerative Medicine, D. Y. Patil, Education Society, Kolhapur and* ***Prof. Dr. Shivaji. H. Pawar****, Emeritus Scientist (CSIR) & Distinguished Professor, Center for Interdisciplinary Research D. Y. Patil Education Society, Kolhapur & Director, Center for Innovative and Applied Research, Anekant Education Society, Baramati for their invaluable guidance, constant encouragement, inspiring and thought provoking discussions throughout my Ph. D. program. I have been able to learn a great deal from them and consider my association with them as a rewarding experience. I greatly appreciate the freedom my supervisors gave me and the opportunity to pursue my research in my own way.*

Besides my guides, I would like to acknowledge to ***Dr. Prakash. B. Behere****, Vice Chancellor, D. Y. Patil, Education Society, Kolhapur for his encouragement and support.*

I must also acknowledge the ***Dr. Vishwanath V. Bhosale****, Registrar and* ***Mr. Sham P. Kole,*** *Finance Officer of D. Y. Patil Education Society, Kolhapur and other staff members who have helped me directly or indirectly during my research work.*

I also express my gratitude to ***Prof. Dr. Chandrakant D. Lokhande****, Research Director and Dean, D. Y. Patil Education Society, Kolhapur and* ***Principal, Dr. Chandrashekhar Murumkar,*** *T. C. College, Baramati for their guidance, constant encouragement, inspiring and thought provoking discussions throughout my Ph. D. Program.*

I would like to acknowledge to ***Dr. Raghvendra Bohara*** *and* ***Ms. Jagruti Meshram****, Center for interdisciplinary research, D. Y. Patil, Education Society, Kolhapur for his valuable discussion and suggestions regarding the manuscript.*

I take this opportunity to convey my hearty admiration to all ***my teachers*** *from my school days to post graduation level.*

A Special thanks to all the group members, ***Dr. Manisha Phadtare****,* ***Dr. Valmiki Koli, Mr. Abhinandan Patil,*** *and* ***Mr. Deepak Sawant*** *without their unconditional help*

and support, this study would not have been successful. I thank all of you for your help, time and input. I am lucky to have had the opportunity to meet all of you. I wish to thank to ***all my friends*** *for being there for me always.*

Last but not least, I would like to thank the special people who supported me throughout my educational endeavour, my father ***Mr. Popat Patil****, my mother* ***Mrs. Kalpana Patil*** *who instilled in me the love of science and the ambition to do my best in every aspect of my life, to my husband* ***Mr. Prakash Shinde*** *who inspired and helped me through this process. It is their constant support; unconditional infinite love and belief in my capabilities which has made me to achieve my goals. I sincerely apologize for any omissions and sincerely thanks all concert.*

Ms. Priyanka P. Patil

CONTENTS

Chapter 1
Introduction

Chapter 2
Nanotechnology and wound dressings: Theoretical background

Chapter 3
Characterization techniques for wound dressing materials

Chapter 4
Synthesis and characterization of Silk Fibroin and its composite films using PVA and ZnO NPs

Chapter 5

Hybrid Chitosan-ZnO NPs coated with a sonochemical technique on SF-PVA composite film

Chapter 6
Biocompatibility study of SF based composite films

Chapter 7
Antibacterial study of SF based composite films

Chapter 8
Evaluation of SF based composite films for their wound dressing application

CHAPTER 1

Introduction

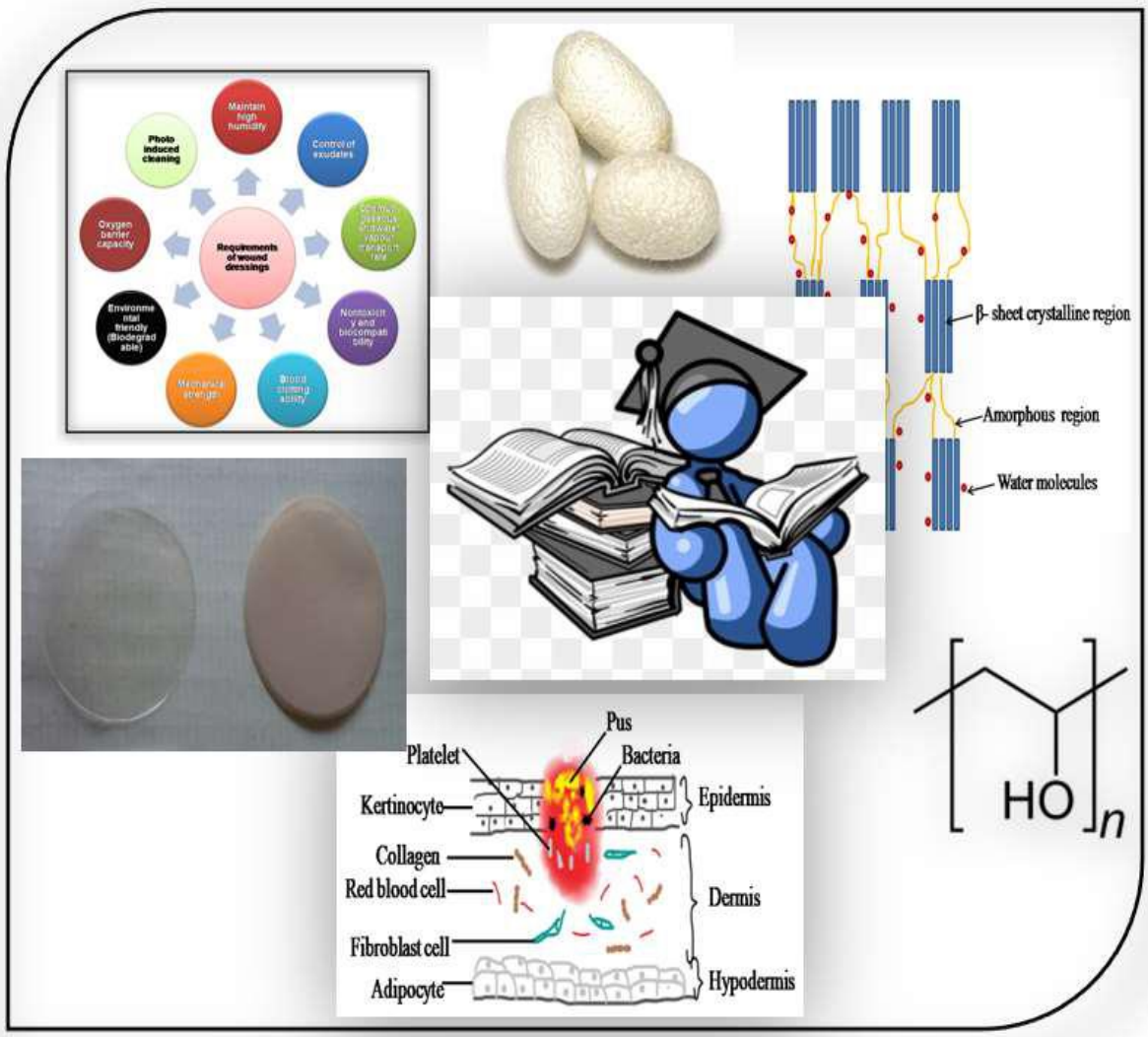

1.1 Introduction

Human skin is one of the important and protective organs of the body. Every year, several million people have affected skin injury of both acute and chronic nature [1, 2]. Worldwide 3, 00,000 people die every year in lower middle-income countries due to the chronic and burn injury [2]. The injuries and its infections are the most painful form of trauma. Wound infections are the growth of microorganisms within the wound area. This infection causes the body's immune system, inflammation and damages the tissue within the wound site. Therefore, it causes delay in wound healing and may come to life-threatening infections [3]. Thus, these bacterial wound infections are serious complications of wound management. Initially, microorganisms of an initial stage of the infected process involved gram-positive *Staphylococcus aureus* (*S. aureus*) and *Streptococcus pyogenes* (*S. pyogenes*) bacteria. Gram- negative bacteria such as *Escherichia coli* (*E. coli*) and *Pseudomonas aeruginosa* (*P. aeruginosa*) etc are involved in later stage of the infectious process that is when a chronic wound is formulated [4]. The main signs of wound infections include pus formation, spreading redness, increased pain or swelling, and fever for patients [5]. This problem can be overcome by protecting the wound from proper antibacterial wound dressing materials. Based on these, different types of dressings are available in the market. Most of these dressing materials are lacking one or the other reasons such as low level of mechanical properties, insufficient blood clotting ability, lower swelling ability, and inadequate antibacterial activity [6, 7]. Hence, there is an immense need to formulate new dressing materials for wound dressing application.

The potential dressings offer the development of antibacterial dressings based on biomaterials has become an important area of research because of the materials are of biological origin [8, 9]. According to the literature study, biomaterials based composite materials have been used as the best wound dressing materials [10]. The main aim of this chapter is to introduce the background of wound and healing process, wound healing model, the necessity of wound dressings, types of dressings and requirements of wound dressing materials. Further, it also focuses on

the different types of biomaterials and the advantages of Silk fibroin (SF) and its composite films for wound dressing applications.

1.2 Wound and wound healing process

1.2.1 Wound

The wound is a type of injury to the body. It damages the underlying tissue with disruption in anatomical structure and function due to accidents, burns, surgery etc. [11]. The wounds are classified into several types according to the wound depth, tissue loss, and type of injury, location or clinical appearance of the wound. Wounds are classified into two types based on wounds with and without tissue damage. Wounds by tissue damage comprise second and third-degree burns wounds, diabetic foot ulcer etc. and wounds without tissue damage comprise first-degree burn wound and laceration etc [12]. According to the time of healing process, wounds are divided into two different types, first acute wound and second chronic wound. The acute wound heals normally 8-12 weeks, and the chronic wound heals very slowly beyond 12 weeks [13]. Wounds involving epidermis only is called a superficial wound whereas wound includes epidermis, deeper dermal layer, blood vessels etc. considered as partial thickness wounds. When wound consisted of epidermis, dermis and subcutaneous tissue may be referred to as full thickness wounds [14].

1.2.2. Wound Healing Process

Wound healing progress is the multistep method for formation of cell growth and tissue regeneration. It is a typical biological process in human anatomy shows in figure 1.1. Regeneration of tissue is achieved by four phases including coagulation or haemostasis, inflammation, proliferation, and remodeling or maturation phase.

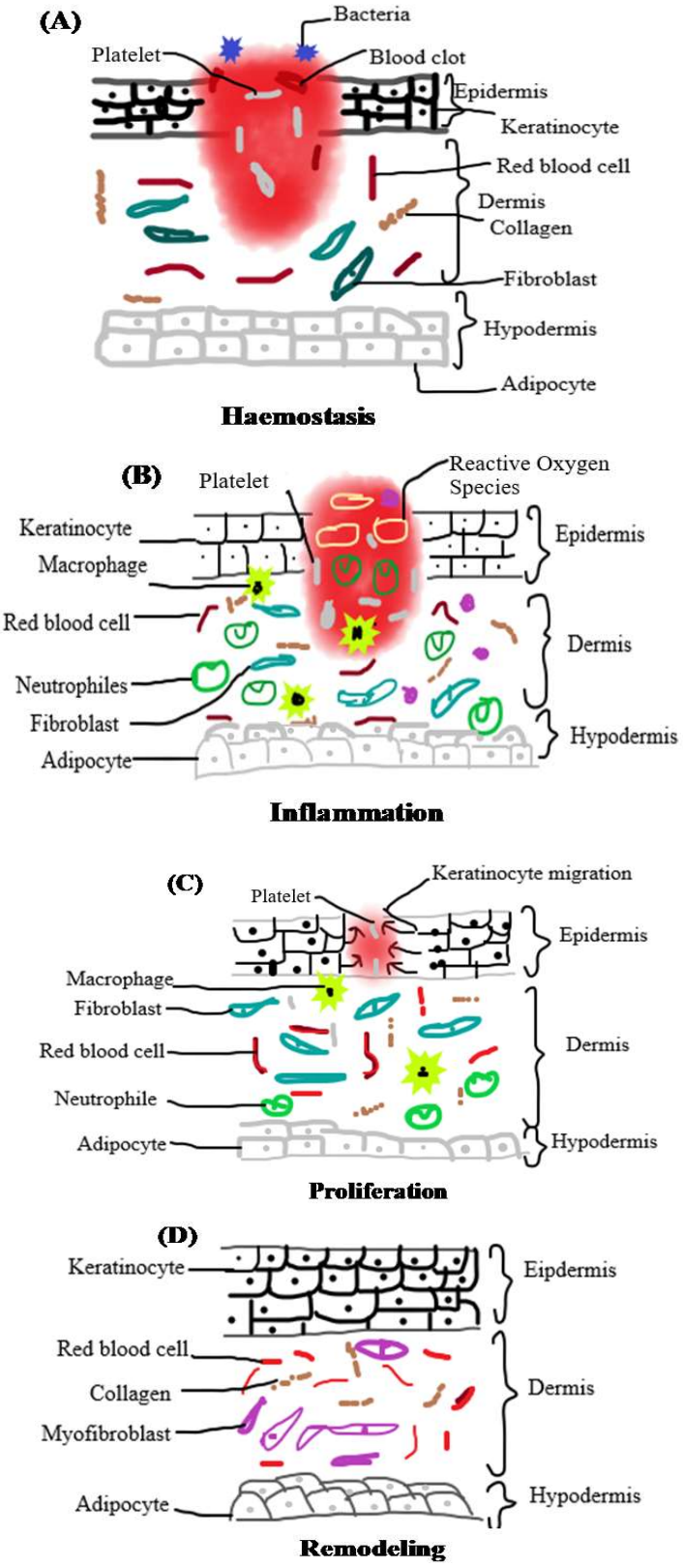

Figure 1.1 Schematic diagram of the wound healing process of **(A)** Haemostasis, **(B)** Inflammation, **(C)** Proliferation and **(D)** Remodeling.

The first phase of hemostasis is within the first few minutes of injury, with the production of a fibrin clot in the blood to the injured site and vascular constriction [15, 16]. Surrounding wound tissue and blood clot release cytokines and growth factors such as interleukin-1 (IL-1) β, tumor necrosis factor (TNF)-α, transforming growth factor (TGF) β, platelet-derived growth factor (PDGF), basic fibroblast growth factor (bFGF), epidermal growth factor (EGF), which causes migration of neutrophils (after 6 hrs), formation of initial matrix for early wound healing by fibrins, lymphocytes and histiocytes (after 12 hrs) [17].

During the inflammation phase, dead and damaged cells are cleared out, along with microorganisms and debris. In this stage, neutrophils appear in the wound area, followed by lymphocytes and monocytes which differentiate into macrophages. This takes place with the process of phagocytosis. In this process, the bacteria, foreign particles and injured tissues are removed. Neutrophils also create substances like proteases and reactive oxygen species (ROS) that cause some supplemental bystanders damage [18]. In the wound healing process, macrophages show various roles. Macrophages release cytokines and cytokines stimulate the inflammatory response by activating additional leukocytes. Macrophages are responsible for inducing apoptotic cells (including neutrophils) thus paving the way for the resolution of inflammation [19].

The proliferative phase is beginning from the 3rd day after the formation of wound and lasts for about 2 weeks thereafter. During the proliferative healing phase, fibroblast migration, deposition, collagen synthesis, angiogenesis and granulation tissue formation takes place in the wounded area. Fibroblasts generate collagen also glycosaminoglycans and proteoglycans that are major constituents of the extracellular matrix (ECM).

In the final remodeling phase, reversion of several newly created tissues occurs. Scar maturation is another major avenue in this phase of healing. Collagen remodeling and maturation continues for two years [20, 21].

1.2.3 Wound Healing Model

The wound healing is explained with a theoretical model on the basis of the mechanism of healing of the wound. The proposed model includes a system of nonlinear partial distinctive equations reporting the interplays in space and time of the various variables. The schematic diagram of theoretical wound healing model is shown in figure 1.2.

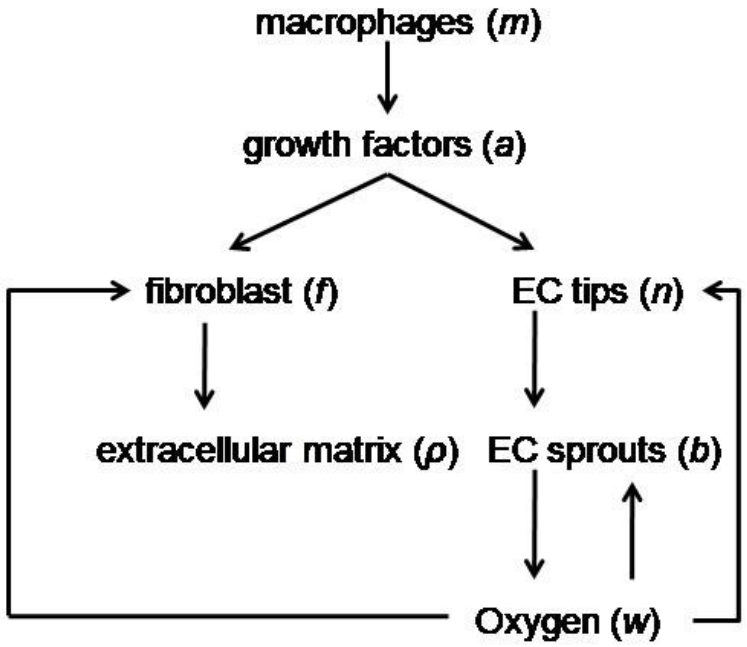

Figure 1.2 Schematic sketch of theoretical model of wound showing seven variables, m, w, a, f, ρ, n and b.

The variable of wound healing models are, m = macrophages, w = oxygen, a = chemoattractants i. e. VEGF, f = fibroblast, ρ = extracellular matrix, n = capillary tips and b = capillary sprouts. These are a different variable. The effect of different variables on wound healing process is explained with the help of seven partial differential equations like $\partial n/\partial t$, $\partial b/\partial t$, $\partial w/\partial t$, $\partial m/\partial t$, $\partial a/\partial t$, $\partial f/\partial t$ $\partial n\partial$ $\partial p/\partial t$. The different key components of the developed models are explained theoretically by Schugart *et al*. [22].

1.3 Wound Dressings

Wound dressings are the materials, which is used for healing or promoting the wound. Wound dressings are formulated to be in direct contact with the wound from materials. These dressing materials are produced depends on the category, severity, and location of the wound.

1.3.1 Necessity of wound dressings

There are multiple factors that affect wound healing process. These are categorized into two factors local or intrinsic and systematic. Local factors are insufficient blood supply, foreign bodies, infection on the wound site, topical steroids and antiseptic. Systematic factors are the overall health or disease, aging and general health of the body [23]. Any wound fails to heal within a few weeks should be expected by a healthcare professional. It might be a chronic wound. This is due to the bacterial infection or might show an underlying disease such as diabetes, fibrosis, jaundice etc [24].

Microbiology of wound is an important infectious complication in patients with skin wounds. Wound infection can occur when the natural cutaneous barrier is broken and exposing underlying tissue. The schematic diagram of wound infection represented in figure 1.3. In the condition of the contaminated wound, comprise of an immunocompromised skin area and the loss of natural protection that is little energy for healing of wound [25]. The major risk of wound infection is increased by the concentration of pathogens and the presence of vascular disease, edemia, malnutrition, diabetes, and corticosteroids. If the wound is deeper or over a large area and the tissue is necrotic then the patient is more susceptible to infection [26]. The main signs of the soft tissue infections are pus formation, increased swelling of the wound site, increased erythema, pain, odor and fever for patients [27].

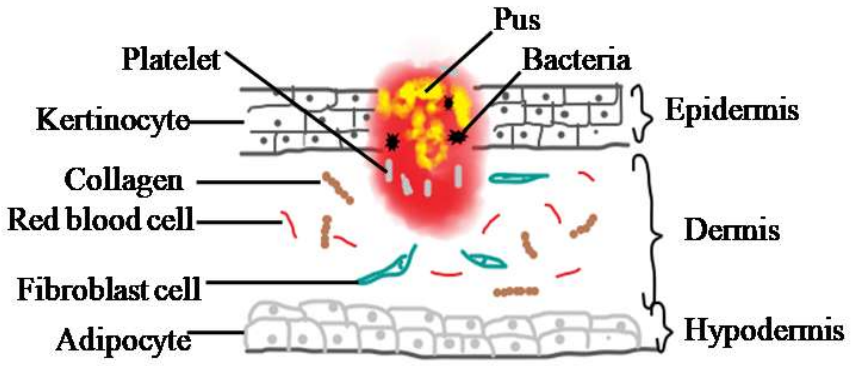

Figure 1.3 Schematic diagram of infections associated on wound area.

The bacterial infections enter into the body and immediately start the growth of microorganisms and its colonies. This can lead to the internal infection or the infection of deeper portion of the tissue. Inadequate care of infections of the wound may also lead to a slow healing process, loss of soft tissue, limb amputation and death [28]. Recent reports observed that microbial contamination and its infectious colonies are the main reason of death for at least 10,000 people for every million wound patients. Other factors are included as oxygenation, age and gender, stress, sex hormones in aged individuals, diabetes, medications, obesity, nutrition, alcohol consumption and smoking. These factors are the main factors for the delay in the process of wound healing [23]. Thus, the ideal wound dressing is the major need in wound care management.

1.3.2 Types of wound dressings

The healing progress of wound is an intricate method that demands a proper environment to encourage the healing steps. With the improvement in processing, more than 3,000 products have been developed for the treatment of various types of wounds by treating different forms of healing. Currently, there are different wound dressings depends on interactive and bioactive materials applicable to the healing process [29]. These are represented in figure 1.4. Many of the new types of dressing materials are constructed to form a moist wound repairing environment that permits wound fluids and growth factors to accelerate wound healing [30].

Basically, suitable dressing materials must be selected for proper care of the wound and faster wound healing process. In an earlier day, the wound dressing materials used for healing are of bandages and gauze, with varying degree of absorption. Recently, researches focusing on the newer type of dressings with rapid healing capability, maintain a moist environment, control of infection, control of wound exudates etc [31].

Wound dressings are categorized into two types, traditional dressings, and current (modern) wound dressings. The natural, synthetic materials, cotton gauzes and wool are traditional dressings. Film, foam, hydrocolloids, alginates, hydrogels, composites, and antimicrobial dressings are modern wound dressing materials [29].

1.3.2.1 Traditional wound dressings

Gauze is the most available wound dressing in use today were made from woven or nonwoven gauze. It is highly absorbent and comparatively non-barrier due to it may promote dryness in wounds. In gauze dressings, sterile gauze pads are selected for absorbing a large volume of wound exudates in an open wound with the use of fibers [32]. Gauze dressings require constant changing to safe from the exhaustion of healthy tissues. These types of dressings are reasonable cost and easy for manufacturing. Gauze becomes moistened due to intense wound effluent. Moreover, it becomes more adhesive to the wound area creating it painful when removing process. For the preparation of gauze bandages, natural cotton wool and cellulose materials are used [33].

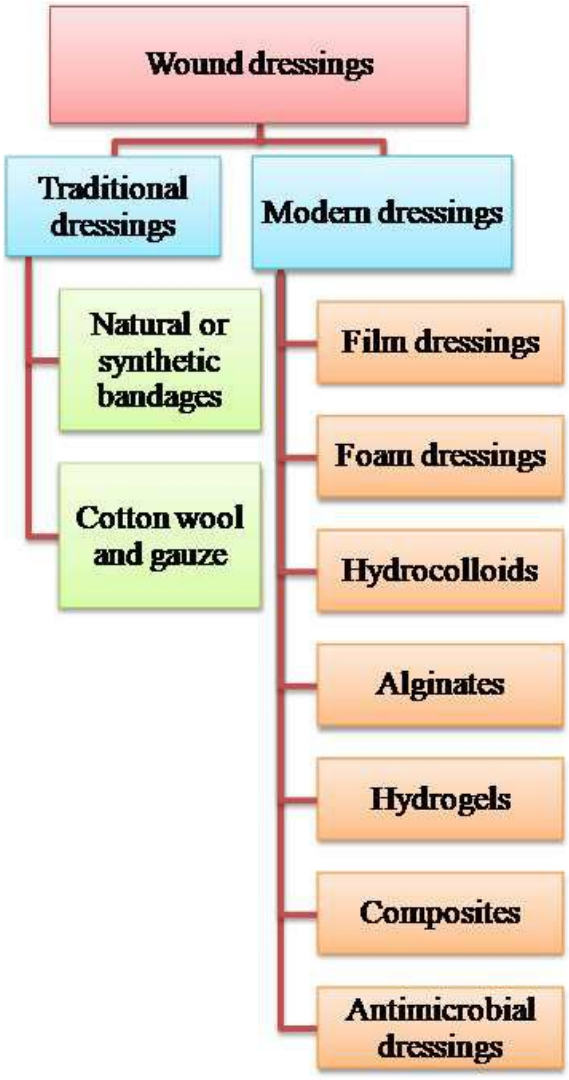

Figure 1.4 Schematic of different types of wound dressings.

1.3.2.2 Modern wound dressings

These are significantly different dressings comprised of traditional in keeping and developing a humid environment around the area of wound facilitating wound steps. The modern types of wound dressings are developed by employing synthetic polymers. These are primarily categorized as foam, film, gel, and hydrocolloids. The modern wound dressings offer preventions of infections to the wound environment [34].

Film dressings are suitable for primary and secondary wound dressings. These are made up of sterile plastic sheets of polyurethane and coated with

adhesive to allow adherence to the skin. These films are permeable to water and air. These materials are flexible and elastic. Film dressings are suggested for epithelializing wound, lower exudates wounds. Examples of film dressings are OpsiteTM (Smith and Nephew, Hull, UK), TegadermTM [35].

Foam dressing consists of porous polyurethane foam or film forms. The outer layer of dressings has hydrophobic. This layer is impermeable to liquid. The inner layer of foam dressing has permeable to water and O_2, CO_2, and water vapor exchange due to its porosity. It is protective, provide thermal insulation, highly absorbent, and maintain a moist environment. These types of dressings are used to prevent infections. Additionally, it is nonadherent, easy to apply and remove processes. The absorbency of foam dressings can be controlled by foam properties. It is available in different sizes or shapes. Foam dressings are recommended for granulating wounds and lower leg ulcers. Some commercially available foam dressings are Allevyn™, Tielle™, and Lyofoam™ (Conva Tec, Princeton, NJ) [36].

Hydrocolloid dressings are consisting of two types of layers an inner layer and outer layer. An inner layer is colloidal, adhesive, jelly, and prepared from hydrophilic colloid materials like carboxymethyl cellulose (CMC), gelatin, an elastomer and pectin etc. [37]. This layer absorbs wound exudates and forms gel-like mass on the surface of the wound. The main aim of this layer is to absorb wound exudates from the wound site. This layer provides thermal insulation to the wound area. Another outer layer is made up of usually polyurethane materials. This layer protects the wound from foreign materials and bacteria. When this hydrocolloids contact with wound exudates, they offer a moist wound environment, protection from contamination and promote cell migration. Hydrocolloid dressings are advised for limited and complete thickness wounds with lower effluents, pressure ulcers and slight burns [38].

Hydrogel-based dressing materials created by natural or synthetic polymers. It is a polymer chain connection which is hydrophilic, hydrophobic, and in some cases, it is found as a colloidal gel in which water is the dispersion medium. The flexibility of hydrogel dressings is very high which is similar to natural tissues, due

to their 70-90 % water content. It promotes granulation tissues and epithelium in a moist area. Currently, hydrogel based scaffolds are used for wound dressings. There are several advantages includes hydrogel scaffolds which are retention of a moist environment, high swelling ratio, supply cooling sensation and healing of wound without scar development [39].

Alginate dressing is prepared from the sodium and calcium salts in the form of foams or fibrous sheets. Due to their high absorption capacity, alginate forms an intense hydrophilic gel, which minimizes wound exudates and reduces bacterial infection. This type of materials have commonly applicable for diabetic wounds, venous wounds, complete thickness burns, pressure ulcer, cavity wound, and chronic ulcers. Alginate activated macrophages to produce TNF-α which initiates inflammatory signals. The ions released, also aids in blood clotting mechanism. Alginate dressings are recommended for heavy exudates wound. These are not suitable for third-degree burn wound, dry wound and severe wounds [40].

Bioactive wound dressings involved biomaterials for the wound healing process. Biomaterials are biocompatible, biodegradable and nontoxic in nature. They are prepared by natural or artificial origins like collagen, hyaluronic acid, chitosan, alginate and elastin. Sometimes, growth factors and antimicrobial agents are incorporated to bioactive dressings for enhancement of healing process [41].

The composite dressings are made up of combination in benefits of multiple layers, allowing more than one function in wound care management. It includes an adhesive border of nonwoven fabric tape or transparent film. The composite dressing contains three layers which bottom layer is consisting of semi or nonadherent materials that prevent sticking to young granulating tissue, the middle layer is composed of absorptive material, which maintains moisture environments and assists autolytic debridement and outer most layer protect the wound from infection. The composite dressings can be utilized as primary or secondary dressings [42].

The main function of antimicrobial wound dressing has to reduce the risk of infection in partial and full thickness wounds. Antimicrobial type of wound dressings is available in the form of film, sponges, impregnate, woven gauzes,

absorptive products, island dressing, nylon fabric, non-adherent barrier, or a combination of materials [43]. Antibacterial dressings are available in the market based on Ag NPs and other antimicrobial agents. The antibacterial effect of these materials depends on their concentration.

Silver (Ag) has been used as an antimicrobial agent in the treatment of burns. Ag ions produces various negatively charged groups or ions that is thiol, phosphates, carbohydrates, hydroxylase, indoles, imidazoles and ROS (Reactive Oxygen Species) which disturb the bacterial cell membrane, leakage of cytoplasm, denaturing DNA, proteins and finally death of microorganisms. Additionally, iodine also used as an antibacterial agent in dressings which lower the microbial load in the chronic wound. Honey is regarded as highly bacterial resistant with hydrogen peroxide activity. Honey is an effective antibacterial agent assist in healing of wounds with excellent wound healing properties. Metronidazole gel is often used as in the management of fungating malignant wounds and also helps to control of odor caused by anaerobic bacteria. Some commercial available antimicrobial dressings are Acticoat, Algidex Ag gel, ALLEVYN Ag adhesive dressing, Aquacel Ag, Arglase, Iodoflex, Inadine, Iodosorb, Manukahd lite etc [44, 45].

1.3.3 Requirements of wound dressings

The identification of requirements for proper wound dressing plays a very important task for the formulation of newer dressings. The requirements of the development of proper dressings are reported in the literature. However, these requirements of wound dressing materials are biocompatible, it should prevent dehydration, maintain appropriate moist humidity to wound area allowing gas permeation, prevention against foreign particles and bacteria. It is nontoxic, it has easy to apply and removing and showing compatible with blood [44].

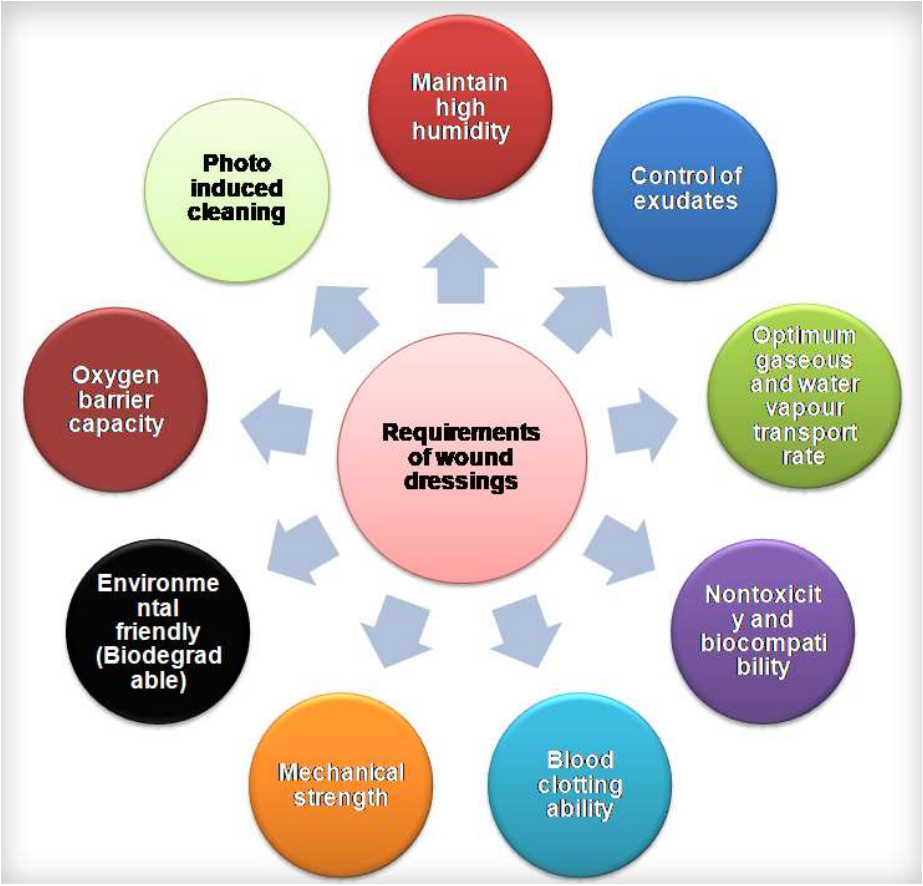

Figure 1.5 Requirements of wound dressing materials.

The requirements of wound dressings are listed in figure 1.5, which are listed below,

- Maintain high humidity
- Control of exudates
- Optimum gaseous and water vapor transport rate
- Nontoxicity and biocompatibility
- Blood clotting ability
- Mechanical strength
- Environmental friendly (biodegradable)
- Oxygen barrier capacity
- Photoinduced cleaning

1.4 Biomaterials for wound dressings

Natural biomaterials used for wound dressings listed in figure 1.6. Biomaterials are the materials used for biomedical applications (It is not only derived from biological things but materials used for biomedical applications). There are varieties of natural biomaterials employed in wound dressing applications, which are classified as polymers and nanobiomaterials. In nanobiomaterials, it is included in ceramics and metals. Ceramic materials are non-metallic, polycrystalline substances specified by mechanical strength, lower density, and corrosion resistance. The type of materials is plastic deformation, sensitive to cracks and other defects. Therefore, ceramic materials are used in fewer amounts with respect to metallic and polymers [45]. The properties of metals are applicable for electrical and thermal conductivity, mechanical strength, corrosion resistance, and reasonable cost. Therefore, metals are largely employed as a biomaterial in the biomedical field and their application in wound dressings [46].

Polymers have special competences like superior biocompatibility, mechanical strength, flexibility, lightweight, and its availability. Polymeric biomaterials have extensively applied in biomedical areas owing to its good properties. Polymers generally prescribed due to various advantages namely tissue engineering, wound healing and dressings [47].

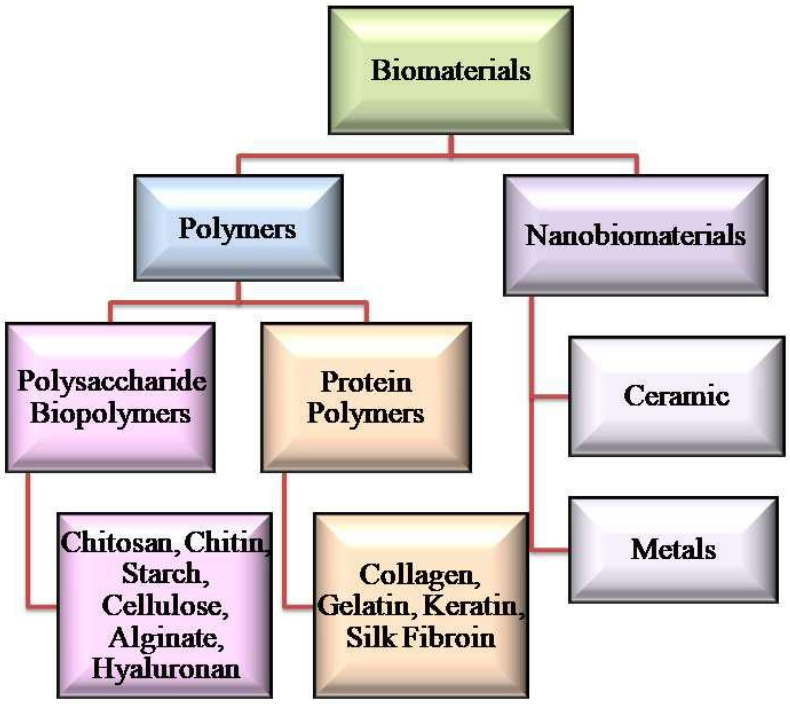

Figure 1.6 Schematic of different types of biomaterials.

According to their origin, polymers are classified into natural (biopolymers) and synthetic polymers. Natural and synthetic polymers are synthesized from renewable sources (animals and plants) and non-renewable sources, respectively [48]. Biopolymers are offered various benefits. The synthetic polymers provide excellent biocompatibility, biodegradability, and uncomplicated manufacturing that can be utilized to produce biocomposite materials. Biopolymers used as biomaterials are biological macromolecules classified into two types that are polysaccharides and proteins [49].

1.4.1 Polysaccharide biopolymers

The most largely used and produced polysaccharide biopolymers are chitosan, starch, cellulose, alginate and hyaluronan etc [50].

Chitosan polysaccharide is the most abundant polymer created by deacetylation of chitin which is different polymeric polysaccharide utilized as biomaterials. Chitosan collected from D-glucosamine and N-acetyl-D-glucosamine linked by glycosidic bonds [51]. Chitosan has been used in several areas such as

cosmetics, photography, and removal of metallic and coloring ions in industrial effluents. It has employed as biomaterial for drug delivery, gene delivery, and in other biomedical applications owing to its compatibility, biodegradability and antibacterial efficacy. Chitosan forms good films generally used in antibacterial food packaging and wound dressing applications [49].

Starch is the vegetable sources and it is collected from potatoes, corn, wheat, and rice. The composition of starch composed of amylase, a linear and crystalline polymer and amylopectin, a branched and amorphous polymer with individual ratios based on the vegetable source. The mechanical property and biodegradability of starch are because of the amount of amylase and amylopectin [52].

Cellulose is an organic polysaccharide consisting of linear and elongated macromolecular series of one repeating component of cellulobiose by plants. Cellulose is much more crystalline compared to starch and is insoluble in organic solvents [53].

Alginate or alginic acid is a polysaccharide extracted from the cell wall of brown algae. Alginate is a linear acid monomer linked to α-L-guluronic acid monomer, through a 1, 4-glycoside linkage in various sequences. Alginate is capable to develop gels in the presence of cations. Alginate-based hydrogels, composites, films are employed as good dressings due to its cooling sensation, biocompatibility, biodegradability, non-immunogenicity and muco-adhesive property under normal physiological conditions [54].

Hyaluronan is an important polysaccharide present in several animal species. Hyaluronan is a polymer of disaccharides composed of D-glucuronic acid and D-N-acetylglucosamine, linked via alternating β-1, 4 and β-1, 3 glycosidic bonds. It has properties of high hygroscopicity, viscoelasticity, and shock-absorbing properties. Hyaluronan has included the capacity to retain water, due to it is dispersed in several tissues of the animal body, appropriate to the skin, the umbilical cord and semen [55].

1.4.2 Protein Biopolymers

Proteins show unique functionalities and potential applications in both biomedical and material sciences. There are various types of proteins that are able to form films. These are performed by the solution casting method. Protein-based films provide mechanical property comparable to those of films produced by synthetic polymers. Some proteins are employed as wounds and burns dressing such as collagen, gelatin, keratins and SF etc [56].

Collagen is extracted by fibroblasts which are the heaviest protein in the human body. It stimulates the wound healing process. Type I collagen that can be produced from animal origins including bovine skin and tendons, porcine skin and rat tail. Collagen is transformed by chemo-physically degraded in order to produce gelatin [57].

Gelatin is formulated by using various animal byproducts and soluble in water. Due to its biocompatibility, biodegradability, gelatin is utilized in biomedical areas like drug delivery systems and wound dressing applications. Gelatin is used in various formulated products that are combined with alginate and hyaluronate materials. The prepared materials are suitable for wound healing properties owing to its physical, mechanical and water vapor barrier capacities [58].

Keratins are fibrous proteins obtained by vertebrate epithelia and corneous tissues like horns, claws, hooves. The functions of keratins are mechanical, protective and show chemical, thermal balance, low sensitivity towards attacking of accepted proteolytic enzymes. Keratin proteins are grouped in soft and hard depends on their amino acid composition, secondary structures, and functions. Keratins are mostly used to their interaction with the proteolytic wound environment facilitating the healing process. In the last few decades, SF offers improved use in biomedical applications [59].

1.4.3 Natural SF biopolymer

1.4.3.1 Sources of SF

Naturally derived biomaterials such as SF protein produced by spiders, silkworm, honey bee, wasp and lacewing. Figure 1.7 shows the sources and structure of SF protein. A large amount of silk can be fabricated from *Bombyx mori* silkworms and spiders. However, spider silk can be extracted from Cannibalistic spiders which are more costly [60]. Obtained silk from silkworm and spider silks bear a great resemblance in their molecular structures and mechanical properties. Silk has been used for thousands of years as a textile for luxury clothing and surgical suture because of its texture, mechanical strength and biocompatibility. In recent years, *Bombyx mori* SF has proven to be interesting biomaterials for wound dressing applications [61].

1.4.3.2 Properties of SF

SF has possessed unique properties such as slow biodegradation, mechanical robustness, transparency, and easy surface patterning. Craig *et al*. reported the silks are fibrous proteins composed of highly repetitive sequences of amino acids [62]. Silk includes fibroin and sericin that is coating the surface of fibroin fiber. Both proteins fibroin and sericin possess excellent biocompatibility, exceptional mechanical properties, biodegradability, nontoxicity, hemostatic properties, and easy processing. Due to these impressive properties in last few decades, SF and sericin proteins have considered as promising candidates in wound dressing applications. Sericin is glue-like amorphous protein, soluble in water and that represent as an adhesive material to carry the structural integrity of the fibers. The amount of SF is approximately 75 % and sericin protein is about 25 %. Thermochemical method can be used for separation of sericin protein to fibers. This process is named as degumming [61].

1.4.3.3 Structure of SF

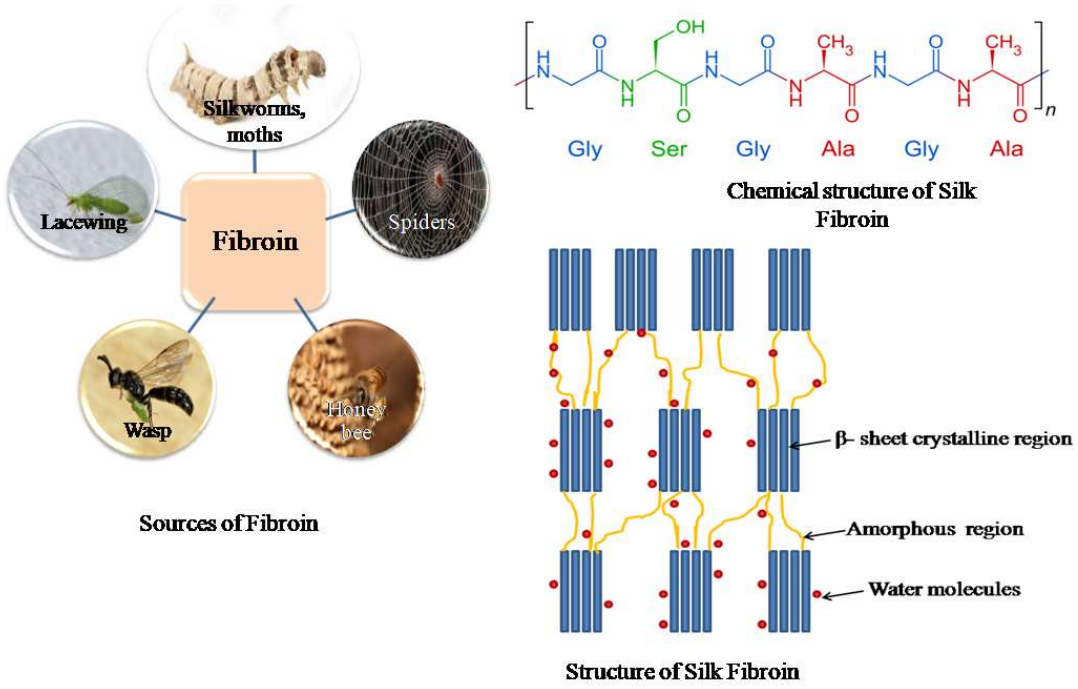

Figure 1.7: Sources of fibroin and structure of SF.

SF made up of a light sequence and heavy sequence. These two sequences linked by a disulfide bond. The heavy sequence of SF comprised of crystalline and amorphous regions. The crystalline parts consist of glycine-alanine repeating compound with serine and tyrosine amino acids. The amorphous part made up of amino acids like aspartic acid [63]. The crystalline parts of SF are rich in hydrophobic β-sheet-forming structures, linked by small hydrophilic linker segments. The interest of the β-sheet-forming structures within the fibroin structure gives the protein-rich materials with the higher mechanical property. The tensile strength of *Bombyx mori* silk fibers is 740 MPa. It contains either a high content of β-sheet or α-helices depending on their equilibrium state. SF is tough due to the β-sheets are surrounded by α-helices and coils, which act as a matrix phase. Silks processed easily semi-crystalline to the crystalline structure by chemical methods such as treatment with methanol and potassium phosphate [64].

1.4.3.4 Applications of SF Proteins

The applications of SF as biomaterials in wound dressings have been growing in recent years. SF fibers are used in textile industries from ancient times due to its softness, lustrous appearance, ease of dyeing and moisture absorption capacity. Apart from this, SF have desirable properties of high strength, biocompatibility, biodegradability, lower adherence of microorganisms, and easy to handle. Therefore, it is mostly applied as suture materials in the medical field. SF can be easily fabricated into nanofibrous mats, scaffolds, sponges, hydrogels, microparticles and nanoparticles (NPs), and composite films for biomedical applications namely tissue engineering, drug delivery, cancer therapy, skin wound healing and wound dressing applications. The advantages of SF in wound dressing applications have shown porosity, high strength, flexibility, oxygen permeability, cell adhesion, migration, proliferation capacity and non-cytotoxicity [65].

1.4.4 SF and PVA composite films

PVA is a synthetic polymer, soluble in water, nontoxic and semicrystalline polymer have been applied in several advanced biomedical applications e.g. wound dressings, drug delivery system, artificial organs and contact lenses. It has possessed various useful properties, such as biocompatibility, gas barrier properties, high strength, flexibility, and excellent membrane-forming properties together with high thermal stability making it an effective polymer to be used in wound dressing applications [66]. Blends of SF and PVA have been extensively used in dressing application since these blends can be prepared with good mechanical, biocompatible and biodegradable properties. Sheik *et al.* developed a biodegradable composite film based on PVA reinforced SF fibers. The results demonstrated that the degradation rate of composite films was improved with the addition of SF fibers. Additionally, the degree of crystallinity, mechanical property, and the thermal property was improved with the incorporation of SF fibers as compared to pure PVA [67]. The blended films of SF, PVA and starch were developed by a solution casting method and examined for their mechanical property, antibacterial efficacy and biodegradability. The blended films has

improved mechanical property, good bacteria killing ability against *S. aureus* and *E. coli* bacteria and showed biodegradability by addition of SF particles. Electrospinning has developed a new and suitable technology for the formation of tissue engineering matrices and PVA is selected as the polymer additive to produce electrospun nanofibrous matrix due to its good fiber forming properties [68]. Zhao *et al.* synthesized membrane based on recombinant spider SF/PVA by electrospinning technique. These membranes applied as a wound dressing for the Sprague Dawley rat model. The results showed that the prepared membrane has porous structure and promote wound healing activity [69].

1.5 Statement of Problem

Fast wound closure is the first aim in the care of acute or chronic wounds, where healing is impaired because of infections. The infectious wound is the large complications in the area of wound care management. These infections can cause a delay in the healing process. Wound infection is caused by indigenous microflora or environments, which grow immediately in the wounded area. This problem can be prevented by protecting the wound with proper antibacterial dressing materials. The control of infections within the area of the wound is due to the antibacterial agents. These antibacterial agents play an essential role to prevent the wound from infections.

SF is one of the natural materials broadly used in wound dressing applications due to its excellent mechanical properties, low immunogenicity, biocompatibility, biodegradability, cell proliferation capability, and water absorption capacity. Similarly, PVA is a synthetic polymer, which is semicrystalline in nature, water-soluble, nontoxic, biocompatible and biodegradable. The blend of SF and PVA has been used earlier for wound dressing applications. According to the reported study, the antibacterial agents such as chitosan, (N-(2-hydroxy) propyl-3-trimethyl ammonium chitosan chlorides (HTCC) are used in addition to SF-PVA composite films for wound dressing applications. Both the composites were used for wound dressing applications. However, the results of the antibacterial study showed that the blended films

inhibited only those organisms that were in direct contact with the active sites of the blended films. Improvement in antibacterial activity of the prepared dressings urgently required, when they are used for infected wound care. SF and PVA do not show any antibacterial activity at neutral pH, which limits their use in infected wound care. This problem can be overcome by the addition of inorganic materials such as metal oxide NPs. Among different metal oxides, ZnO NPs are important and are considered as reinforcing fillers for a polymer matrix due to their excellent antibacterial activity. Moreover, they do not show any adverse effects on normal cells when used in appropriate concentrations. In addition, ZnO NPs release Zn^{+} ions, and they can improve keratinocytes migration towards the wound area and enhance the healing process [70].

Hence, the present thesis is focused on the synthesis and characterization of ZnO NPs embedded SF-PVA and hybrid chitosan-ZnO NPs coated SF-PVA composite films for enhancing the antibacterial and mechanical properties. In light of this problem we carried out the work in this thesis with the following objectives:

- To synthesize the pure materials of SF, PVA and ZnO NPs. SF is synthesized by chemical desolvation method, while the ZnO NPs are synthesized by the reflux method.
- To synthesize hybrid chitosan-ZnO NPs by mixing the chitosan and ZnO NPs by desolvation method.
- To synthesize composite films of SF-PVA, ZnO NPs embedded SF-PVA by casting method at room temperature.
- To synthesize hybrid chitosan-ZnO NPs coated SF-PVA composite films by sonochemical coating technology.
- To explore the physical-chemical characterizations of pure materials as well as composite films.
- To investigate the biological, physical and environmental (biodegradable) properties of SF-PVA, ZnO NPs embedded SF-PVA, and hybrid chitosan-ZnO NPs coated SF-PVA composite films. Biological properties include antibacterial activity and biocompatibility whereas physical properties include swelling study and mechanical properties.

- To evaluate the comparative study of SF-PVA, ZnO NPs embedded SF-PVA and hybrid chitosan-ZnO NPs coated SF-PVA composite films for wound dressing application.

References

1. Y. Chen, M. Fischbach, Y. Belkaid, 2018, Nature, 553, 427-436.
2. A. S. Vidyadhar, and A. M. Vartak, J Burn Care Res, 2017, 39, 109-116.
3. W. Yiwei, J. Beekman, J. Hew, S. Jackson, C. A. I.-Fisher, R. Parungao, S. S. Lajevardi, L. Zhe, and P. K. Maitz, Adv Drug Deliver Rev, 2018, 123 3-17.
4. M. Sulca, C. Remuzgo, J. Cardenas, S. Kiyota, E. Cheng, M. Bemquerer, M. Machini, 2017, Toxicon, 134, 30-40.
5. M. Kuehl, R. Moriarty, T. Richards, R. Verhofstad, M. Borens, O. Kates, S. Morgenstern, Injury, 2018, 49, 511-522.
6. M. Fonder, G. Lazarus, D. Cowan, B. aronson-Cook, A. Kohli, A. Mamelak. J. Am Acad Dermatol, 2008, 58, 185-206.
7. Y. Zhou, D. Yang, X. Chen, Q. Xu, F. Lu, J. Nie, Biomacromolecules, 2008, 9 349−354.
8. Z. Hussain, H. Thu, A. Shuid, H. Katas, F. Hussain, Current drug targets, 2018, 19, 527-550.
9. S. Ahmed, S. Ikram, S. Kanchi, K. Bisetty, In Biocomposites, 2018, 17, 295-316.
10. T. Khampieng, S. Wongkittithavorn, S. Chaiarwut, P. Ekabutr, P. Pavasant, P. Supaphol, J Drug Deliv Sci Tec, 2018, 44, 91-100.
11. S. Eming, P. Martin, M. Tomic-Canic, Sci Transl Med, 2014, 6, 265sr6-265sr6.
12. B. Lipsky, M. Silverman, W. Joseph, Open Forum Infect. Dis., Oxford University Press, 2017, 4, 1-8.
13. C. Thompson, M. Fuhrman, Nutr Clin Pract, 2005, 20, 331-347.
14. A. R. Siddiqui, J. Bernstein, Clin Dermatol, 2010, 28, 519-526.
15. M. Flanagan, J Wound Care, 2000, 9, 299-300.
16. S. Singh, A. Young, C. Mcnaught, Surgery (Oxford), 2017, 35, 473-477.
17. M. Berthet, Y. Gauthier, C. Lacroix, B. Verrier, C. Monge, Trends Biotechnol., 2017, 35, 770-784.
18. P. Martin, S. Leibovich, Trends Cell Biol., 2005, 15, 599-607.
19. N. Fujiwara, K. Kobayashi, Curr Drug Targets Inflamm Allergy, 2005, 4, 281-286.

20. T. Velnar, T. Bailey, V. Smrkolj, J Int Med Res, 2009, 37, 1528-1542.
21. W. Stadelmann, A. Digenis, G. Tobin, Am J Surg, 1998, 176, 26S-38S.
22. R. Schugart, A. Friedman, R. Zhao, C. Sen, Proc. Nati. Acad Sci, 2008, 105, 2628-2633.
23. S. Guo, L. DiPietro, J Dent Res, 2010, 89, 219-229.
24. P. Carpenter, C. Kitko, S. Elad, M. Flowers, J. Gea-Banacloche, J. Halter, F. Hoodin, L. Johnston, A. Lawitschka, G. McDonald, A. Opipari, Bio Blood Marrow Transplant, 2015, 21, 1167-1187.
25. M. Fonder, G. Lazarus, D. Cowan, B. Aronson-Cook, A. Kohli, A. Mamelak, J Am Aca Dermatol, 2008, 58, 185-206.
26. D. Church, S. Elsayed, O. Reid, B. Winston, R. Lindsay, Clin Microbiol Rev, 2006, 19, 403-434.
27. A. Martín-Aspas, F. Guerrero-Sánchez, F. García-Colchero, S. Rodríguez-Roca, J. Girón-González, Infect Drug Resist. 2018, 11, 861-872.
28. T. Jerry, A. T. Queen, I. Tersagh, E. Esther, J Clin Case Rep, 2018, DOI: 10.4172/2165-7920.10001083
29. G. Mogoşanu, A. Grumezescu, Int J Pharm, 2014, 463, 127-136.
30. V. Andreu, G. Mendoza, M. Arruebo, S. Irusta, Materials, 2015, 8, 5154-5193.
31. N. Rajendran, S. Kumar, N. Houreld, H. Abrahamse, Int J Biol Macromol, 2018, 115, 165-175.
32. A. Hussain, P. Cahalan, L. Cahalan, I. Ension, Methods of making bioactive collagen wound care dressings. U.S. Patent Application 15/790, 2018, 851.
33. H. Onishi, Y. Machida, E. Santhini, K. Vadodaria, Advanced Textiles for Wound Care, 2019, 211-260, 2nd edition, Elsevier, Woodhead Publishing.
34. S. Rajendran, Advanced textiles for wound care, 2018, 169-192, 2nd edition, Elsevier, Woodhead Publishing.
35. A. Ahmed, J. Boateng, Therapeutic Delivery, 2018, 9, 185-204.
36. P. Kalowes, V. Messina, M. Li, Am J Crit Care, 2016, 25, 108-119.
37. A. Leon, F. Hebal, C. Stake, K. Baldwin, K. Barsness, Inter Wound J, 2019, 16, 41-46.
38. V. Tsioli, P. Gouletsou, A. Galatos, D. Psalla, A. Lymperis, A. Sideri, L.

Papazoglou, J Am Anim. Hosp Assoc, 2018, 54, 125-131.

39. I. Negut, V. Grumezescu, A. Grumezescu, Molecules 2018, 23, 2392, (1-23).
40. F. Momoh, J. Boateng, S. Richardson, B. Chowdhry, J. Mitchell, Int J Biol Macromol, 2015, 81, 137-150.
41. J. Koehler, L. Verheyen, S. Hedtrich, F. Brandl, A. Goepferich, J Biomed Mater Res A, 2017, 105, 3360-3368.
42. M. Joshi, R. Purwar, Advanced Textiles For Wound Care 2nd edition, 2019, 313-327. Woodhead Publishing.
43. N. Mao, S. Russell, 2004, Textile Progress, 36, 1-57.
44. A. Abdelgawad, S. Hudson, O. Rojas, Carbohydr Polym, 2014, 100, 166-178.
45. K. Mahyar, I. Gibson, M. Goldberg, J. Nomani, G. Littlefair, Sci Adv Mater, 2016, 1491-1511.
46. A. Moghadam, E. Omrani, P. Menezes, P. Rohatgi, Compos B Eng, 2015, 77, 402-420.
47. M. Maitz, Biosurf Biotribol, 2015, 1, 161-176.
48. L. Yu, K. Dean, L. Li, Prog Polym Sci, 2006, 31, 576-602.
49. L. Nair, C. Laurencin, Prog Polym Sci, 2007, 32, 762-798.
50. G. Mogosanu, A. Grumezescu. "Pharmaceutical Natural Polymers: Structure and Chemistry." Handbook of Polymers for Pharmaceutical Technologies: Structure and Chemistry, 2015, 1, 477-519.
51. El-Sherbiny, M. Ibrahim, M. Nancy El-Baz., Springer, 2015, 173-208.
52. G. Madhumitha, J. Fowsiya, S. Roopan, and V. Thakur, Int J Polym Anal Ch. ,2018, DOI: 10.1080/1023666X.2018.1447260
53. D. Klemm, B. Heublein, H. Fink, A. Bohn, Chemie International Edition, 2005, 44, 3358-3393.
54. L. N. Gerschenson, A. M. Rojas, and E. N. Fissore, Nutr. Res Anal Chem, 2017, 39-101.
55. J. Fraser, T. Laurent, U. Laurent, J Intern Med.1997, 242, 27-33.
56. F. Antonio, M. Fernandes, G. Rocasalbas, S. Gautier, T. Tzanov. Adv Poly Medicine, Springer, 2015, 401-431.
57. C. Sayani, and R. Raines, Biopolymers, 2014, 101, 821-833.

58. M. Dan, A. Grumezescu, Int J Pharm, 2014, 463, 127-136.
59. G. Mogosanu, A. Grumezescu, M. Chifiriuc, Currt Drug Targets, 2014, 15, 518-530.
60. T. Scheibel, Microbial cell factories, 2004, 3, 1-10
61. Y. Qi, H. Wang, K. Wei, Y. Yang, R.-Y. Zheng, I. S. Kim, and K.-Q. Zhang. Int J Mole Sci, 2017, 18, 1-21.
62. C. Catherine, C. Riekel, Comp Bioche Physiol B Biochem Mol Biol, 2002, 133, 493-507.
63. A. Gregory, F. Diaz, C. Jakuba, T. Calabro, R. Horan, J. Chen, H. Lu, J. Richmond, D. Kaplan., Biomaterials, 2003, 24, 401-416.
64. D. Rockwood, R. Danielle, T. Preda, X. Yücel, M. Wang, L. Lovett, and D. Kaplan, Nat Protoc, 2011, 6, 1612–1631.
65. T. Ponrasu, B. Ramachandran, R. Kannan, V. Muthuvijayan. J Biomed Mater Res Appl Biomater, 105, 2017, 1401-1408.
66. K. Elbadawy, X. Chen, S. Mohamed. M. Eldin, E. Kenawy, Arab J Chem, 2015, 8, 1-14.
67. S. Sheik, G. Nagaraja, J. Naik, R. Bhajanthri, Int J Plast Tech, 2017, 21, 108-122.
68. D. Chouhan, G. Janani, B. Chakraborty, S. Nandi, B. Mandal. J Tissue Eng Regen M, 2018, 12, 1559-1570.
69. Z. Liang, D. Chen, Q. Yao, M. Li., Int J Nanomed, 2017, 12, 8103-8114.
70. Y. Xingxing, L. Fan, L. Ma, Y. Wang, S. Lin, F. Yu, X. Pan, G. Luo, D. Zhang, H. Wang, Mater Design, 2017, 119, 76-84.

CHAPTER 2

Nanotechnology and Wound Dressings: Theoretical Background

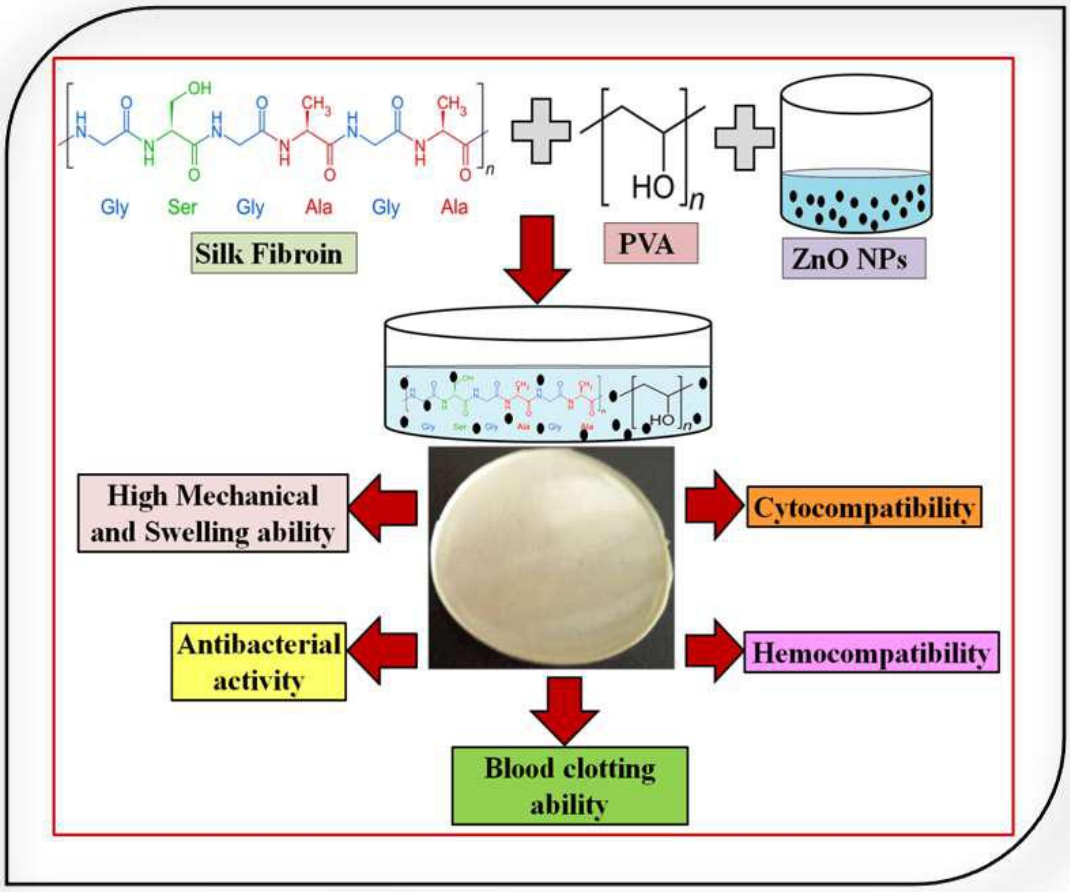

Reference - P. P. Patil, J. V. Meshram, R. A. Bohara, S. G. Nanaware and S. H. Pawar, New Journal of Chemistry, 2018, 42, 14620-14629.

2.1 Introduction

The remedy of wound has derived from ancient times. The main purpose of development of wound dressings was to secure the wound from bacterial infection, inhibition of bleeding, and faster wound healing process. Wound dressings are categorized into three types, biological, synthetic and combination of biological and synthetic dressings [1]. Biological dressings are employed for short term treatment of open wounds by preventing the wound and controlling the microbial contamination but biological dressings have few limitations like limited availability, higher level of antigenicity, imperfect adhesiveness and possibility of infections [2]. Synthetic types of dressings are modeled after biological dressings and possess long durability, stimulate minimum inflammatory reaction and support for prevention of bacterial contamination. The combinations of biological and synthetic type of materials are bilayered and they have higher polymer content and biological materials [1]. The design of ideal wound dressings was carried out by maintaining a moist environment at the wound interfaces, provide softness, flexibility, provide antibacterial activity, cytocompatibility, should be allowing water and vapor permeability, easily removable and promoting faster wound healing process [3,4].

Significant advances in the area of wound dressing materials have enormous demands of wound cares. One of the keys to advancing this field lies in the development of systematically designed materials. Such the wound dressing materials can be derived directly from nature, or synthesized in the laboratory in the form of synthetic polymers, metals, alloys, and ceramics. These are easily obtainable biomaterials that require minimum processing, possess antibacterial activity and support wound healing process [5]. One of the most promising technologies in wound dressings is the nanotechnology-based dressings that are ability to accelerating the wound healing.

2.2 Nanoscience and Nanotechnology

There are a various type of engineered nanotechnology have been offered exhibiting unique properties and various functions that address particular problems

related to wound reformation mechanism. The scientist Richard Feynman discovered the new science namely nanoscience and nanotechnology in 1959. The term nanotechnology is referred as, the branch including the designing, formulation, identification, and applications of materials that are designing by at the minimum size in nanometre range. There are two types of aspects are used in nanotechnology such as "bottom-up" approach and "top-down" approach. In "bottom up" view nanoscale materials are developed by breakage of larger materials particularly physical breakage or chemical breakage. In "top-down" approach nanoscale materials are collected atom by atom or molecule by molecule. Nanoscience is involving the development and application of physical, chemical and biological system at nanoscale range [6].

Nanotechnology offers the main properties of materials are controlling the size of materials in the nanoscale range. The main aim of controlling the size in nanometres range of materials is its novel properties such as size-dependent properties. These properties are listed below [7],

- Thermal- Melting temperature
- Electrical- Tunneling current
- Chemical-Reactivity, catalysis
- Magnetic-Superparamagnetic effect
- Optical-Absorption and scattering of light.
- Mechanical-Adhesion, capillary forces.

Due to these good properties, nanotechnology is effectively utilized in different areas such as electronics, health care, agriculture, food, textiles, water treatment, environment, and many more. Figure 2.1 depicts the schematic diagram of applications of nanotechnology in various fields. In healthcare field, NPs have been contributing different the healthcare areas like tissue engineering, controlled drug and gene delivery, wound healing and wound dressings. The size, shape, design, and high surface area to volume ratio of NPs made it easier for the NPs to be incorporated into various biomedical devices. Hence, recently NPs have been used to be effective treatments for preventing various diseases such as cancers, infections, diabetes, allergies, and wound healing and dressings [8].

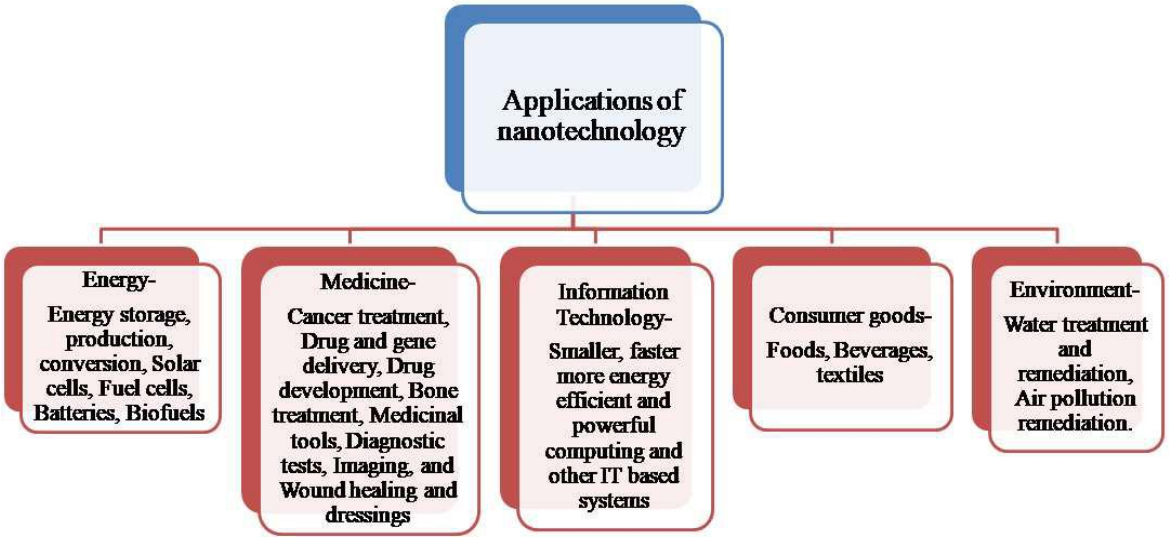

Figure 2.1 schematic representations of applications of nanotechnology in various fields.

Nanotechnology-based dressings are an innovative aspect which focuses for promoting wound healing and finally repairing the damaged tissue. It can be tailored for specific types of wounds, for example, to prevent the deterioration of chronic wounds. There is different nanoscale designs were analyzed for targeting particular phases of wound repair, including nanomaterials. The significant feature which supports nanomaterials application in wound dressing is the dimension (1-100 nm). The nanomaterials size is related to biological molecules. Hence, these materials can be suitable for *in vivo* and *in vitro* applications. There are various types of nanomaterials used in wound dressings but the metallic and metal oxide NPs are the best in all nanomaterials due to providing mechanical strength, therapeutic advantages and support antibacterial activity [9].

2.3 Nanomaterials

Nanomaterials are included in ceramics, polymers, carbon-based, lipid contained and metallic and metal oxide NPs. Ceramic materials are non-metallic, polycrystalline substances described by mechanical strength, stiffness, stability, low density, and corrosion resistance. The type of materials are plastic deformation, sensitive to cracks and other defects therefore, ceramic materials are

used in less amount in respect to metallic and polymers [10]. Ceramic materials are silica, calcium salts etc. The polymers are synthetic and natural polymeric materials. These are mostly biomaterials. Synthetic polymers are classified as polyethylene, polypropylene, polystyrene, polyvinyl chloride, polytetrafluoroethylene, and polyurethanes. The natural polymers are gelatin, collagen, hyaluronic acid, SF etc. The manufacturing of polymers is easy and low cost and its high flexibility property is the most important use in various types of dressings. Carbon-based nanomaterials are included in the fullerene, carbon nanohorn, carbon nanotubes, and graphene. Carbon-based materials have gained interest in nanomedicine due to its versatile use in advanced imaging, drug, gene delivery, and tissue engineering. Lipid contained nanomaterials are liposomes. A very interesting application of liposomes is it accelerates wound closure. Metal oxide NPs are Ag NPs, iron oxide, gold, TiO_2 and ZnO NPs. The properties of metals are good mechanical, thermal, electrical as well as cost effective. Therefore, metals are largely employed as a biomaterial in biomedical filed and their application in wound dressings [11].

2.4 Nanotechnology and SF based dressings

SF is the most important medical biotextile materials used in wound dressing applications. The combination of nanotechnology and medical biotextile offers a new technology called as bionanotextiles [12]. The modification of various properties of SF is based on the use of nanotechnology. These properties are included in the improvement of antibacterial activity, mechanical property, thermal stability etc. There are various types of materials have been prepared by using the integration of NPs to SF and modification of SF based on NPs. These materials can be prepared with simple and advanced methods. The simple method includes freeze drying, casting, and salt leaching etc. while advanced method is the electrospinning method. SF has formulated different types of dressings, which are capable to accelerate the wound healing. Nanotechnology has offers a combination of NPs and SF, which is gained much more advantages than traditional technology.

There are various reports indicated that the SF and NPs based different derivatives used as advanced dressing materials for wound healing [13].

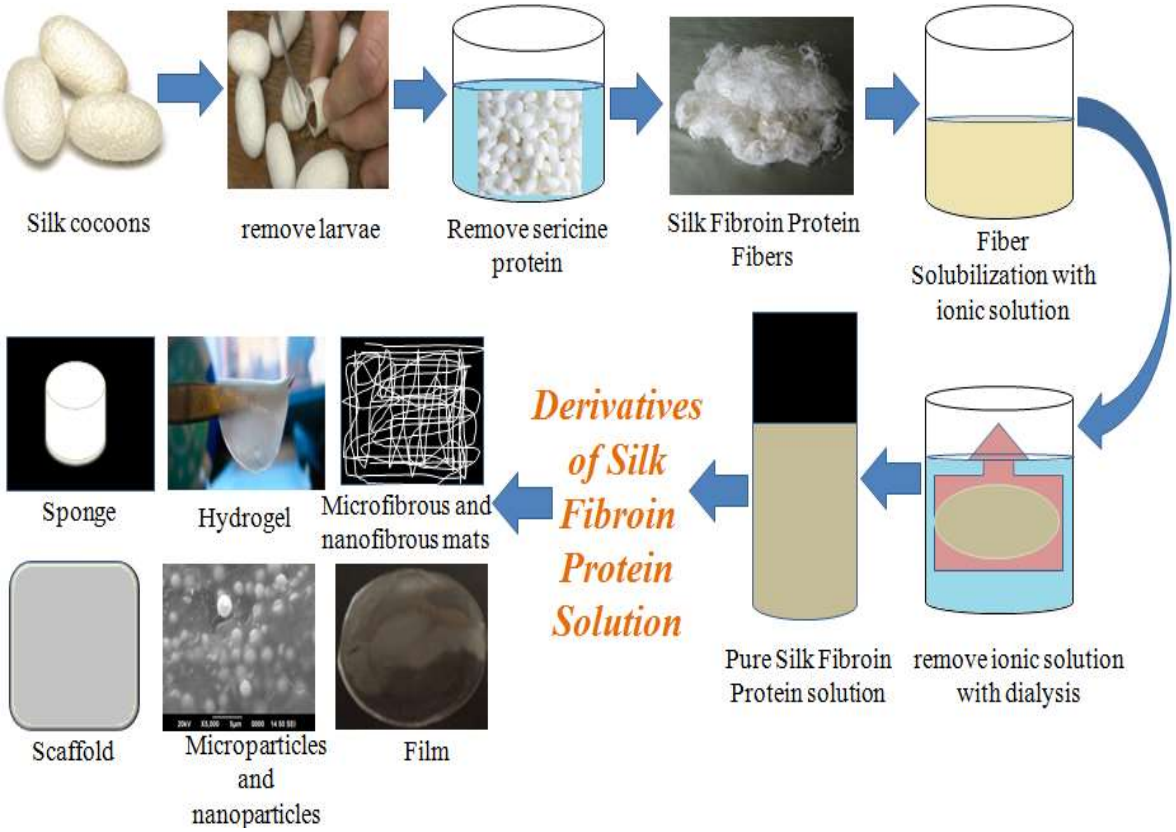

Figure 2.2 Synthesis processes of SF solution and its different NPs based derivatives used as the wound dressing materials.

Figure 2.2 is shown in the synthesis process of SF and its different nanomaterials based derivatives used for wound dressing applications. These are nanofibrous matrices and scaffolds, hydrogels, sponges, microparticles, NPs and NPs based SF composite films.

2.4.1 Scaffolds and nanofibrous matrices

Silks are in the form of fibrous architectures formed in nature. Microfibers (diameters in micrometer) and nanofibers (diameters less than 1 μm) have shown excellent materials as tissue engineering for skin replacement [14, 15]. Fibers can mimic native tissue while providing topographical and biological cues for healing.

The advantages of these micro-nanofibers are high porosity, applicable pore size distribution, high oxygen permeable, high surface to volume ratio and strong mechanical properties [16]. The fibers have been inserted into 2-D mats with a high surface to mass ratio which provides excellent mechanical property. Such fibers can be synthesized by different methods like phase separation, self-assembly and electrospinning technique [17, 18]. The phase separation method of fibers formation can be carried out by thermodynamic mixing of a homogenous solution into polymer rich phase and polymer poor phase [19]. These phases can be formed by exposure of the SF solution to different immiscible solvent. Another method for the formation of SF fibers is self-assembly. It occurs by the spontaneous hierarchical organization to higher order structures [17, 19]. Self-assembly method produced very fine fibers, which can often act as precursors to microscopic silk fibers [20]. Electrospinning is one of the advanced technologies has been evolved to fabricate nanofibrous scaffolds with unique properties because electrospinning technique is a facile, rapid and efficient method for production of silk and its composites based nanofibers by applying a high voltage to electrically charged liquid [21, 22]. Electrospinning is a highly scalable method for development of nano and microfibers of pure silks as well as silk composites [21]. Electrospun SF based fibers can be sterilized by using 70 % ethanol. The morphology and diameter of synthesized nanofibrous mats are investigated by using Scanning Electron Microscopy (SEM) study. This morphology and secondary structure of SF mats is depended on the electrospinning voltages, the concentration of SF solution, flow rate and receive distance [22]. If the concentration of SF is less, therefore the prepared SF mats observed clustered or beaded fibers [23, 24]. During the process of electrospinning technique, the different spinning solvents have been used such as Polyethylene Oxide (PEO), Hexafluoroisopropanol (HFIP) and formic acid [25]. Recently, biocompatible Manuka honey/SF fibrous matrices were developed by electrospinning procedure of aqueous PEO solution as wound dressing materials. In this study, *in-vivo* wound healing assay indicates that the prepared Manuka honey/SF fibrous matrices demonstrated excellent biocompatibility and enhanced wound healing process

[26]. Guldmet *et al.* prepared nanofiber webs based on olive leaf extract loaded SF/hyaluronic acid for wound dressing applications. The cytotoxicity of prepared nanofiber webs was evaluated *in-vitro* against the human epidermal keratinocytes cells. These results suggested that the developed electrospun nanofibers were nontoxic and good candidates for wound dressing materials [10]. Shadai *et al.* developed starch NPs as a vitamin E-TPGS carrier incorporated SF/PVA/Aloe Vera nanofibrous by electrospinning technique. These results indicated that the prepared nanofibrous dressing of SF/PVA/Aloe Vera containing 5% Vitamin-E-loaded starch NPs can be a potential dressing for treating skin wounds [22]. Similarly, the addition of Ag and TiO_2 NPs was found to improve the antibacterial property of SF mats [27, 28]. Minsung *et al*. prepared Ag NPs incorporated SF for the fabrication of antibacterial wound dressings [27]. Win *et al*. prepared electrospun SF/TiO_2 nanofibrous mats for wound dressings. In this study, the antibacterial effect of prepared mats was demonstrated against *E. coli* bacteria were under UV-A light exposure using the antibacterial drop-test method. The results of this study suggested that the inclusion of TiO_2 NPs into SF nanofibrous mats showed bactericidal ability against *E.coli* and the ability of photocatalytic degradation of methylene blue under UV irradiation [28]. Xingwo *et al.* prepared polyethyleneimine/SF multilayers nano fabrics for cell culture [29]. Cai *et al.* demonstrated chitosan and SF composite nanofibrous membrane was fabricated by electrospinning. The antibacterial activity of composite nanofibrous membrane was studied by the turbidity measurement method against *S. aureus* and *E. coli* bacteria. The results concluded that the bacteria killing activity of composite nanofibers varied on the type of bacteria. The biocompatibility study of synthesized nanofibers was studied by hematoxylin, eosin staining, and MTT assay. The prepared membranes were found to promote cell attachment and proliferation. The obtained results of this study suggested that the SF based composite nanofibrous matrix could be good candidates for wound dressings. [30].

Due to the excellent properties like high biocompatibility, cytocompatibility, biodegradability and flexibility of SF is considered as promising Scaffolding material [31]. 3-D structure biomaterials are the ideal material for

tissue engineering, wound healing and wound dressing applications because 3-D structures mimic the *in-vivo* physiological environment more closely than 2-D structures. Scaffolds are three-dimensional porous structures. These scaffolds are construct of ceramic, polymer and metals or composites of all these materials. SF based scaffolds must be biocompatible, excellent mechanical property and high porosity. Different types of scaffolds have been formulated using SF based materials [32, 33]. SF/amniotic 3-D bi-layered artificial skins were developed as scaffolds for the reformation of skin *in-vivo*. This scaffold promoted the regenerating of an extracellular matrix. *In-vivo* results indicated that the prepared artificial skin may be considered as a clinically translational product with stem cells to guide scarless healing of 3rd-degree burn injuries [34]. A novel anti-adhesion nonwoven mat prepared by SF by electrospinning technique for wound management in robotic surgery. SF based electrospun mats prepared by addition of synthetic polymers such as SF/PVA, SF/polyethylene glycol (PEG), and SF/polyethylene oxide (PEO). The results showed that the all non-woven mats were composed of submicron-fibers and showed no cytotoxicity towards skin cells such as fibroblast cells. Additionally, the prepared mats improved the anti-adhesion ability, good flexibility, high mechanical properties, promoting the biocompatibility and anti-inflammatory effects. Furthermore, *in-vivo* studies of SF and SF/PVA treated mats both have superior collagen regeneration and wound closure ability [35].

2.4.2 Hydrogels

SF based hydrogels are produced via sol-gel transition through aggregation of SF molecules into β-sheets or cross-linking of fibroin molecules to form an interconnected network in aqueous solution [36]. The gelation process is formed via heat/cold procedures, change of pH, cross-linking by usage of ionic species like Ca^{2+} ions and mechanical agitation/sonication, vortexing process [37]. The SF solution concentration is increased in hydrogels while enhanced tensile strength, modulus and strain. The increasing temperature of the gelation process similarly increase mechanical properties because of reduction of pore size. The prepared SF

hydrogels can be characterized by differential scanning calorimetry (DSC) to verify the melting point (~206 ^{o}C for hydrogels) [25]. Rheology study was used to investigate the stiffness of hydrogels. The adhesive properties of SF hydrogels were determined by using dynamic mechanical analyzer using stainless steel fixtures [38]. Due to the high water content and biocompatibility of SF based hydrogels applying for biological applications such as wound healing and wound dressings. The resulting hydrogels based on SF protein was improved cell attachment and proliferation when it was used in wound dressing applications. The prepared hydrogels were observed to be a suitable for wound repairing owing to its high effectiveness and easy application [39]. Burn wound care is one of the most critical problems in current surgery. Recently, chitosan-based hydrogels loaded with SF and L-Proline have been prepared and investigated. In this study, the cell attachment and proliferation improved by chitosan blending with SF and L-Proline. Due to the presence of numerous cationic sites, chitosan does not have better cell attachment and proliferation of the hydrogels. The prepared hydrogels showed better results than other polymers and used as an alternative wound dressing material in the *in-vivo* system in chronic wounds like diabetic and burn wounds [36]. *Y. huang et al.* prepared successfully composite hydrogel based on SF and polyurethane. The results showed that the excellent swelling and deswelling behaviors and good mechanical property of composite hydrogel and prepared composite hydrogels can be a potential material for biomedical applications [9]. The advantages of the utilization of hydrogels in the dressings are absorbed and retain the wound exudates, cooling sensation around the wound, stimulate fibroblast proliferation and keratinocytes migration. These activities are very necessary for complete epithelialization and healing of the wound [40]. Moreover, the advantages of hydrogels in wound dressing materials showed hydrogel structure prevents the wound from infections. [41]. However, hydrogel structures induce antibacterial agents and antibiotics [42]. The significant advances in wound dressing materials fabricated by antibacterial agent incorporated SF hydrogels. Therefore recently, curcumin loaded SF e-gel scaffolds prepared for wound healing applications. In this study, SF gel was formed with weak electric

fields which are 3-D scaffolds formed and studied for wound dressing materials. The observed results suggested that the curcumin-loaded SF gel scaffolds could improve the wound healing activity and be potentially used as wound dressing materials [43].

2.4.3 Sponges

Sponges based on SF can be obtained by utilizing SF solution by freeze-drying, gas foaming, and particle-leaching using porogens. For the freeze-drying process, silk cocoons dissolved in salt solutions of calcium chloride, and lithium bromide and dialyzed to 2-8 days wt % SF aqueous solution [44]. The porosity of sponges can be controlled by the usage of concentration, freezing temperature, and salt leaching. The pore size ranging from 490-900 μm was achieved by salt leaching technique. The porosity can be controlled by the size and quantity of particles. The methanol/salt technique is used to induce molecular crystallization into β-sheets so as to impart water stability and mechanical integrity [45]. In gas foaming type of process for the preparation of sponges is involving the addition of ammonium bicarbonate into SF solution and then by sublimation of ammonium bicarbonate in hot water [25]. The prepared sponges provide 3–D porous scaffolds for wound dressing applications. The 1, 1, 1, 3, 3, 3-hexafluoro-2-propanol (HFIP) can be employed for the preparation of sponges. The HFIP based sponges provide smoother surfaces along the pores and possess greater mechanical strength [45]. The developed SF based sponges can be characterized by morphology and pore structures by SEM. The porosity study can be determined by liquid (alcohol) displacing method. The SF sponges can be sterilized by using autoclaving, ethylene oxide, γ-radiation, or 70 % ethanol [25].

Blended chitin whisker reinforced SF nanocomposite sponge was developed and the effects of synthesized sponge were studied by using rat model. The results demonstrated that the wound healing effect of chitin whisker reinforced SF sponge was the best than other treatments including SF and chitin during the development of new tissue. The wound healing impact of the blended sponge was mediated by re-epithelialization and collagen deposition through fibroblasts proliferation. It

may be clinically useful for skin wound treatment [46]. Xiaomeng *et al.* (2014) developed SF/HTCC (N- (2-hydroxy) propyl-3-trimethyl ammonium chitosan chloride/ PVA composite sponge for wound dressings. The blended sponge prepared by the freeze-drying method and studied using chronic wound rat model. The obtained results suggest that the composite sponge performed better results than commercially available oil-containing non-woven fabrics [47].

2.4.4 Microparticles and NPs

SF microparticles and NPs can be prepared by using diverse methods such as self-assembly [48], freezing process [49], desolvation [50], spray drying [51], laminar jet break up [52], milling [53], capillary microdots [54] and electrospray techniques [55]. Self-assembly is extensively used to prepare SF micro and NPs with highly controlled diameters. SF molecules can be arranged in hydrophilic (Tyr, Ser) and hydrophobic (Gly, Ala) segments. The addition of a certain amount of ethanol to SF solution is permitting SF molecules to form particles by a self-assembly mechanism [48]. The size of microparticles is 0.2 to 1.5 μm, which can be controlled by the concentration of SF aqueous solution and amount of ethanol to be added. These microparticles have distinctive properties namely subcellular size, stability, high surface to volume ratio, high carrier capacity [48]. Wang *et al.* indicated that the blending of PVA to SF molecules to form SF micro and NPs [56]. Lammel *et al*. studied that the addition of Potassium phosphate to SF molecules to obtained SF micro and NPs ranging from 500 nm to 2 μm [57]. Milling is another physical method for production of SF micro and NPs. It does not use any chemicals, particles obtained by grinding, miller and the aperture of the vibratory sieve shaker. The cellular uptakes of SF NPs make for more efficient that of microparticles. SF NPs have been tested in wound healing and dressing applications [53]. Lee *et al*. developed SF NPs incorporated hydrocolloid dressings (SFNHD). In this study, results suggested that the SFNHD showed structural stability, improved water uptake and swelling ratio and increase cell growth rate compared to commercially available dressing. Additionally, SFNHD could reduce the burn size of rats and accelerate the growth of collagen fibers compared to

Neoderm® dressing. This study showed that the SFNHD may be the better choice for burn wounds. Lee *et al*. prepared insulin- functionalized SF dressing for chronic wound healing. The results from the *in-vivo* test using diabetic rat model suggested that the insulin-functionalized SF dressing provides a new treatment for chronic wound due to the prepared dressing showed wound closure, collagen deposition, and vascularization [58].

2.5 NPs based antimicrobial wound dressings

Now a day's NPs have emerged as an important platform to treat skin wound. The significant feature which supports NPs application in wound dressings is the dimension less than 100 nm, because of which there is the high surface to volume ratio [59]. Using NPs have attracted much attention for their well defined characteristics, and that are inaccessible in traditional microscopic materials. The flexibility of materials is in shape that is from NPs, nanofibers, nanotubes, nanocrystals, nanowires, and quantum dots, etc. which gives freedom for selection of application based nanomaterials. Incorporation of NPs into materials is to enhance mechanical and therapeutic advantages [60]. The ongoing worldwide research of nanotechnology is predicted to influence different fields of biomedical and engineering applications. NPs-assisted cancer therapy, drug delivery, cell imaging are most important areas in biomedical applications [61].

2.5.1 Ag NPs and SF based composite films

Over the last few decades, NPs based wound dressing materials have become an important area in research. Ag is a well-known metal applicable for a prolonged period as an antibacterial agent. This material is in the type of metallic Ag and Ag sulfadiazine ointments. It possesses fast, broad-spectrum antibacterial activity [62]. In recent years Ag based composite films improved various activities. Therefore, many researchers have focused on the composite materials based on Ag and SF. The blended SF and Ag NPs films are developed either by *in-situ* synthesis of Ag NPs using precursors or by mixing of NPs into SF aqueous solution by vigorous stirring [63]. The bacterial wound infection is the serious

problem of wound management. Recently Ag oxide NPs embedded SF spun were prepared by microwave mediated and studied their synergistic wound healing and antibacterial activity. The *in-vitro* wound healing (scratch assay) demonstrated that fast migration of the T3T fibroblast cells through the scratch area, treated with the Ag_2O-SF spuns and the area was completely cover within 24 h. The prepared spuns also showed biocompatible nature and used an ideal material for wound dressing and antibacterial applications [64]. In another study developed chitosan-SF composite materials with incorporation of Ag NPs for infected wound repair. The scaffolds of chitosan-SF-Ag NPs were synthesized by a freezing method. The embedded particles were observed using TEM and SEM examination. The asymmetric wettability of prepared scaffolds was measured using a contact angle measurement study. The results suggested that the prepared scaffolds showed high porosity, moisture retention capability, appropriate mechanical stiffness, good antibacterial activity, and highly biocompatible dressing. The *in-vivo* healing measured in mice infected wound models. The prepared dressing offers the potential for infected wound tissue repaired and regeneration. Ag NPs also employed in functionalization of Silk biomaterials for wound healing and dressing applications [65]. Gil *et al*. formed Ag sulfadiazine and epidermal growth factor (EGF) functionalized SF biomaterials and studied with a cutaneous excisional mouse wound model. The prepared materials increased wound healing rate, re-epithelialization, cell proliferation, collagen synthesis and reduce scar formation than control Tegaderm tape and Tegaderm hydrocolloid dressings [66]. Yu *et al*. reported in situ assemblies of Ag NPs on porous silkworm cocoon based wound film. The prepared film showed excellent antibacterial performance, biocompatibility and good extensibility. The in-vivo study was evaluated by using infected white rabbits and results observed the formation of broad epidermis during 14 days [67]. Coatings of Ag NPs on SF biomaterials have advanced technology for designing the newest wound dressing materials due to improving its antibacterial activity. Uttayarat *et al.* reported SF mats coated with Ag NPs for wound dressing application. The results indicated that the Ag NPs coated SF mats inhibit the growth of *S. aureus* and *P. aeurogenosa* and prepared mats can be used

as a prototypic wound dressing application with antibacterial properties [68]. In previous years several reports have been published describing the usage of Ag NPs in an enormous variety of antibacterial applications. They have been used as antibacterial filler in several wound dressing materials. Pei *et al.* studied the developed composite sponge, which are synthesized by using Ag NPs, SF and Carboxyethyl chitosan. The antibacterial study was carried out by disc diffusion and bacterial suspension assay, which showed that prepared sponge indicated effective for controlling infections of *S. aureus, P. aeruginosa* as compared to AQUACEL® Ag dressing. Also, the antibacterial activity of Ag NPs treated silk, offers excellent bacteria killing activity and certain antioxidant activity [69]. Calmak *et al*. developed bio-nanotextiles using Ag NPs and SF. Ag NPs containing SF bio-nanotextiles showed strong antibacterial activity [70]. Several excellent reviews on Ag NPs based biomaterials for antibacterial wound healing applications have been published in recent years [71]. All these studies have demonstrated that the novel fabrication of SF based composites is considerable in wound dressings and that Ag NPs present in the composite aid in the increased antibacterial activity.

2.5.2 TiO_2 NPs and SF based dressings

TiO_2 NPs have the promising potential nanomaterials used in various biomedical applications due to the TiO_2 NPs have nontoxic, long-lasting and inexpensive nanomaterials. It showed strong bactericidal and photocatalytic activities. In recent years there are various reports indicated that the TiO_2 photocatalyst illuminated by UV-A light, which showed high disinfection efficiency against *E. coli* bacteria. Recently electrospinning technique is a very popular and effective way for fabricating varieties of nanofibers. Jao *et al*. synthesized SF/TiO_2 nanofibrous mats for wound dressing application. The nanofibrous mats were synthesized by electrospinning technique. The size of prepared nanofibrous mats was 385 ± 63 nm. The water vapor transport rate, hemocompatibility, cytocompatibility, antibacterial activity, and cell attachment study using L929 fibroblasts cells were evaluated. The obtained results concluded

that the porous structure of mats provides high water vapor transmission rate, moisture absorption capacity, blood compatibility and cell adhesion and growth of L929 fibroblast cells. In addition, it observed bactericidal activity against *E. coli* bacteria [72]. Another study observed that the biocompatible wound dressing bandage was prepared by using chitin, SF and TiO_2 NPs. This bio-nanocomposite scaffold was prepared by freeze-drying method. This study investigated that the insertion of chitin to SF greatly enhanced the SF biodegradability whereas the addition of TiO_2 NPs into it showed good antibacterial and antifungal activities. Furthermore, this study observed that the prepared bio-nanocomposite scaffolds have good biocompatibility, cytocompatibility, biodegradability, good blood clotting ability and it has good potential application in wound dressings. The mechanism of antibacterial activity of TiO_2 NPs observed in the various reported study. The bacterial cells destroyed by photocatalytic peroxidation, which causes a change in cell permeability and leakage of the cell cytoplasm. Another important mechanism of prevention of infections of TiO_2 NPs are a generation of hydroxyl and peroxide radicals on the surface of TiO_2 NPs under the UV-irradiation attack on polyunsaturated phospholipids in the cell membrane and damage the bacterial cell [73]. Table 2.1 shows the different wound dressing materials on the basis of nanotechnology and SF along with their highlights.

Table 2.1: The different nanotechnology and SF based dressing materials in variety of forms along with their highlights.

No.	Matrix	Name of materials	Highlights	Refere-nces
1.	Scaffolds and nanofibrous matrices	SF/Manuka honey/PEO	In vivo wound healing assay observed excellent biocompatibility and enhanced wound healing process.	Yang *et al.* 2017
		SF/Olive leaf extract/ hyluronic acid	Nontoxic and good candidates for wound dressings	Guldm *et al.* 2016.
		SF/Vitamin E/PVA/Alovera	Antibacterial and potential dressing for treating skin wounds	Shadai *et al.*

				2018
		SF/Ag NPs	Antibacterial	Minsung *et al.* 2007
		SF/TiO_2	Antibacterial activity demonstrated against *E coli* bacteria under UV light	Win *et al.* 2012
		SF/Chitosan	Antibacterial, biocompatible	Cai *et al.* 2010
		SF/Amniotic 3 D bilayered artificial skin scaffold	Promoted the remodeling of an extracellular matrix healing of 3 rd degree burn injuries.	Mazaher *et al.* 2018
		SF/Chitin/Ag NPs Scaffold	Observed good antibacterial activity, biodegradability, mechanical property, cytocompatibility, proliferation, and cell attachment with $nHFFF_2$ cells.	Mojtaba *et al.* 2018
2.	Hydrogels	SF/Calcium alginate/Carboxyethyl Chitosan	Excellent cell adhesion and biocompatible for the healing of second degree burns, faster healing.	Woo *et al.* 2014
		SF/Chitosan/L-Proline	Improved cell attachment, proliferation when applied in chronic wound like diabetic, burn wounds.	Thangavel *et al.* 2017
		SF/Polyurethane	Excellent swelling, deswelling behavior and good mechanical property	Huang *et al.* 2013
		Curcumin loaded SF gel	Improved the wound healing activity.	Karahliloglu *et al.* 2018
3.	Sponges	SF/Alginate	Re-epithelialization and collagen deposition.	Dae-Hyun *et al.*

				2006
		SF/ HTCC/PVA	Studied for chronic wound, composite sponge performed better results than commercially available oil containing non woven fabrics.	Xiaomeng *et al.* 2014
		SF/Carboxyethyl chitosan/ AG NPs	High antibacterial activity against *S. aureus*, and *P. aeruginosa* than AQUACEL Ag.	Pei *et al.* 2015
4.	Microparticles and NPs	SF NPs based hydrocolloid dressing	Structural stability, improved water uptake and swelling ratio and increased cell growth rate compared to commercially available dressing, reduce burn size and accelerate growth of collagen fibers compared to Neoderm dressing	Lee *et al.* 2016
		Insulin functionalized SF	Chronic wound, showed wound closure, collagen deposition and vascularization	Lee *et al.* 2015
5.	Composite films	SF/chitosan	Good oxygen and water vapour permeability, hemostatic activity, biodegradability.	Kweon *et al.* 2001
		SF/glucose	High absorption capacity, good flexibility and biocompatibility	Haeyong *et al.* 2001
		SF/chitosan/alginate dialdehyde	Enhanced the stability and promote cell proliferation	Gue *et al.* 2013
		Growth factor functionalized SF	Enhanced macrophage adhesion and higher wound healing capacity	Bienert *et al.* 2017
		PVA reinforced SF	Biodegradability, degree of crystallinity, mechanical property, thermal property was improved	Sheik *et al.* 2014
		Recombinant spider SF/PVA	Porosity, promoting wound healing when it applied for Sprague Dawley rat model	Zhuo *et al.* 2017
		Asymmetric wettable chitosan SF/Ag NPs	High porosity, moisture retention capacity, appropriate mechanical stiffness, antibacterial activity and	Liu *et al.* 2017

	composite film	highly biocompatible	
	Epidermal growth factor functionalized SF film	Increased wound healing rate, re-epithelialization, cell proliferation, collagen synthesis and reduce scar formation compared to Tegaderm tape (3M)	Gil *et al*. 2013

2.5.3 ZnO NPs

The advantage of using the metal oxide NPs for biomedical applications is that it has a unique structure, interesting catalytic effects, high surface area, strong mechanical stability, biocompatibility and antibacterial activity [74]. Among the metal oxide NPs, ZnO NPs are of special interest. ZnO NPs belongs to inorganic, metal oxide NPs are increasingly important as one of the newest class of materials. Due to its antibacterial, biocompatible, and tissue adhesive properties, ZnO NPs are capable and best filler in wound dressing application. ZnO NPs have gained much of interest as future materials due to their interesting effects namely large surface-to-volume ratio, high surface reaction activity, high catalytic effects, and strong adsorption capacity, which make ZnO NPs are suitable candidates for a broad range of applications. ZnO NPs are excellent candidate with a direct band gap (3.37 eV) and it is a semiconducting material. ZnO NPs are widely used in near UV-emission, piezoelectric, nanosensors, energy storage, transparent conductor, cosmetics etc applications. ZnO NPs crystals form hexagonal wurtzite and cubic zinc blend structure showed in figure 2.3. The most general and stable structure at atmospheric condition of ZnO NPs are hexagonal wurtzite structure. Another structure, zinc blend can be stabilized by formation of ZnO on substrates with a cubic lattice form. The centers of zinc and oxide are tetrahedral in both type of structure.

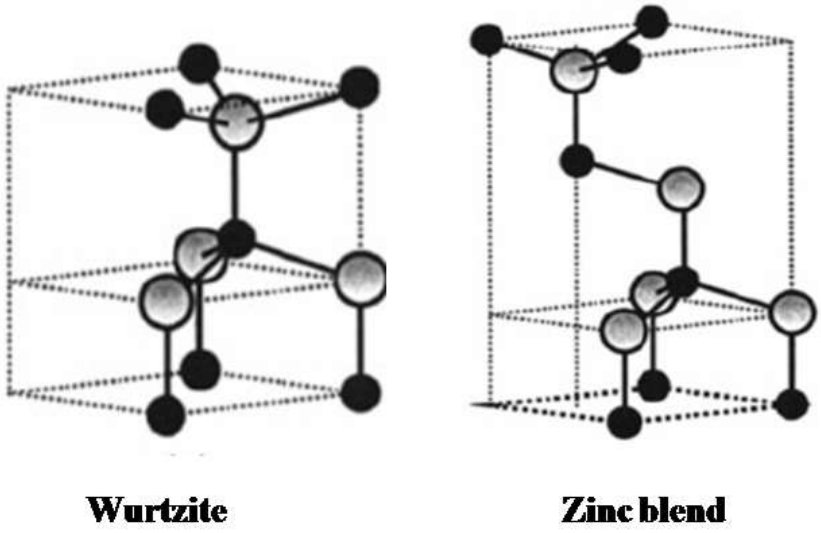

Figure 2.3 Structures of ZnO NPs [75].

ZnO NPs have been formulated by interested high temperature solid-state method. In large scale, ZnO NPs can be synthesized by low coast simple solution based chemical precipitation, sol-gel type and hydrothermal reaction method. The hydrothermal process is important for controlling the particle size of ZnO NPs. These types of NPs have described wide interest because of its high stability, less cytotoxicity than Ag NPs, good photocatalytic activity and from use in electronics and solar cells to biomedical application. The production of the hydrogen peroxide at its surface results in outstanding antibacterial activity therefore, the utilization of these ZnO NPs in various hydrogen-based dressing materials. ZnO NPs shows good biocompatibility and tissue adhesive properties. Based on these interesting properties ZnO NPs can be used in wound healing application. In a recent study, ZnO NPs have added into a microporous chitosan materials. The developed bandage examined high swelling capacity and formation of platelets and blood clotting. Additionally, this study demonstrated that prepared material showed essential infection prevention properties and cytocompatibility as it supported re-epithelialization and collagen deposition [76].

2.6. Comparison of SF based dressings with other natural polymer materials

There are different dressing materials available in the market based on natural biopolymers such as collagen, elastin, and SF etc. Among these, collagen dressings are mostly used to support cell activities, differentiation, and migrations. Collagen has synthesized by animal sources, it may stimulate immunological responses and transfer pathogens to the host tissue. The synthesis of collagen is not easy and it's challenging from a cost perspective. The mechanical strength of collagen is very poor. These disadvantages of collagen restrict its applications for wound dressings. Elastin is natural biopolymers. Due to its elasticity property, it is used in commercial dressings. The highly cross-linked structure of elastin hinders its processability and decreases its solubility. Therefore, its limited supplies because of it originate from biotechnology-derived sources, whereas SF has high solubility in aqueous salt solutions and easily processed into various structures. Additionally, it shows beneficial characteristics such as abundant supplies, high water absorption capacity, cost effectiveness, and high flexibility. Due to excellent properties SF based dressings are used appropriate supports for complete of healing of the wound. In addition, the SF wound dressing materials have been modified with nanotechnology for their added advantages like Photoinduced cleaning, enhancing antibacterial activity, strengthening mechanical property and extending durability etc. This makes nanotechnology enable SF based film is more promising in future [77].

2.7 Role of antimicrobial agents in wound dressings

Antimicrobial agents perform a vital role in inhibiting the growth of microorganisms. There are varieties of antimicrobial agents employed in biomedical applications. These are classified into two groups, inorganic and organic agents. Inorganic antibacterial agents are metals, metal oxides, and metal phosphates materials. The organic antibacterial agents are phenols, halogenated compounds, and quaternary ammonium salts. All the antibacterial agents are used in various biomedical applications such as tissue engineering, drug delivery, and wound healing and dressing applications [78]. Inorganic antibacterial materials of

metal oxides such as ZnO and TiO_2, NPs have played an essential role in wound dressing applications. These inorganic NPs are used to incorporate other organic and polymer materials for the production of antibacterial composite materials. The incorporation of these antibacterial agents is aimed to prevent wound infections in patients at high risk when it is used in wound dressing applications. If the antibiotics have been used as antibacterial agents, then the antibiotic-resistant bacteria grow and spread the infections. Thus, the selection of proper antibacterial agents can help to enhance the prevention of infections. Wound infection causes delayed in the healing process or extends the time of wound closure. Therefore if the infections prevent, simultaneously prevents the extended time of wound closure [79].

2.8 NPs embedded composite films

NPs embedded composite materials that have the structure comprising two or more different phases arranged and size of one of the materials is measured in nanometer so as to bring benefits that do not possess individually. Schematic diagram of the NPs embedded composite film showed in figure 2.4. A significant advancement in the development of novel composite film is of great interest for biomedical applications such as tissue engineering, drug delivery and, cellular therapies. Incorporation of NPs into the matrix is a drastic improvement in properties such as mechanical strength and toughness, thermal stability, electrical conductivity, surface appearance etc. The percentage of nanofiller is about 0.5 to 5 % is the best effectiveness due to low filler shows high aspect ratio [80].

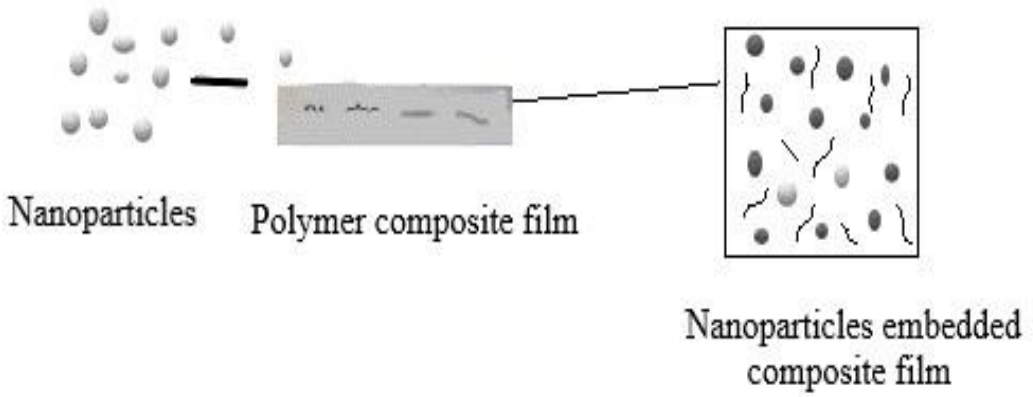

Figure 2.4 Schematic diagram of NPs embedded composite film.

2.9 NPs surface coated composite films

Recently, the antimicrobial coatings on the surfaces of polymer matrices play a significant role to enhance the antibacterial activity against pathogenic bacteria. Surface coating techniques are improving the mechanical and antibacterial activity against microorganisms of composite materials. Figure 2.5 represented the schematic diagram of NPs surface coated composite films. If the NPs are coated on the surface of the polymer matrix, then the thermal property of the polymer materials are increased and improving the abrasion resistance, barrier properties including corrosion resistance of the coatings without losing their other properties. The varieties of NPs have coated on the surface of polymer matrix such as TiO_2, ZnO, $AgNO_3$, SiO_2 etc. The TiO_2 and ZnO NPs have generally coated for the reason of antibacterial activity as well as UV-blocking gents. The SiO_2 NPs have coated for abrasion resistance of the coatings. The coatings are offers much greater surface area to volume ration of the materials. There are many surface coating techniques that are Plasma irradiation, hydrothermal method, microwave, screen printing, etc [81]. In an attempt to these facing the complications namely pre and post-treatment, long processing time as well as expensive. Sonochemical surface coating technique appeared as a simple, fast, easy, efficient, and inexpensive for coating of different substrates. Sonochemical coating technique prevents the aggregation to NPs due to the application of high-intensity ultrasound

and the acquired coatings are uniformly deposited on the surface of substrates [82]. Antimicrobial coating of composite films improved the thermal, mechanical, antibacterial properties of composite films. According to the literature the antibacterial agents of ZnO NPs coated on the surface of polymer matrices by a screen printing technique. The results concluded that the coating enhanced the tensile strength and % elongation, thermal stability, antibacterial activity against gram positive and gram-negative bacteria. Another study revealed that the antibacterial activity, swelling ability, mechanical property, of composite films increased with increase in the concentration of coatings of NPs. [83]

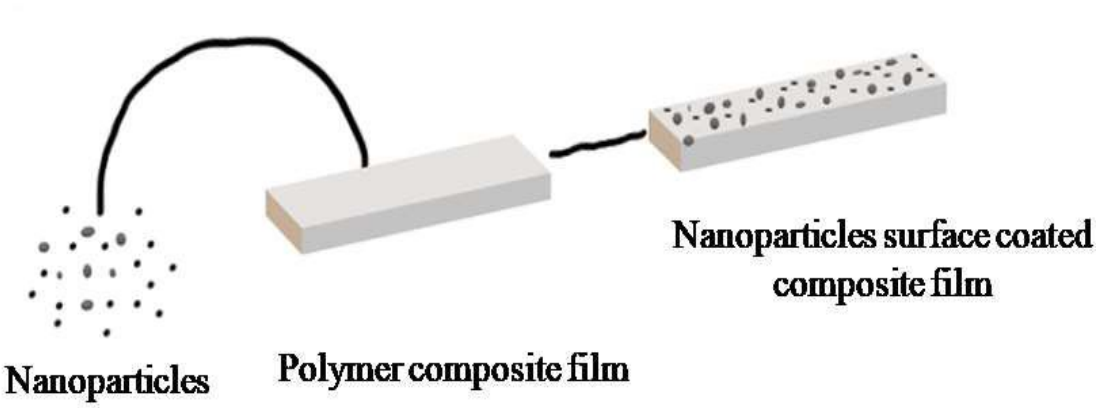

Figure 2.5 Schematic diagram of NPs surface coated composite film.

2.10 Conclusions

Nanoscience and nanotechnology is an emerging field in biomedical applications particularly in wound healing and wound dressing applications. SF has amazing natural materials for fabrication of different kinds of materials based on NPs and with great potential for various biomedical applications. Wound healing is an intricate process involving skin repairs itself after injury. SF and NPs are excellent dressing materials for wound healing purpose are well studied in the literature. In this chapter, we focused the recent advances of SF and NPs based materials such as scaffolds and nanofibrous matrices, hydrogels, sponges, SF micro and NPs, and composite films in the wound dressings. Nanofibrous matrix and scaffolds of SF improved porosity, oxygen permeability, and mechanical property. Electrospinning is the advanced technique for fabrication of nanofibrous

mats and scaffolds. Hydrogels of SF may be considered as an important material for burn dressing due to its adhesive strength and water content. Moreover, SF based hydrogels provide the moist environment in wound interfaces. The sponges based on SF and NPs have the properties of higher porosity, greater mechanical strength, the rapid proliferation of epithelial cell and collagen deposition via fibroblast proliferation. SF microparticles and NPs have shown unique properties such as subcellular size, stability, high carrier capacity, improved swelling ratio and increased cell growth of collagen fibers. To improve the properties of wound healing SF and NPs based composite films have been developed by using different types of polymers such as PEG, PVA, alginate, and hyaluronic acid. It is strongly proved that the nanotechnology-enabled SF composite films are excellent antibacterial activity, mechanical property, non-cytotoxicity, cell attachment property, and permeability to water and vapor and it is considered as NPs enabled SF materials could be excellent materials for wound dressing application.

References

1. M. Mir, M. Ali, A. Barakullah, A. Gulzar, M. Arshad, S. Fatima, M. Asad, Prog Biom, 2018, 7, 1-21.
2. S. Mehrotra, and A. Misir, Current Pediatr Rev, 2018, 14, 28-33.
3. H. Shihao, S. Bi, D. Yan, Z. Zhou, G. Sun, X. Cheng, X. Chen, Carbohydr Polym, 2018, 184, 154-163.
4. P. Nakod, The Development of a Textile Wound Dressing for Vacuum Assisted Wound Therapy, 2017.
5. A. Singh, D. Gemmate, A. Kanase, I. Pandey, V. Misra, V. Kishore, T. Jahnke, J Veins Lymphatics, 2018, 7:7196, 1-47
6. J. Curtis, M. Greenberg, J. Kester, S. Phillips, G. Krieger, Toxicol Rev, 2006, 25, 245-260.
7. A. Arico, P. Bruce, B. Scrosati, J. Tarascon S. Van, Materials for sustainable energy, 2011, 148-159.
8. R. Lehner, X. Wang, S. Marsch, P. Hunziker, Nanomed-Nanotechnol, 2013, 9, 742-57.
9. Y. Huang, B. Zhang, G. Xu, W. Hao, Compos Sci Technol, 2013, 84, 15-22.
10. K. Mahyar, I. Gibson, M. Goldberg, J. Nomani, G. Littlefair, Sci Adv Mater, 2016, 8, 1491-1511.
11. L. Ng, A. Mohammad, C. Leo, N. Hilal, Desalination, 2013, 308, 15-33.
12. S. Calamak C. Erdogdu, M. Ozalp, K. Ulubayram, Mater Sci Eng C, 2014 43, 11-20.
13. Z. Hussain , H. Thu, A. Shuid, H. Katas, F. Hussain, Curr Drug Targets, 2018 19, 527-50.
14. P. Quynh , U. Sharma, A. Mikos, Biomacromolecules, 2006, 10, 2796-2805.
15. D. Michael, D. Boyd, A. Adams, F. Ligler, Adv Health Mater, 2015, 4, 11-28.
16. S. Sivolella, G. Brunello, N. Ferrarese, A Puppa, D. Avella, E. Bressan, B. Zavan, Intl J Mol Sci, 2014, 15, 3088-3117.
17. L. Smith, P. Ma. Colloids Surf, B, 2004, 39, 125-131.
18. B. Nandana, S. Kundu, Biotechnol Adv, 2010, 28, 325-347.
19. C. Ping, D. Lin, C. Shih, A. Dwan, C. Gryte. J Polym Sci, Part B: Polym. Phys, 1999, 37, 2079-2092.

20. L. Qiang, H. Zhu, C. Zhang, F. Zhang, B. Zhang, D. Kaplan. Biomacromolecules, 2012, 13, 826-832.
21. Z. Xiaohui, M. Reagan, D. Kaplan, Adv Drug Delivery Rev, 2009, 61, 988-1006.
22. K. Alsadat, J. Nourmohammadi, H. Tabesh, B. Bagheri. Colloids Surf, B, 2018, 166, 9-16.
23. A. Martins, R. Reis, N. Neves. Int Mater Rev, 2008, 53, 257-274.
24. A. Nasim, M. Nouri, M. Kish, Fiber Polym, 2009, 2, 167-176.
25. D. Rockwood, R. Danielle, T. Preda, X. Yücel, M. Wang, L. Lovett, and D. Kaplan, Nat Protoc, 2011, 6, 1612–1631.
26. Y. Xingxing, L. Fan, L. Ma, Y. Wang, Si Lin, F. Yu, X. Pan, G. Luo, D. Zhang, H. Wang, Mater Design, 2017, 119, 76-84.
27. K. Minsung, R. Jung, H. Kim, J. Youk, H. J. Nanosci Nanotechnol, 2007, 7, 3888-3891.
28. J. Win Chun, M. Yang, C. Lin, C. Hsu. Polym Adv Technol, 2012, 23, 1066-1076.
29. Y. Xinguo, S. Li, X. Chen, Y. Zhan, X. Li., Int J Biol Macromol, 2017, 94, 492-499.
30. Z. Cai, X. Mo, K. Zhang, L. Fan, A. Yin, C. He, H. Wang., Int J Mole Sci, 2010, 11, 3529-3539.
31. R. Nazarov, H. Jin, D. Kaplan. Biomacromolecules, 2004, 5, 718-726.
32. W. Yun, E. Bella, C. Lee, C. Migliaresi, L. Pelcastre, Z. Schwartz, B. Boyan, A. Motta, Biomaterials , 2010, 31, 4672-4681.
33. U. Kim, J. Park, H. Kim, M. Wada, D. Kaplan, Biomaterials, 2005, 26, 2775-2785.
34. G. Mazaher, S. Ali, M. Alexander, S. Aleksandra, M. Urbanska, H. Ghanbarian, J. Hardy, M. Omrani, R. Reis, S. Kundu, Biomed Mater, 2018, 13, 035003.
35. W. Yu-Chi, M.-Y. Bai, W.-Y. Hsu, and M.-H. Yu, J Biomed Mater Res Part A, 2018, 106, 221-230.
36. T. Ponrasu, B. Ramachandran, R. Kannan, V. Muthuvijayan., J Biomed Mater Res Part B, 2017, 105, 1401-1408.
37. Y. Qi, H. Wang, K. Wei, Y. Yang, R. Zheng, I. Kim, K. Zhang., Int. J. Mole. Sci. 2017, 18, 237, 1-21.
38. T. Hoare, D. Kohane, Polymer, 2008, 49, 1993-2007.
39. N. Peppas, P. Bures, W. Leobandung, H. Ichikawa, Eur J Pharm Biopharma,

2000, 50, 27-46.

40. R. Optveld, O. Boomen, D. Lundvig, E. Bronkhorst, P. Kouwer, J. Jansen, E. Middelkoop, J. Von den Hoff, A. Rowan, F. Wagener, Biomaterials, 2018, 181, 392-401.
41. J. Woo, O. Lee, B. Moon, F. Sheikh, J. Lee, J. Kim, H. Park, Tissue Eng Regen Med, 2014, 11, 203-210.
42. J. Boateng, K. Matthews, H. Stevens, G. Eccleston., J Pharm Sci, 2008, 97, 2892-2923.
43. M. Fini, A. Motta, P. Torricelli, G. Giavaresi, N. Aldini, M. Tschon, R. Giardino, C. Migliaresi, Biomaterials, 2005, 26, 3527-36.
44. C. Craig, C. Riekel. Comp. Biochem. Physiol., Part B: Biochem Mol Biol, 2002, 133, 493-507.
45. V. Charu, D. Kaplan, Progr. Prog Polym Sci, 2007, 32, 991-1007.
46. D. Roh, S. Kang, J. Kim, Y. Kwon, H. Kweon, K. Lee, Y. Park, J Mater Sci: Mater Med, 2006, 17, 547-552.
47. X. Li, B. Li, J. Ma, X. Wang, S. Zhang, J Bioact Compat Polym, 2014, 29, 398-411.
48. C. Zhengbing, X. Chen, J. Yao, L. Huang, Z. Shao, Soft Matter, 2007, 3, 910-915.
49. W. Lu, Z. R. Xia, L. L. Lv, Q. Tang, and M. Z. Li, Adv Mater Res, 2011, 236, 1902-1905.
50. J. Kundu, C. Yong, H. Young, T. Giyoong S. Kundu, Int J pharm, 2010, 388, 242-250.
51. H. Tomoaki, M. Tanimoto, S. Shimabayashi, J Colloid Interface Sci, 2003, 266, 68-73.
52. E. Wenk, A. Wandrey, H. Merkle, L. Meinel, J Controlled Release, 2008, 132, 26-34.
53. R. Rangam, L. Wang, and X. Wang, Pow Tech, 2008, 185, 87-95.
54. Z. Zheng, Y. Li, M. Xie, Int J Mole Sci, 2015, 16, 4880-4903.
55. Y. Wang, M. Bai, W. Hsu, M. Yu, J Biomed Mater Res, Part A, 2018, 106, 221-230.
56. X. Wang, T. Yucel, Q. Lu, X. Hu, D. Kaplan, Biomaterias, 2010, 31, 1025-1035.
57. A. Lammel, X. Hu, S. Park, D. Kaplan, T. Scheibel, Biomaterials, 2010, 31, 4583-4591.
58. L. Joo, J. Kim, B. Moon, J. Chao, H. Ju, J. Lee, Tissue Eng Regen Med, 2016, 13,

218-226.

59. W. Jolanta, T. Rydzkowski, G. Borowski, M. Szczypiński, T. Klepka, V. Thakur, Int J Polym Anal Charact 2018, 23, 383-95.
60. A. Tiwari, A. Bajpai, J. Bajpai, R. Saini, P. Agrawal, Smart Biomaterial Devices: Polymers in Biomedical Sciences, 1st Edition, CRC Press, 2016, 1-242.
61. J. Boateng, K. Matthews, H. Stevens, G. Eccleston, J pharm Sci, 2008, 97, 2892-2923.
62. M. Rai, A. Yadav, A. Gade, Biotechnol Adv, 2009, 27, 76-83.
63. K. Thitikan, S. Wongkittithavorn, S. Chaiarwut, P. Ekabutr, P. Pavasant, P. Supaphol, J Drug Delivery Sci Tech, 2018, 44, 91-100.
64. L. Zhisong, J. Xiao, Y. Wang, M. Meng, J Colloid Interface Sci, 2015, 452, 8-14.
65. B. Jayasekhar, M. Doble, A. Raichur, J Colloid Interface Sci, 2018, 513, 62-71.
66. G. Seok, B. Panilaitis, E. Bellas, D. Kaplan, Adv Healthc, Mater, 2013, 2, 206-217.
67. Y Kun, F. Lu, Q. Li, H. Chen, B. Lu, J. Liu, Z. Li, F. Dai, D. Wu, G. Lan. Sci Rep, 2017, 7, 2107.
68. U. Pimpon, S. Jetawattana, P. Suwanmala, J. Eamsiri, T. Tangthong, S. Pongpat, Fiber Polym, 2012, 13, 999-1006.
69. P. Zejun, Q. Sun, X. Sun, Y. Wang, P. Zhao. Bio-Med Mater Eng, 2015, 26 S111-S118.
70. C. Semih, E. Aksoy, C. Erdogdu, M. Sagıroglu, K. Ulubayram, J Nano Res, 2015, 17, 87.
71. S. Kumar, D. Sundar, N. Rajendran, N. Houreld, H. Abrahamse, Int J Biol Macromol, 2018.
72. W. Jao, M. Yang, C. Lin, C. Hsu, Polym Adv Technol, 2012, 1066-76.
73. M. Mehrabani, R. Karimian, R. Rakhshaei, F. Pakdel, H. Eslami, V. Fakhrzadeh, M. Rahimi, R. Salehi, H. Kafil, Int J Biol Macromol, 2018 , 116, 966-76.
74. A. Kołodziejczak-Radzimska , T. Jesionowski, Materials, 2014, 7, 2833-81.
75. P. Espitia, N. Soares, J. Coimra, E. Mediros, Food Sci Technol, 2012, 5, 1447–1464.
76. Z. Lu, J. Gao, Q. He, J. Wu, D. Liang, H. Yang, R. Chen. Carbohyd poly, 2017, 156, 460-469.
77. M. Faokhi, F. Mottaghitalab, Y. Fatahi, A. Khademhosseini, D. Kaplan, Trends

Biotechnol, 2018, 36, 907-922.

78. D. Rahmani, A. Bakhshayesh, N. Annabi, R. Khalilov, A. Akbarzadeh, M. Samiei, E. Alizadeh, M. Alizadeh-Ghodsi, S. Davaran, A. Montaseri, Artif Cells Nanomed Biotechnol, 2018, 46, 691-705.
79. C. L. Ventola, Pharm Ther, 2015, 40, 277- 283.
80. M. Khorasani, A. Joorabloo, A. Moghaddam, H. Shamsi, Z. MansooriMoghadam, Int J Biol Macromol, 2018, 114, 1203-1215.
81. N. Shaigan, W. Qu, D. Ivey, W. Chen, J Power Sources, 2010, 195, 1529-1542.
82. R. Gottesman, S. Shukla, N. Perkas, L. A. Solovyov, Y. Nitzan, A. Gedanken, Langmuir, 2010, 27, 720-726.
83. J. Meshram, V. Koli, M. Phadatare, S. Pawar, Mater Sci Eng C, 2017, 73, 257-266.

CHAPTER 3

Characterization Techniques for Wound Dressing Materials

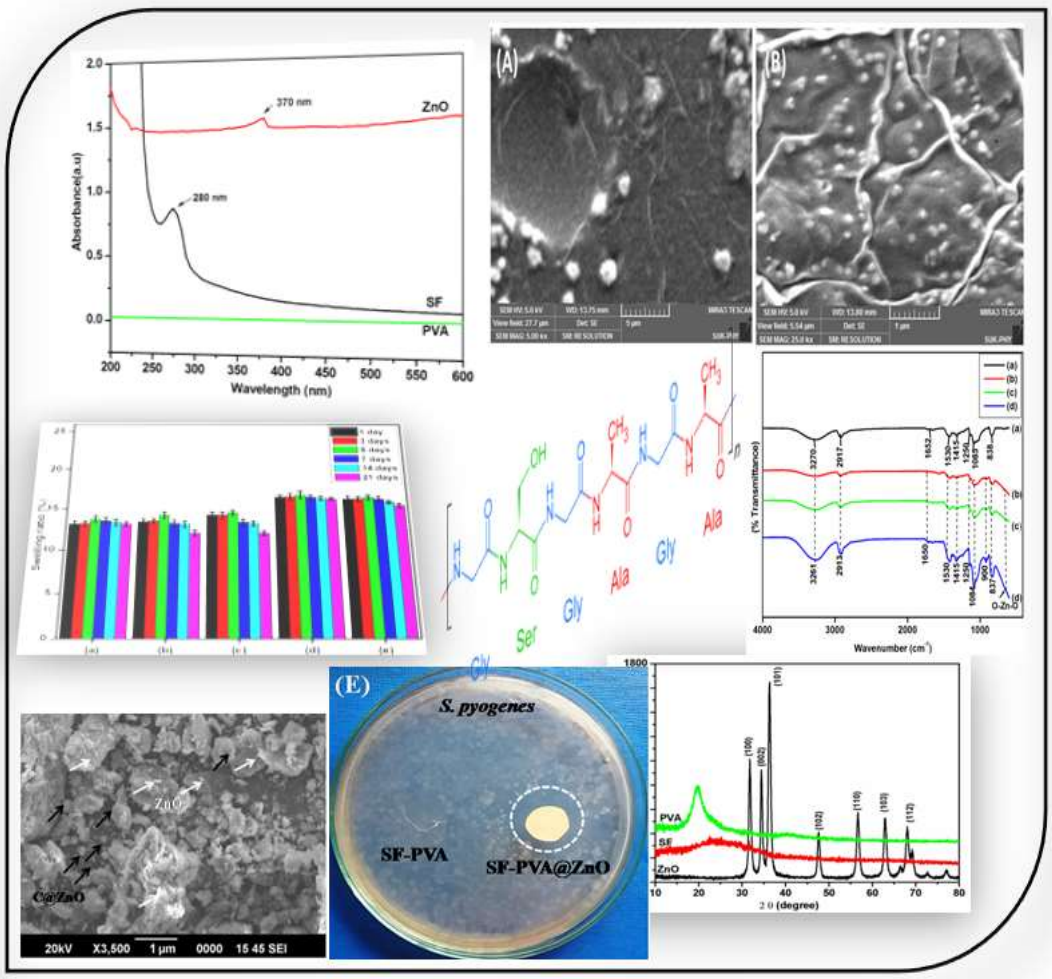

3.1 Introduction

The properties of materials are changed dramatically when their size is reduced to nanoscale range. The measurement of these nanodiamension materials is not a very easy task. These nanoscale composite materials are studied by employing appropriate characterization techniques [1]. The study of different characterization techniques are required for better understanding of synthesized nanodiamension materials. These characterization techniques give the detailed information about the materials size, shape, morphology, chemical composition and other novel properties [2]. The important characterization techniques used for analysis of ZnO NPs and composite films explained in this chapter. These characterization techniques are including physico-chemical characterizations, morphological, thermal, mechanical, surface area, porosity and biological characterization techniques.

The physico-chemical characterizations of materials are basically depends on the method adopted for the synthesis of materials. The understanding of morphological, mechanical, surface area, porosity and biological characterization techniques is very important for wound dressing applications [3]. The present chapter deals with the characterization techniques for wound dressings, their working principle, and operation are mentioned below.

3.2. Characterization Techniques

3.2.1. Structural and surface characterization techniques

3.2.1.1 X-ray diffraction

X-ray diffraction (XRD) is a strong technique which is noncontact and nondestructive employed to identify crystalline phases of materials. XRD is used to measure structures, phases, grain size, epitaxy, preformed orientation and crystal defects. In addition, XRD is employed to examine the thickness of films, multilayers, and arrangements of atomic in amorphous type of materials [4].

The instrument of XRD is consists of incident X rays, sample holder and detector. The monochromatic source X-rays entered through a monochromator to develop Kα radiation from the respective metal. The intensity of diffraction is

measured as a function of 2θ and the orientation of the specimen, which yields the diffraction pattern. The X-ray wavelength λ is typically 1 Å, which corresponds to X-ray energies of 6-17 KeV.

The working principle of XRD instrument is observed in reported literature. This is based on the monochromatic source X-rays and crystalline materials. The X-rays interact with crystalline materials to forms diffraction owing to the atomic planes. One of the scientists Bragg's reported the mathematical equation based on the diffraction from crystalline material. It is called as Bragg's low and which is expressed as below,

$$2\,d\sin\theta = n\,\lambda \qquad (3.1)$$

Where,

d= interplaner spacing

θ= diffraction angle

λ= wavelength of X-ray

n= order of diffraction

A process of fulfilling Bragg's condition is devised and that can be alone by continuously varying either λ or θ during the experiment. Hence, depending on the methods these quantities are varied. It differentiated into the three main diffraction systems such as laus system, rotating crystal and powder system. Among these three processes, the powder system was selected during the whole proposed work. In this process, the crystal to be detected is reduced to a fine powder of particles and situated in a monochromatic X-rays. The particles are the tiny crystals, or assembly of smaller crystals, oriented at random with respect to incident beam. In this method, some of the crystals will be correctly oriented so that their (100) planes can be reflect the incident beam. Other crystals will be properly oriented for (110) reflections and so on. These results indicated that every set of lattice planes will cause reflection. Figure 3.1 (a) shows the schematic representation of typical XRD, depending on the Bragg's- Bentano geometry and figure 3.1 (b) shows the photograph of the XRD instrument.

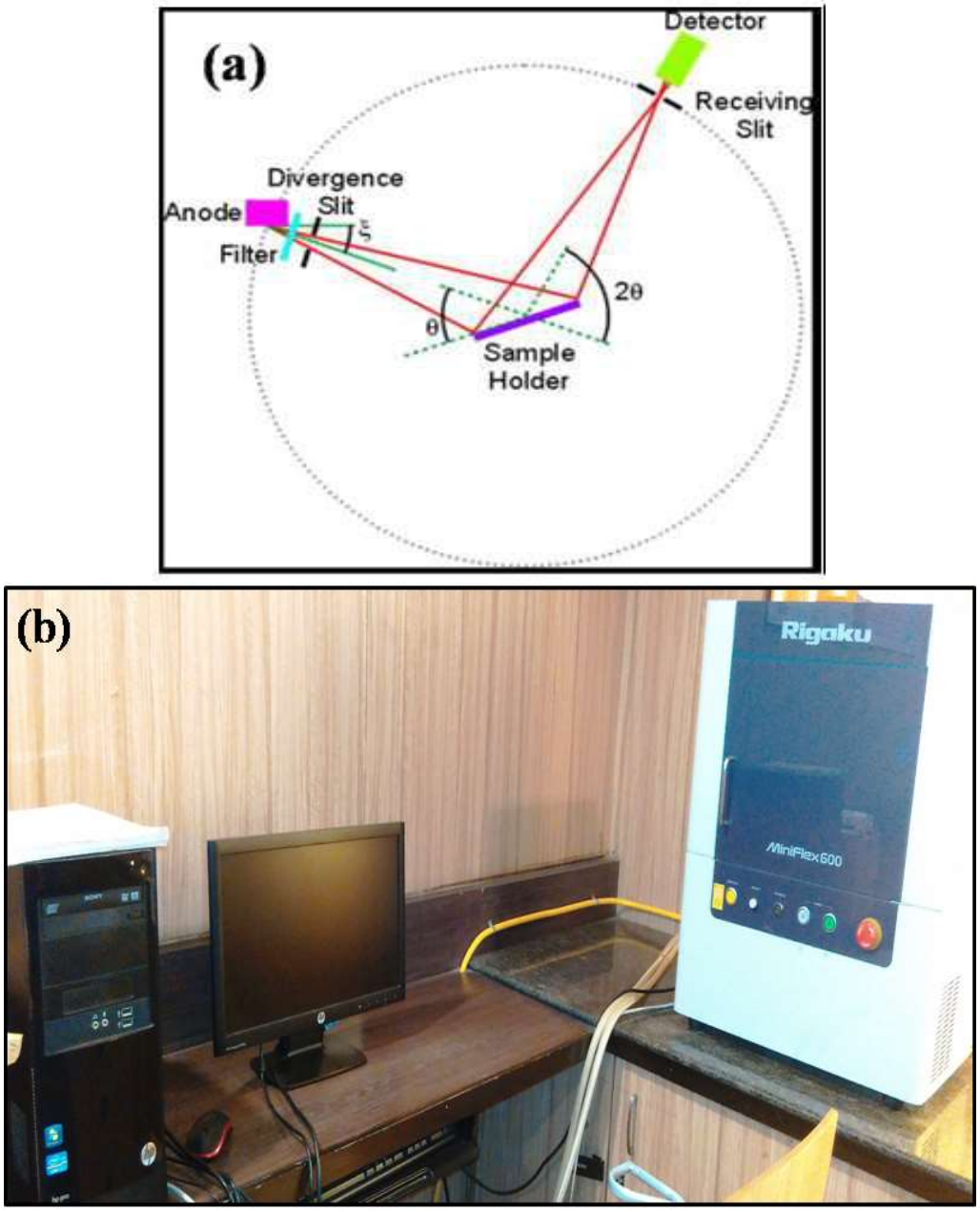

Figure 3.1 (a) Schematic representation of X-ray diffractometer, **(b)** Photograph of X-ray diffraction instrument [5].

XRD is also used for identification of crystalline Phases by comparing the data from the sample with peaks and relative intensities with known Standard Joint Committee on Powder Diffraction Standards (JCPDS) file. Reflections can be indexed with Miller indices. If the size of diffraction tiny crystal is small, there is no more complete destructive interference at $\theta \pm d\theta$, which broadness the peak

corresponding to the diffraction beam in proportion to the size of little crystal. The broadening of diffraction peak can be employed to estimate the particle size. The relation is given by Scherer's formula [6],

$$t = \frac{0.9\lambda}{\beta \cos\theta} \quad (3.2)$$

Where,

t = Particle size

θ = diffraction angel

λ = Wavelength of X-rays

β = Full width at half maximum (FWHM)

The phase composition, lattice parameter and the crystallite size of ZnO NPs and prepared composite films were estimated by XRD (RIGAKU Miniflex 600) equipped with a crystal monochromator used to Cu-Kα radiation of wavelength 1.5406 Å in the 2θ range from 20 to 100^{o}.

3.2.1.2 BET surface area and porosity

Physical gas adsorption method is important and standard method for the determination of surface area and porosity of materials. The scientist Stephen Brunauer, Paul Huge Emmet, and Edward Teller in 1938 introduced this theory and consist of their family named as Brunauer-Emmet-Teller (BET) method. An inert gas mostly nitrogen is adsorbed on the surface of solid materials [7]. This method is widely utilized for determination of specific surface area and porosity of materials.

Adsorption is the process by which atoms, ions or molecules are attracted to and retained at the surface of a solid or liquid. An adsorption isotherm is acquired by measuring the amount of gas adsorbed over a wide range of relative pressures at a constant temperature. Conversely desorption isotherms are attained by measuring gas removed as pressure is reduced.

In BET analysis, nitrogen gas is mostly used as the probe molecule and is exposed to a solid under investigation at liquid nitrogen conditions. The amount of nitrogen gas adsorbed is proportional to the total surface area of the particles including pores in the surface. Before the specific surface area of the sample can

be determined, it is necessary the sample is degassed in a vacuum at high temperatures to remove gases, vapors and other contamination. The nitrogen gas is inserted into the sample cell with a calibrated piston. The specific surface area may be the dead volume in the sample tube before and after the analysis. For the blank, run of helium gas, because it does not adsorb on the sample surface. The dead volume in the sample must be determined before and after each measurement. The determination of nitrogen gas is then displayed in the form of a BET isotherm. This data plots the amount of gas adsorbed as a function of the relative pressure. The BET adsorption isotherm equation is given below,

$$\frac{\mathrm{P}}{V(Po-P)} = \frac{\mathrm{P}}{Vm-C} + \frac{(\mathrm{C}-1)\,\mathrm{P}}{CVm-Po} \qquad (3.3)$$

Where,

V = amount of nitrogen gas adsorbent at a given pressure P.

Vm = monolayer capacity of the volume of gas adsorbed at standard temperature and pressure (STP).

P_O = saturation vapor pressure of the adsorbate.

C = dimensionless constant.

When the BET model holds, a plot of V vs. P/Po is a straight line with slope is equal to (C-1)/ CVm and y intercept is equal to 1/VmC. For the slope and y intercept Vm can be evaluated. Once Vm is obtained, the sample specific surface area is calculated by using equation,

$$S = \frac{\mathrm{Vm\ Nv\ Am}}{\mathrm{Mv}} \qquad (3.4)$$

Where,

S = specific surface area

Nv =Avagadro constant ($6.022\times10\ mol^{-1}$)

Am = effective cross sectional area of nitrogen gas adsorbed ($0.162\ nm^2$)

Mv = molar volume of the adsorbed gas at STP ($2.414 mol^{-1}$)

Surface area and porosity of prepared composite films were studied by using a Smartscrb 93, Novachrom instrument.

Porosity and pore structure

Pore size distribution and pore volume of prepared materials was determined by the Barrett-Joyner-Halenda (BJH) method. Pores volume was reachable to condensed adsorbate.

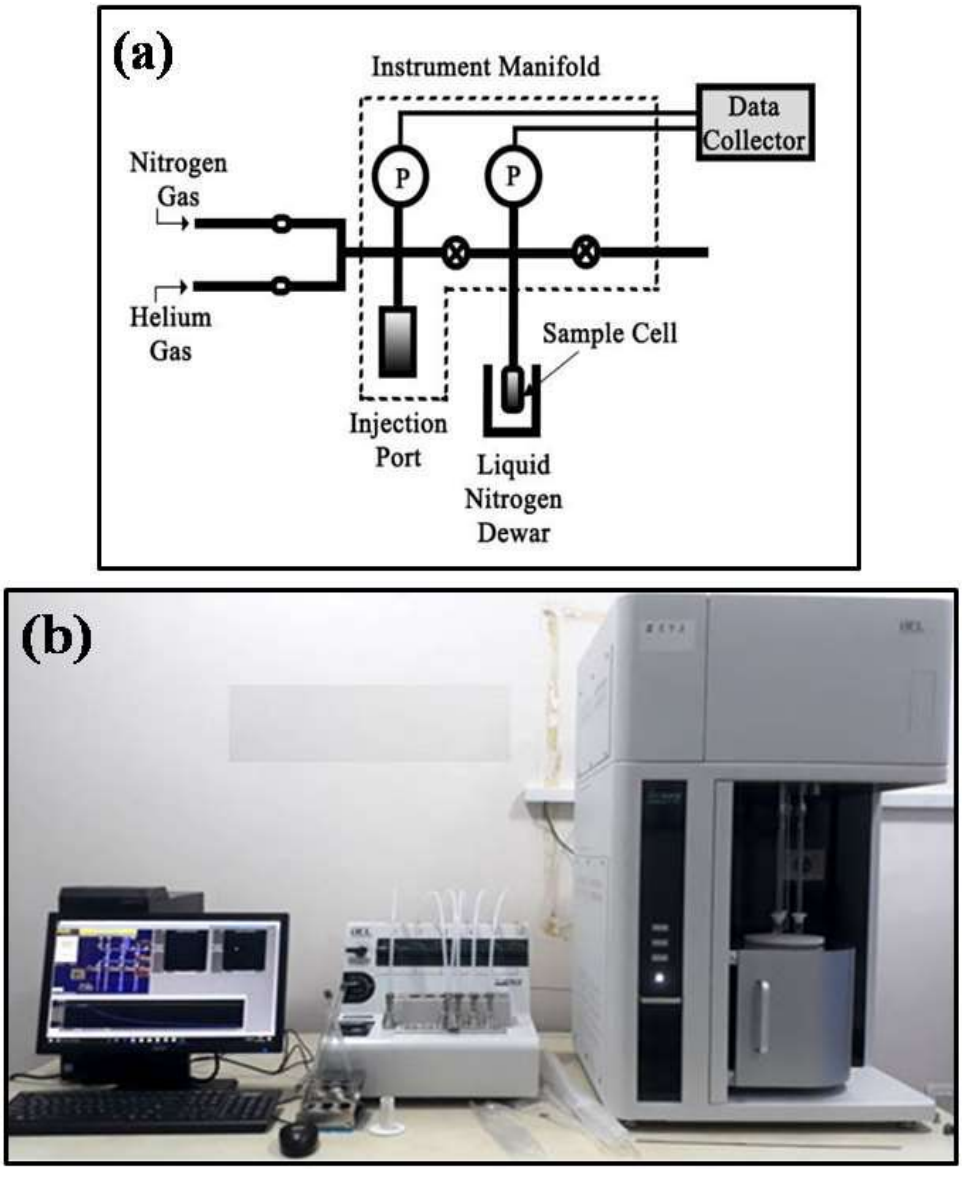

Figure 3.2 (a) Schematic representation of the BET instrument, **(b)** Photograph of BET instrument [8, 9].

According to the IUPAC (International Union of Pure and Applied Chemistry) classification pores are of three types such as microporous (less than 2 nm), mesopores (between 2 to 50 nm) and macrospores (greater than 50nm). The

total pore volume of the materials is derived from the amount of vapor adsorbed at a relative temperature close to unity (assuming pores are filled with liquid adsorbate)

$$Vliq = \frac{\text{Pa Vads Vm}}{\text{RT}} \quad (3.5)$$

Where,

Vads = Volume of gas adsorbed.

Vliq = Volume of liquid N_2 in pores

Vm = molar volume of liquid adsorbate (N_2= 34.7 cm^3/mol)

Pa = ambient pressure

T = ambient temperature

The average pore size of the materials can be determined from the pore volume. Assuming cylindrical pore geometry (type A hysteresis) average pore radius (γp) can be expressed as,

$$\gamma P = \frac{\text{2 V liq}}{\text{S}} \quad (3.6)$$

Other pore geometry models may require further information on the isotherm hysteresis before applying appropriate model [10, 11].Figure 3.2 (a) shows the schematic representation of the BET instrument, and (b) Photograph of BET instrument.

3.2.2 Spectroscopic Techniques

3.2.2.1 UV- visible spectroscopy

UV-visible spectroscopy uses light near the UV and infrared ranges named as visible and adjacent respectively. In this method, the absorption and reflectance in the visible range, it's directly affects the perceived color of the chemicals involved. In an area of the electromagnetic spectrum, molecules and atoms undergo electronic transitions. Absorption spectroscopic technique is corresponding to florescence spectroscopy, in that florescence deals with transition from the excited state to the ground state, whereas absorption measures transitions from the ground state to the excited state. The electronic excitations take place in the range from 200 to 780 nm, while the region from 10 to 200 nm is known as far

or vacuum ultraviolet region. A molecule contains two types of electrons that is π-electrons or non-bending electrons. These electrons absorb energy in the form of ultraviolet or visible light to stimulate the electrons, the longer the wavelength of light it can absorb.

The instrument used in ultraviolet visible spectroscopy is named as UV-visible spectrophotometer. This instrument measure the intensity of light passing through the sample (*I*), and compares it to the intensity of light before it passes through the sample (*Io*). The transmittance is the ratio of *I/Io* and it expressed as a percentage (%T). The absorbance, A is based upon transmittance expressed as below,

$$A = \log (\% T/100 \%) \quad (3.7)$$

The UV-visible spectrophotometer can also be assembled to measure reflectance which is expressed as (% R).

The basic parts of instruments are a light source, a sample holder, a diffraction grating in a monochromator or a prism to separate the different wavelengths of light and a detector. Figure 3.3 (a) shows the block diagram and (b) shows the photograph of UV-visible spectrophotometer. There are four different radiation sources such as tungsten filament (300-250 nm), deuterium arc lamp (190-400 nm), Xenon arc lamp (160-2000) and light emitting diodes for the visible wavelengths. All monochromator or filters contains the different component parts, such as an entrance slit, collimating lens, dispersing device, focusing lines and an exit slit. There are three different types of filters, glass filters, gelatin filters and inter ferometric filters. Glass filters made up of pieces of colored glass. These pieces transmit limited wavelength range and spectrum with wide band width 150 nm. Gelatin filters are mixture of dyes placed in gelatin and sandwiched between glass plates with band width 25 nm. Furthermore, inter ferometric filters consists of band width of 5 nm. The samples are placed in a transparent cell to the radiation which will pass through them called as cuvette. Silica glasses can be used for the manufacture of these cuvettes. The shape of cuvette is rectangular and width of cuvette is 1 cm. The detectors of UV-visible spectroscopy consist of three common types named as barrier layer cell, photo cell detector and photomultiplier.

UV-visible spectrophotometer can be either of single beam or double beam. In the single beam system, light passes through the sample cell while in the double beam system, light is split into two beams before it reaches the sample. In this system, one beam passes through the reference and other beam passes through the sample cell. The intensity of reference beam is taken as 100 % transmittance or zero absorbance. The measurement recorded in the ratio of two beam intensities [12, 13].

In the present investigation, UV-visible spectra of materials were recorded at room temperature between 200-500 nm using Shimadzu UV 1600 spectrophotometer.

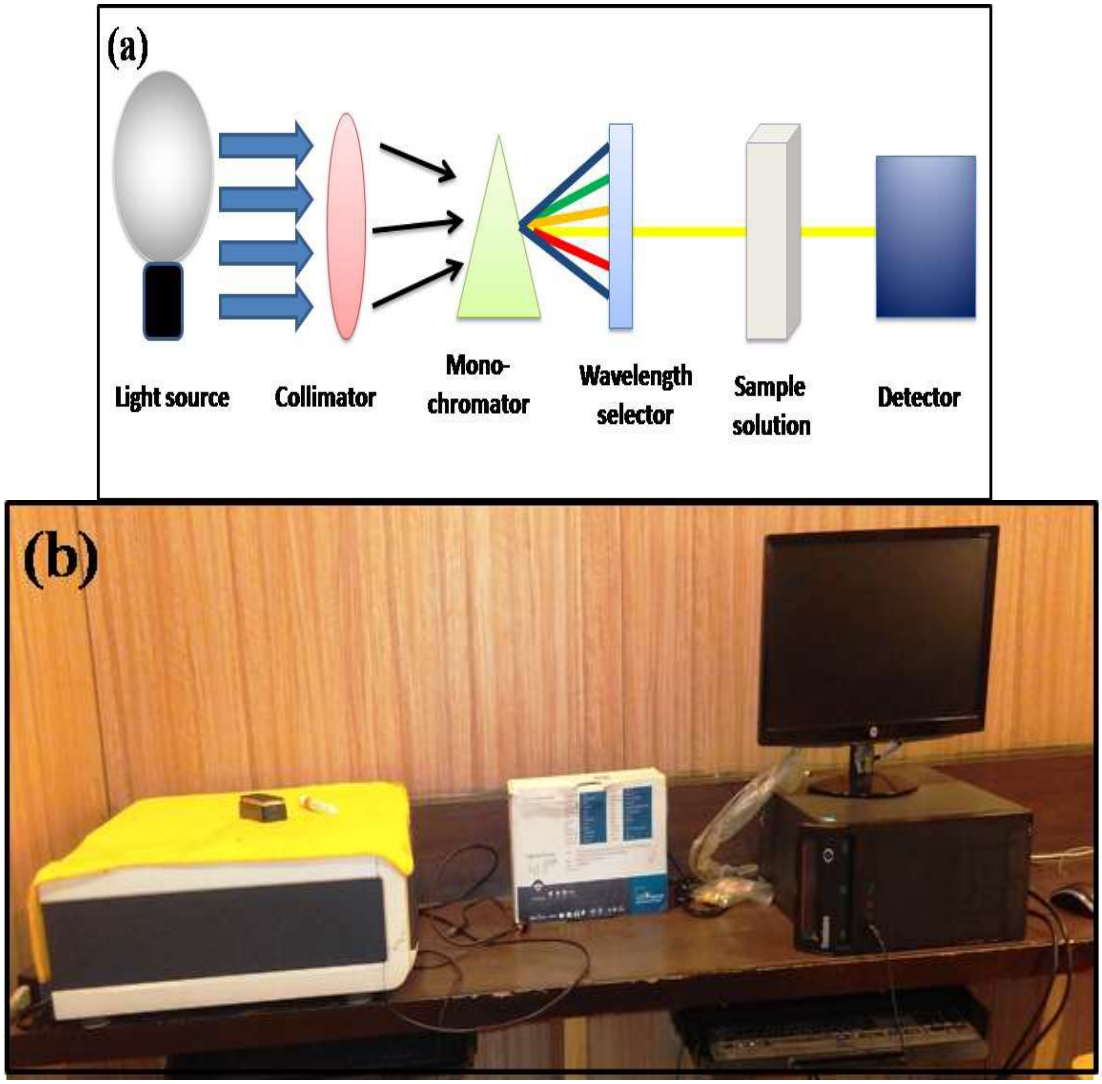

Figure 3.3 (a) Schematic overview of a UV-visible spectrophotometer, **(b)** Photograph of UV–visible spectrophotometer

3.2.2.2 Fourier Transform Infrared Spectroscopy

Fourier Transform Infrared Spectroscopy (FTIR) is a well known powerful technique used to characterize functional moieties of organic and inorganic compound. It is also useful in determination of quality, consistency and amount of components of a sample. In this technique, the infrared radiation (IR) is absorbed by the sample and it is proportional to its concentration. The IR spectrum peaks show the excitation of vibrational mode of the molecules and are related with the functional group present in the sample. It has been noted that IR includes a spectral region from red end of the visible spectrum (12,500 cm^{-1} to 0.8 mm) to the microwave (10 cm^{-1} to 1000 mm) in the electromagnetic spectrum. Based upon application instrumentation is divided into three region such as near (12,500 to 4000 cm^{-1}), Mid IR (4000 to 400 cm^{-1}) and far IR (400 to 10 cm^{-1}). It is found that Mid-IR region is most important region as most of the fundamental vibrations take place in that region.

Figure 3.4 (a) shows the typical FTIR instrument and figure 3.4 (b) represents the block diagram. FTIR spectrometer is based upon Michelson interferometer and it consist of first Nernst filament (ZrO_2+Y_2O_3) or Globar (SiC), second is the monochromatic, in which the beam is guided and focused by the mirrors aluminized or silverized on their surfaces and last is detectors for detecting heat radiations. The specifications of instrument that have been used in the proposed work are Perkin Elmer and range from 400-4000 cm^{-1}[14].

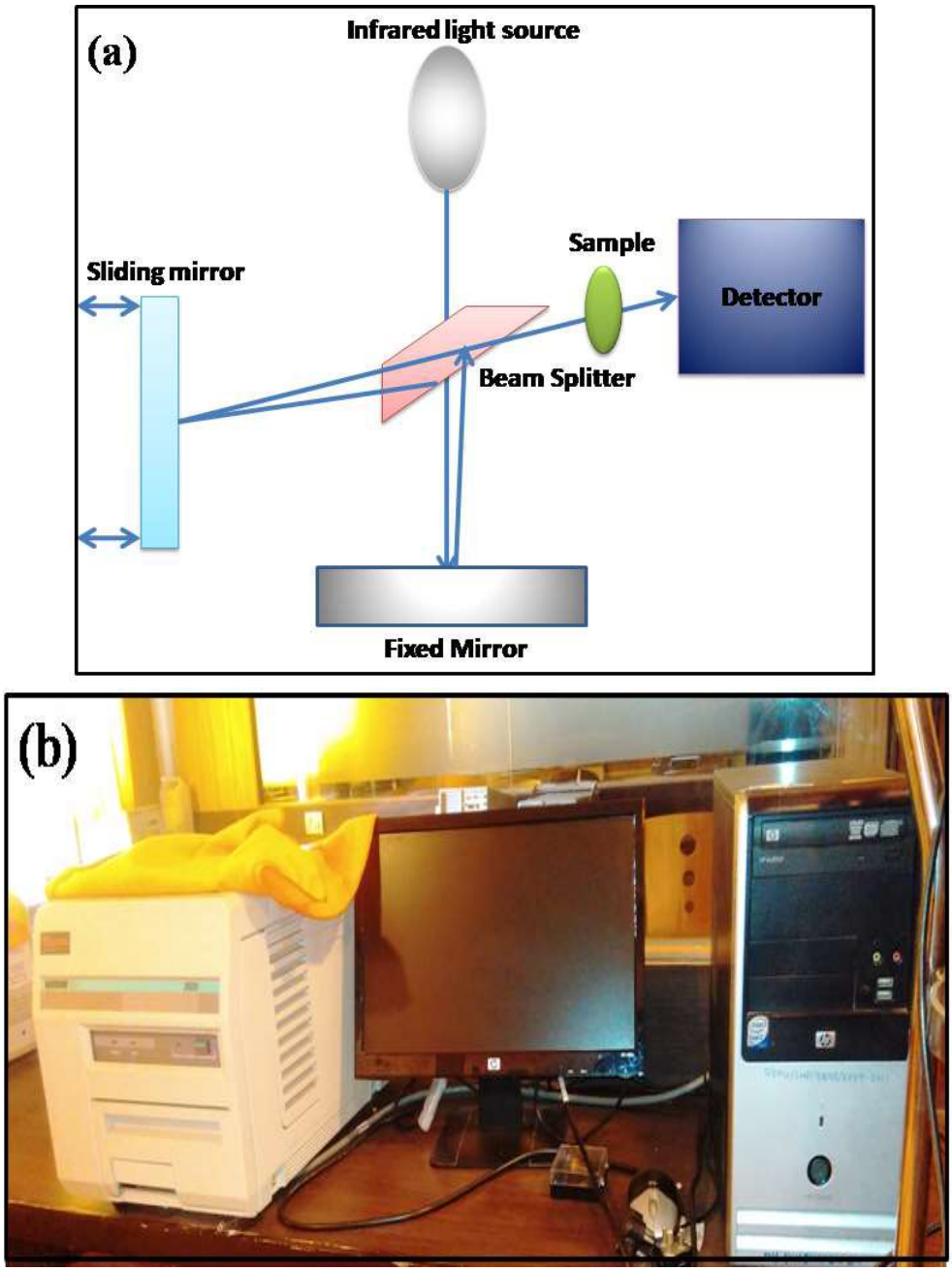

Figure 3.4 (a) Block diagram of the Fourier Transform Infrared Spectrometer and **(b)** A typical FTIR instrument.

3.2.3 Morphological Techniques

3.2.3.1 Scanning Electron Microscopy

Scanning electron microscopy (SEM) is a type of electron microscopy used to study the morphology, topography and composition of sample [15]. It produces images based upon the principle by scanning the surface with a focused beam of

electrons. When the electrons interact with atoms of the sample, leads to inelastic and elastic scattering. In the case of inelastic scattering with electrons, few amount of energy is transferred to the other electron. On condition of the transferred energy is very small then the emitted electron will likely not have sufficient energy to exit the surface. If the transferred energy is exceeds, then the emitted electron can exit the solid. In the case of energy of the emitted electron is less than about 50 eV, by conventions it is called to as secondary electrons (SE). Theses emitted secondary electrons are produced mostly within the first few nm of the surface and much deeper in the material. When the electrons that exit the specimen with energy are greater than 50 eV, then it is referred as backscattered electrons (BSEs). Most of the BSEs have energies comparable to the energy of the primary beam. If the atomic number of a material is higher, the more probably it is that backscattering will occur. There are two types of detectors are used for detecting samples. First is n-type silicon diodes coated with a layer of gold and second is scintillator photo multiplier detector. First type of detector is used to convert the incident BSEs into electron-hole pairs at the rate of 1 pair per 3.8 eV. It is used to separate atomic number contrast from topographical contrast. Second type detector was used for materials that will fluorescence under the bombardment of the type energy BSEs to produce a light signal that can be further amplified.

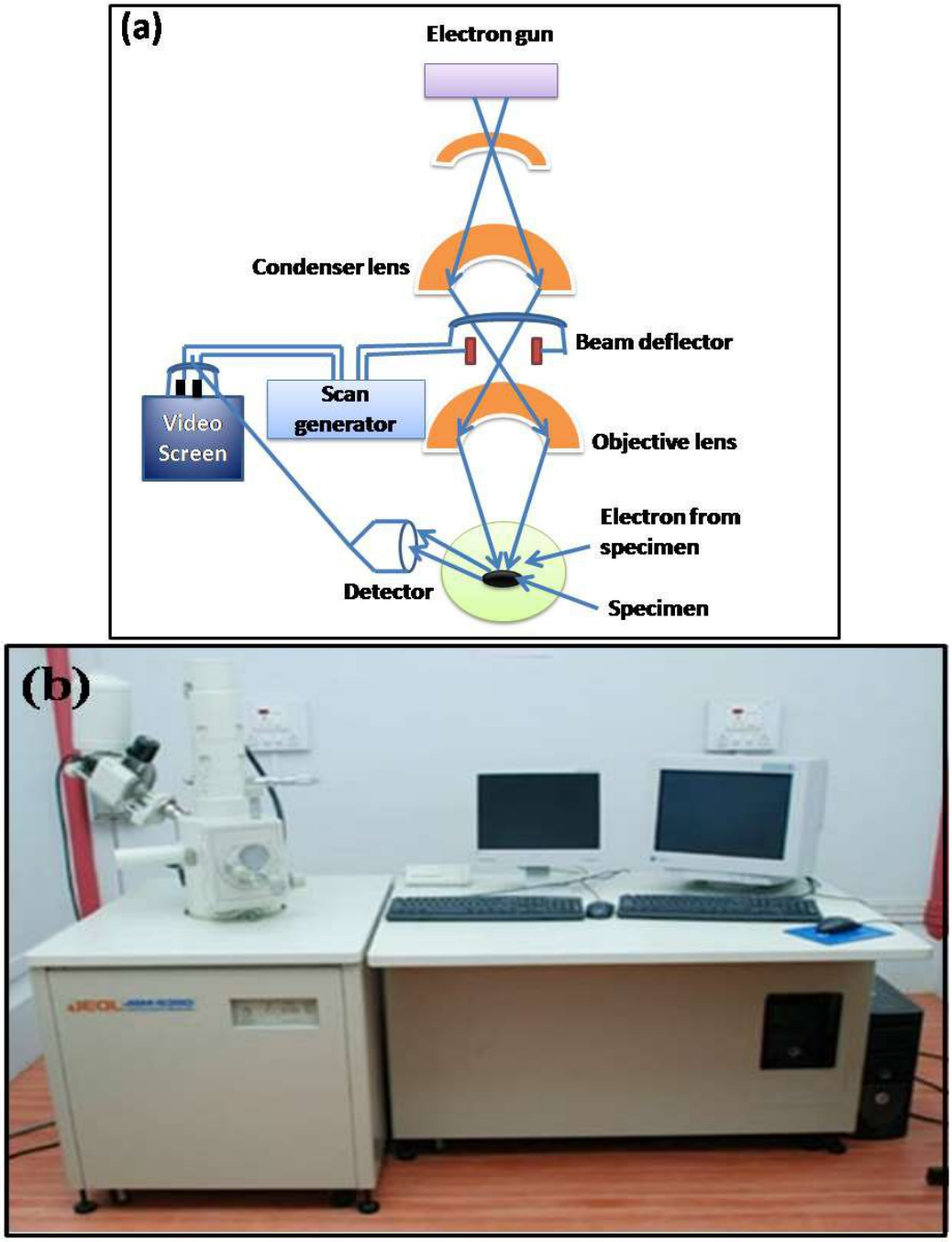

Figure 3.5 (a) Ray diagram of Scanning Electron Microscopy and **(b)** photograph of typical SEM instrument.

Preparation of samples for SEM is carried out with vacuum conditions at high energy beam of electrons. Samples are mounted to a specimen holder with the help of conductive adhesive and sputter coated with gold or gold/palladium alloy

before examination in microscope. Figure 3.5 (a) shows the ray diagram and (b) shows the typical photograph of SEM instrument.

SEM is used in conjunction with EDX. This technique detects X-rays emitted from the sample during bombardment by an X-ray beam to characterize the elemental composition of the analyzed volume. The tested sample consists of electrons which are bound to the nucleus and present in an unexcited state. The incident beam may excite an electron in an inner shell and ejecting it from the shell and generating an electron hole. The high energy shell fills this hole and the difference between the energy levels of high energy shell and energy levels of lower energy shell is released in the system of X-ray [16].

The specifications of instruments that have been used in the proposed work are JOEL JSM 6360 with accelerating voltage 20 KV and energy scan range 0-20 KeV.

3.2.3.2 Transmission Electron Microscopy

Transmission Electron microscopy (TEM) is useful characterization with higher resolution for the analysis of structure and morphology of materials. Additionally, TEM gives information about atomic resolution lattice images as well as chemical information at a spatial resolution in nanometers. Regular (Conventional) TEM uses only the transmitted beams or some of the forward scattered beams to generate a diffraction contrast image while high resolution transmission electron microscopy (HRTEM) uses the transmitted and the scattered beams to create an interference image.

Figure 3.6 (a) shows ray diagram and (b) shows the photograph for TEM. It consist of an electron gun at top generates the stream of monochromatic electrons. This is focused to a small, thin, coherent beam by the use of two coherent lenses. When this small focused beam of electron falls on the specimen variety of the interaction takes place. This transmitted part is focused by the objective lens into an image. The sample image is created by the transmitted electron beams that make the bright field image and by diffracted or deflected electron beams that

make dark field image. The sample, which is used for TEM analysis should be extremely thin and should range between 0.1 to 1.0 µm [17].

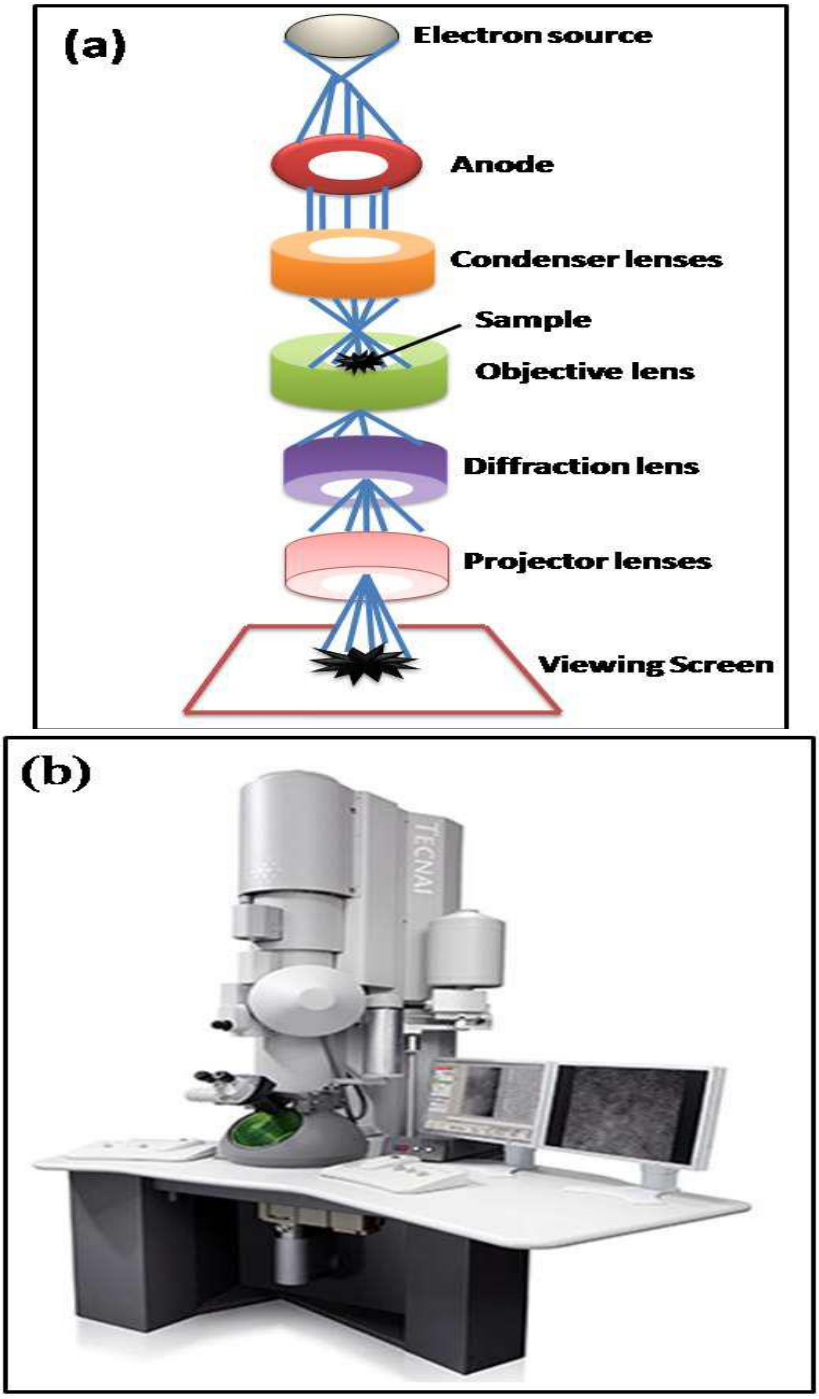

Figure 3.6 (a) Schematic representation of Transmission Electron Microscopy and **(b)** A typical instrument of TEM [18].

Preparation of sample for TEM analysis is the essential step and comes lots of weightage. The procedure involves dispersed in some dispersive media such as water to form colloidal solution, then a drop of colloidal solution is kept on conducting grid of copper or silver (sq. size is ~ 1µm) and dried. Further this dried grid is used for analysis of the sample. In the present study, the instrument used is high resolution TEM (HR-TEM) with TECNAJF 20 Philips operated at 200 KV.

3.2.4 Particle Size Analysis

3.2.4.1. Dynamic Light Scattering

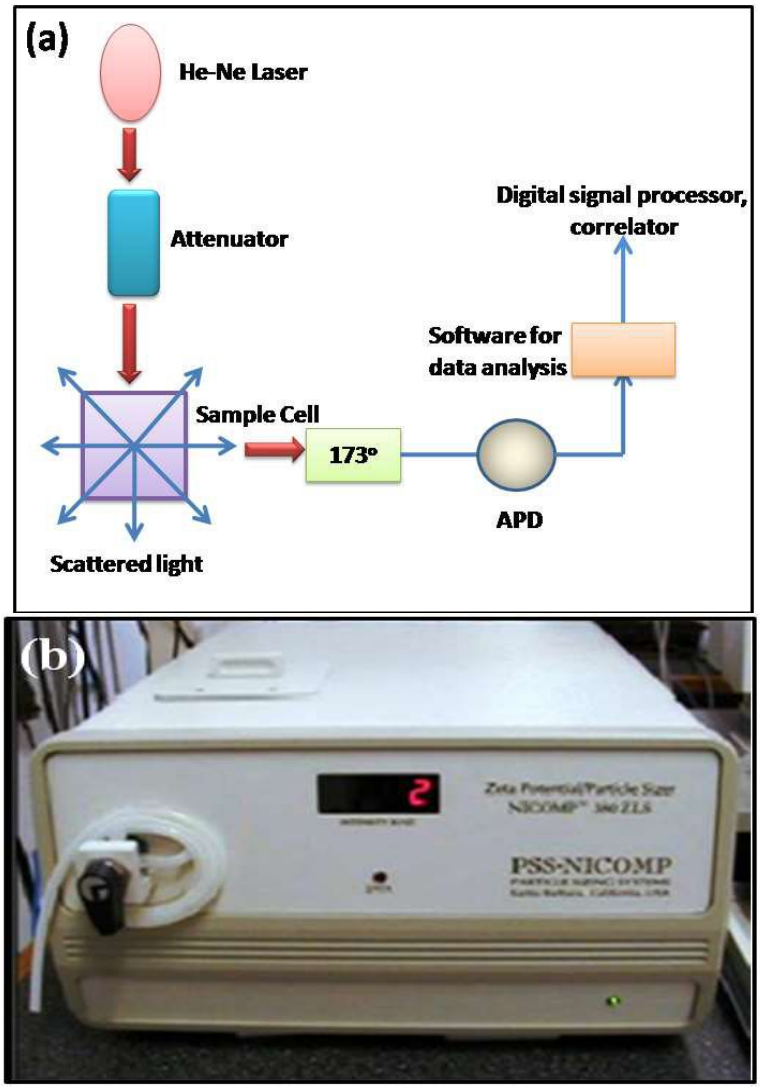

Figure 3.7 (a) Schematic representation of Dynamic Light Scattering and **(b)** A typical instrument of DLS.

Dynamic Light Scattering (DLS) technique is used to determine the size of particles suspended in suspension. DLS is one of the most popular techniques in nanotechnology. DLS measures the translational diffusion coefficient and relates it to the hydrodynamic diameter of the particles [19]. In the present work, DLS is used to determine the size of the synthesized ZnO NPs.

In DLS technique, a light beam will scatter the light from a laser that passes through a colloidal solution which is proportional to the size of the particles. It is used to determine the smaller particles which are less than 1 μm. DLS technique is also referred photon correlation spectroscopy (PCS) or quasi-elastic light scattering (QELS) Technique. The particles suspended in suspension are in Brownian motion due to random collisions with solvent molecules. This change is either faster or slower depends upon the movement of colloids. How quick the colloids movements determined by the signal intensity of scattered light. It is then detected over time and the gained values used to create an intensity autocorrelation function. Thus, DLS measuring the agglomeration state of NPs as a function of time or suspending solution.

In present study, DLS of the ZnO NPs were measured using a PSSI NICOMP 380 ZLS particle sizing system (Santa Barbara, CA, USA) with a red He-He laser diode at 632.8 Å in a fixed angle 90^{o} plastic cell. Synthesized samples were measured in disposable polystyrene cuvette at a temperature of 25^{o} C + 1^{o}C. Obtained data is in the automatic mode. The software (DTS Vs 03) incorporates a data quality report that indicates good quality for all data obtained and provides both the size mean and polydispersity index. All the measurements were conducted in triplicates. Figure 3.7 (a) shows block diagram and (b) shows typical DLS instruments.

3.2.5 Thermal testing

3.2.5.1 Differential Scanning Calorimetry (DSC)

Differential Scanning Calorimetry (DSC) is the thermoanalytical technique used to obtain the phase transition temperatures and the crystalline behavior of the materials.

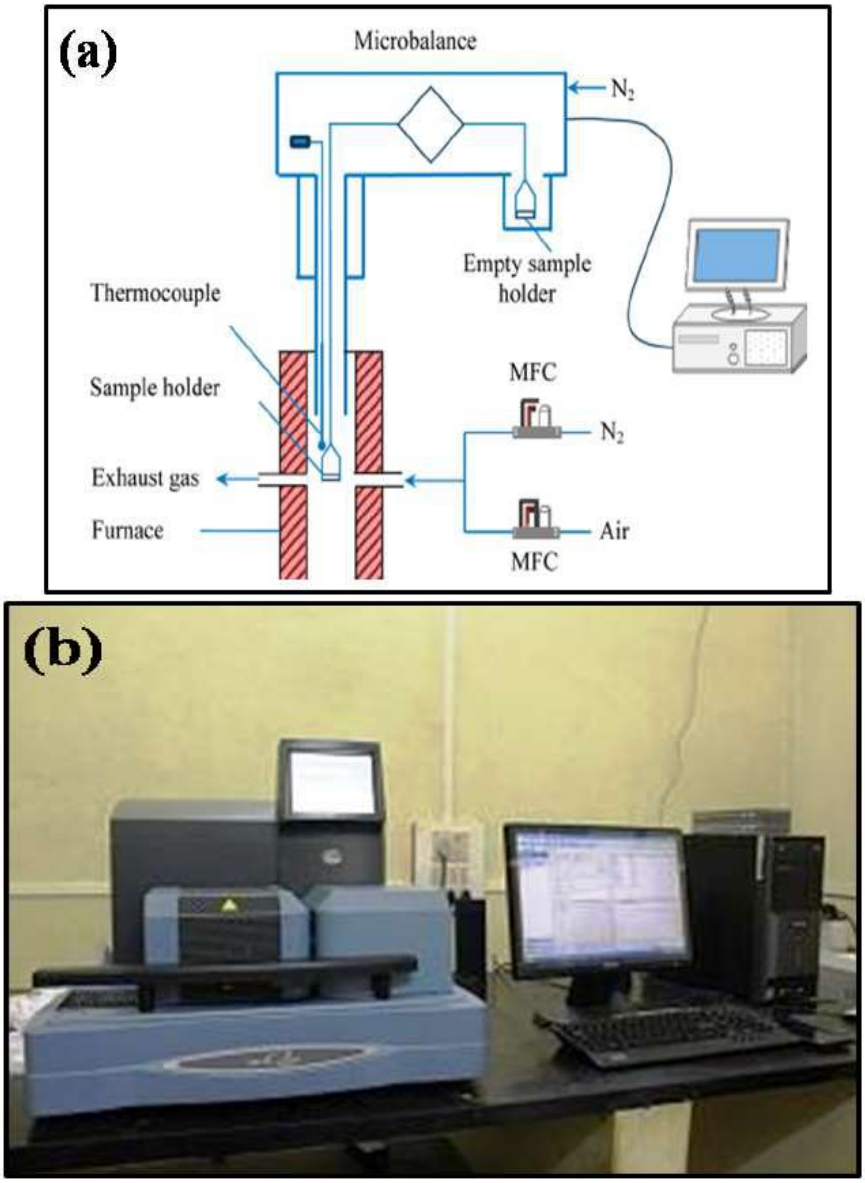

Figure 3.8 (a) Schematic representation of DSC thermal analyzer and **(b)** Photograph of instrument of DSC [20].

Figure 3.8 (a) shows the schematic representation and (b) shows the photograph of DSC thermal analyzer. It needs more or less heat from 10 to 250 ^{o}C at heating rate of 10^{o} C/min in nitrogen environment. This is depending on whether the process is exothermic or endothermic. The glass transition temperature (Tm) was confirmed as the inflection point of the specific heat capacity while the melting temperature (Tm) was set as the peak temperature of melting endotherm [21]. The results of DSC analysis are the data of heat vise time. The data curve of

DSC can be used to examine enthalpies of transitions. This calculation is done by combining the peak corresponding to the transition. The enthalpy of transition can be expressed using the following equation,

$$\Delta H = KA \tag{3.8}$$

Where,

ΔH = enthalpy of transition

K = calorimetric constant

A = area under curve

The DSC thermal analysis of composite films was carried out using the DSC, SDT Q 600 instrument.

3.2.6 Mechanical Testing

Universal testing machine (UTM) is applied to investigate the mechanical properties of materials. It is employed to examine the tensile strength and percent elongation of materials such as polymers and particularly metallic films deposited onto polymeric substrates [22]. In the working principle, UTM is by hydraulic transmission of load from the test sample to a separately housed load indicator. The hydraulic setup is best because it replaces transmission of load: through levers and knife edges, which are prone to wear and damage due to shock on rupture of test pieces. The load is put into hydrostatically lubricated ram and main cylinder pressure is transmitted to the cylinder of the pendulum dynamometer system housed in the control panel. Additionally, the cylinder of the dynamometer is of self lubricating design. The load transmitted to the cylinder of the dynamometer is transferred through leverage to the pendulum. Figure 3.9 (a) shows the schematic representation and (b) shows the typical instrument of UTM. (The UTM consist of 5 main parts straining unit, control panel power pack, hydraulic controls, load indicator system, automatic continuous roll load.)

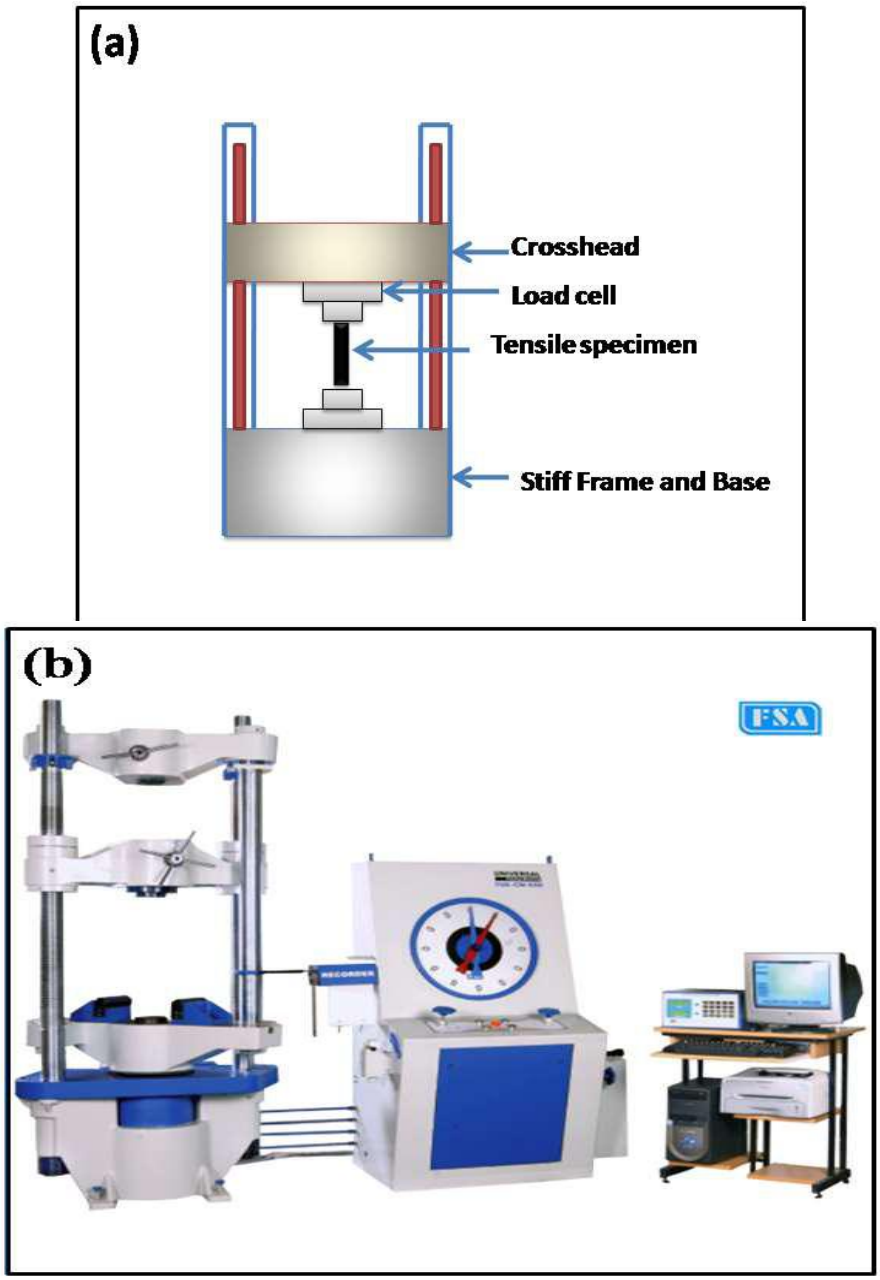

Figure 3.9 (a) Schematic diagram of a Universal Testing machine, **(b)** A typical instrument of UTM [23].

The mechanical property test was conducted using rectangular geometries of films of 40 mm length, 5 mm wide and 0.125 mm thick. The thickness of tested sample was studied using digital digimatic calipers and three measurements were taken. The displacement velocity of the movable crosshead during tensile experiments was maintained at 0.01 mm/s.

The tensile strength and % elongation of composite films was investigated by using the Winsoft tensile and compression testing machine (Shimadzu AG) 100 KN load cell at 25 ^{o}C.

3.2.7 Biological characterizations

3.2.7.1 Swelling behavior

Swelling behavior of materials is the increase of volume of materials due to absorption of a solvent, especially for polymers. It is used to determine water uptake capacity of materials. In this method, the prepared composite films dipped into Phosphate Buffer Saline (PBS) solution of pH 7.4 at room temperature until saturation and the swelling ratio of composite films are examined by measuring the weight of swollen films divided by weight of completely dried films. The study of water uptake capacity of composite films is very important for wound dressing application, because this study measure the absorption capacity of composite films of wound exudates. The swelling ratio was estimated using the following formula [24],

$$\text{Degree of Swelling } (DS) = \frac{W_s - W_d}{W_d} \times 100 \qquad (3.9)$$

Where,

Ws = the weight of swollen films

W_d = the weight of completely dried films.

3.2.7.2 Biocompatibility

Biocompatibility study is the ability to measure how compatible of material is with biological system [25]. The aim of performing biocompatibility testing is how biomaterials interact with the human body and to see whether a use of the material can have any potentially harmful physiological effects. In detail study of nanocomposite biocompatibility has been formulated as an essential field of research. In the present thesis, biocompatibility of materials is carried out by using hemocompatibility, blood clotting ability and cytocompatibility or cytotoxicity.

3.2.7.2.1 Hemocompatibility

Hemocompatibility is the compatibility of material with blood; it is in-vitro assay. This assay is employed to evaluate the probability of a test causes adverse effects on red blood cells (hemolysis) thrombosis, coagulation, platelets and complement process. The hemocompatibility study is carried for composite films with hemolytic assay. In this assay, water is used as a negative control and PBS is used as a positive control. The percentage of hemolysis is calculated by using absorbance of test sample divided by absorbance of positive control. As per the ASTM-756-08, percentage of hemolysis is less than 2 % is considered as nonhaemolytic, 2-5% is slight haemolytic and more than 5 % is hemolytic [26]. The hemolytic percentages (HP) of the composite films were calculated using the following equation.

$$HP(\%) = \frac{D_t - D_{nc}}{D_{pc} - D_{nc}} \times 100 \qquad (3.10)$$

Where,

D_t = the absorbance of the test sample,

D_{pc} = the absorbance of the positive control and

D_{nc} = the absorbance of negative control.

3.2.7.2.2. Blood clotting ability

The ideal wound dressing should possess the blood clotting ability [27]. Clotting is also called as coagulation. It is the process to prevent excessive bleeding when cut the skin and internal vessels. Clotting is possibility results in hemostasis, the stopping of blood loss from injured vessels, followed by reformation. The principle mechanism of clotting involves activation, adhesion and aggregation of platelate together with deposition and maturation of fibrin. Bleeding of the skin is an injury to the blood vessels has damaged, platelate are activated at the site of injury called as primary hemostasis. Secondary hemostasis is the addition of coagulation factors or clotting factors for production of fibrin stands. In the process of platelate activation, large protein developed by the cells of the vessel wall. These proteins collagen and thrombin act at the site of injured area

to cause platelates to stick together. The platelates release proteins and other substances that entrap more platelets and clotting proteins in the enlarging plug that becomes a blood clot. Blood clotting factors generate thrombin, which converts fibrinogen. This blood clotting factor dissolved in blood and form more platelets and blood cells. Calcium and phospholipids are also used for the tenase and prothrombinase complexes to function.

3.2.7.2.3. Cytocompatibility study

The cytocompatibility or cytotoxicity study of nanomaterials is most important indicators of the biological evaluation system *in-vitro*. The fast development of nanotechnology has been most important correlated to desirable effects of nanomaterials, including human health and environment impact. Cytotoxicity study is the study of the nanomaterials quality of being toxic to cells. In this study it is identify that the cell cultures are sensitive to change in their environment such as fluctuation in temperature, nutrient and waste concentration of the potentially toxic agent being tested. There are different types of assays can be employed for the determination of toxic effects of the nanomaterials on cell cultures are listed below,

- lactate dehydrogenase (LDH)
- Leakage,3-(4-5-diamethylthiazol-z-yl)-2,5-diphenyltetrazolium bromide (MTT) assay
- Dye exclusion assay (Trypan blue)
- Test of Cytokine/Chemokine creation etc.

Selection of accurate assay is important to the correct assessment of nanomaterials toxicity. In the present thesis, MTT assay has used to evaluate the in-vitro cytocompatibility of prepared nano-composite films of mammalian cell line (L929). The assay is simple and easy to evaluate. The apoptic or necrosis effect of nano composite films was visualized by alcidine orange and ethidium bromide staining method. These methods are described in briefly MTT assay [28]. This assay is a colorimetric assay, which is used to estimating cell viability. The reduction of MTT (tetrazolium salts) is currently accepted as a best method to

determine cell proliferation. The yellow 3-(4,5-dimethylthiazolyl-2)-2, 5- diphenyl tetrazolium bromide (tetrazolium MTT) is make lower by metabolically active cells in turn by dehydrogenase enzymes, to create reducing equivalents like NADH and NADPH. This reduction process produces intracellular purple formazan which can be solubilize and quantified by spectrophotometrically. The cell proliferation can be determined by using MTT cell proliferation assay. The MTT assay calculates the cell proliferation rate when metabolic events cause to necrosis or apoptosis, the reduction in cell viability. The cell viability was determined with the equation,

$$\text{Cell viability} = A_{\text{treated}} / A_{\text{control}} \times 100 \qquad (3.11)$$

Where, $A_{treated}$ and $A_{control}$ is the test sample and control sample respectively. Figure 3.10 shows schematic of cytotoxicity tests.

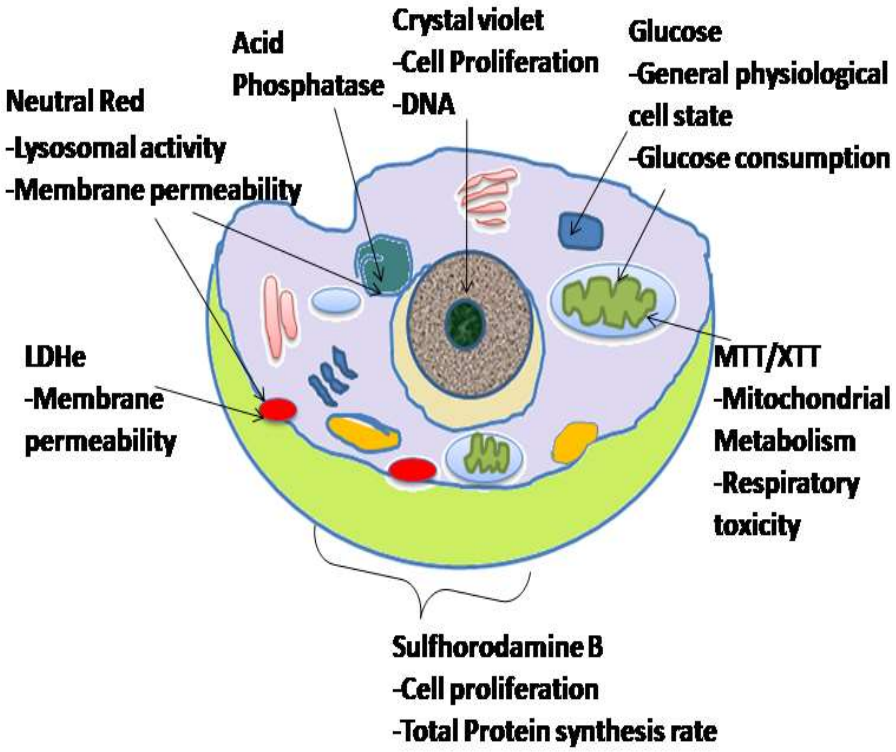

Figure 3.10 Cytotoxicity Screening Test Systems.

3.1.7.3 Antibacterial activity

Antibacterial activity is involving two basic activities such as bactericidal activity and bacteriostatic activity. The bactericidal activity is the use of antibacterial agents or other substances that kill the bacteria, whereas the bacteriostatic activity is defined as the use of antibacterial agents or other substances that kill the bacterial growth. Antibacterial materials are used to fight against infections. Hence, there are different methods employed for investigation of antibacterial activity of different antibacterial agents or other substances. These methods are listed below [29],

- Agar disc diffusion method
- Agar well diffusion method
- Shake flask method

3.1.7.3.1 Agar disc diffusion method

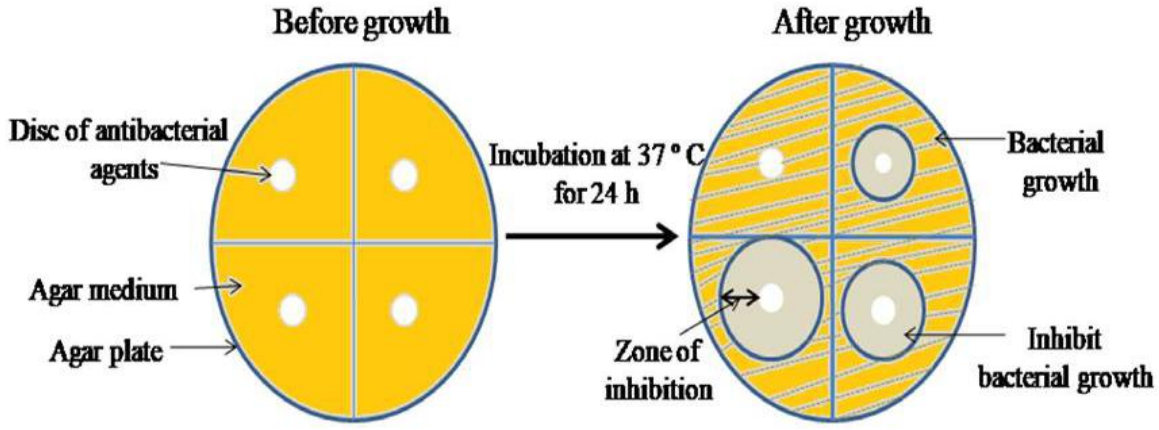

Figure 3.11 Schematic representation of the agar disc diffusion method for antibacterial activity.

The disc diffusion method is easy, important and most widely method for antibacterial activity study. In the disc diffusion method the first target organism suspension spread on the surface of nutrient agar medium and then the paper disc of antibacterial agents or tested samples deposited on the surface of sterile medium plate. Further, the tested sample discs diffused in medium by plates kept in refrigerator for 10 min. After the plates are incubated at 37 ° C for 24 h, the zone of inhibition (ZOI) around each discs are determined by using the scale in

millimeter. Figure 3.11 shows the schematic representation of agar disc diffusion method for antibacterial activity.

3.1.7.3.2 Agar well diffusion method

In agar well diffusion process, the wells (6 mm in diameter) are prepared by applying sterile cork borer and the target organism suspension is spread over the nutrient agar medium. The tested liquid sample of volume 70-80 µl is aseptically dispensed into each well and plates are kept at 4º C for 10 min to facilitate the diffusion of sample in the agar medium. After plates are incubated at 37 º C for 24 h and the ZOI is measured around each well. Figure 3.12 shows the schematic representation of agar well diffusion method for antibacterial activity

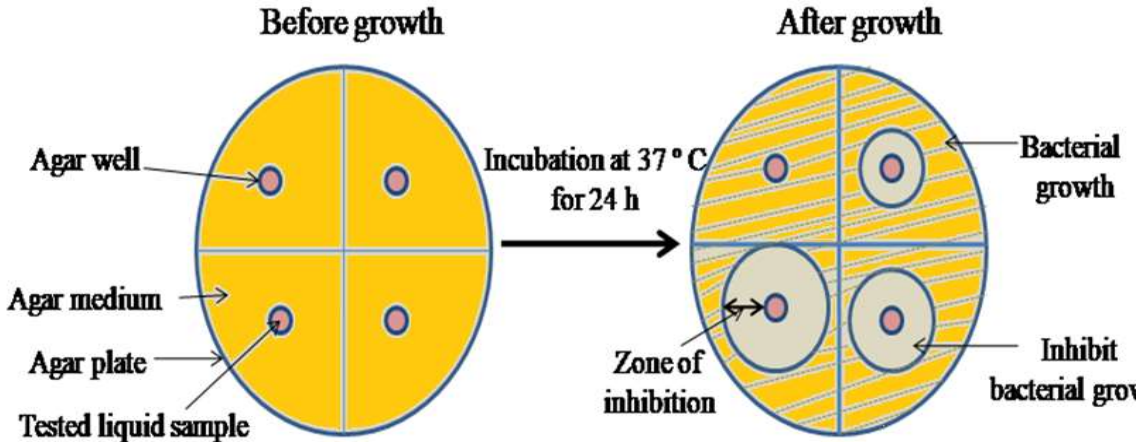

Figure 3.12 Schematic representation of the agar well diffusion method for antibacterial activity.

3.1.7.3.3 Shake flask method

In this method, the nutrient broth are prepared and dispensed in flask aseptically. The tested samples as well as microbial suspension are aseptically dispensed into the flask and the flasks are kept in shaking incubator at 180 rpm for 24 h at 37 º C. The growth of organisms is observed in the form of turbidity. The growth of organism is determined by using optical density. Figure 3.13 shows the schematic representation of shake flask method for antibacterial activity.

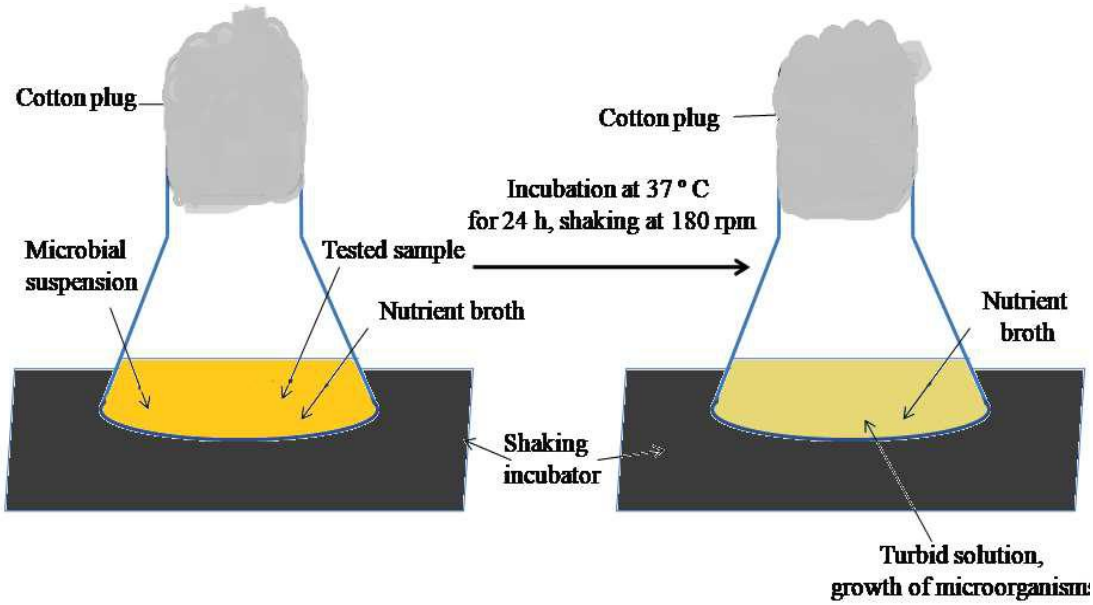

Figure 3.13 Schematic representation of shake flask method for antibacterial activity.

3.1.7.3.4 Minimum Inhibition Concentration

Minimum inhibition concentration (MIC) refers the lowest concentration of antibacterial agents which restrict the growth of bacteria. The determination of MIC of antibacterial agents are carried out in two different methods, which are listed below [30],

- Agar dilution method
- Broth dilution method.

In agar dilution method, the defined number of bacterial cell suspension deposited directly onto the sterile medium plates that have integrated different antibacterial agent concentrations. After, incubation period the presence of the bacterial growth on the plates displays the growth of the organisms. This process is generally applicable for antibiotics available in ample amounts. The advantages of this method are to determine large number of bacterial isolates simultaneously under exactly identical condition.

In broth dilution method, the liquid growth medium is used for determination of MIC. In this method, the liquid growth medium incorporated the concentrations of antibacterial agents, which is inoculated with a defined number of bacterial

cells. The final volume of the sample is prepared, whether the method is termed microdilution. When using a total volume is 2 ml. The microdilution is achieved in Microtiter plates using < 500 µl per well. The presence of turbidity of samples indicates the growth of organisms, after incubation period. Both the method of MIC is calculated as the lowest concentration of antibacterial agent, which restricts the growth of bacteria. This method is applicable for testing the different antibiotics as well as other antibacterial agents [31].

In the present work, the antibacterial activity of pure materials as well as composite films was investigated by using agar disc diffusion procedure. The paper discs of pure materials were prepared using Whatman filter paper. The MIC study was done by using broth dilution method.

References:

1. A. Seaton, L. Tran, R. Aitken, K. Donaldson, J. R. Soc. Interface, 2009, 7, 119-129.
2. M. Naito, T. Yokoyama K. Hosokawa K. Nogi, Nanoparticle technology handbook. 3rd edition, Elsevier, 2018, 1-904.
3. N. Capanema, A. Mansur A. De Jesus, S. Carvalho, L. De Oliveira, H. Mansur, Int. J. Biol. Macromol.2018, 106, 1218-1234.
4. P. Chu, L. Li, Mater. Chem. Phys., 2006, 96, 253-277.
5. http://pd.chem.ucl.ac.uk/pdnn/inst1/optics1.htm
6. "X-ray diffraction by polycrystalline materials" R. Guinebretière, 2013, John Wiley & Sons, 1-351.
7. S. Brunauer, P. H. Emmett, E. Teller, J. Am. Chem. Soc. 1938, 60, 309-319.
8. http://particle.dk/methods-analytical-laboratory/surface-area-bet-2/
9. http://www.velsuniv.ac.in/common-instrumentation-centre.asp
10. S. Brunauer, L. Deming, W. Deming, E. Teller, J. Am. Chem. Soc.1940, 62, 1723-1732.
11. M. Lawrence, and Y. Jiang, In Bio-aggregates Based Building Materials, Springer Dordrecht, 2017, 23, 39-71.
12. F. Rocha, A. Gomes, C. Lunardi, S. Kaliaguine, G. Patience, Can. J. Chem Eng. 2018, 96, 2512-2517.
13. S. Gorog, Ultraviolet-Visible Spectropy In Pharmaceutical Anaysis, 1st Edition, 2018, Taylor and Francis, CRC press 1- 405.
14. W. Doyle, Process Control Qual. 1992 2, 11-41.
15. "Scanning electron microscopy and X-ray microanalysis". J. Goldstein, D. Newbury, J. Michael, N. Ritchie, J. Scott, D. Joy, 2017, 4th Edition, Springer 1-550.
16. R. White, A. Owens, J Forensic Sci, 1987, 32, 1595-603.
17. L. Gremillet, G. Bonnaud, F. Amiranoff, Phys Plasma. 2002, 9, 941-948.
18. http://www.crestgroup.net/frmClientProductNEW.aspx?type=p&selectedindustry=4
19. S. Bhattacharjee, J. Controlled Release, 2016, 235, 337-51.

20. Source:https://www.researchgate.net/figure/263958136_fig2_Figure-2-Schematic-of-the-TGA
21. C. Demetzos, J. Liposome Res. 2008, 18, 159-73.
22. M. Ramesh, K. Palanikumar, K. Reddy, Composites Part B, 2013, 48, 1-9.
23. https://www.indiamart.com/sr-entps-hyderabad/f-s-a-machine.html
24. R. Jindal, B. Kaith, R. Sharma. J. Polym. Environ, 2018, 26, 999-1011.
25. J. Anderson, Annu. Rev. Mater. Res, 2001, 31, 81-110.
26. S. Logothetidis, M Gioti, S. Lousinian, S. Fotiadou, Thin Solid Films, 2005 482, 126-32.
27. K. Madhumathi, P. Kumar, S. Abhilash, V. Sreeja, H. Tamura, K. Manzoor, S. Nair, R. Jayakumar, J. Mater. Sci. - Mater. Med, 2010, 21, 807-13.
28. D. Gerlier, N. Thomasset, J. Immunol. Methods, 1986, 94, 57-63.
29. J. Parekh, S. Chanda, Afr. J. Biomed. Res., 2007, 10, 2.
30. J. Andrews, J. Antimicrob. Chemother, 2001, 48, 5-16.
31. A. Neill, I. Chopra, Expert Opin. Inv. Drug, 2004, 13, 1045-63.

CHAPTER 4

Synthesis and Characterization of Silk Fibroin and Its Composite Films using PVA and ZnO NPs

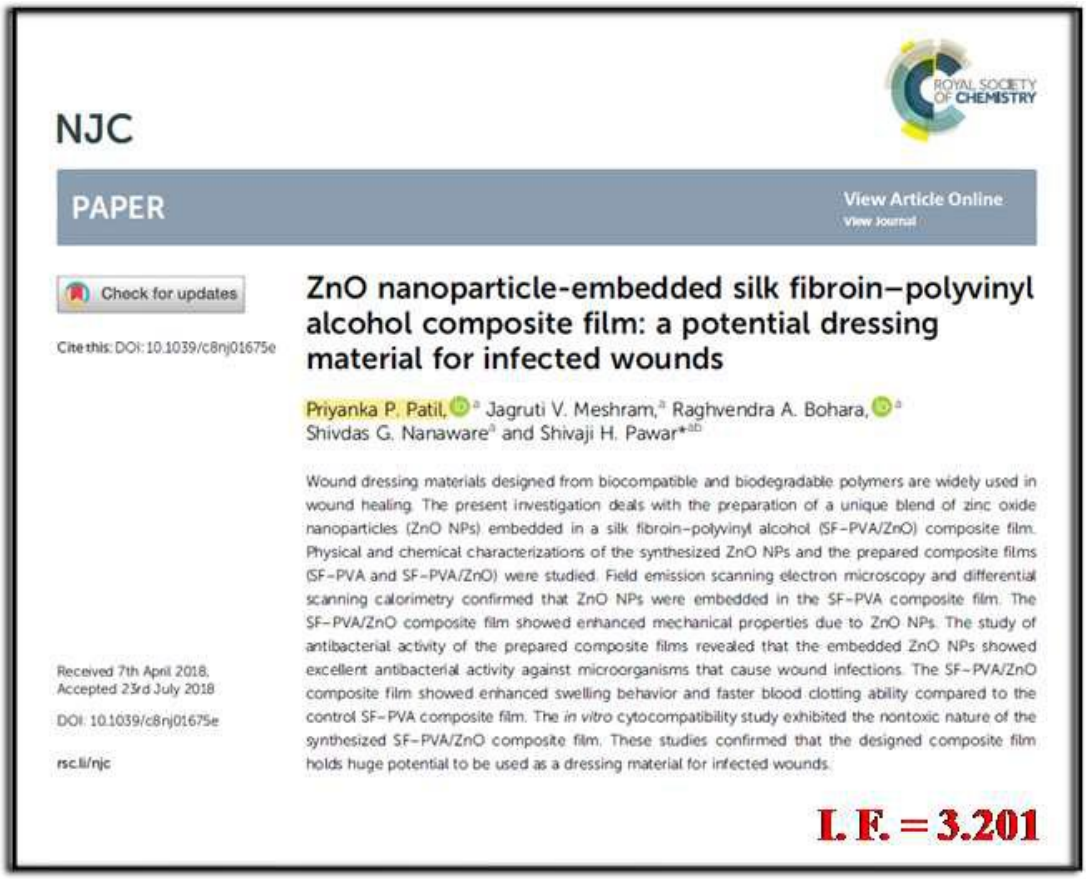

NJC

PAPER

View Article Online
View Journal

Check for updates

Cite this: DOI: 10.1039/c8nj01675e

ZnO nanoparticle-embedded silk fibroin–polyvinyl alcohol composite film: a potential dressing material for infected wounds

Priyanka P. Patil,[a] Jagruti V. Meshram,[a] Raghvendra A. Bohara,[a] Shivdas G. Nanaware[a] and Shivaji H. Pawar*[ab]

Wound dressing materials designed from biocompatible and biodegradable polymers are widely used in wound healing. The present investigation deals with the preparation of a unique blend of zinc oxide nanoparticles (ZnO NPs) embedded in a silk fibroin–polyvinyl alcohol (SF–PVA/ZnO) composite film. Physical and chemical characterizations of the synthesized ZnO NPs and the prepared composite films (SF–PVA and SF–PVA/ZnO) were studied. Field emission scanning electron microscopy and differential scanning calorimetry confirmed that ZnO NPs were embedded in the SF–PVA composite film. The SF–PVA/ZnO composite film showed enhanced mechanical properties due to ZnO NPs. The study of antibacterial activity of the prepared composite films revealed that the embedded ZnO NPs showed excellent antibacterial activity against microorganisms that cause wound infections. The SF–PVA/ZnO composite film showed enhanced swelling behavior and faster blood clotting ability compared to the control SF–PVA composite film. The *in vitro* cytocompatibility study exhibited the nontoxic nature of the synthesized SF–PVA/ZnO composite film. These studies confirmed that the designed composite film holds huge potential to be used as a dressing material for infected wounds.

Received 7th April 2018,
Accepted 23rd July 2018

DOI: 10.1039/c8nj01675e

rsc.li/njc

I. F. = 3.201

4.1 Introduction

In nanotechnology, the size, shape, and morphology of nanostructured materials play a very important role in wound dressing application due to improvement of physical, chemical, biological properties, and functionality. Therefore, the ability to synthesize and the processing of nanomaterials are involved in the first step in nanotechnology [1]. The formation of effective, easy and simple methods for the fabrication of nanomaterials have become more important to control the size, shape, and morphology of nanomaterials. Another important aspect of the nanoscale materials is the characterization study. Hence, characterization study of nanomaterials is necessary to analyze their various properties [2].

The present chapter focuses on the synthesis and characterization studies of pure materials of SF aqueous solution, PVA, ZnO NPs and the composites of SF-PVA and ZnO NPs based SF-PVA (SF-PVA/ZnO NPs) films which will be discussed in details. The composite films prepared based on a tailor-made synthesis of ZnO NPs-embedded optimum blend of SF-PVA. The SF-PVA composite films were prepared by the casting method at room temperature. Physical and chemical characterizations of SF, PVA and ZnO NPs and the prepared composite films were done. Further, the composite films were evaluated for their mechanical properties, surface morphology, swelling property, porosity, DSC thermal analysis and biodegradability. These studies confirmed the designed composite films hold a potential to be used in wound dressing materials.

4.2 Experimental

Cocoons of Thai silkworms *Bombyx Mori* were purchased from the Abhilasha Silk and Silk Products Pvt. Ltd. India. PVA was purchased from Sigma Aldrich. The average molecular weight of the PVA was approximately 56,000. Dialysis membrane-150 with flat width: 42.44 mm, and average diameter: 25.4 mm were purchased from Himedia Laboratories Pvt. Ltd. Mumbai, India. Sodium carbonate (Na_2CO_3), lithium bromide (LiBr), calcium chloride ($CaCl_2$), zinc acetate ($C_4H_6O_4Zn$), sodium hydroxide (NaOH), diethylene glycol (DEG) and

ethanol were purchased from Merck Specialties Pvt. Ltd, Mumbai. All the chemicals were of analytical grade (AR grade) and used without further purification. Double distilled water was used throughout the experiments.

4.2.1 Synthesis of composite films based on SF, PVA and ZnO NPs

4.2.1.1 Synthesis of SF aqueous solution

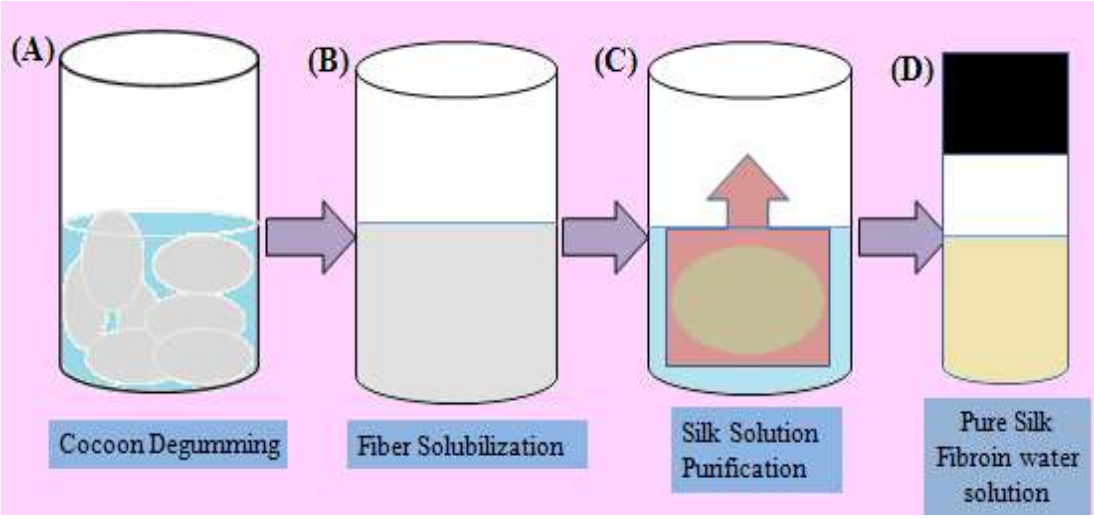

Figure 4.1 Schematic representations of steps involved in synthesis of SF aqueous solution of **(A)** Cocoon degumming, **(B)** Fiber solubilization, **(C)** Silk solution purification, and **(D)** Pure SF water solution.

Cocoons of *Bombyx mori* silkworm were degummed in 0.5% (w/v) Na_2CO_3 solution at 100 ^oC for 30 min and then rinsed with double distilled water to remove the sericin protein or wax. This process was repeated three times to completely remove the sericine protein and wax. SF was dried and stored at room temperature for overnight. 2.5 g of SF was dissolved in 10 ml of LiBr solution (9.5 Mol/L) for 2 h. Further, the solutions were dialyzed against double distilled water to extract the salts and small molecules. After, the SF solution was purified by centrifugation to obtain the final pure SF solution. Final concentration of SF solution was 5% (w/v). The obtained solutions were preserved at 4 ^oC to avoid precipitations of solution [3-5]. Figure 4.1 shows the schematic representation of steps involved in synthesis of SF aqueous solution.

4.2.1.2 Synthesis of ZnO NPs

ZnO NPs were synthesized using reflux method [6, 7]. Briefly, 0.06M Zn $(CH_3COO)_2 .H_2O$ was mixed to DEG in a flask and refluxed at 160 ^oC for 1 h. DEG was used to assisted hydrolysis of zinc acetate. The completion of reaction white colloidal solution forms at the bottom of the flask. The solution was centrifuged at 10,000 rpm for 20 min, and the supernatant was removed. Followed by the washing treatment was done with double distilled water and ethanol. After, the sol was dried at 100 ^oC for 2 h to remove the water molecules. Figure 4.2 (A) shows the schematic representation of the synthesis of ZnO NPs and, (B) shows the photograph of the reflux instrument used for the synthesis of ZnO NPs.

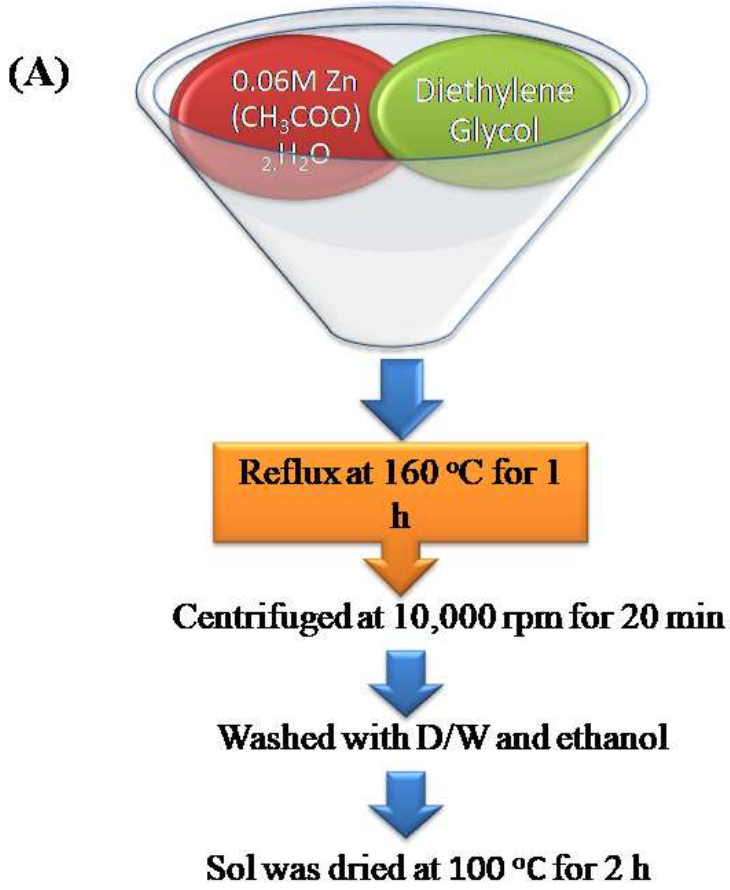

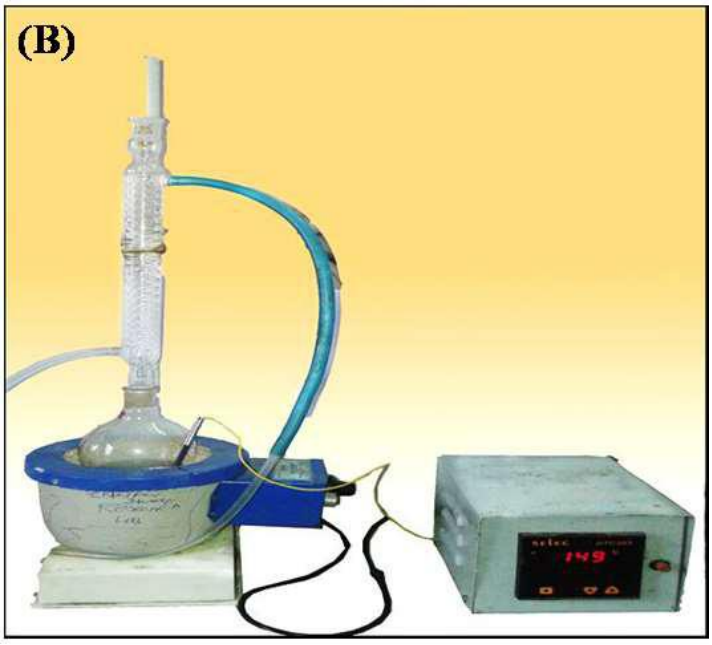

Figure 4.2 (A) Schematic representation of synthesis of ZnO NPs and **(B)** Photograph of reflux instrument used for synthesis of ZnO NPs.

Mechanism of synthesis of ZnO NPs

In this study, the reflux method was used for the synthesis of ZnO NPs as mentioned in above. The reaction mechanism for the formation of ZnO NPs is expressed below [7]:

$$nZn(CH_3COO_2).\ 2H_2On + nDEG \rightarrow [Zn(OH)_2 - DEG]\ n \quad (4.1)$$

$$[Zn(OH)_2\text{-}DEG]n \rightarrow [ZnO\text{-}DEG]n + nH_2O \rightarrow ZnO \quad (4.2)$$

In the above reaction, Zn $(CH_3COO_2).2H_2O$ is dissolved in DEG solvent forming [ZnO $(OH)_2$−DEG] n as shown in equation 4.1. The [ZnO $(OH)_2$−DEG] n formed is a complex with DEG molecules. The hydroxyl group present on ZnO surface interacts with other molecules. This might be due to the electrostatic interaction between the hydroxyl groups present on the surface of NPs. The complex compound of [ZnO $(OH)_2$- DEG] n is then broken at a given temperature to release water molecules and then forming ZnO NPs as described in equation 4.2. The prepared solution is washed using double distilled water and ethanol resulting in the formation of pure ZnO NPs.

4.2.1.3 Preparation of SF-PVA composite film

The concentration of 5wt % of PVA was added to water and stirred at 80 ^{o}C for 2 h. The extracted SF aqueous solution was added to PVA solution at a concentration of 1:2 wt. ratios and stirred for 1 h. Further, the blended solution was transferred to Petri dishes and dried at room temperature for 48 h. The dried films of SF-PVA were then peeled off using forceps and stored at room temperature for further study [8].

4.2.1.4 Preparation of ZnO NPs embedded SF-PVA (SF-PVA/ZnO NPs) composite film

SF-PVA/ZnO NPs composite film was developed by casting method at room temperature. First, the stock solutions of SF and PVA were prepared at a concentration of 5 wt % and the stock solution of ZnO NPs was formed at a concentration of 1wt %. The blending of the films was performed by mixing the SF: PVA: ZnO NPs wt. ratio 1:4:1. After mixing, the solutions were stirred at 150 rpm for 2 h at room temperature; the pH was adjusted to a neutral value and then, the solutions were transferred to petri dishes. All the petri dishes were placed at room temperature to dry overnight. The dried composite films were stored at room temperature. Figure 4.3 shows the schematic representation of the formation of SF-PVA and SF-PVA/ZnO NPs composite films and photographs of SF-PVA and SF-PVA/ZnO NPs composite films.

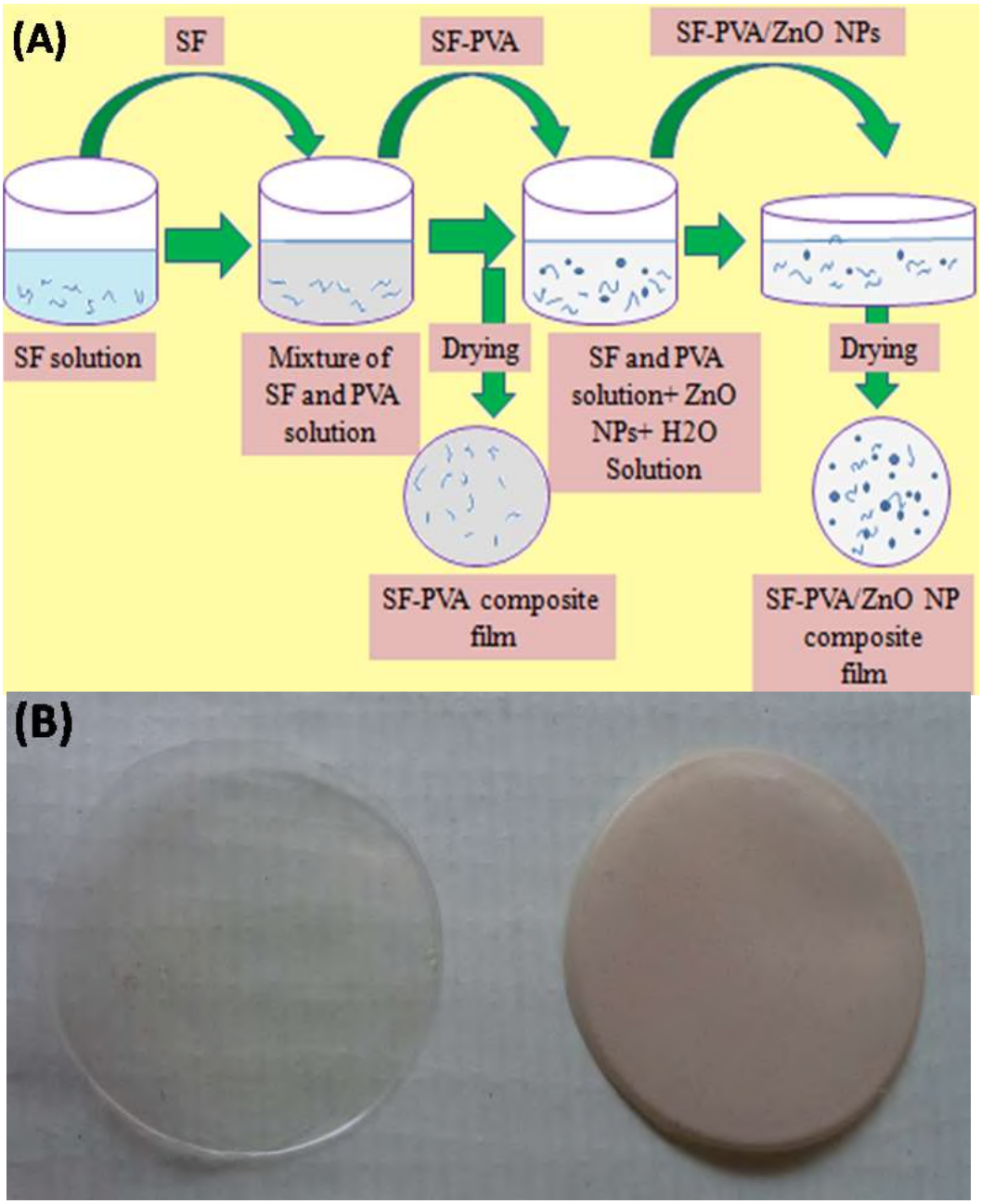

Figure 4.3 (A) Schematic representation of preparation of SF-PVA and SF-PVA/ZnO NPs and **(B)** Photographs of SF-PVA and SF-PVA/ZnO NPs composite films.

4.2.2 Characterization Studies

4.2.2.1 Structural analysis

The synthesized pure materials of SF, PVA, ZnO NPs and prepared composite films of SF-PVA and SF-PVA/ZnO NPs were characterized using X-ray diffraction (XRD) (Rigaku 600 Miniflex X-ray diffraction instrument) in the range of 10^{o}-80^{o}.

4.2.2.2 Spectroscopic analysis

The functional groups present in the synthesized SF, PVA, ZnO NPs and prepared composite films were examined using fourier transform infrared (FTIR) spectroscopy. FTIR spectra were recorded in the wave number range from 4000 to 600 cm^{-1}.The UV-visible spectroscopic study of pure materials and prepared composite films was recorded using Shimadzu UV 1600 spectrophotometer in the range of 300-600 nm.

4.2.2.3 Morphological analysis

The surface morphologies of SF, PVA, ZnO NPs and prepared composite films were studied by field emission-scanning electron microscopy (FE-SEM). Images were recorded on a 5KV (JEOL Model JSM - 6390LV) instrument.

4.2.2.4 Particle size distribution of ZnO NPs

The size of the synthesized ZnO NPs was studied using TEM analysis. TEM images were obtained by 200 kV (Jeol/JEM 2100) instrument. The size distribution was examined on at least 200 particles visualized on the TEM images. The size of ZnO NPs was also determined by a particle size analyzer (Particle Sizing Systems, Inc. Santa Barbara, Calif., and the USA) with an autotitrator.

4.2.2.5 DSC thermal analysis

Thermal properties of SF, PVA, ZnO NPs and prepared composite films were studied through differential scanning colorimetry (DSC) (SDT Q600). 5 mg of samples were heated in an aluminum crucible from 10 ^{o} to 600 ^{o}C with a

constant rate of 10 ^{o}C min^{-1} in a nitrogen atmosphere, and the weight loss was recorded.

4.2.2.6 Mechanical properties

The mechanical properties of prepared composite films were characterized using Universal Testing Machine (UTM) with Winsoft tensile and compression testing machine (Shimadzu AG) 100 kN load cell at 25 °C. Composite films were cut into double shaped strips measuring 40mmlong and 10mmwide. The tensile strength per cross-sectional area and the ratio of the relative elongation to the initial film length at break (%) were determined from the stress and strain data. The thickness of each sample was measured using digital digimatic callipers and average of three measurements was taken.

4.2.2.7 Porosity study by gas volumetric analysis

Nitrogen gas adsorption was used to determine Brunauer-Emmet-Teller specific surface area (BET) and porosity characteristics of composite films. 0.1–0.2 g films samples were first degassed in the Quantachrome Instruments Version 3.0 (Nova Station 0) automated system at 150 °C for 8 h. The specific surface area (S_{BET}) was determined by the BET method based on nitrogen adsorption isotherm data. The average pore diameter was estimated by Barrett-Joyner-Halenda method (BJH) [9].

4.2.2.8 Degree of Swelling

Swelling degree of composite films was studied by reported method [8]. Briefly, the synthesized composite films cut into the uniform size and weight and dipped into Phosphate Buffered Saline (PBS) of pH 7.4 at room temperature until saturation. Then the composite films were removed, their surfaces were scrubbed softly, and composite films pieces were weighted. The degree of swelling was calculated. The swelling ratio was calculated using the formula 3.9.

4.2.2.9 Biodegradation study

The biodegradation of composite films was evaluated by preparing a medium of phosphate buffer solution (PBS) of pH 7.5 containing lysozyme enzyme. The composite films were cut into the similar size and weight, after cutting the composite films immersed in PBS containing lysozyme (10,000U/mL) and incubated it at 37^{o} C for 21 days. The degradation rate is calculated by using the following formula,

$$\text{Degradation (\%)} = \frac{(Wi - Wt)}{Wi} \times 100 \qquad (4.3)$$

Here, Wi is the initial weight and Wt is the dry weight of composite films.

4.3 Results and discussion

4.3.1. Studies on SF, PVA and ZnO NPs

4.3.1.1 Structural Analysis

X-ray Diffraction

Figure 4.4 represents the XRD data of SF, PVA and ZnO NPs. The synthesized powder of ZnO NPs and pure films of synthesized SF and PVA were used for analysis of XRD. The XRD spectra analyses confirm the pure synthesis of SF, PVA and ZnO NPs. The characteristic peaks of 2θ values at 23.20 ^{o} and a small peak of 2θ = 28.50 ^{o} exhibits the silk II, the β-sheet crystalline structure of SF [10]. Pure PVA shows the characteristic peaks at 2θ = 19.90^{o} and 40.10^{o}, could be assigned to the semicrystalline nature of PVA [11]. The XRD spectrum of ZnO NPs depicts the diffraction peaks of 2θ = 31.74^{o}, 34.4^{o}, 36.29^{o} 47.5^{o}, 56.5^{o}, 63.7^{o}, 67.6^{o}, 68.5^{o} and 69.68^{o} arising from the reflection planes of (100), (002), (101), (102) and (110), (103), (200), (112), (201), respectively and it matched with hexagonal wurtzite structure of ZnO NPs, corresponded to JCPDS File Card No. 36-1451. The XRD spectra confirm the synthesis of amorphous SF, semi-crystalline nature of PVA and crystalline form of ZnO NPs. The most intense peak is used for calculation of crystallite size of ZnO NPs. The crystallite size of ZnO NPs calculated by using the Scherrer's formula is estimated to be ~ 13 nm [12].

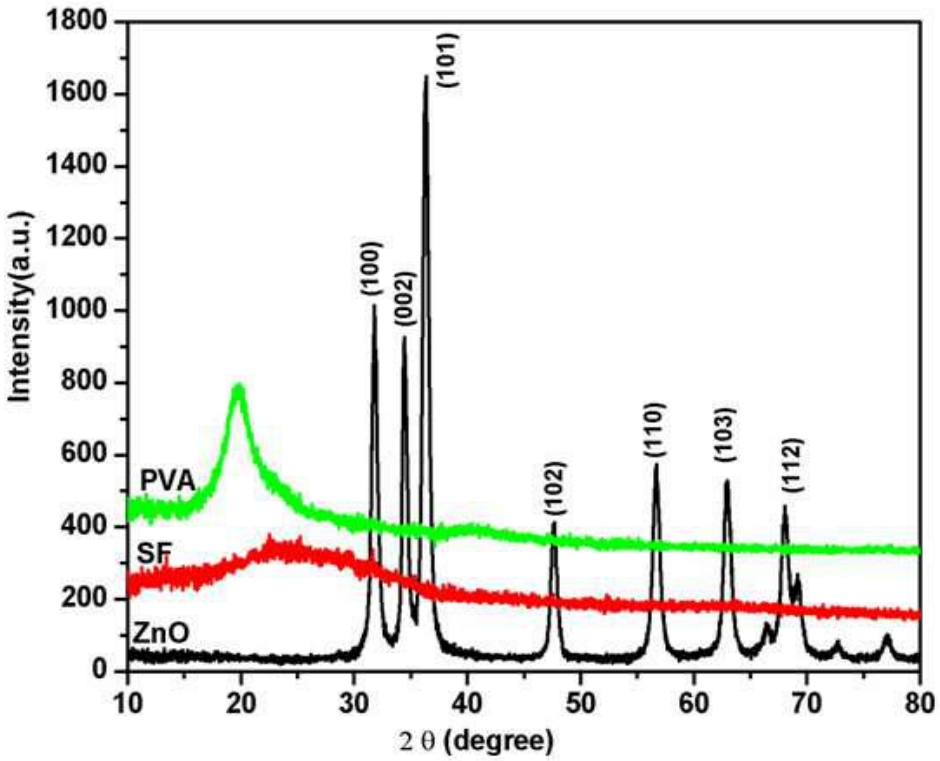

Figure 4.4 XRD spectra of SF, PVA and ZnO NPs

4.3.1.2 Spectroscopic Analysis

Fourier Transform Infrared Spectroscopy

FTIR spectra helped in understanding the functional groups present in the sample. Figure 4.5 depicts the FTIR data of SF, PVA and ZnO NPs, which represent broad peaks centered at 3415 cm^{-1} of SF, 3450 cm^{-1} of PVA and 3421.44 $cm^{-1}$of ZnO NPs related to the stretching of hydroxyl groups. The characteristic peaks of about 2879 cm^{-1} of PVA and 2889 cm^{-1} of ZnO NPs are assigned to the asymmetric CH_2 stretching. The peak position at about 1594 cm^{-1} and 1405 cm^{-1} of SF indicated that the random coil structure of amide I (C-O stretching), and amide II (N-H deformation), respectively. The absorption peaks of 1474 cm^{-1} and 1483 cm^{-1} are appeared due to the stretching mode of vibration of C=O resonance. The peak of 1631.89 cm^{-1} could be referred to asymmetric stretching of zinc carboxyl and a strong peak at 889 cm^{-1} and 564 cm^{-1} indicates the stretching vibrations of ZnO NPs [13].

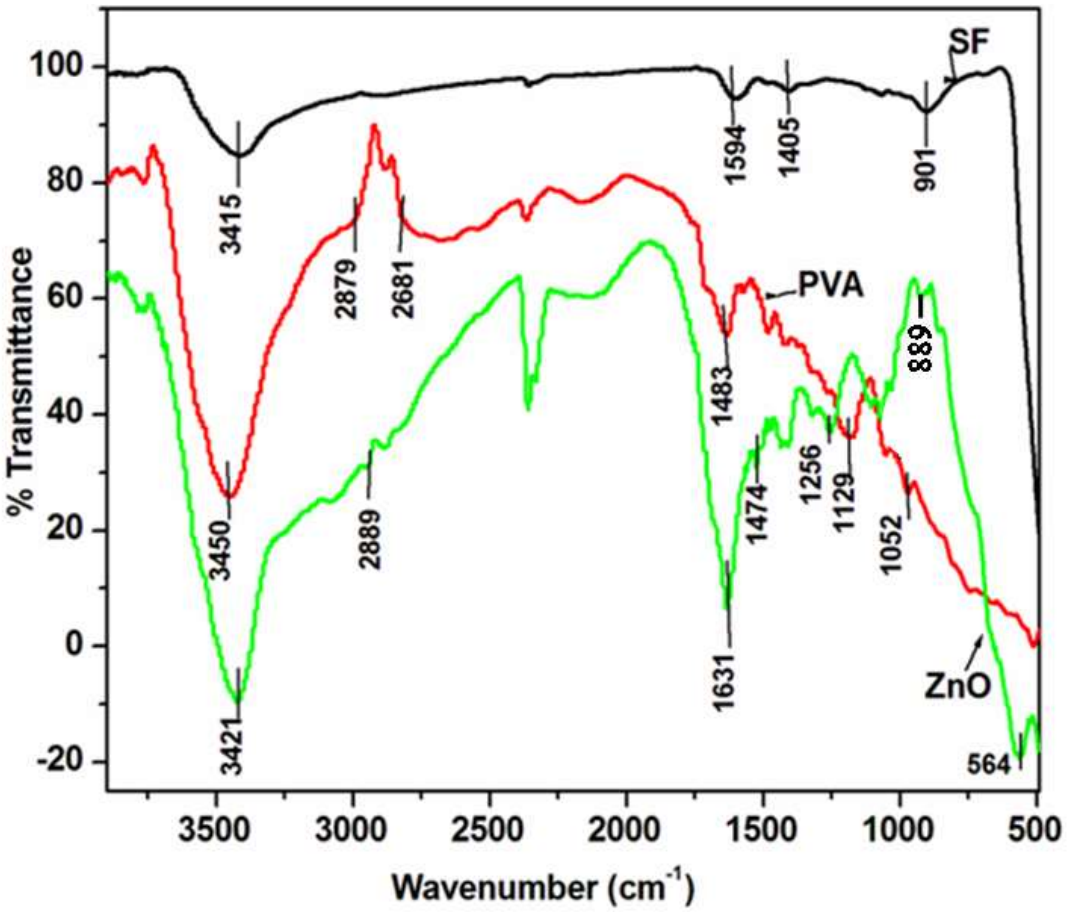

Figure 4.5 FTIR spectra of SF, PVA and ZnO NPs

UV-visible spectroscopy

The UV-visible spectroscopy study of SF, PVA and ZnO NPs is represents in figure 4.6. The SF shows the absorption peak of 280 nm, which confirms the small traces of tyrosine present in SF. The pure PVA does not show the absorption peak in the UV region. The synthesized ZnO NPs shows the sharp absorption peak in the UV region at 370 nm. This absorption peak of ZnO NPs represents the monodispersed nature of ZnO NPs [14]. UV-visible absorption spectroscopy confirms the synthesized ZnO NPs are wurtzite hexagonal in structure.

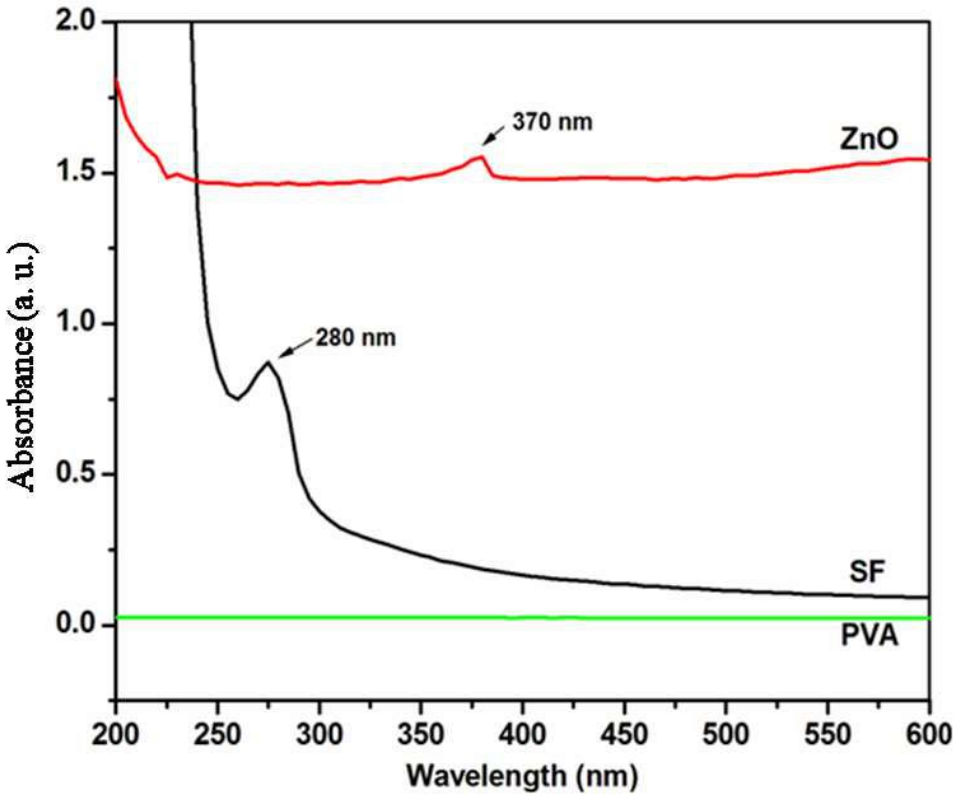

Figure 4.6 UV-visible spectra of SF, PVA and ZnO NPs

4.3.1.3 Morphological Analysis

FE-SEM Analysis of SF, PVA and ZnO NPs

Surface morphology of SF, PVA and ZnO NPs are observed in figure 4.7 (A), (B), and (C) respectively, with FE-SEM at an accelerated voltage of 5 KeV. It is observed that SF shows a porous structure, as well as PVA, shows uniform and plane platform. FE-SEM image of ZnO NPs shows the spherical shaped structure and the size of ZnO NPs is ~ 100 nm.

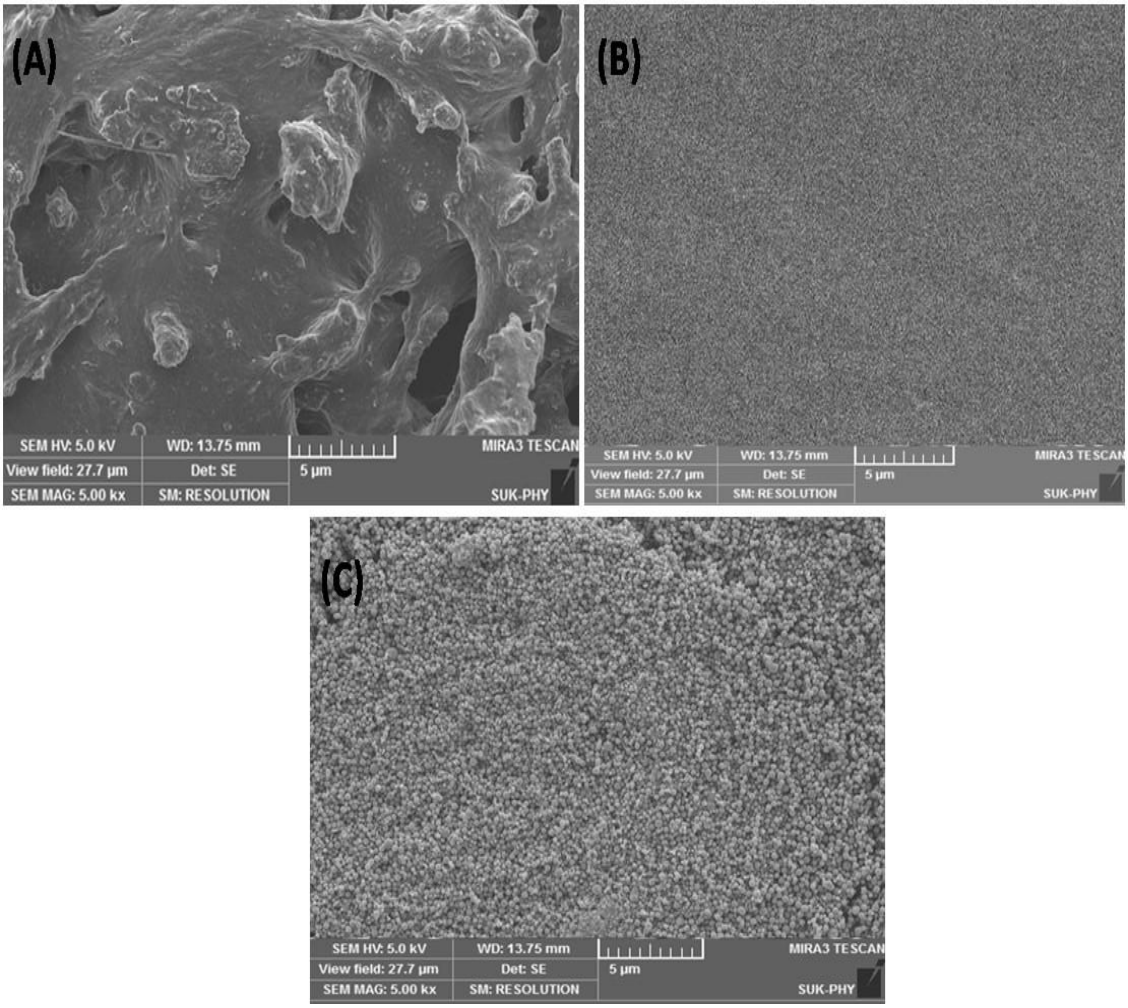

Figure 4.7 (A) FE-SEM images of SF, **(B)** PVA, and **(C)** ZnO NPs at 5,000X magnifications.

4.3.1.4 Particle size distribution of ZnO NPs

TEM of ZnO NPs

Transmission Electron Microscopy (TEM) is the most important technique, which is used for the measurement of particle size, size distribution and surface morphology of the sample. TEM analysis was conducted to measure the size of the synthesized ZnO NPs. Figure 4.8 represents the TEM image of ZnO NPs. The size of ZnO NPs is in the range of ~ 100 nm.

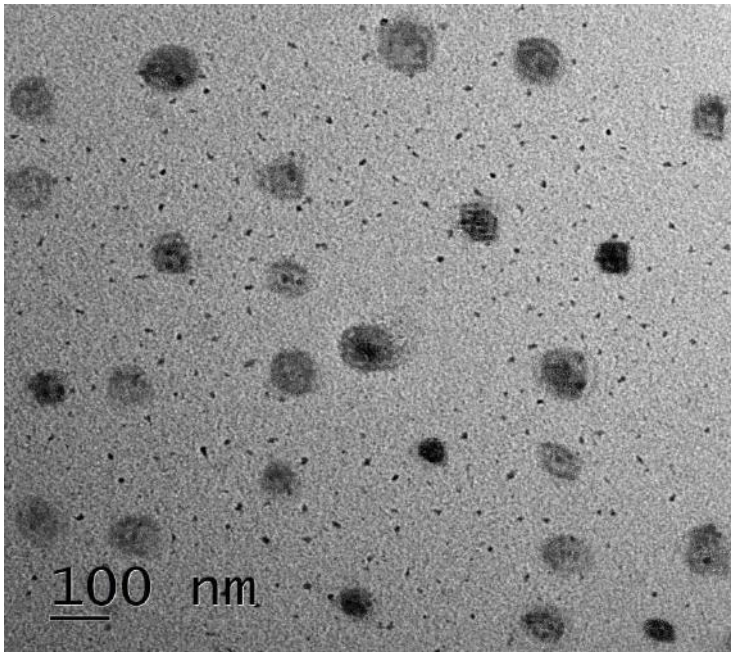

Figure 4.8 TEM of ZnO NPs

DLS of ZnO NPs

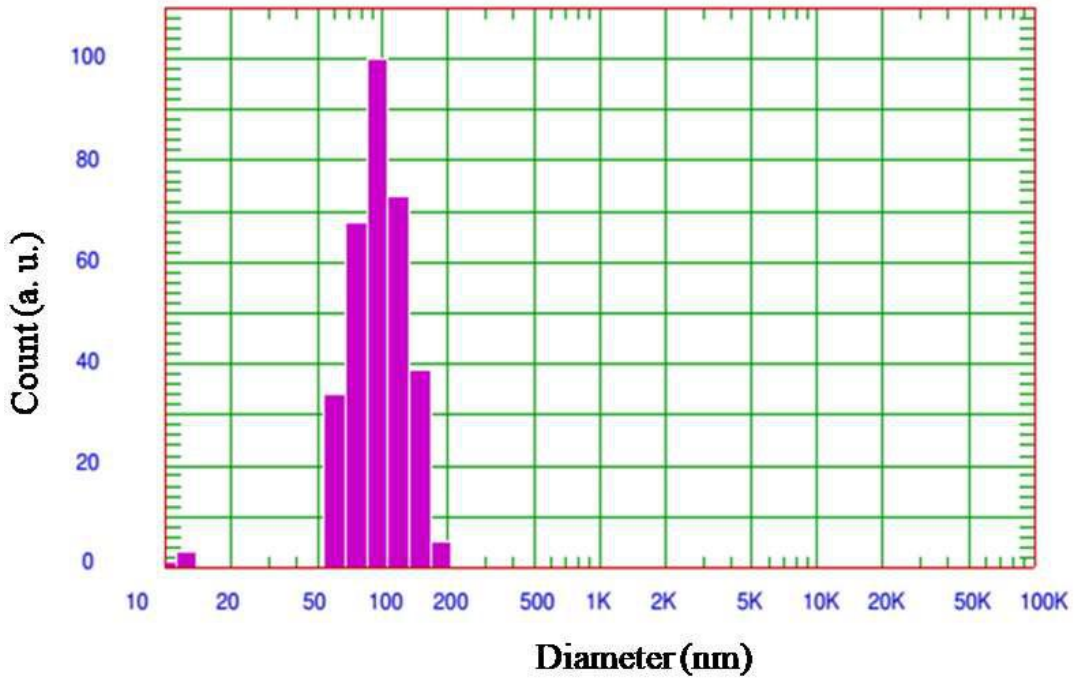

Figure 4.9 DLS of ZnO NPs

Dynamic light scattering (DLS) was employed to study the precise particle size of the NPs. Figure 4.9 shows the DLS data of ZnO NPs. The average maximum size of ZnO NPs is ~110 nm. The variation in size measurement from TEM and DLS technique is observed due to the hydrodynamic size distributions. ZnO NPs interacts with water molecules present in the solution. In addition, an increase in the hydrodynamic size of ZnO NPs is owing to aggregations of NPs.

4.3.1.5 DSC Thermal study of SF, PVA and ZnO NPs

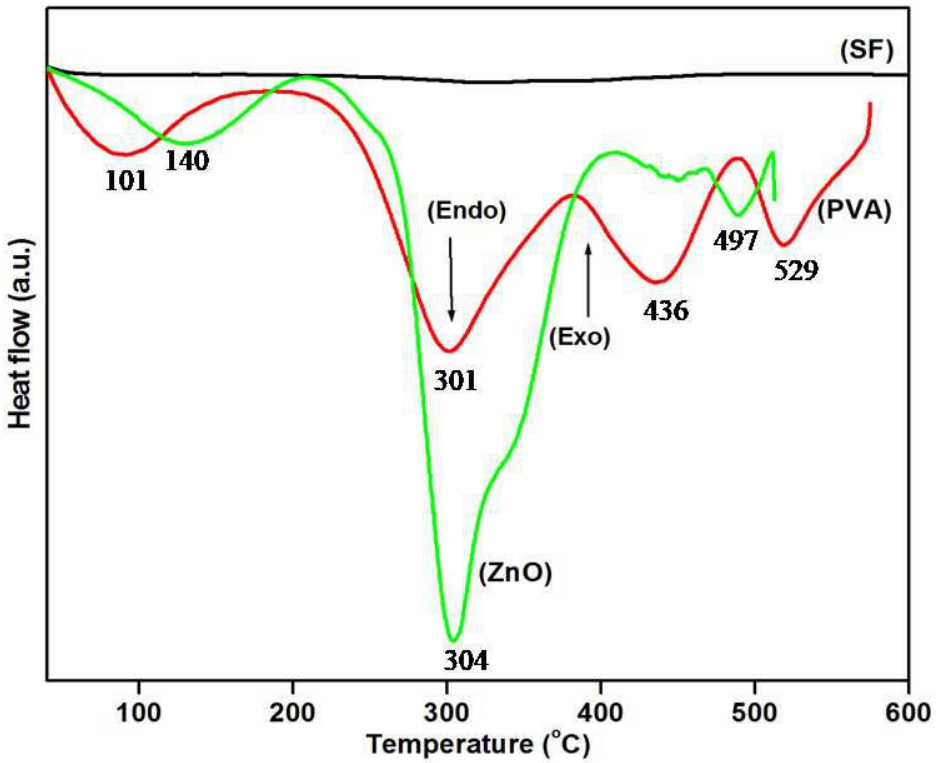

Figure 4.10 DSC thermal spectra of SF, PVA and ZnO NPs

Figure 4.10 depicts the DSC thermograms of pure SF, PVA and ZnO NPs. The endothermic peaks at 101 ^{o}C, 140 ^{o}C show the PVA and ZnO NPs, respectively. These peaks observe due to the evaporation of water molecules. The endothermic peaks of PVA at 301 ^{o}C and 436 ^{o}C could be assigned to the crystallization during heating from PVA molecules [15]. The endothermic peaks of ZnO NPs are at 304 ^{o}C and 497 ^{o}C. These peaks could be assigned to the

crystallization of ZnO NPs during heating [16]. The endothermic peak at 529 ^{o}C shows the melting temperature of PVA.

4.3.2 Studies on SF-PVA and SF-PVA/ZnO NPs composite films

4.3.2.1 Structural

X-ray diffraction analysis

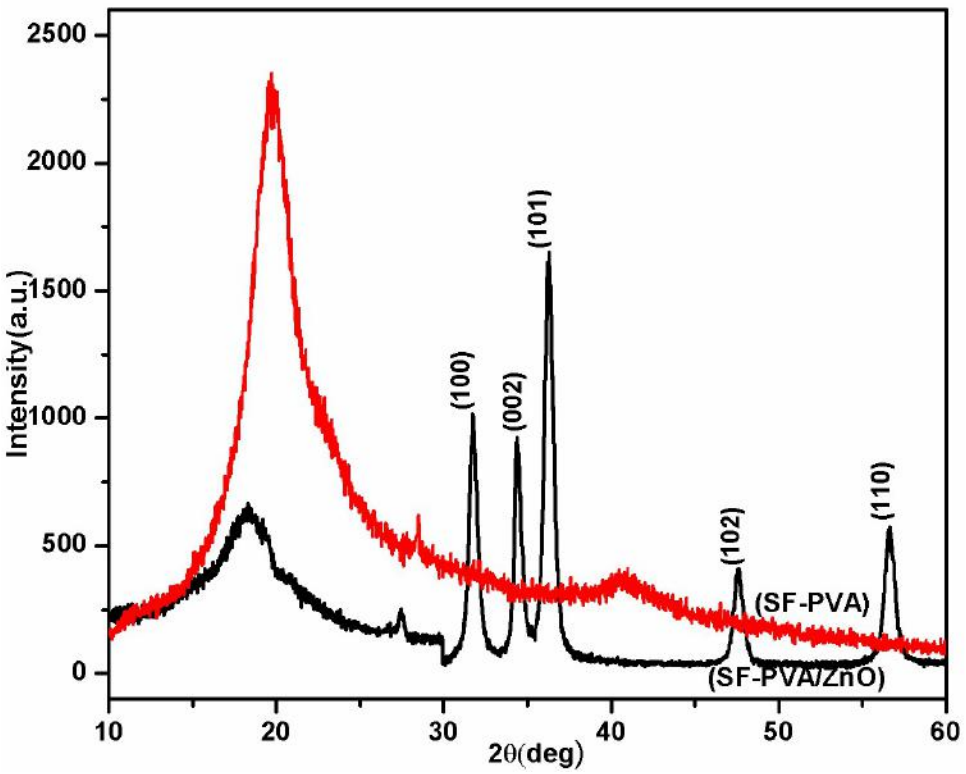

Figure 4.11 XRD spectra of SF-PVA and SF-PVA/ZnO NPs composite films

XRD analysis was carried out to study the crystalline nature of composite films. XRD spectra of prepared composite films are shown in figure 4. 11. Both spectra of the composite films of SF-PVA and SF-PVA/ZnO shows the prominent peaks at 2θ = 19.98^{o}, 23.26^{o}, 28.56^{o} and 40.96^{o}. The diffraction peaks at 2θ = 19.98^{o} and 40.96^{o} could be assigned to the semi-crystalline nature of PVA. The diffraction peaks at 2θ = 23.26^{o} and 28.56^{o} exhibits to silk II, β- sheet crystalline structure of SF [17]. The XRD spectrum of the SF-PVA/ZnO composite film depicts different diffraction peaks at 2θ = 36.1^{o}, 41.66^{o} and 56.60^{o} which are ascribed to the (101), (002), (101), (102) and (110) planes, respectively. The

intensities of the diffraction peaks that correspond to SF-PVA are very high compared to those of the SF-PVA/ZnO composite film because the concentration of PVA is higher than that of ZnO NPs [18].

4.3.2.2 Spectroscopic

UV-visible analysis of composite films

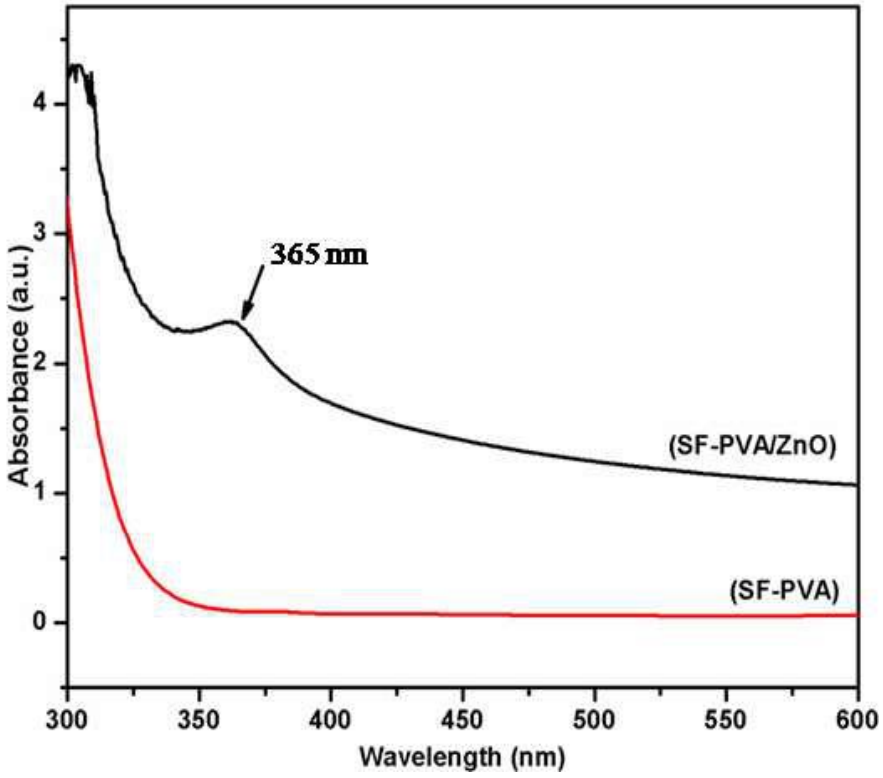

Figure 4.12 UV-visible spectra of SF-PVA and SF-PVA/ZnO NPs composite films

Figure 4.12 represents the UV-visible spectra of SF-PVA and SF-PVA/ZnO composite films. The absorption peak of the SF-PVA/ZnO composite film shows in the region of 350-400 nm with a peak at 365 nm for ZnO NPs [14]. Pure ZnO NPs shows an absorption peak in the UV region at 370 nm. The peak shows blue shift for the SF-PVA/ZnO composite film compared to ZnO NPs. The shift in the absorbance is due to ZnO NPs embedded into the SF-PVA composite film.

FTIR analysis of composite films

Figure 4.13 shows the FTIR study of composite films. The FTIR spectrum of the SF-PVA composite film shows the characteristic peak at about 3267.93 cm^{-1} which is assigned to the stretching vibration of a hydroxyl group (OH) and the peaks at about 2920.53 cm^{-1}, and 2851.30 cm^{-1} are assigned to the asymmetric CH_2 stretching.

The peak position at about 1018.15 cm^{-1} is assigned to the (C-O) resonance. The absorption bands at 1631.05 cm^{-1} indicate random coil structure of amide I (C-O stretching), and that at 1545 cm^{-1} corresponds to amide II (NH deformation and N-stretching). The FTIR spectrum of the SF-PVA/ZnO composite film shows a characteristic absorption peak of PVA at about 3267.93 cm^{-1} due to the stretching vibration of a hydroxyl group (OH) and the peaks at about 1018.15 cm^{-1} and 1413.21 cm^{-1} are due to the C-O group. The two bands observed at 2920.53 cm^{-1} and 2851.30 cm^{-1} are assigned to the asymmetric CH_2 stretching. The peak positions at 1631.05 cm^{-1} indicate a random coil structure of amide I (C-O stretching). The peak at around 1579.46 cm^{-1} is amide II (N-H deformation and C-N stretching) and those at 1250 cm^{-1} indicate random coil structure of amide III (C-N stretching and N-H deformation). Metal oxides generally exhibit absorption bands in the fingerprint region, i.e., below 1000 cm^{-1} due to inter-atomic vibrations [19]. The absorption peak at about 1413.21 cm^{-1} appeared the stretching mode of vibration of C=O. Also, the bands at 835.77 cm^{-1} and 668.30 cm^{-1} indicate the stretching vibrations of ZnO NPs [13].

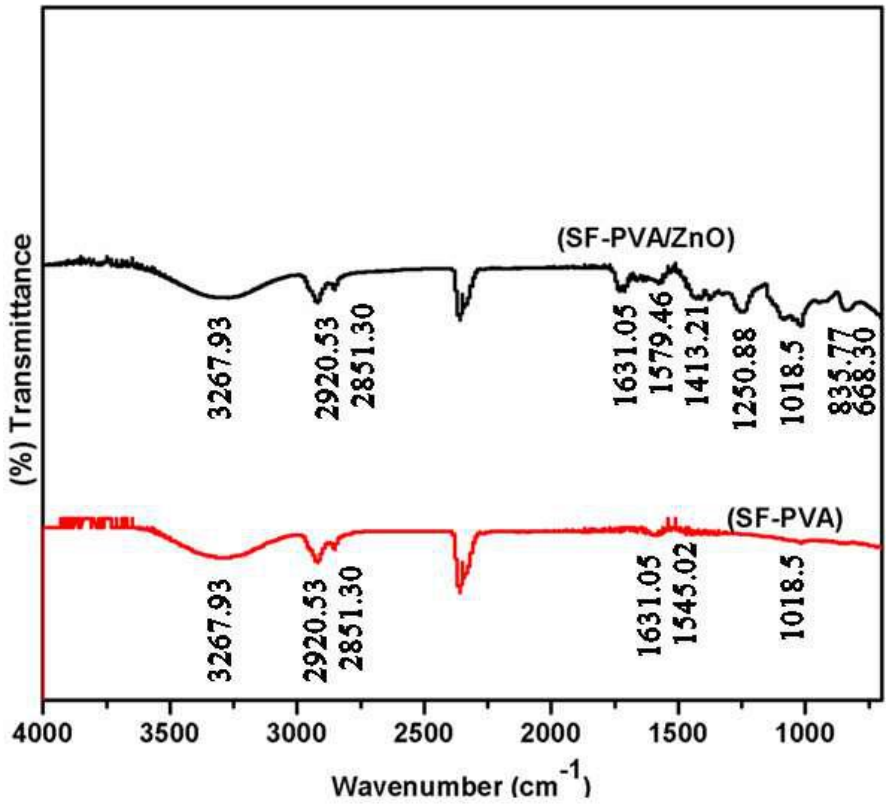

Figure 4.13 FTIR spectra of SF-PVA and SF-PVA/ZnO NPs composite films

4.3.2.3 Morphological Analysis

FE-SEM analysis of composite films

Surface morphologies of the prepared SF-PVA and SF-PVA/ZnO composite films are shown in figure 4.14 (A) and (B) respectively, using field emission scanning electron microscopy at an accelerated voltage of 5 KeV. The addition of SF to the PVA matrix, the SF-PVA composite film shows microspheres of SF due to the combination of SF and PVA [20]. Additionally, the SF-PVA composite film shows a porous structure. It is observed that ZnO NPs possesses a spherical-shaped structure in the SF-PVA/ZnO composite film, and ZnO NPs are inserting into the pores that are formed by the SF-PVA composites. However, the roughness of the composite film is observed by increasing the concentration of ZnO NPs [21]. Figure (B) clearly shows that ZnO NPs are embedded in the SF-PVA composite film. This result indicates that ZnO NPs are

uniformly dispersed into the SF-PVA composite film. This will result in uniform antibacterial activity and reduction in infection.

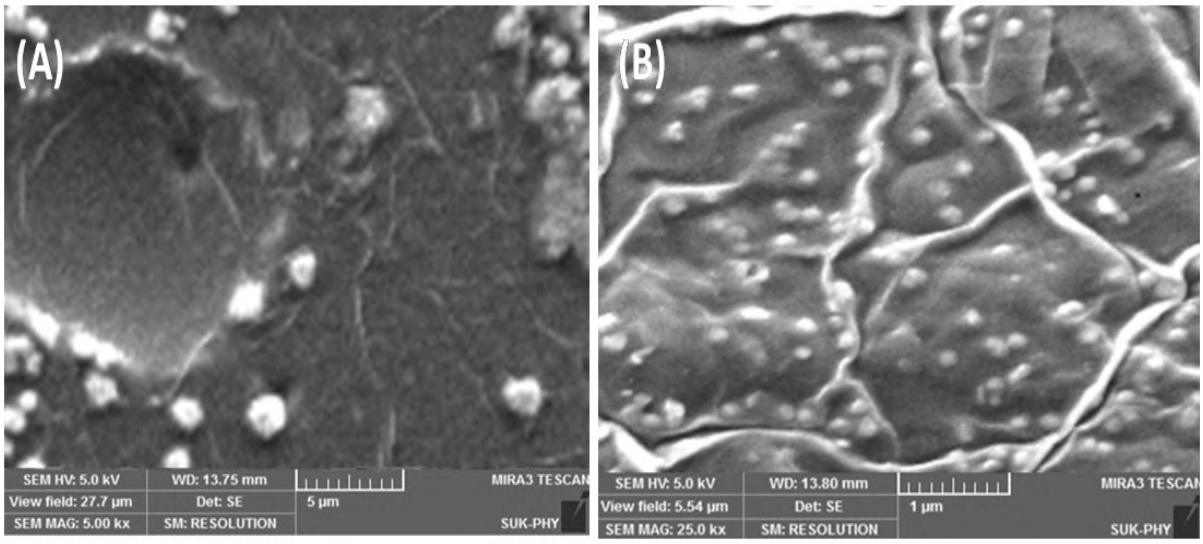

Figure 4.14 FE-SEM images of **(A)** SF-PVA and **(B)** SF-PVA/ZnO NPs composite films at 5,000X and 25, 000X magnifications, respectively.

4.3.2.4 DSC Thermal analysis of composite films

Figure 4.15 shows the DSC thermograms for SF-PVA composite and SF-PVA/ZnO NPs composite films. For the SF-PVA composite film, endothermic peaks at 205 ^{o}C and 302 ^{o}C are observed for SF and PVA exhibits due to evaporation of water molecules. Exothermic peaks of SF-PVA at 222 ^{o}C and 329 ^{o}C could be assigned to crystallization during heating from Silk I, Silk II and PVA molecules [22]. The composite film of SF-PVA/ZnO NPs exhibits endothermic peaks at 210 ^{o}C and 263 ^{o}C for SF and PVA, respectively. The slight shift of endothermic peak of PVA to a lower temperature and the observed intense peaks confirms the presence of ZnO NPs in the SF-PVA matrix. Exothermic peaks of SF-PVA/ZnO composite film at 226 ^{o}C and 318 ^{o}C could be assigned to the crystallization of Silk, PVA, and ZnO NPs during heating. The broadness of exothermic peak of 318 ^{o}C confirms the ZnO NPs are embedded in the SF-PVA composite film. The melting temperature (Tm) of the SF-PVA composite film slightly shifts towards a higher temperature, i.e. from 429 ^{o}C to 452 ^{o}C with the addition of ZnO NPs.

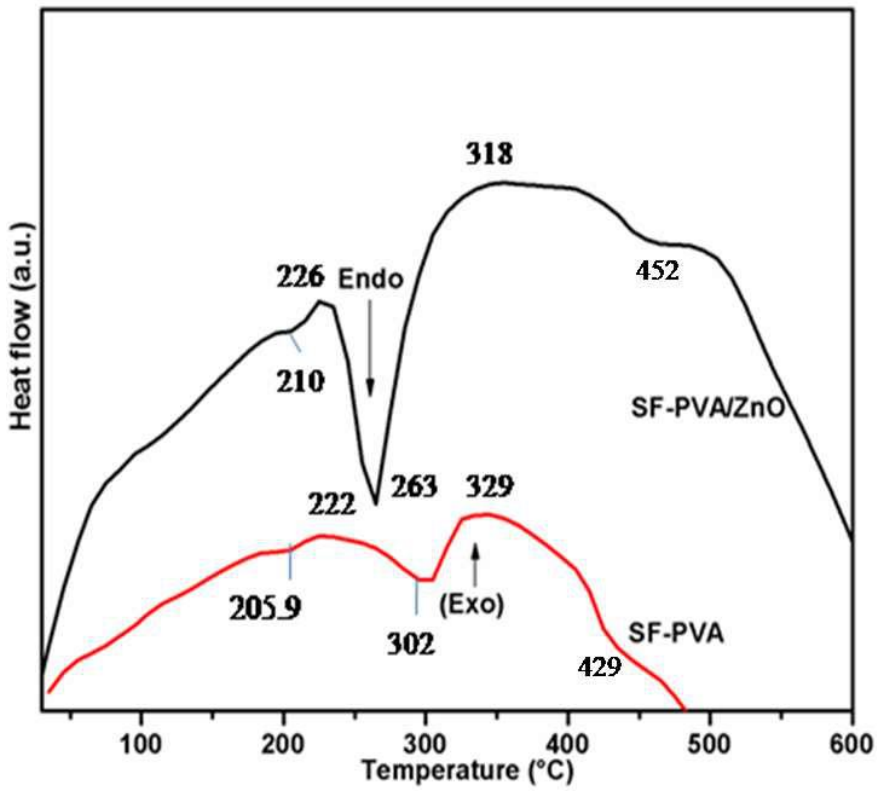

Figure 4.15 DSC thermal studies of SF-PVA and SF-PVA/ZnO NPs composite films.

4.3.2.5 Mechanical property of composite films

Figure 4.16 depicts the tensile strength and % elongation data of SF-PVA and SF-PVA/ZnO NPs composite films. The results show the tensile strength of the SF-PVA composite film is about 3. 125 MPa and % elongation is about 178 %. SF-PVA/ZnO NPs composite film is a tensile strength of about 3. 791 MPa and % elongation is about 207 %. However, the tensile strength and % elongation of the SF-PVA/ZnO NPs composite film increased by the addition of ZnO NPs. The obtained tensile strength and % elongation are higher than those reported for the β-chitin hydrogel/ZnO NPs composite bandage. [23]. Therefore, it is concluded that the obtained tensile strength and % elongation of prepared SF-PVA/ZnO NPs composite film are sufficient for wound dressing applications.

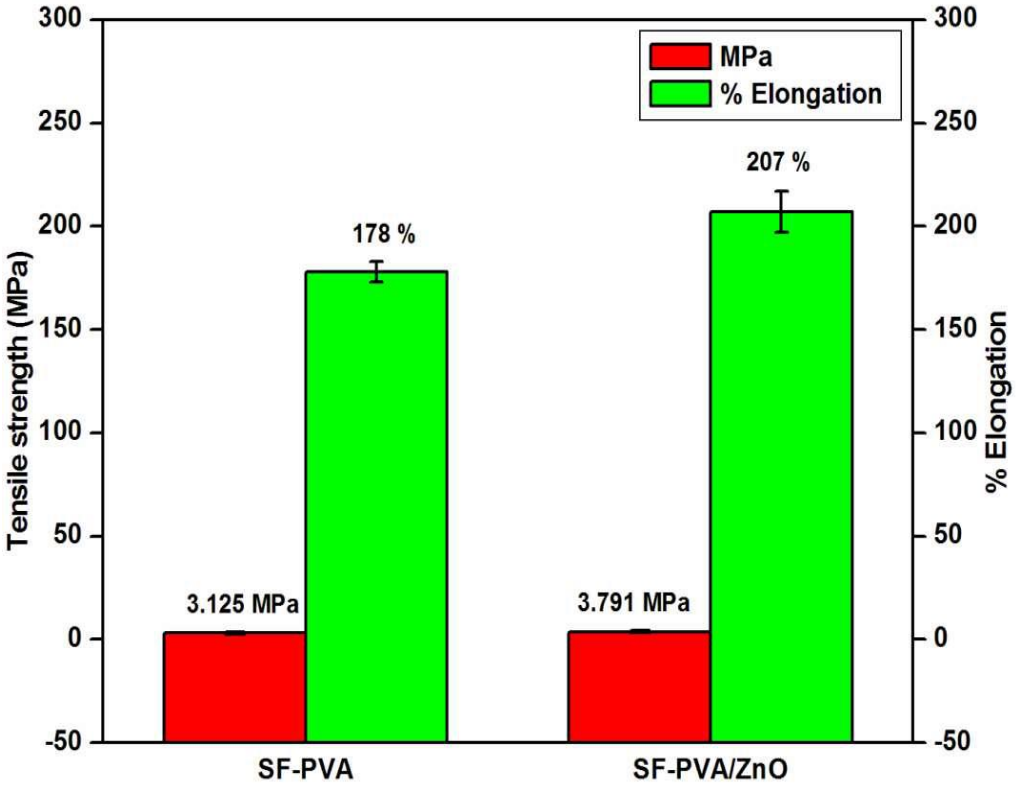

Figure 4.16 The Mechanical properties of SF-PVA and SF-PVA/ZnO NPs composite films

4.3.2.6 Porosity study by BET analysis

Porosity study of SF-PVA and SF-PVA/ZnO NPs composite films was carried out by the BJH method in figure 4.17. The SF-PVA composite film shows higher pore diameter of about 1.64 nm and the radius of 0.0055 cc/g. The SF-PVA/ZnO NPs composite film shows the pore diameter is about 1.57 nm and radius of 0.0043 cc/g. According to the IUPAC terminology the obtained data depicts the embedded ZnO NPs in SF-PVA composite film shows the mesopores adsorbents. The addition of ZnO NPs into SF-PVA matrix is slightly decreased pore diameter and pore volume as compared to SF-PVA composite film.

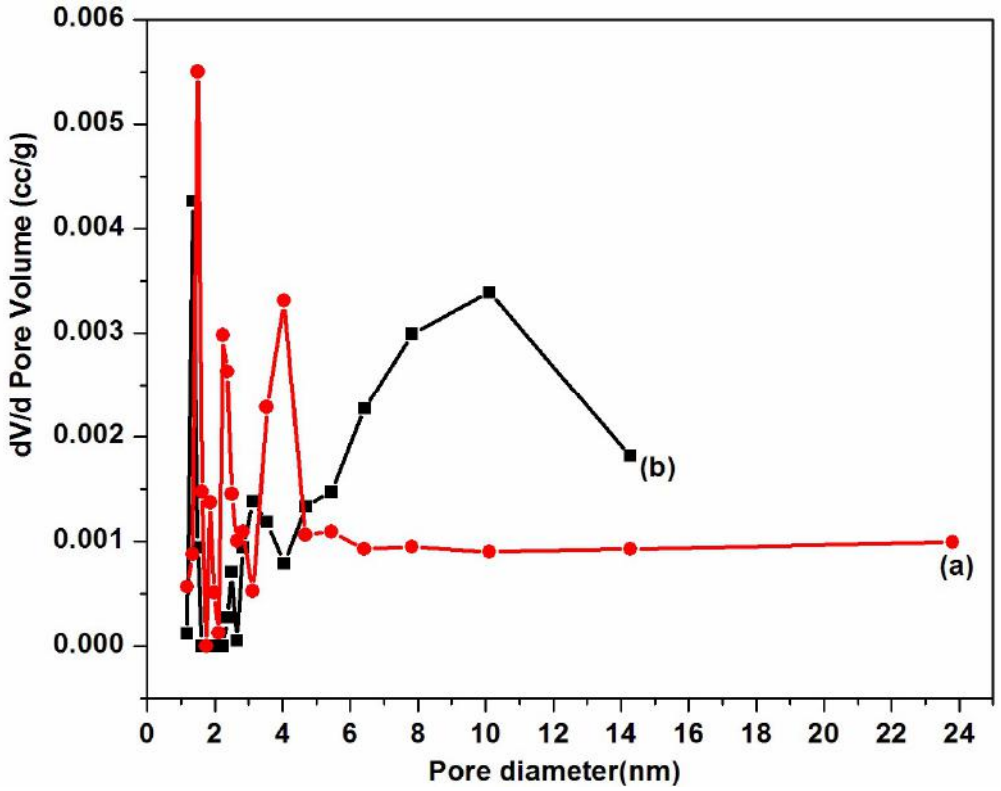

Figure 4.17 Porosity of **(a)** SF-PVA and **(b)** SF-PVA/ZnO NPs composite films.

4.3.2.7 Swelling behavior of composite films

Figure 4.18 represents the swelling ratios of SF-PVA and SF-PVA/ZnO composite films. The swelling ratio of SF-PVA composite film shows slightly higher value as compared to that of SF-PVA/ZnO NPs composite film. The presence of ZnO NPs slightly reduces the swelling ratio since the composite film containing ZnO NPs shows lower porosity compared to SF-PVA composite film. Both SF and PVA materials are hydrophilic in nature. The water uptake and retention capacities of SF and PVA are higher compared to ZnO NPs, due to it slightly reduces the swelling ratio. Additionally, this can be due to interactions among SF, PVA and ZnO NPs. The swelling ratios of composite films increase after 7 days of incubation compared to those obtained for 1-day incubation. The water uptake capacity of the composite films decreases after 14 days and the composite films start to degradation. Therefore, the swelling behavior data

indicates that the composite film can absorb a large volume of liquid in which it is immersed, and there is no change in the dressing for up to 1 week.

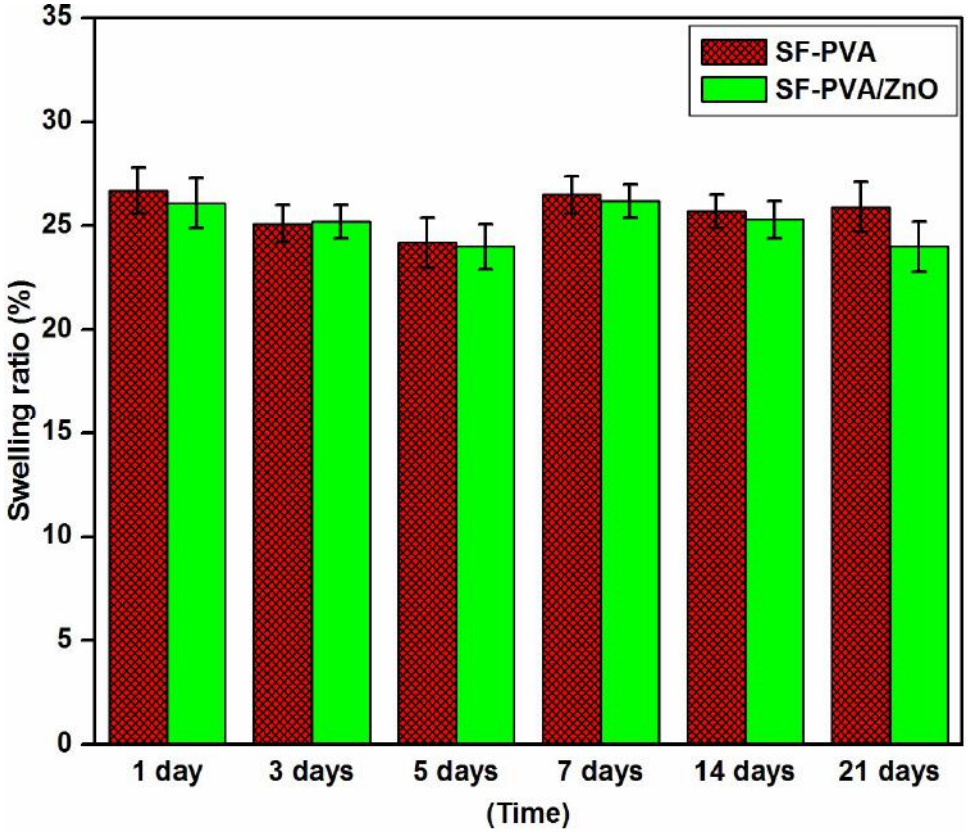

Figure 4.18 Swelling behavior of SF-PVA and SF-PVA/ZnO NPs composite films

4.3.2.8 Biodegradation study of composite films

Biodegradation study of composite films is very important due to the degradation nature of composite films would be helpful to attain better-wound healing process. Figure 4.19 shows the biodegradation of composite films of SF-PVA and SF-PVA/ZnO NPs. The data reveals that the composite film by SF-PVA showed 50-55% of degradation after 7 days, 55-60% degradation after14 days and 60-65 % degradation after 21 days. The data reveals that the ZnO NPs embedded SF-PVA composite film showed degradation 30-35 % after 7 days, 14 days and 35-40% after 21 days. The obtained results concluded that the degradation rate decreased after incorporation of ZnO NPs into SF-PVA matrix. The degradation rate of both composite films increased with increasing the time duration.

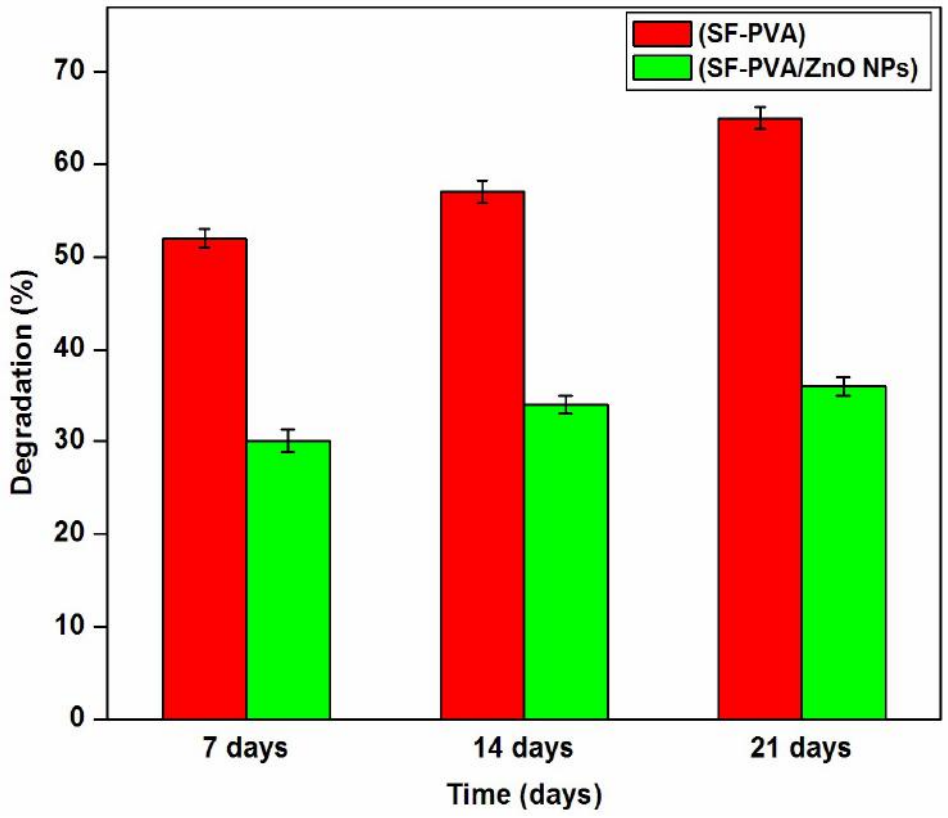

4.19 Biodegradation study of SF-PVA and SF-PVA/ZnO NPs composite films

4. 3 Effect of embedded ZnO NPs into SF-PVA composite films

The structural and spectroscopic analysis of composite films showed the addition of ZnO NPs into SF-PVA composite film have increased crystalline nature of composite films. SF-PVA composite film is amorphous in nature. The crystallinity of composite films increased with increase in the concentration of ZnO NPs. The mechanical property of ZnO NPs embedded SF-PVA composite film showed the increased tensile strength and % elongation compared to control SF-PVA composite film. The porosity study of composite films concluded that the addition of ZnO NPs to SF-PVA composite film, the pore diameters slightly decreased. Similarly, the swelling study of composite films concluded that the addition of ZnO NPs slightly reduced the swelling ability. The biodegradation study revealed that the ZnO NPs embedded SF-PVA composite film shows the degradation rate decreased, these are increased with increase in the time duration. Hence, the obtained results of mechanical property, swelling behavior, and

biodegradation capacity of prepared SF-PVA/ZnO NPs composite films are higher than those reported β-chitin hydrogel/nZnO composite bandages.

4.4 Conclusions

The ZnO NPs are successfully synthesized by reflux method and composite films of SF-PVA and SF-PVA/ZnO NPs are prepared by casting method at room temperature. The XRD analysis indicates that the SF is amorphous in nature, pure PVA shows semicrystalline nature and ZnO NPs shows the crystalline structure. The XRD spectrum confirms the exact synthesis of the nano-crystalline structure of ZnO NPs with hexagonal wurtzite structure. The crystallite size of ZnO NPs is estimated to be ~ 13 nm. The functional groups present in the synthesized pure materials of SF, PVA, ZnO NPs and composite films are studied by using FTIR analysis. The size of ZnO NPs is confirmed by TEM and DLS analysis. In TEM image, the size of ZnO NPs is confirmed by the approximately 100 nm. DLS analysis shows the particle hydrodynamic size distribution is approximately 110 nm. FE-SEM images and DSC analysis confirms the ZnO NPs are embedded in the SF-PVA composite film. The SF-PVA/ZnO composite film shows higher tensile strength and % elongation as well as appropriate swelling behavior, porous, and biodegradable in nature which is helpful for absorbing large volumes of wound exudates. This work provides simple methods which will be helpful in order to fabricate SF, PVA, ZnO NPs and composite films of SF-PVA, and SF-PVA/ZnO NPs. All these obtained data revealed that the composite films of SF-PVA and SF-PVA/ZnO NPs have the potential to be applied for wound dressings.

References

1. A. Nel, T. Xia, L. Mädler, N. Li, Science, 2006, 311, 622-627.
2. K. Powers, S. Brown, V. Krishna, S. Wasdo, B. Moudgil, S. Roberts, Toxicol Sci, 2006 90, 296-303.
3. Y. Kishimoto, F. Ito, H. Usami, E. Togawa, M. Tsukada, H. Morikawa S. Yamanaka, Int J Biol Macromol, 2013, 57, 124–128.
4. M. Sah K. Pramanik, Int J Environ Sci Dev, 2010, 1, 404-408.
5. A. Aykac, B. Karanlik, A. Sehirli, Gene, 2018, 641, 287-291.
6. K. Lin, H. Cheng, H. Hsu, L. Lin W. Hsieh, Chem Phys Lett, 2005, 409, 208–211
7. J. Meshram, V. Koli, S. Kumbhara, L. Borde, M. Phadatare, S. Pawar, Mater Res Express, 2018, 5, 045016.
8. P. Patil, J. Meshram, R. Bohara, S. Nanaware S. Pawar, New J Chem, 2018, 42, 14620-14629.
9. T. Li, N. Bao, A. Geng, A. H. Yu, Y. Yang, X. Dong, 2018. R Soc Open Sci, 5, 171788-171788.
10. F. Miroiu, G. Socol, A. Visan, N. Stefan, D. Craciun, V. Craciun, G. Dorcioman, I. Mihailescu, L. Sima, S. Petrescu, A. Andronie, Mater Sci Eng B, 2010, 169, 151-158.
11. J. Liang, Y. Huang, L. Zhang, Y. Wang, Y. Ma, T. Guo, Y. Chen, Adv Funct Mater, 2009, 19, 2297-2302.
12. H. Klug, L. Alexander, X-Ray Diffraction Procedures: For Polycrystalline and Amorphous Materials, 2nd Edition, by Harold P. Klug, Leroy E. Alexander, ISBN 0-471-49369-4. Wiley-VCH, 1974, 992.
13. S. Azizi, M. Ahmad, F. Namvar R. Mohamad, Mater Lett, 2014, 116, 275–277.
14. L. Luo, Y. Zhang, S. Mao L. Lin, Sensor Actuat A-Phys, 2006, 127, 201–206.
15. J. Friedrich, Rev Adhes Adhes, 2018, 6, 253-328.
16. M. Ramesan, M. Varghese, P. Periyat, Adv Polym Tech, 2018, 37, 137-143.

17. H. Zhu, J. Shen, X. Feng, H. Zhang, Y. Guo J. Chen, Mater Sci Eng Carbon, 2010, 30, 132–140. .
18. A. Roy, S. Gupta, S. Sindhu, A. Parveen P. Ramamurthy, Composites Part B, 2013, 47, 314–319.
19. A. Janaki, E. Sailatha S. Gunasekaran, Spectrochim. Acta, Part A, 2015, 144, 17–22.
20. S. Calamak, C. Erdogdu, M. Ozalp K. Ulubayram, Mater Sci Eng Carbon, 2014, 43, 11–20.
21. D. Fernandes, A. Hechenleitner, S. Lima, L. Andrade, A. Caires and E. Pineda, Mater Chem Phys, 2011, 128, 371–376.
22. K. Lee, D. Baek, C. Ki Y. Park, Int J Biol Macromol, 2007, 41, 168–172.
23. S. Kumar, V. Lakshmanan, M. Raj, R. Biswas, T. Hiroshi, S. Nair, R. Jayakumar, Pharm Res, 2013, 30, 523-537.
24. A. Ranella, M. Barberoglou, S. Bakogianni, C. Fotakis, E. Stratakis, Actabiomaterialia, 2010, 6, 2711-2720.
25. I. Degasne, M. Basle, V. Demais, G. Hure, M. Lesourd, B. Grolleau, L. Mercier, D. Chappard, Calcif Tissue Int, 1999, 64, 499-507.
26. G. Zhao, Z. Schwartz, M. Wieland, F. Rupp, J. Geis-Gerstorfer, D. Cochran, and B. Boyan, J Biomed Mater Res B, 2005, 74, 49-58.

CHAPTER 5

Hybrid Chitosan-ZnO NPs Coated with a Sonochemical Technique on SF-PVA Composite Film

International Journal of Biological Macromolecules 122 (2019) 1305–1312

Contents lists available at ScienceDirect

International Journal of Biological Macromolecules

journal homepage: http://www.elsevier.com/locate/ijbiomac

Hybrid chitosan-ZnO nanoparticles coated with a sonochemical technique on silk fibroin-PVA composite film: A synergistic antibacterial activity

Priyanka P. Patil [a], Raghvendra A. Bohara [a,c], Jagruti V. Meshram [a], Shivdas G. Nanaware [a], Shivaji H. Pawar [a,b,*]

[a] Centre for Interdisciplinary Research, D. Y. Patil University, Kolhapur 416006, India
[b] Center for Research and Technology Development, Sinhgad Institute, Solapur 413255, MS, India
[c] CÚRAM, Centre for Research in Medical Devices, National University of Ireland Galway, Ireland

ARTICLE INFO

Article history:
Received 30 March 2018
Received in revised form 12 September 2018
Accepted 14 September 2018
Available online 15 September 2018

Keywords:
Hybrid C@ZnO NPs
Sonochemical coatings
Antibacterial activity
Cytocompatibility

ABSTRACT

The hybrid chitosan-ZnO nanoparticles (C@ZnO NPs) are synthesized and coated on Silk fibroin-polyvinyl alcohol (SF-PVA) composite film by a sonochemical coating process. These are systematically studied for their synergistic antibacterial activity and reported. The coated composite films show the excellent antibacterial activity against Gram-positive and Gram-negative bacteria. The composite films are characterized by using X-ray diffraction (XRD), Fourier transform infrared spectroscopy (FTIR), and Scanning Electron Microscopy (SEM) studies. The specific surface area and porosity are studied by Brunauer-Emmett-Teller (BET) analysis under nitrogen gas adsorption. The swelling degree, mechanical property and cell viability study of coated and uncoated composite films are investigated. The results showed that the specific surface area, porosity, swelling degree, and mechanical property of coated composite films increased with increasing the concentrations of C@ZnO NPs on SF-PVA composite film. Cell viability study confirmed the cytocompatible nature of all the C@ZnO NPs coated composite films. Thus, obtained properties of composite films reveal the potential of this material which can be used as antibacterial wound dressing applications.

I. F. = 3.909

5.1 Introduction

In recent years, researchers have largely focused on the development of newer technology in the nanotechnology area. The surface coating technology has newer technology for the development of novel materials especially nanomaterials due to increased the availability of NPs and advancements in coating methods. This coating process provides excellent properties including morphology, composition, structure, and adhesion. Surface coatings of materials or functionalization of NPs are applied in order to selectively change the properties of materials [1]. In this method, the surface of materials can be coated with an advanced substances and NPs. This process generates single or multilayers that can be either complete layer or incomplete layer. These coated particles increase the stability, wettability, improve physical and chemical functions, increases efficiency, prevention of particle core dissolution, biocompatibility, and functionality when it is employed in biomedical applications [2].

Over the last few decades, the preparation of antibacterial dressings based on ZnO NPs with polymers has become an important area of research [3]. ZnO NPs have attracted significant interest due to its good tissue adhesive property, high ability and antibacterial activity [4]. In addition, this system gives the flexibility to enhance the biocompatibility by modifying the surface with biocompatible polymers [5].

The present chapter focuses on the synthesis of hybrid chitosan-ZnO NPs and synthesized chitosan-ZnO NPs coated on the surface of SF-PVA composite film. Chitosan has properties of biocompatibility, biodegradability, non-toxicity, moisture retentive ability, antibacterial activity and cost effective, hence this material is widely suited in wound dressing applications [6]. The present efforts are aimed, to study the physical-chemical properties of composite films by surface modification of chitosan-ZnO NPs hybrid system. The surface modification is done by keeping in mind the end application of wound dressing and for this we have selected sonochemical method [7]. Sonochemical coating technique prevents the aggregation of NPs due to the application of high-intensity ultrasound and the acquired coatings are uniformly deposited on the surface of substrates [8]. The role

of coated hybrid chitosan-ZnO NPs on structural and morphological properties was studied. The specific coated surface area of prepared composite films was evaluated.

5.2 Experimental

Cocoons of Thai silkworms *Bombyx Mori* were obtained from the Abhilasha Silk and silk Products Pvt. Ltd. India. PVA was purchased from Sigma Aldrich. The average molecular weight of the PVA was approximately 56,000. Dialysis membrane-150 with flat width: 42.44 mm and average diameter: 25.4 mm were purchased from Himedia Laboratories Pvt. Ltd. Mumbai, India. Sodium carbonate (Na_2CO3), calcium chloride ($CaCl_2$), zinc acetate (ZnAc), sodium hydroxide (NaOH), diethylene glycol (DEG), chitosan (degree of deacetylation 75% and molecular weight 156,000 Da, as determined by a viscometric method) and ethanol were purchased from Merck Specialties Pvt. Ltd, Mumbai. All the chemicals were of analytical grade (AR grade) and used without further purification. Double distilled water was used throughout the experiments.

5.2.1 Sonochemical surface coating technique

Recently, researchers are focused on the new approaches of surface coatings on nanomaterials. The surface coating technique offers many advantages due to their stability, wettability, biocompatibility, homogenous distribution on solid surfaces and improved cytotoxicity properties due to low metal concentration dissolution rate [1]. The surface coating techniques such as plasma irradiation, microwave method, screen printing technique, spray pyrolysis technique and sonochemical coating technique are reported [12].

The sonochemical coating process is a simple, one-step process of coating of nanomaterials on the surface of fabrics, papers, ceramics, and polymeric materials. This method has resulted for the formation of smooth and homogeneous coatings on the surfaces. It is also called ultrasound irradiation technique due to it requires high intensity ultrasound for the coating process. This method prevents the coated NPs aggregation and the obtained coatings are stable and uniformly

deposited on the surfaces. In addition, the sonochemical coating process provides strong adherence to the surface of substrates [8, 13].

5.2.2 Need of hybrid NPs coatings

Nanomaterials have wide applications in many fields, especially in biomedical applications. It has to bear some excellent properties i.e. high surface to volume ratio, size, stability, absorption capacity etc. However, most of the materials have relatively unstable, their stability and toxicity of cells [9]. There are different factors are included to cause nanomaterials toxicity. These are size, inherent properties, and surface chemistry. The term nanomaterials toxicity referred to as nanotoxicology [10]. The research work is being carried to improving the performance and reducing toxicity of nanomaterials by a mixing of these NPs with biocompatible materials or biodegradable/biocompatible nanomaterials. Mostly the metal oxide NPs show toxic effects as a therapy in humans or their effects on human health. Optimizing the ZnO NPs concentrations to nonhazardous levels without affecting their functional properties would be a way to diminish the cytotoxic effect of these systems. This issue is achieved by a combination of the metal oxide NPs with biocompatible materials that enhance their stability and efficacy [11].

5.2.3 Synthesis procedures

5.2.3.1 Synthesis of hybrid Chitosan-ZnO NPs

Hybrid chitosan-ZnO NPs was prepared by blending of chitosan and ZnO NPs. Chitosan 2 % solution was prepared using 4% acetic acid solution and stirred for 4 h. An undissolved chitosan particles removed by using muscling cloth. The process was repeated 2 to 3 times to prepared homogenous chitosan solution. Deposition of ZnO NPs was achieved by direct addition of ZnO NPs in prepared chitosan solution at a concentration of 1:1 ratio and stirred continuously for 2 h. After stirring hybrid chitosan-ZnO NPs solution was prepared, the hybrid solution dried in an oven at 50 ^{o}C to formed powder of chitosan-ZnO NPs.

5.2.3.2 Mechanism of synthesis of hybrid chitosan-ZnO NPs

Hybrid chitosan-ZnO NPs were successfully synthesized due to chitosan strongly forms complexes with ZnO NPs because of its free amino groups. There are two ways to form chitosan-ZnO NPs, the pendant way and the bridge way. In pendant way ions are bounds to only one amino group of chitosan and in bridge way ions are bound to several nitrogen atoms and hydroxyl groups of one or bridging more chitosan chain [14]. Figure 5.1 shows the structure of hybrid chitosan-ZnO NPs.

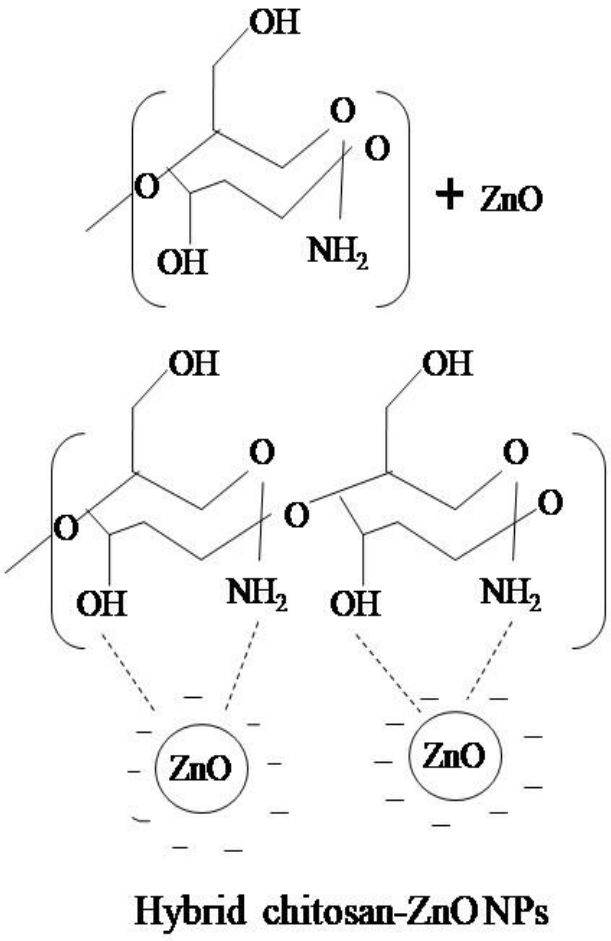

Figure 5.1 Chemical structure of hybrid chitosan-ZnO NPs

5.2.3.3 Preparation of surface coated chitosan-ZnO NPs on SF-PVA composite films

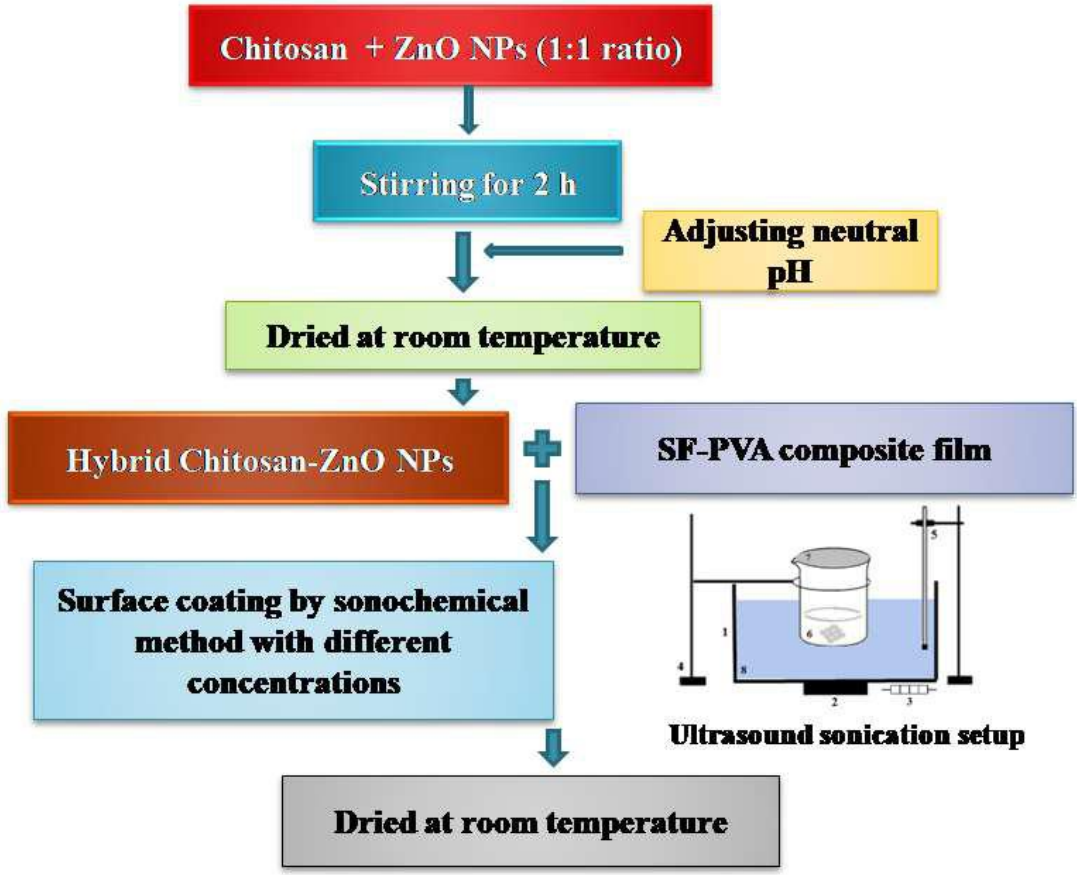

Figure 5.2 Schematic representation of preparation of surface coated SF-PVA composites with hybrid chitosan-ZnO NPs by sonochemical technique.

Surface coating of chitosan-ZnO NPs on SF-PVA composite film was carried out by a sonochemical method using ultrasonic transducer (Ti-horn, 20 KHz, 600W, Sonics and Materials VCX 600). Figure 5.2 depicts the schematic representation of the formation of hybrid chitosan-ZnO NPs coated SF-PVA composite films. During the process of coating, the concentrations of chitosan-ZnO NPs were varied, which was 0.2 wt %, 0.5 wt % and 1 wt %. The composite films was held immersed in a solution of hybrid chitosan-ZnO NPs in water, the solution was irradiated for 15 min with a high intensity ultrasonic horn in different

flasks. After sonication, the coated composite films were dried at room temperature.

5.2.3.4 Mechanism of Sonochemical coating of hybrid chitosan-ZnO NPs on SF-PVA composite films

In the first step of the experiment, hybrid chitosan-ZnO NPs mixed in water by adjusting a neutral pH. The composite film of SF-PVA cut into a similar size of 1cm × 1cm. After addition of SF-PVA composite film in the solution of hybrid chitosan-ZnO NPs, the films are settling down in the beaker containing the solution. After starting the process of sonication the hybrid chitosan-ZnO NPs simultaneously deposited on the surfaces of SF-PVA composite film. The literature protocol shows the phenomenon of the sonochemical coating process, in this process irradiation of liquid solution causes the effects of cavitation and heating [13]. When the microscopic cavitation bubbles collapsed near the surface of the solid materials, they create powerful shock waves and microjets that cause effective mixing of the adjacent liquid layer. These ultrasound waves promote the fast migration of the hybrid chitosan-ZnO NPs on the surface of SF-PVA composite film. The synthesized hybrid chitosan-ZnO NPs coated SF-PVA composite film revealed the synergistic enhancement of the antibacterial activity.

5.2.3.5 Characterization of hybrid chitosan-ZnO NPs and composite films

Studies on hybrid chitosan-ZnO NPs

Particle size and surface morphology of prepared hybrid chitosan-ZnO NPs was determined by Scanning Electron microscopy (SEM). The particle size of synthesized hybrid chitosan-ZnO NPs was also studied using the Transmission Electron Microscopy (TEM).

Studies on hybrid chitosan-ZnO NPs coated composite films

Structural analysis

The synthesized chitosan-ZnO NPs coated SF-PVA and uncoated SF-PVA composite films were characterized using X-ray diffraction (XRD) Rigaku 600

Miniflex X-ray diffraction instrument in the range 10^{o}-60^{o}. XRD (X-ray diffraction) analysis was used to study the crystalline structure of synthesized composite films.

Spectroscopic analysis

The functional groups presented in prepared composite films were examined using Fourier transform infrared (FTIR) spectroscopy. FTIR analysis was recorded on a Bruker ALPHA 100508, the USA in the range 4000-400 cm^{-1}.

Morphological analysis

The surface morphology of the coated and uncoated composite films was determined with an SEM (Scanning Electron microscopy), Model (JEOL Model JSM - 6390LV).

Energy Dispersive X-Ray Analysis (EDX)

The elemental analysis of hybrid chitosan-ZnO NPs coated SF-PVA and uncoated SF-PVA composite films was done by Energy Dispersive X-ray (EDX) spectroscopy using Zeiss Ultra FEG 55.

Mechanical properties

The mechanical properties of as-prepared SF-PVA and hybrid chitosan-ZnO NPs coated SF-PVA composite films were characterized using universal testing machine (UTM) with a Winsoft tensile and compression testing machine (Shimadzu AG) 100 KN load cell at 25 ^{o}C. Composite films were cut into double shaped strips measuring 4 cm long and 1 cm wide. The gauge length was 2 cm between clamps. These were examined at a crosshead speed of 5 min^{-1}. The tensile strength % elongation of coated and uncoated composite films was determined from the stress and strain data.

Porosity study by gas volumetric analysis

Nitrogen gas adsorption was used to determine Brunauer-Emmet-Teller specific surface area (BET) and porosity characteristics of composite films. 0.1-0.2 g films samples were first degassed in the Quantachrome Instruments Version 3.0 (Nova Station 0) automated system at 150 ^{o}C for 8 h. The specific surface area (S_{BET}) of composite films was determined by the BET method based on nitrogen adsorption isotherm data. The average pore diameter was estimated by Barrett-Joyner-Halendar method (BJH) [15].

Swelling study

Swelling degree of composite films was studied by reported method [4]. Briefly, the synthesized composite films cut into the uniform size and weight and dipped into Phosphate Buffered Saline (PBS) of pH 7.4 at room temperature until saturation. Then the composite films were removed, their surfaces were scrubbed softly, and composite films pieces were weighted. The degree of swelling was calculated using the formula 3.9.

Biodegradation study

The biodegradation of coated and uncoated composite films was evaluated by preparing a medium of PBS of pH 7.5 containing lysozyme enzyme. The composite films were cut into the similar size and weight, after cutting the composite films immersed in PBS containing lysozyme (10,000U/mL) and incubated at 37^{o} C for 21 days. The degradation rate is calculated by using the formula 4.3.

5.3 Results and Discussion

5.3.1 Studies on synthesized hybrid chitosan-ZnO NPs

5.3.1.1 SEM

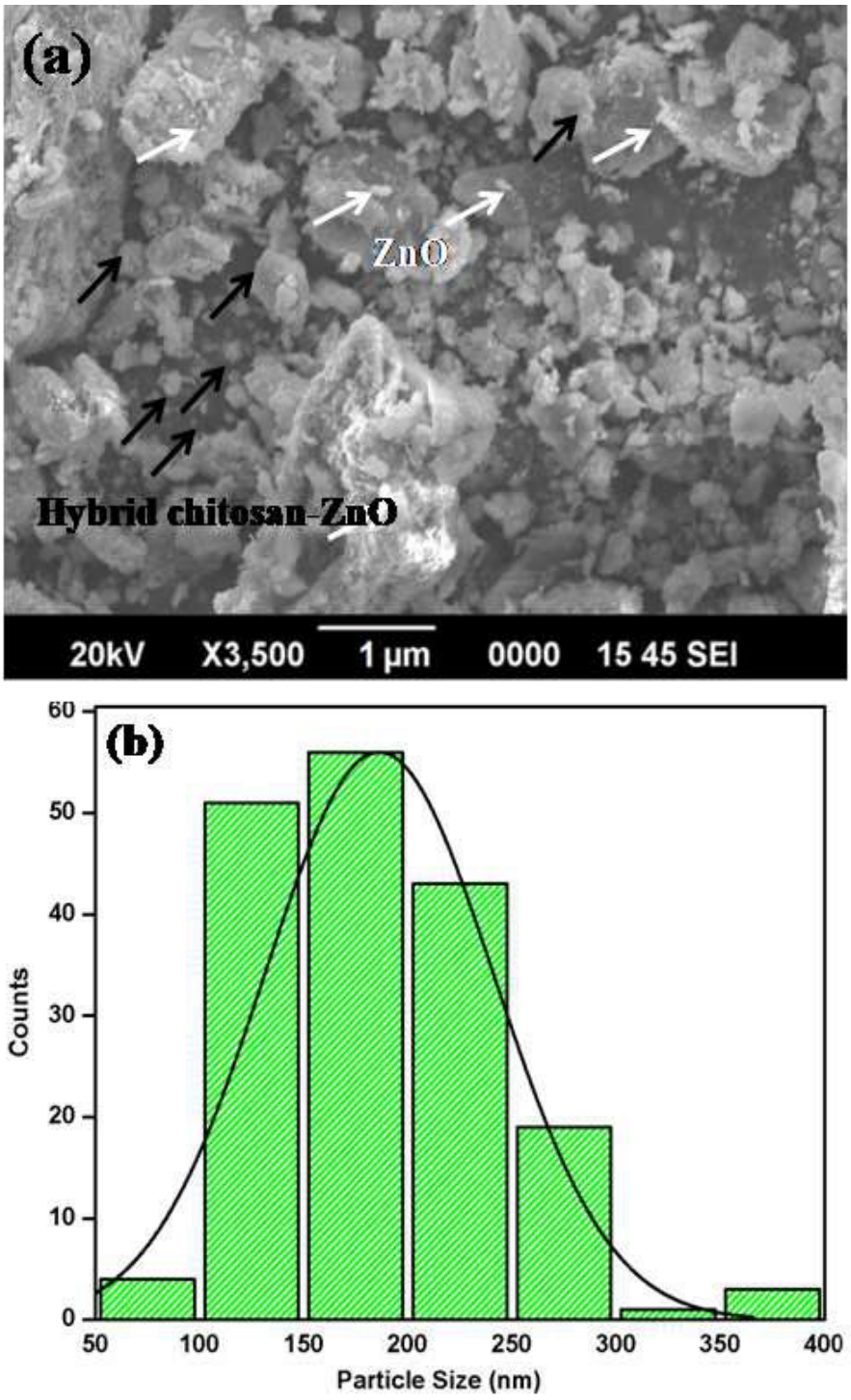

Figure 5.3 (a) surface morphology and **(b)** particle size of chitosan-ZnO NPs**.**

Figure 5.3 (a) shows the SEM image of synthesized hybrid chitosan-ZnO NPs. The image clearly observed that the ZnO NPs and chitosan are combined together. The white arrows show the ZnO NPs and black arrows observed the hybrid chitosan-ZnO NPs. Figure 5.3 (b) shows the particle size distribution of hybrid chitosan-ZnO NPs. The average particle size of synthesized chitosan-ZnO NPs is measured using the Image J software. The average particle size of synthesized chitosan-ZnO NPs is ~ 168 nm.

5.3.1.2 TEM of chitosan-ZnO NPs

The particle size of synthesized chitosan-ZnO NPs was measured using the TEM analysis. Figure 5.4 represents the TEM image of hybrid chitosan-ZnO NPs. The average particle size of synthesized chitosan-ZnO NPs is ~ 150-160 nm.

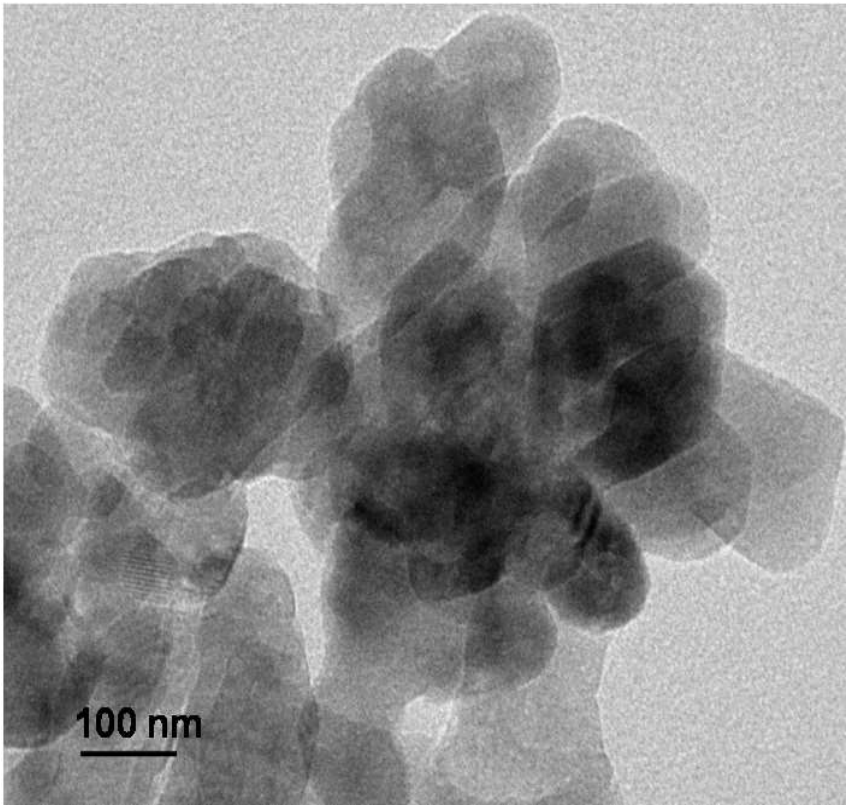

Figure 5.4 TEM of hybrid chitosan-ZnO NPs.

5.3.2 Studies on hybrid chitosan-ZnO NPs coated composite films

5.3.2.1 X-ray diffraction study

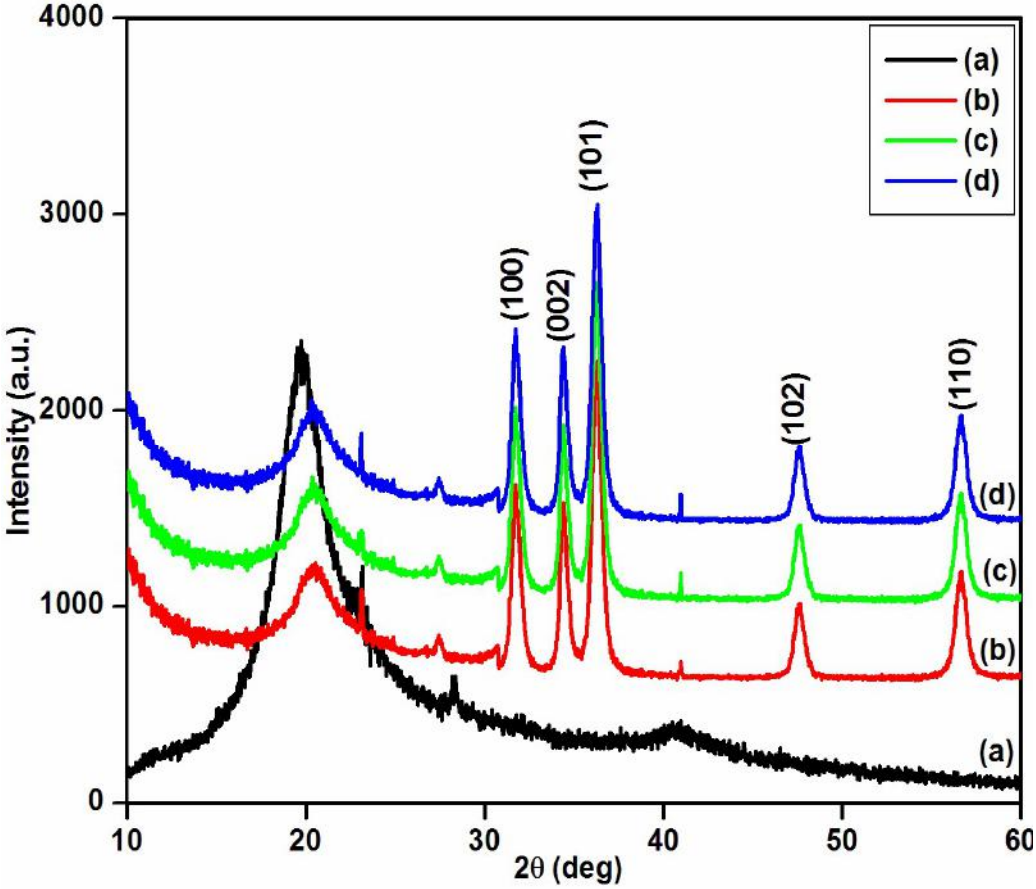

Figure 5.5 XRD spectra of **(a)** SF-PVA, **(b)** 0.2 wt %, **(c)** 0.5 wt %, and **(d)** 1 wt % hybrid chitosan-ZnO NPs coated SF-PVA composite films.

Figure 5.5 shows the XRD patterns of chitosan-ZnO NPs coated SF-PVA composite films with different coating concentrations and uncoated SF-PVA composite film. Figure 5.5 (a) shows the XRD pattern of SF-PVA composite film. Two broad signals at 2θ = 19.9° and 40.1° are attributed to the amorphous SF-PVA composite film [16]. The diffraction peaks at 2θ = 23.1° and 2θ = 28.5° attributed to silk II, β- sheet crystalline structure, and silk I of SF, respectively. Figure 5.5 (b) shows the XRD pattern of 0.2 wt % coated composite film, Figure 5.5 (c) shows the XRD pattern of 0.5 wt % coated composite film and Figure 5.5 (d) shows the XRD pattern of 1 wt % coated composite film. All the chitosan-ZnO

NPs coated composite films depicts the peaks at $2\theta = 10^{o}$, and $2\theta = 20.3^{o}$ is the chitosan and peaks at $2\theta = 19.98^{o}$, 23.1^{o}, 40.1^{o}, and 28.5^{o} corresponds to silk II, β-sheet crystalline structure, PVA, and silk I of SF respectively [16, 17]. All the coated composite films are observed the diffraction peaks at $2\theta = 31.7^{o}$, 34.4^{o}, 36.2^{o}, 47.5^{o}, 56.6^{o}, are assigned to (100), (002), (101), (102) and (110) planes of ZnO NPs [18]. The diffraction peaks of ZnO NPs matches with the JCPDS card No. 39-1451.

These results proved the successful coating of chitosan-ZnO NPs on SF-PVA composite film. The most intense peak (101) is used to calculate the FWHM for determination of crystallite size (D) by Scherer's formula, 3.2 [18]. The average crystallite size calculated by equation (3.2) is found to be ~ 13 nm. In addition, the peaks of coated composite films appeared intense after coating with chitosan-ZnO NPs. The increase in intensity is due to the effect of increased concentration of chitosan-ZnO NPs on SF-PVA composite film.

5.3.2.2 FTIR spectroscopy analysis

Figure 5.6 represents the FTIR spectra of hybrid chitosan-ZnO NPs coated SF-PVA and uncoated SF-PVA composite films. Figure 5.6 (a) shows the FTIR spectra of SF-PVA composite film. It shows the absorption band at 3270 cm^{-1} is attributed to hydroxyl groups (OH). The absorption bands at 2917 cm^{-1} referred to stretching of CH_2 groups. The peak position at 1652 cm^{-1} indicates random coil structure of amide I (C-O stretching). The peaks at around 1530 cm^{-1} shows amide II (N-H deformation) and those at 1250 cm^{-1} indicates random coil structure of amide III (C-N stretching) [19]. The peaks at around 1085 cm^{-1} and 1415 cm^{-1} attributed to C-O resonance.

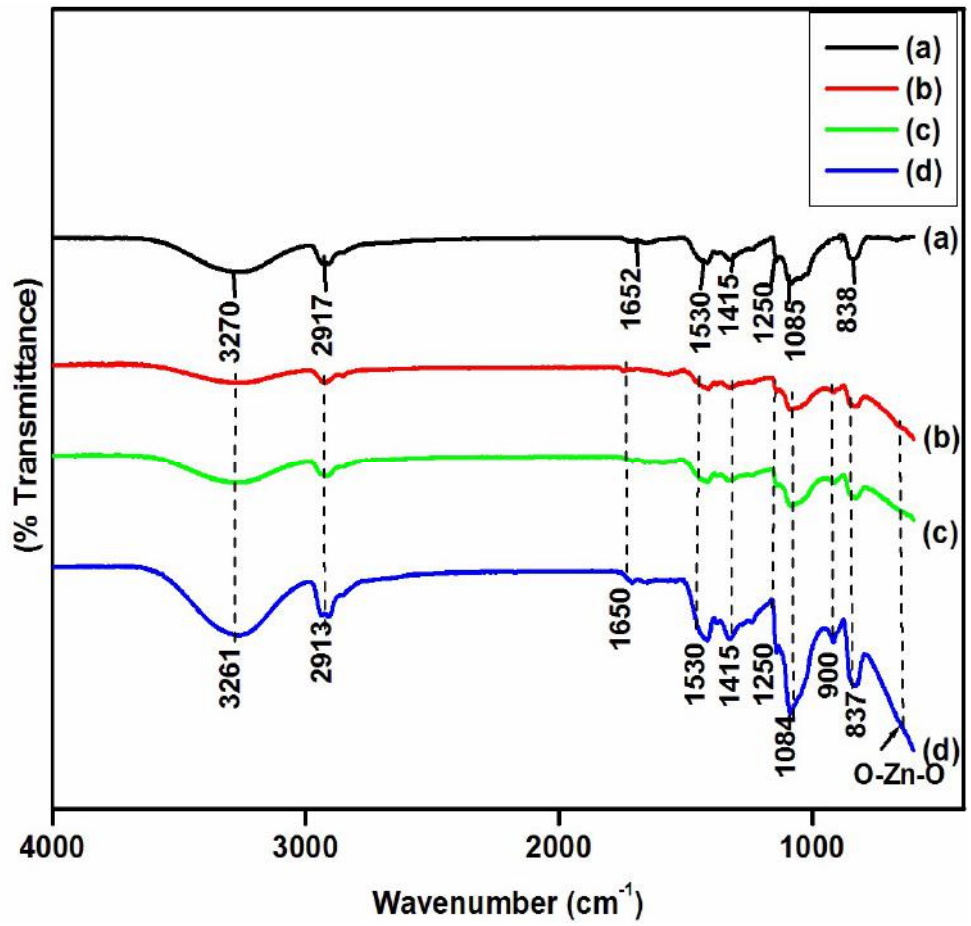

Figure 5.6 FTIR spectra of **(a)** SF-PVA, **(b)** 0.2 wt %, **(c)** 0.5 wt %, and **(d)** 1 wt % hybrid chitosan-ZnO NPs coated SF-PVA composite films

Figure 5.6 (b), (c), and (d) shows the FTIR spectra of 0.2 wt %, 0.5 wt % and 1 wt % hybrid chitosan-ZnO NPs coated composite films, respectively. It represents absorption bands in the range of 3261 cm^{-1} attributed to OH groups and NH stretching bands. The absorption peaks at 2913 cm^{-1} are stretching bands of CH_2. The absorption peaks of chitosan and SF are attributed to C=O stretching (amide I) at 1650 cm^{-1}, NH bending (amide II) at1530 cm^{-1} and C-N stretching (amide III) at 1250 cm^{-1}. The absorption bands at around 900 cm^{-1}, which are attributed to the saccharide structure of chitosan [20]. The peaks at around 1084 cm^{-1}, 1415 cm^{-1}, and 837 cm^{-1} are attributed to C-O resonance. Compared with uncoated SF-PVA composite film, a new broad absorption band at the range of 450 cm^{-1}- 550 cm^{-1} are found in the FTIR spectra of all the coated SF-PVA

composite films, which are ascribed to the vibration of O-Zn-O groups [21]. This band increases with increase in the concentration of hybrid chitosan-ZnO NPs. The characteristic peaks of OH group of coated composite films are shifted to a slightly lower wavenumber, due to the formation of strong hydrogen bonding between hybrid chitosan-ZnO NPs and SF-PVA composite film.

5.3.2.3 Surface morphology

Surface morphology of coated and uncoated composite films was observed with SEM at an accelerated voltage of 20 KV. Figure 5.7 (a) depicts the surface morphology of uncoated, SF-PVA composite film. It is distinctly noticed that the SF microspheres are present into the PVA matrix. The detected SF microspheres are round and spherical in shape and the size of SF microspheres is between 2 to 3 μm. Figure 5.7 (b) represents the SEM image of ZnO NPs and it is a spherical shaped structure. The SEM, of coated composite films with different concentrations of 0.2 wt %, 0.5 wt %, and 1 wt % are shown in Figure 5.7 (d) and (e), respectively.

It is clearly observed that the coated composite films show the slight aggregation of chitosan-ZnO NPs on SF-PVA composite films. The hybrid NPs left over in the solution after the sonication process, which shows aggregated morphology of coated composite films. This may be due to the higher concentration of hybrid chitosan-ZnO NPs on SF-PVA composite films.

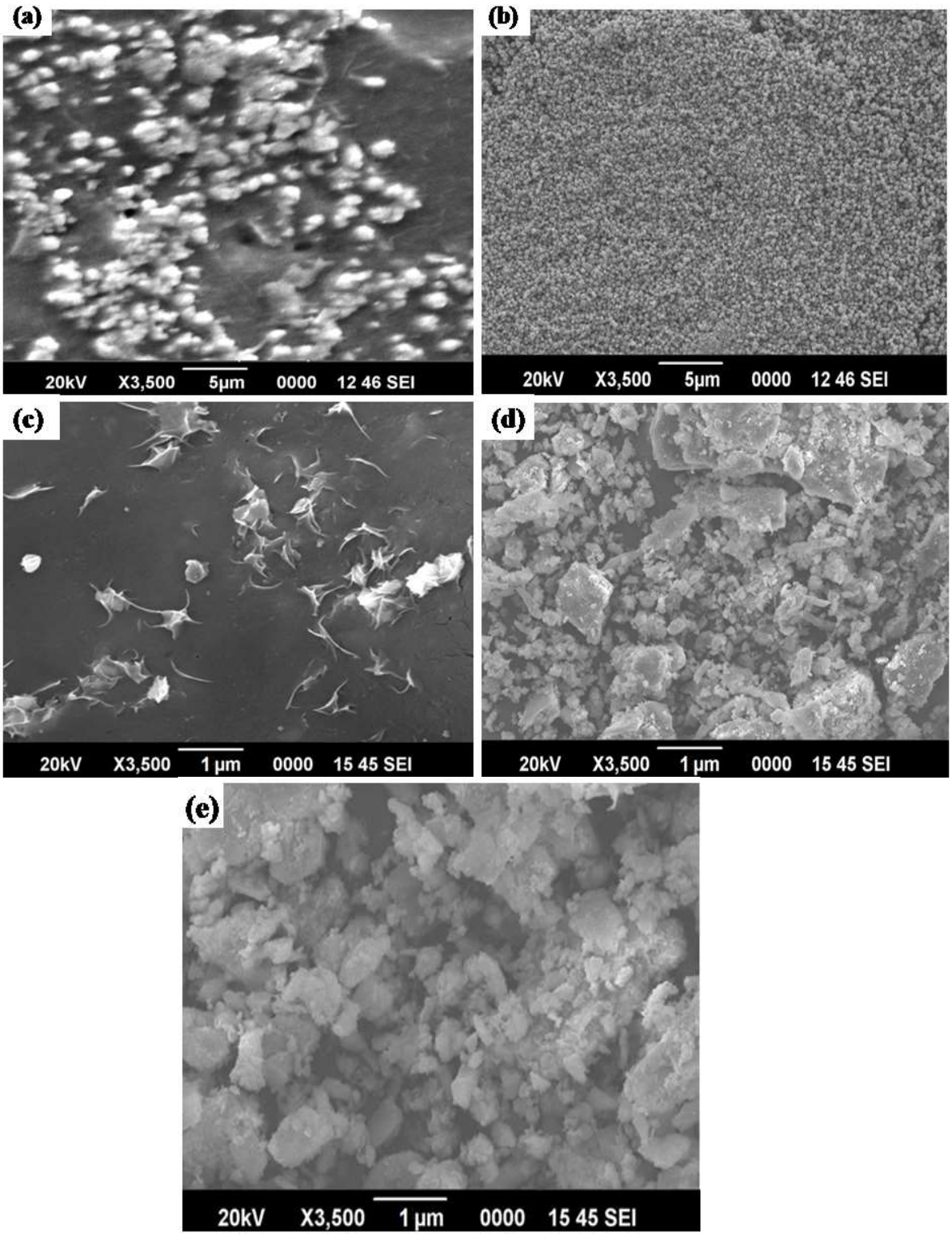

Figure 5.7 SEM images of **(a)** SF-PVA, **(b)** ZnO NPs **(c)** 0.2 wt %, **(d)** 0.5 wt %, and **(e)** 1 wt % hybrid chitosan-ZnO NPs coated SF-PVA composite films examined at 3,500 X magnifications.

5.3.2.4 Surface area and porosity by gas volumetric analysis

The specific surface area of coated and uncoated composite films was investigated by measuring nitrogen adsorption desorption isotherms in Fig. 5.8 (A) at 77 K. According to the IUPAC terminology, all the sorption isotherms are of type IV, which involves adsorption on mesopores adsorbents (2 - 50 nm) [22]. The specific surface area of the composite films is determined from the adsorption isotherms at a relative pressure below 0.99 using BET analysis. The SF-PVA composite film shows the specific surface area is about 12.17 m^2/g. The obtained surface area is due to the silk microspheres present in the PVA matrix. The 0.2 wt % hybrid chitosan-ZnO NPs coated composite films shows the specific surface area is about 12.75 m^2/g, 0.5 wt % coated composite film shows the specific surface area is 19.28 m^2/g and 1 wt % coated composite film shows the specific surface area is about 41.39 m^2/g. Additionally, the Sterizone dressing shows the specific surface area is about 18.14 m^2/g. All the coated composite films have a higher specific surface area than uncoated SF-PVA and Sterizone dressing, which can give uniform antibacterial activity as well as reduce the infection.

Pore size distribution analysis was carried out by (BJH) method [15]. Pore size distribution shows mesopores ranging from 2 to 24 nm (Fig. 5.8, B). The SF-PVA composite film shows the pore diameter is about 1.231 nm. The 0.2 wt % hybrid chitosan-ZnO NPs coated composite films shows the pore diameter is about 1.486 nm, 0.5 wt % coated composite film shows the pore diameter is 2.358 nm and 1 wt % coated composite film shows the pore diameter is about 3.551 nm. The Sterizone dressing shows the pore diameter is about 3.442 nm. The appearance of larger pores is assigned to the coating of a higher concentration of hybrid chitosan-ZnO NPs. These results collectively suggest the coating of hybrid chitosan-ZnO NPs on SF-PVA composite film with great porosity.

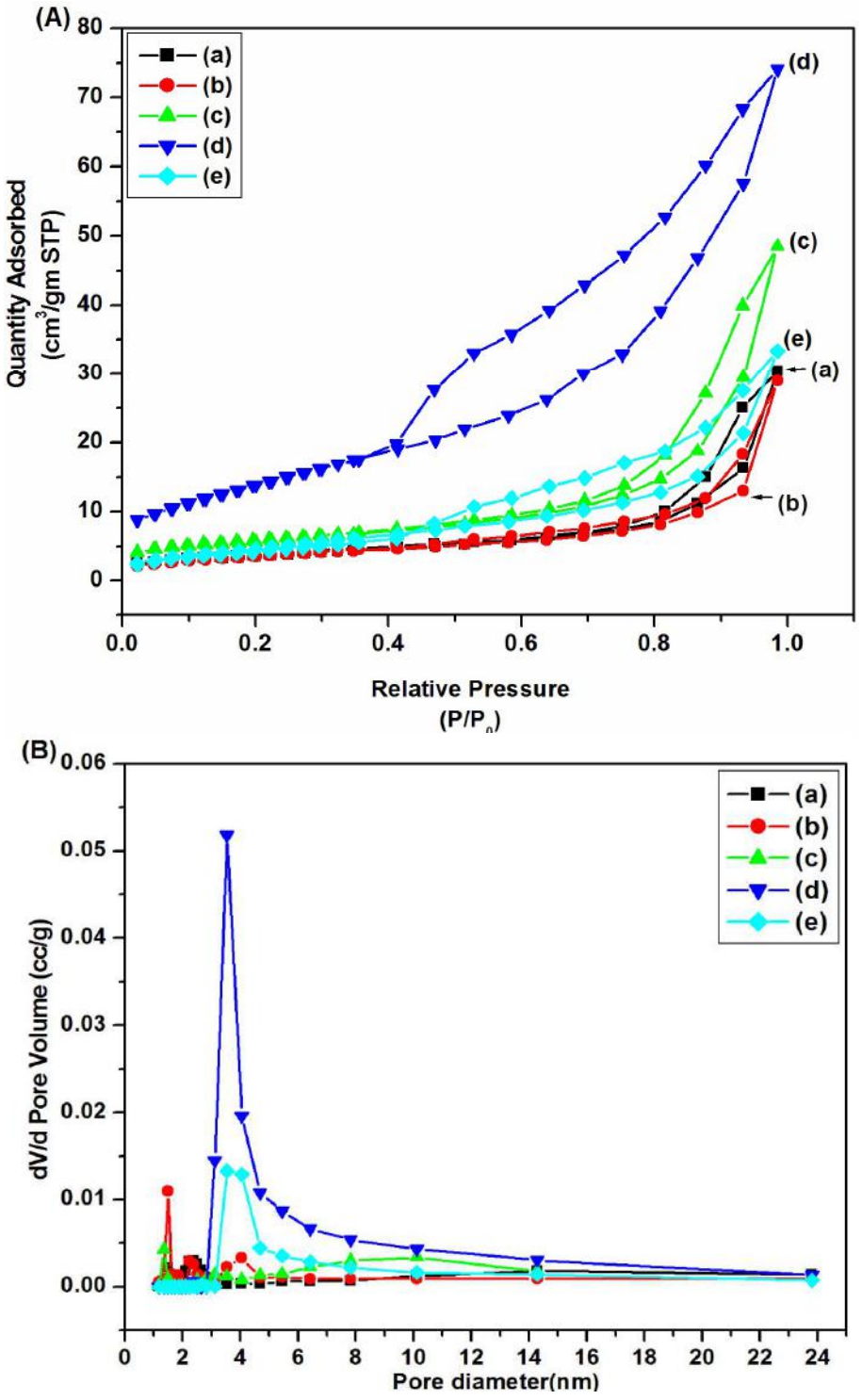

Figure 5.8 (A) N_2 adsorption desorption isotherms and **(B)** BJH mesopores size distribution of **(a)** SF-PVA **(b)** 0.2 wt %, **(c)** 0.5 wt %, **(d)** 1 wt % hybrid chitosan-ZnO NPs coated SF-PVA composite films and **(e)** Sterizone dressing.

5.3.2.5 EDX Analysis

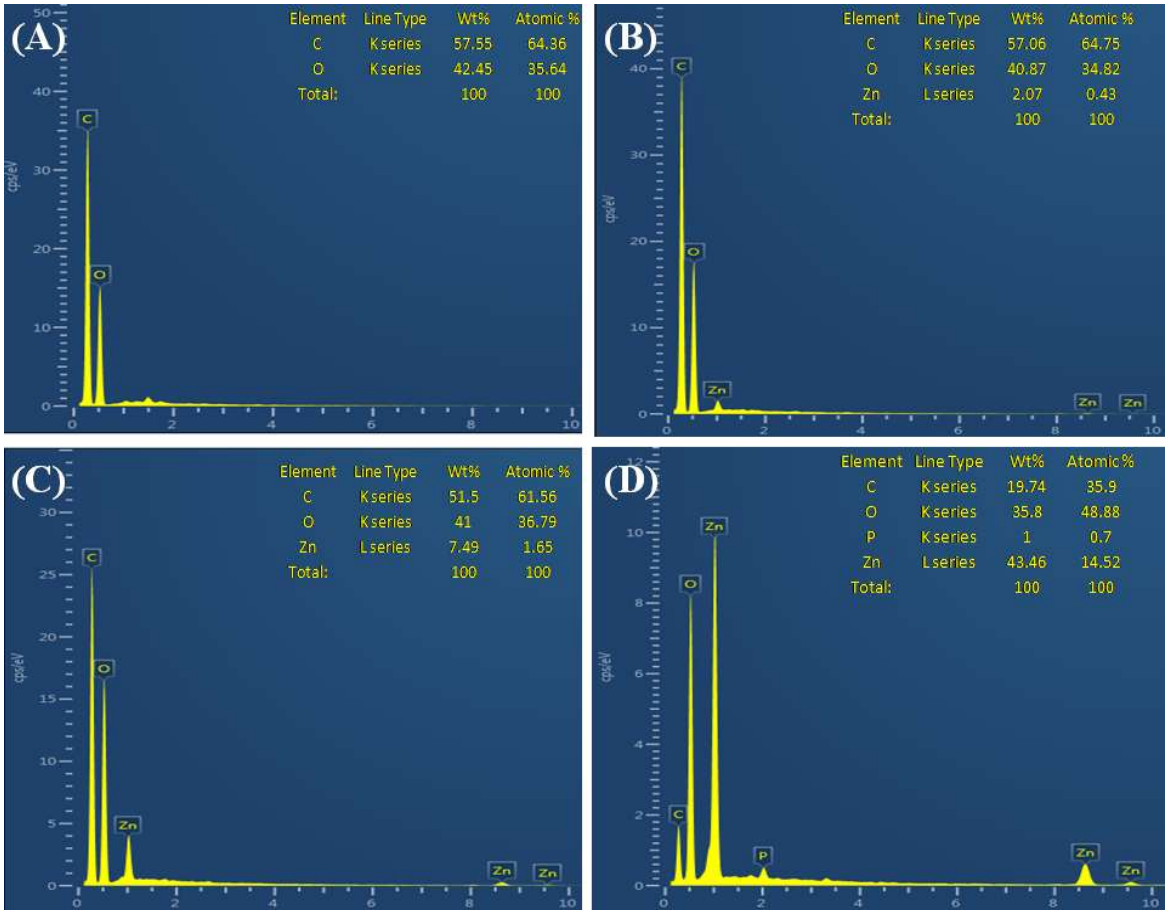

Figure 5.9 EDX studies of **(A)** SF-PVA **(B)** 0.2 wt %, **(C)** 0.5 wt % and **(D)** 1 wt % hybrid chitosan-ZnO NPs coated SF-PVA composite films

The elemental analysis of coated and uncoated composite films was studied by EDX analysis. Figure 5.9 (A) depicts the EDX of SF-PVA composite film. The EDX study observed presence of C and O elements, which confirms the developed composite films are of impurity free. Figure 5.9 (B), (C) and (D) shows the EDX of 0.2 wt %, 0.5 wt % and 1 wt % hybrid chitosan-ZnO NPs coated SF-PVA composite films respectively. It is identified only carbon, zinc, oxygen, and phosphorus elements. This analysis suggests that hybrid chitosan-ZnO NPs are successfully prepared and it deposited on the surface of SF-PVA composite films.

5.3.2.6 Mechanical property of chitosan-ZnO NPs coated SF-PVA Composite films

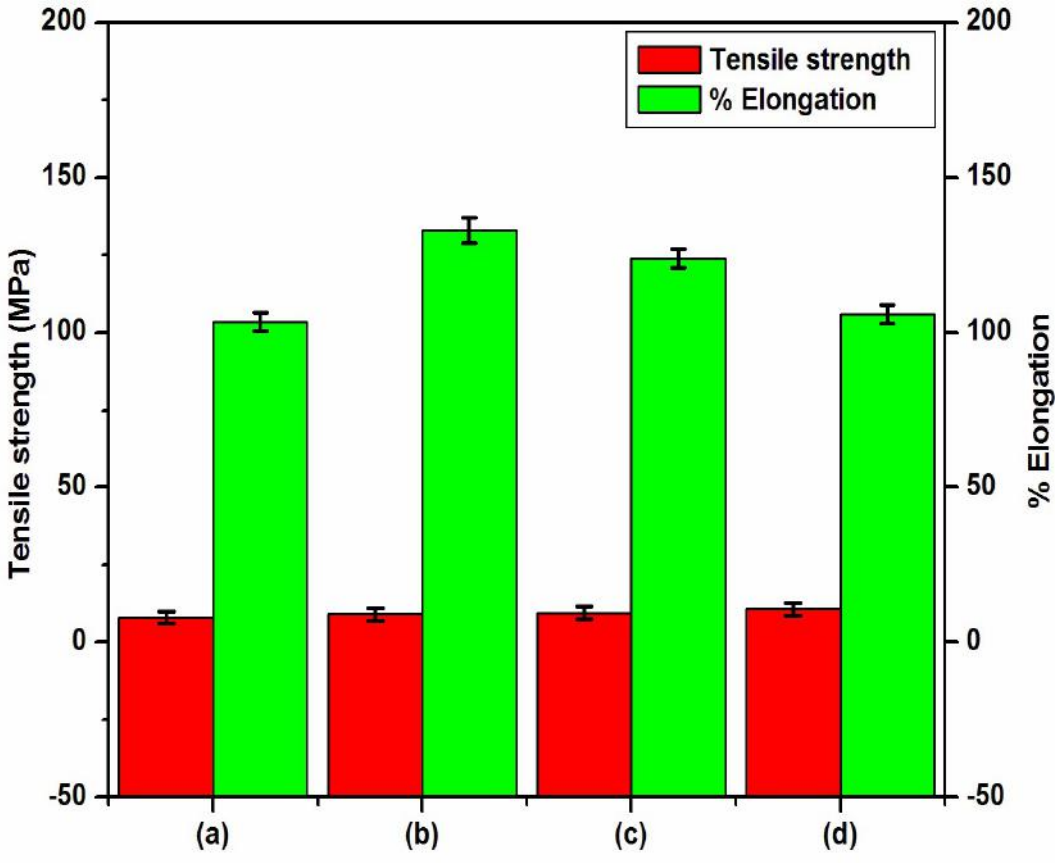

Figure 5.10 Mechanical properties of **(a)** SF-PVA, **(b)** 0.2 wt %, **(c)** 0.5 wt %, and **(d)** 1 wt % chitosan-ZnO NPs coated SF-PVA composite films.

Figure 5.10 represents the mechanical property of coated and uncoated composite films. The uncoated figure 5.10 (a) SF-PVA composite film shows the tensile strength of 8 MPa and percent elongation of 103 %. The coated composite film of figure (b) 0.2 wt % shows the tensile strength of 9 MPa and percent elongation of 133 %. The figure (c) 0.5 wt % depicts the tensile strength of about 9.4 MPa and percent elongation of about 124 %. The figure (d) 1 wt % represents the tensile strength of 10.6 MPa and percent elongation of 106 %. It could be concluded that the coating of a higher concentration of hybrid chitosan-ZnO NPs on SF-PVA composite films shows enhanced tensile strength and reduced the percent elongation of coated composite films. The mechanical properties of all the

coated composite films are better than uncoated SF-PVA composite film. The obtained tensile strength and percent elongation of all the composite films are excellent for wound dressing applications [23]. Hybrid chitosan-ZnO NPs forms the intermolecular hydrogen bonding between –OH and $–NH_2$ group, which are easily rotated the molecular chain of chitosan. When chitosan-ZnO NPs coated on the surface of SF-PVA composite film the intermolecular bonding of hydrogen were weakened and formed new hydrogen bonding between chitosan-ZnO NPs and SF-PVA matrix. Therefore, the tensile strength of coated composite films is increased compared to uncoated SF-PVA composite film. The reported study suggests that the mechanical property of composite films increased when 1 wt % of ZnO NPs are incorporated into composite films [24]. Our results of mechanical properties show coating of 1 wt % concentration of hybrid chitosan-ZnO NPs to SF-PVA composite film is highest mechanical property than other less concentration coating process.

5.3.2.7 Swelling study

The figure 5.11 shows the swelling ratio of (a) uncoated SF-PVA composite film, (b) 0.2 wt % coated SF-PVA, (c) 0.5 wt % coated SF-PVA, (d) 1 wt % coated SF-PVA, and (e) Sterizone dressing. The concentration of 1 wt % hybrid chitosan-ZnO NPs coated SF-PVA composite film shows higher swelling ratio compared to control uncoated SF-PVA composite film and Standard Sterizone dressing. This is due to the chitosan-ZnO NPs present on the surface of SF-PVA composite film and has more porosity compared to control. The swelling ratio of composite films was increased with increasing the concentration of coated hybrid chitosan-ZnO NPs on SF-PVA composite films as well as the time after 7 days of immersion in PBS. The results suggest that the coated composite films will have better exudates uptake capacity of up to 1 week, which is important in a wound dressing. Therefore, the results concluded that there is no need to change the dressing for up to 1week.

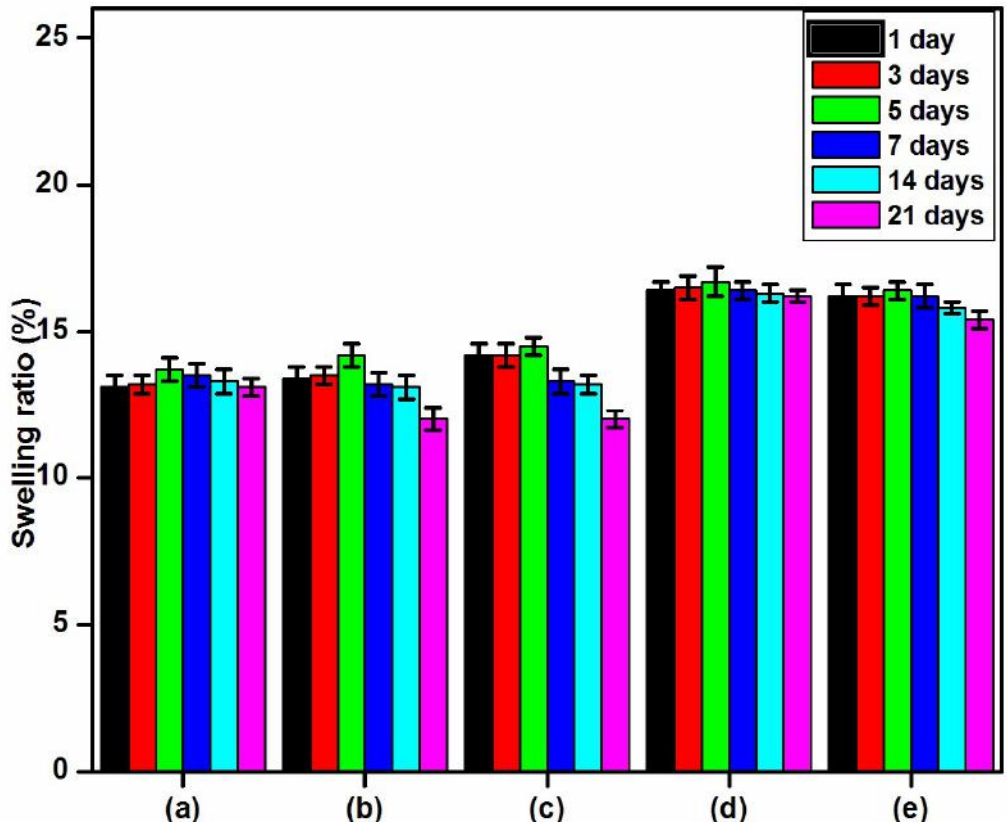

Figure 5.11 Swelling ratio of **(a)** SF-PVA, **(b)** 0.2 wt %, **(c)** 0.5 wt %, **(d)** 1 wt % hybrid chitosan-ZnO NPs coated SF-PVA composite films and **(e)** Sterizone dressing.

5.3.2.8 Biodegradation study of hybrid chitosan-ZnO NPs coated SF-PVA Composite films

Biodegradation study of hybrid chitosan-ZnO NPs coated and uncoated SF-PVA composite films is represented in figure 5.12. It is observed that the composite film of SF-PVA shows 40-50 % degradation after 7 days, 14 days and 21 days. The degradation of 0.2 wt % and 0.5 wt % chitosan-ZnO NPs coated SF-PVA composite film shows 35-40 % after 7 days, 14 days and 40-45 % after 21 days. The degradation of 1 wt % chitosan-ZnO NPs coated SF-PVA composite film shows 40-45 % after 7 days and 45-50 % after 14 days and 21 days. The degradation rates of Sterizone dressing observe 35-40 % after 7 days, 14 days and 21 days. The results indicate that all the hybrid chitosan-ZnO NPs coated SF-PVA composite films have higher degradation as compared to Sterizone dressing. The

rate of degradation increases with increase in the concentration as well as the duration of time. The degradation rate of SF-PVA composite film has higher as compared to all coated composite films and Sterizone dressing due to both the SF and PVA are higher biodegradable agents as compared to pure ZnO NPs.

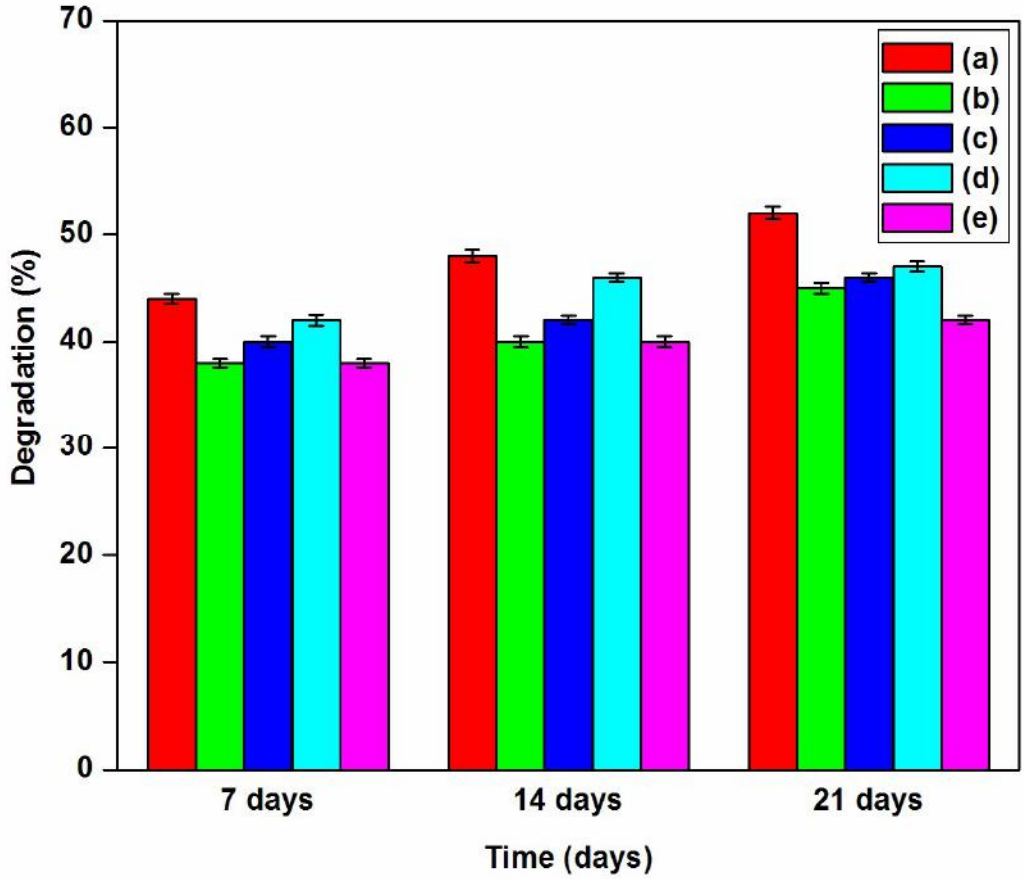

Figure 5.12 Biodegradation study of **(a)** SF-PVA, **(b)** 0.2 wt %, **(c)** 0.5 wt %, **(d)** 1 wt % hybrid chitosan-ZnO NPs coated SF-PVA composite films and **(e)** Sterizone dressing.

5.4 Effect of coated hybrid chitosan-ZnO NPs on SF-PVA composite film

During the process of coating of hybrid NPs on SF-PVA composite films, the hybrid NPs mixed in the water at concentrations of 0.2 wt %, 0.5 wt %, and 1wt % and adjusting a neutral pH. If the pH was acidic or alkaline, then the composite film of SF-PVA was shrinking during the coatings process. The physicochemical characterizations of coated composite films were done. The XRD

and FTIR spectra of coated composite films observed the crystalline nature and chemical composition. The morphological study indicated that the SF-PVA composite film contains SF microspheres inserted into SF-PVA composite films while the hybrid chitosan-ZnO NPs coated composite films reveals that the hybrid NPs coated on the surface of SF-PVA composite films. The coating was enhanced by increasing the concentrations of hybrid NPs. The surface area and porosity of composite films were determined by adsorption-desorption isotherms of BET analysis. The SF-PVA composite film show the specific surface area about 12.17 m^2/gm whereas the coated composite films shows the specific surface area about 12.75-41.39 m^2/gm. The specific surface area of coated composite films is increased with increase in the concentration of hybrid NPs. The SF-PVA composite film shows the pore diameter is 1.64 nm and the coated composite films show the pore diameter is about 2-24 nm. The mechanical property of all the coated composite films is higher tensile strength and % elongation compared to SF-PVA composite film. The swelling study concluded that the 1 wt % hybrid NPs coated composite films shows the higher swelling ability than other coated composite films, uncoated SF-PVA composite films and Sterizone dressing. The biodegradation study indicated that the uncoated SF-PVA and hybrid NPs coated composite films have a higher degradation rate compared to Sterizone dressing. For comparative study, SF-PVA composite films show higher biodegradation rated than hybrid NPs coated composite films due to both the SF and PVA are higher biodegradable agents than ZnO NPs.

5.5 Conclusions

The high surface area and synergistic antibacterial activity of hybrid chitosan-ZnO NPs coated SF-PVA composite films provide potential dressing materials for antibacterial wound dressings. It has been seen that hybrid chitosan-ZnO NPs successfully coated on the surface of SF-PVA composite films by using sonochemical coating techniques. The hybrid chitosan-ZnO NPs are developed by mixing the chitosan and ZnO NPs. It is noticed that the SF-PVA composite film shows the specific surface area is 12.17 m^2/g and the diameter of the mesopores is

~2-24 nm. Hybrid chitosan-ZnO NPs coated composite films have a higher specific surface area than uncoated SF-PVA and Sterizone dressing, which can give uniform antibacterial activity as well as reduce the infection. The elemental analysis of coated and uncoated composite films is carried out by EDX spectroscopy. It is observed that synthesized composite films are impurity free, suggested that hybrid chitosan-ZnO NPs are successfully coated on the surface of SF-PVA composite films. The swelling degree, mechanical property and biodegradability study of coated composite films increases with increasing the concentrations of chitosan-ZnO NPs on SF-PVA composite film as compared to uncoated SF-PVA and Sterizone dressing. The obtained results encourage the use of 1 wt % of hybrid chitosan-ZnO NPs coated SF-PVA composite films could be used as an excellent materials for antibacterial wound dressings.

References

1. A. Gupta, M. Gupta, Biomaterials, 2005, 26, 3995-4021.
2. Y. Lvov, P. Pattekari, X. Zhang, V. Torchilin, Langmuir, 2010, 27, 1212-1217.
3. A. Khalid, R. Khan, M. Ul-Islam, T. Khan, F. Wahid, Carbohydr Polym, 2017, 164, 214-221.
4. P. Sudheesh Kumar, V. Lakshmanan, T. Anilkumar, C. Ramya, P. Reshmi, A. G. Unnikrishnan, R. Jayakumar, ACS Appl Mater Interfaces, 2012, 4, 2618-2629.
5. N. Padmavathy, R. Vijayaraghavan, Sci Technol Adv Mater, 9, 2008, 035004-035004.
6. M. Khorasani, A. Joorabloo, A. Moghaddam, H. Shamsi, Z. Mansoori Moghadam, Int J Biol Macromol, 2018, 114, 1203-1215.
7. M. Salat, P. Petkova, J. Hoyo, I. Perelshtein, A. Gedanken, T. Tzanov, Carbohydr Polym, 2018, 189, 198-203.
8. P. Kamali, N. Talebian, J Coat Technol Res, 2018, 15, 1133-1144.
9. A. Burns, W. T. Self, Smart Nano Biomed, 2018, 159-169.
10. A. Clippinger, D. Allen, H. Behrsing, P. Hinderliter, R. Landsiedel, E. Reinke, V. Stone, Appl In Vitro Toxicol, 2018, 4, 82-88
11. S. Marpu, E. Benton, Int J Mol Sci, 2018, 19, 1795-1795.
12. S. Kango, S. Kalia, A. Celli, J. Njuguna, Y. Habibi, R. Kumar, Prog Polym Sci, 2013, 38, 1232-1261.
13. I. Perelshtein, G. Applerot, N. Perkas, G. Guibert, S. Mikhailov, A. Gedanken, Nanotechnology, 2008, 19, 245705-245705.
14. M. AbdElhady, Int J Carbohyd Chem, 2012, 840591, 1-6.
15. H. Sehaqui, Q. Zhou, L. A. Berglund, Compos Sci Technol, 2011, 71, 1593-1599.
16. J. Kundu, L. Poole-Warren, P. Martens, S. Kundu, Acta Biomater, 2012, 8, 1720-1729
17. R. Salehi, M. Arami, N. Mahmoodi, H. Bahrami, S. Khorramfar, Colloids

Surf B, 2010, 80, 86-93.

18. P. Chang, J. Yu, X. Ma, D. Anderson, Carbohydr Polym, 2011, 83, 640-644.
19. Y. Park, H. Ju, J. Lee, D. Kim, O. Lee, B. Moon, H. Park, J. Jeong, Y. Yeon, C. Park, Int J Biol Macromol,2016, 93, 1567-1574.
20. Z. Gu, H. Xie, C. Huang, L. Li, and X. Yu, Int J Biol Macromol, 2013, 58 121-126.
21 H. Toiserkani, Compos Interface, 2016, 23, 175-189.
22. F. Marrakchi, M. Auta, W. Khanday, B. Hameed, Adv Powder Technol, 2017, 321, 428-434
23. W. Lin, C. Lien, H. Yeh, C. Yu, S. Hsu, Carbohydr Polym, 2013, 94 603-611.
24. L. Li, J. Deng, H. Deng, Z. Liu, L. Xin, Carbohydr Res, 2010, 345, 994-998.

CHAPTER 6

Biocompatibility Study of SF based Composite Films

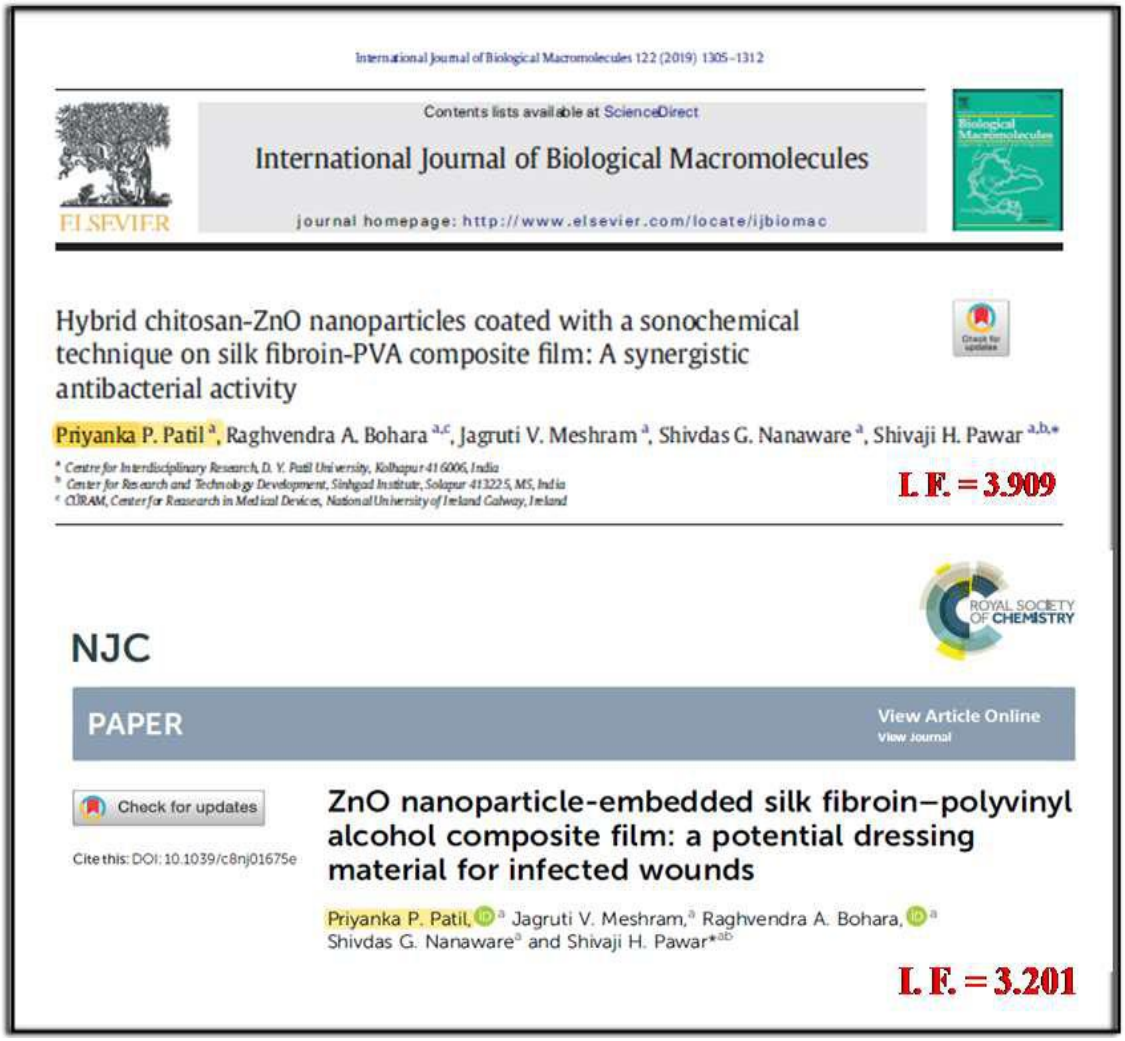

International Journal of Biological Macromolecules 122 (2019) 1305–1312

Contents lists available at ScienceDirect

International Journal of Biological Macromolecules

journal homepage: http://www.elsevier.com/locate/ijbiomac

ELSEVIER

Hybrid chitosan-ZnO nanoparticles coated with a sonochemical technique on silk fibroin-PVA composite film: A synergistic antibacterial activity

Priyanka P. Patil [a], Raghvendra A. Bohara [a,c], Jagruti V. Meshram [a], Shivdas G. Nanaware [a], Shivaji H. Pawar [a,b,*]

[a] Centre for Interdisciplinary Research, D. Y. Patil University, Kolhapur 416006, India
[b] Center for Research and Technology Development, Sinhgad Institute, Solapur 413255, MS, India
[c] CURAM, Center for Research in Medical Devices, National University of Ireland Galway, Ireland

I. F. = 3.909

NJC

ROYAL SOCIETY OF CHEMISTRY

PAPER

View Article Online
View Journal

Check for updates

Cite this: DOI: 10.1039/c8nj01675e

ZnO nanoparticle-embedded silk fibroin–polyvinyl alcohol composite film: a potential dressing material for infected wounds

Priyanka P. Patil,[a] Jagruti V. Meshram,[a] Raghvendra A. Bohara,[a] Shivdas G. Nanaware[a] and Shivaji H. Pawar*[ab]

I. F. = 3.201

6.1 Introduction

The biocompatibility study of nanobiomaterials becomes an important issue in nanotechnology. The term biocompatibility is defined as the capability of biomaterials to perform host response to biomaterials [1]. The capability of biomaterials is to be in contact with a living system without producing adverse effects. Hence, the evaluation of biocompatibility is one of the important parts of the overall safety assessment of nanomaterials. The composite materials include a variety of different materials. To consider the biocompatibility in nanocomposite materials, one should examine all the materials which are coming in biocompatibility of materials on humans may vary based on its application [2]. Therefore, the biocompatibility of nanomaterials is becoming an increasingly important issue regarding nano-bioapplications, especially in wound healing and dressing applications [3]. According to the literature, there is a number of research articles published regarding nanomaterials toxicity and it has published in the subject of dressing bandages. Further, the detailed study indicated that the biocompatibility involves cytotoxicity, sensitization, genotoxicity, implantation, hemocompatibility, and blood coagulating testing etc [4]. Among these studies, the cytotoxicity, hemocompatibility, and blood coagulation test play a important role for the formation of novel dressing materials [3].

The ISO 10993 device category has an essential role in understanding the biocompatibility study of materials, which is based on the Biological Evaluation of Medical Devices (BEMD) [5]. The standard study describes the test on toxicology, hemocompatibility, and blood clotting ability etc. The *in vitro* test is used because it can be a biological reaction in the occupation of materials when they are established on or onto tissue cells, experimentally controllable, repeatable, quick, low cost, ethical and legal issues, human genes carrying transgenic cells can be employed and a small amount of materials has required.

Nanomaterials toxicity indicates the capability of the materials to adversely affect the general physiology along with directly interrupt the normal structure of organs and tissues [6]. Hemocompatibility is referred to as the materials compatibility with blood. It plays an essential role when designing novel dressing

materials. Blood clotting ability of materials is the test of coagulation of blood. This test is important for controlling excessive bleeding in abnormality cases. The present chapter focuses the biocompatibility study of prepared SF-PVA, ZnO NPs embedded SF-PVA and hybrid chitosan-ZnO NPs coated SF-PVA composite films on L929 mouse fibroblast cell lines by using MTT assay. In addition, the experiments of hemocompatibility and blood clotting ability of prepared composite films were studied.

6.2 Experimental

A blood sample was obtained from slaughterhouse and they have no ethical issues for human and animal right in the ethical statement section. The present study does not involve the use of human and animal subjects. All the chemicals were analytical grade (AR grade) and used without purification. Double distilled water was used throughout all the experiments.

6.2.1 Biocompatibility studies of SF-PVA, SF-PVA/ZnO NPs, and hybrid chitosan-ZnO NPs coated composite films.

6.2.1.1 Hemocompatibility

Hemocompatibility study of composite films was carried out by using hemolysis assay. The hemolysis is a process in which RBCs ruptured and hemoglobin is released. The content of hemoglobin is measured in percentage. Hemolysis percentage represents the limit of RBCs broken by the composite films in contact with blood. The hemolysis percentage value is increased with increase in the number of ruptured red cells. The hemolytic assay is represented in figure 6.1.

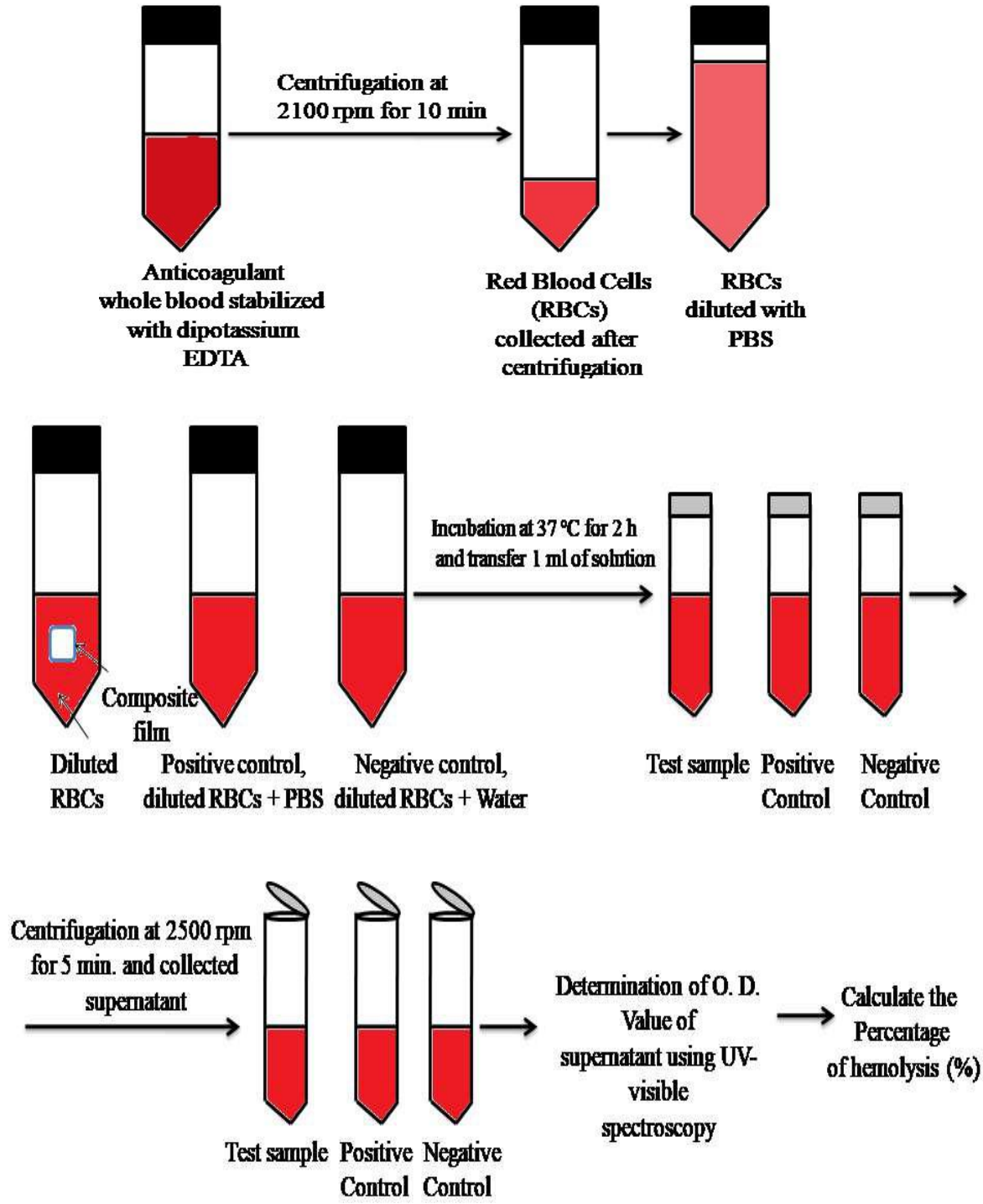

Figure 6.1 Schematic representation of hemolysis assay.

In this assay, the blood was obtained from slaughterhouse and it was stabilized with dipotassium EDTA (1.5 mg L^{-1}). A pretreatment procedure was conducted to obtain healthy red blood cells (HRBCs) for the hemolysis assay [7].

HRBCs were isolated from fresh blood by centrifugation at 2100 rpm for 10 min and purified by successive rinsing with PBS for five times. After that, HRBCs were diluted ten times with the PBS buffer. The diluted HRBCs suspension (0.2 mL) was mixed to 0.8 mL of water (negative control), pure PBS (positive control), and PBS buffer containing composite films (cut into 1 cm × 1 cm). After gentle shaking, the mixtures were kept at 37 ^{o}C for 2 h and 20 h of incubation time. Then, centrifuge the mixture at 2500 rpm for 5 min and the absorbance of the supernatant hemoglobin was recorded by using a Perkin Elmer Lambda 25 UV–vis spectroscopy at a wavelength of 540 nm. The hemolytic percentages (HP) of the composite films were calculated using the formula 3.10.

6.2.1.2 Blood clotting ability

A wound dressing material should have good capacity to stop bleeding faster. Hence, the determination of blood clotting ability of prepared composite films has important and interesting property. The blood clotting abilities of prepared composite films were determined by blood clotting method [8]. It is also called as anticoagulant assay. The schematic representation of blood clotting assay is represented in figure 6.2. In this method, the composite films were cut into small pieces (2 cm × 2 cm). The anticoagulant blood (100 µL, collected from the slaughterhouse) was poured onto the surfaces of composite films, and 10 µL of 0.2 M $CaCl_2$ was added onto them to initiate the clotting. The films were kept for incubation at 37 ^{o}C for 20 min on a shaking incubator. After the incubation period, 5 mL of double distilled water was added dropwise onto the mixture, without disturbing the clot. Further, the solutions were taken from the test tubes and centrifuged at 1000 rpm for 1 min. The supernatant of each sample was collected and kept at 37 ^{o}C for 1 h. Blood clotting was determined by measuring the optical density at wavelength of 540 nm using UV-visible spectroscopy.

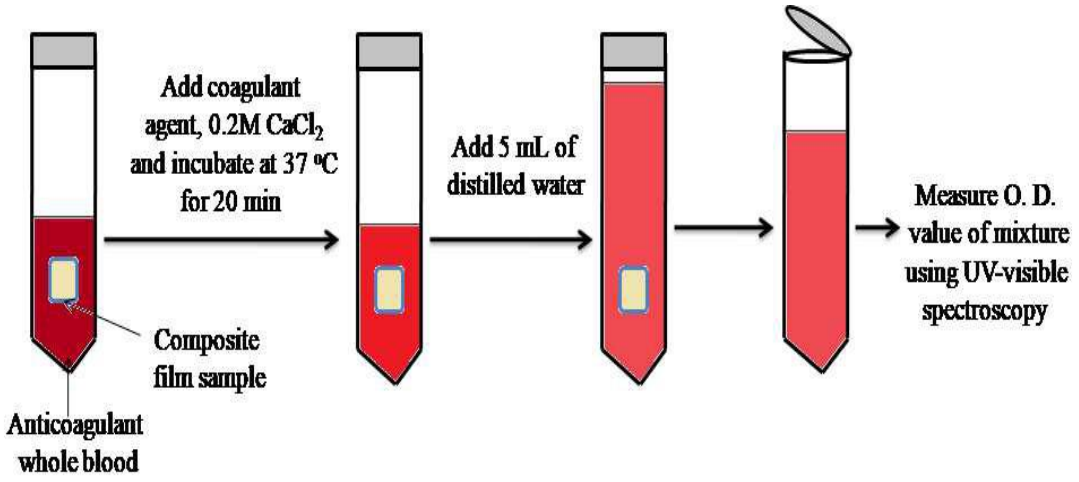

Figure 6.2 Schematic representation of blood clotting assay.

6.2.1.3 Cell viability study of composite films

The cell viability studies of composite films were evaluated by MTT assay using mammalian fibroblast L929 cell lines [9, 10]. Composite films were first sterilized overnight using UV. Cells were cultured in Dulbecco's minimal essential medium (DMEM) supplemented with 10% fetal bovine serum (FBS) and 1% antibiotic penicillin solution (1000 U/mL penicillin G), and 100 µg/mL streptomycin. Cells were seeded into 96-well plates at a seeding density 1 × 104 cells/well with DMEM containing serum and incubated for overnight in a humidified incubator. The sterilized composite films pieces were incubated in serum-containing media for 24 h, 48 h, and 72 h at 37 °C. Uncoated SF-PVA composite film and the standard Sterizone dressing was considered as control. After 24 h, 48 h, and 72 h incubation treatment, the media was removed. Cells were washed with phosphate buffer saline at pH 7.2 and addition of 100 µL of MTT (0.5 mg/mL) prepared in serum-free medium to each well and incubated for 4 h. The medium removed and 100 µL of dimethyl sulphoxide (DMSO) was added to each well to solubilize the formazan crystals. The concentration of formazan was determined using a multiwell plate reader at 570 nm absorbance. The cell viability was determined with the equation 3.11

.

6.3 Results and Discussion

6.3.1 Hemocompatibility study

6.3.1.1 Hemocompatibility of SF-PVA and SF-PVA/ZnO NPs composite films

Compatibility to blood is one of the most important studies that have to be addressed before the materials, especially materials that need to be in contact with blood. A percentage of hemolysis of less than 2% is considered as nonhemolytic, 2-5% is slightly hemolytic and more than 5% is hemolytic as per ASTMF-756-08 [11]. Figure 6.3 shows the hemolytic behavior of SF-PVA/ZnO and SF-PVA composite films. The obtained results indicate that the hemolytic percentage of SF-PVA/ZnO composite film is higher as compared to SF-PVA composite film. The induced hemolysis percentage of the SF-PVA composite film is 2.1% and 2% for 2 h and 20 h of incubation times, respectively. However, the hemolysis percentage for the SF-PVA/ZnO composite film is found to be 3.4% for 2 h and 2.7% for 20 h of incubation. The hemolysis percentages of both the films show below 5%, indicating that both films are slightly hemolytic materials. The obtained results show that the hemolysis percentage decreased with the increasing incubation period of up to 20 h. ZnO NPs cause hemolysis when in contact with blood in a concentration-dependent but nnot in a shape –dependent manner [12]. The results indicate that the composite film of SF-PVA/ZnO is hemostatic in nature, and it can be used to stop bleeding faster.

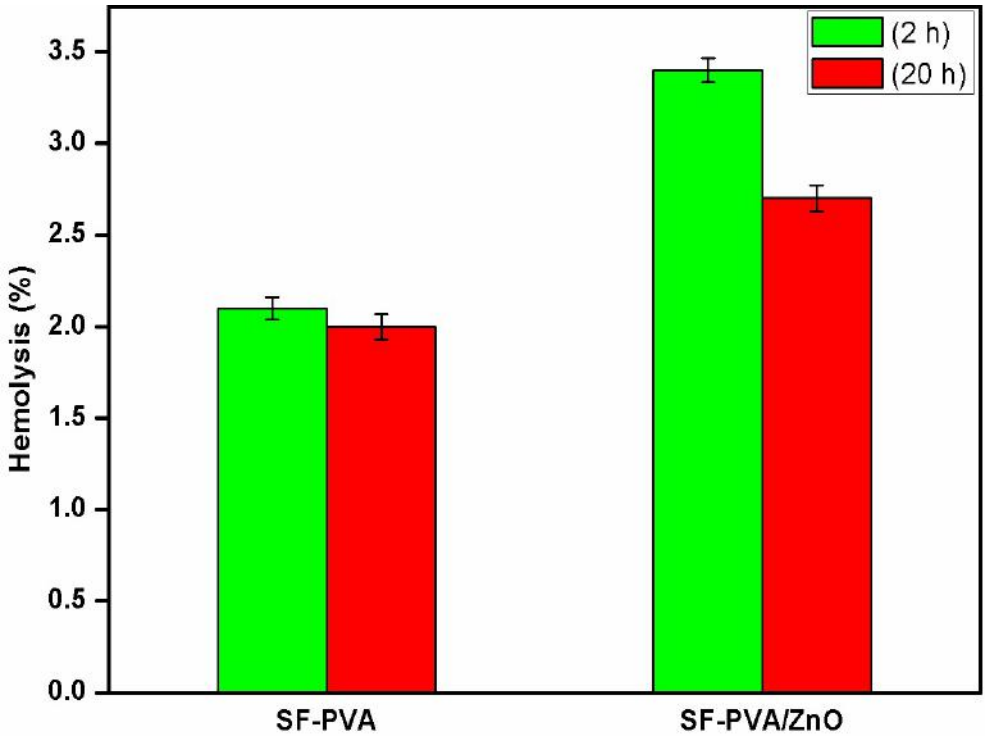

Figure 6.3 Hemolysis percentages of SF-PVA and SF-PVA/ZnO composite films.

6.3.1.2 Hemocompatibility of hybrid chitosan-ZnO NPs coated SF-PVA composite films

Figure 6.4 represents the hemolytic percentages of hybrid chitosan-ZnO NPs coated SF-PVA composite films. The results indicate that the hemolytic percentage of hybrid chitosan-ZnO NPs coated SF-PVA composite film is lower as compared to SF-PVA composite film and Sterizone dressings. The induced hemolysis percentage of SF-PVA composite film is 2.1% and 2% for 2 h and 20 h of incubation times, respectively. However, the hemolysis percentage for 0.2 wt % hybrid chitosan-ZnO NPs coated SF-PVA composite film is found to be 2 % for 2 h and 1.8 % for 20 h of incubation. The hemolysis percentage for 0.5wt % hybrid chitosan-ZnO NPs coated composite film is found to be 1.7 % for 2 h and 1.6 % for 20 h of incubation. The hemolysis percentage for 1wt % hybrid chitosan-ZnO NPs coated SF-PVA composite film is found to be 1.5 % for 2 h and 1.3 % for 20 h of incubation and the hemolysis percentage for commercial Sterizone dressings is found to be 1.8 % for 2 h and 1.6 % for 20 h of incubation. The hemolysis percentage of all the coated composite films shows below 2 %. It can be concluded

that all the coated composite films are increases hemocompatibility with increase in the concentration of coating of hybrid chitosan-ZnO NPs. The hemolysis percentage of all the coated composite films and Sterizone dressings show below 2 %, indicating that all the films have non-hemolytic materials. The obtained results also indicate that the hemolysis percentage is decreased with the increasing incubation period of up to 20 h. The hybrid chitosan-ZnO NPs coated SF-PVA composite films are hemocompatible to blood and it can be used to stop bleeding faster.

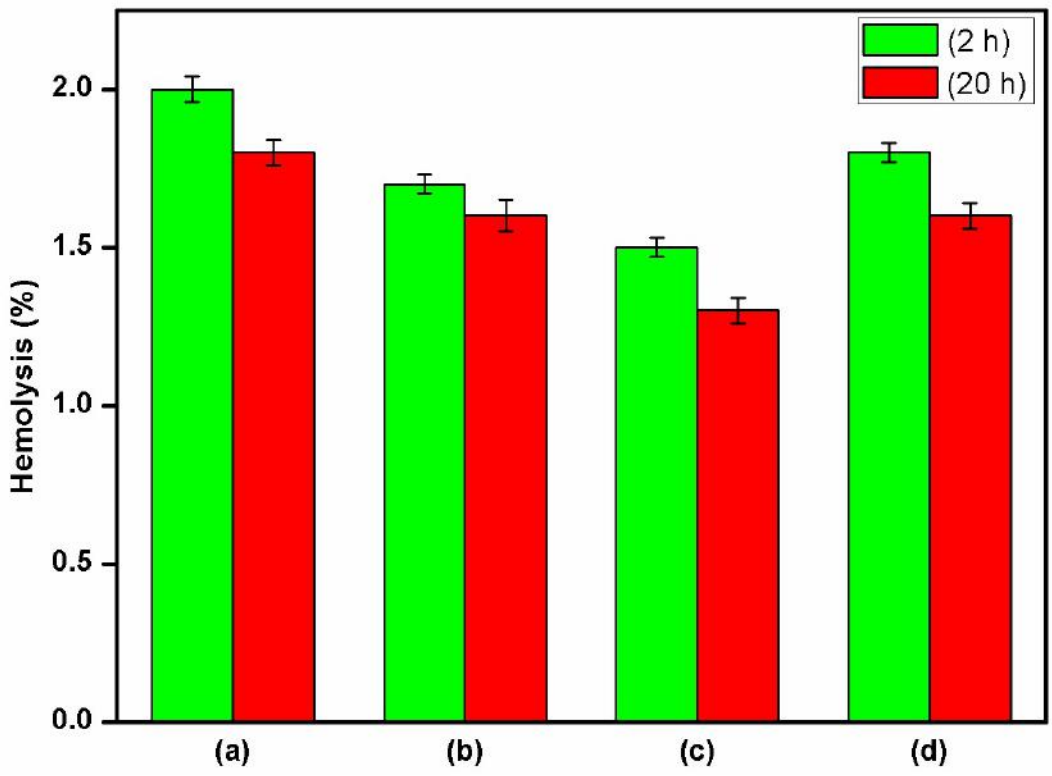

Figure 6.4 Hemolysis percentages of **(a)** 0.2 wt % **(b)** 0.5 wt %, **(c)** 1 wt % hybrid chitosan-ZnO NPs coated SF-PVA composite films and **(d)** Sterizone dressing.

6.3.2 Blood clotting study

6.3.2.1 Blood clotting ability of SF-PVA and SF-PVA/ZnO NPs composite films

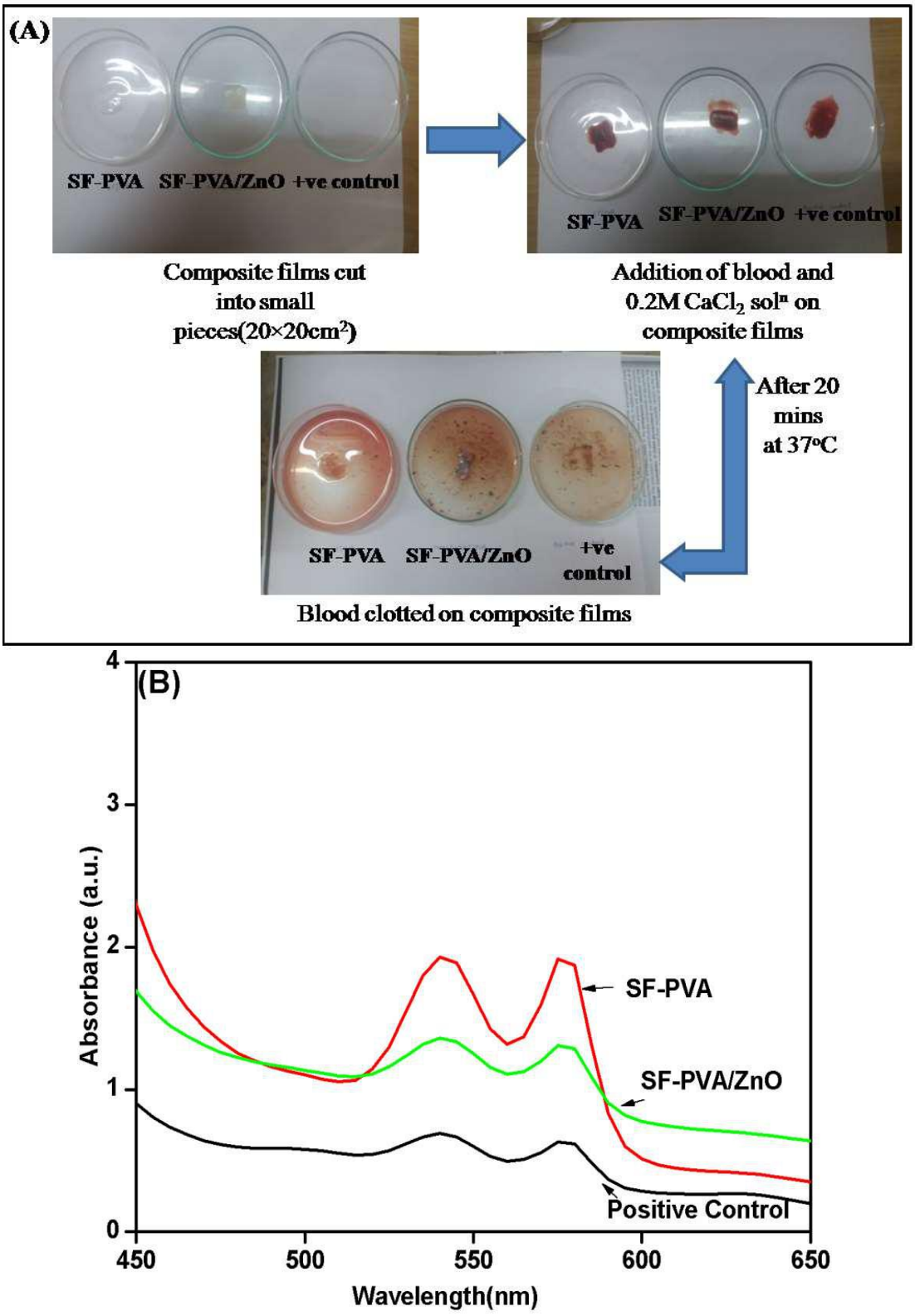

Figure 6.5 (A) Blood clotting abilities, **(B)** absorbance at wavelength 540 nm of SF-PVA and SF-PVA/ZnO composite films.

Figure 6.5 (A) it can be observed that the blood clotting ability of the ZnO NPs embedded composite film is higher than that of the SF-PVA composite film. Figure 6.5 (B), shows lower optical density of SF-PVA/ZnO composite film; this means that it shows more blood-clotting capability. ZnO NPs is hemostatic, as ZnO NPs can form a certain complex with fibrin, which is the most abundant protein in blood plasma, thus decreasing fluorescence in the presence of ZnO NPs [13]. Pure SF shows poor blood clotting ability when it is used as a blood-contact [14]. Blood clotting property of SF is improved with the help of heparin and ferulic acid [15, 16]. Our results indicate that the blood clotting ability of the SF-PVA/ZnO composite film is enhanced by the integration of ZnO NPs because ZnO NPs denatured anticoagulant proteins and affected the intrinsic pathway of blood coagulation by producing a short clotting time [17].

6.3.2.2 Blood clotting ability of hybrid chitosan-ZnO NPs coated SF-PVA composite films

Figure 6.6 (A) represents the blood clotting ability of the (a) SF-PVA, (b) 0.2 wt % (c) 0.5 wt %, (d) 1 wt % hybrid chitosan-ZnO NPs coated SF-PVA composite films (e) Sterizone dressing, and (PC is Positive Control). All the coated composite films show higher blood clotting ability than the control SF-PVA and Sterizone dressing. Figure 6.6 (B), it can be observed that the hybrid chitosan-ZnO NPs coated composite films shows lower optical density; it means that it shows more blood-clotting capability. ZnO NPs and chitosan both are hemostatic, as hybrid chitosan-ZnO NPs can form a certain complex with fibrin, which is the most abundant protein in blood plasma, thus decreasing fluorescence in the presence of ZnO NPs and chitosan. SF-PVA composite film shows poor blood clotting ability when it is used as a blood-contact.

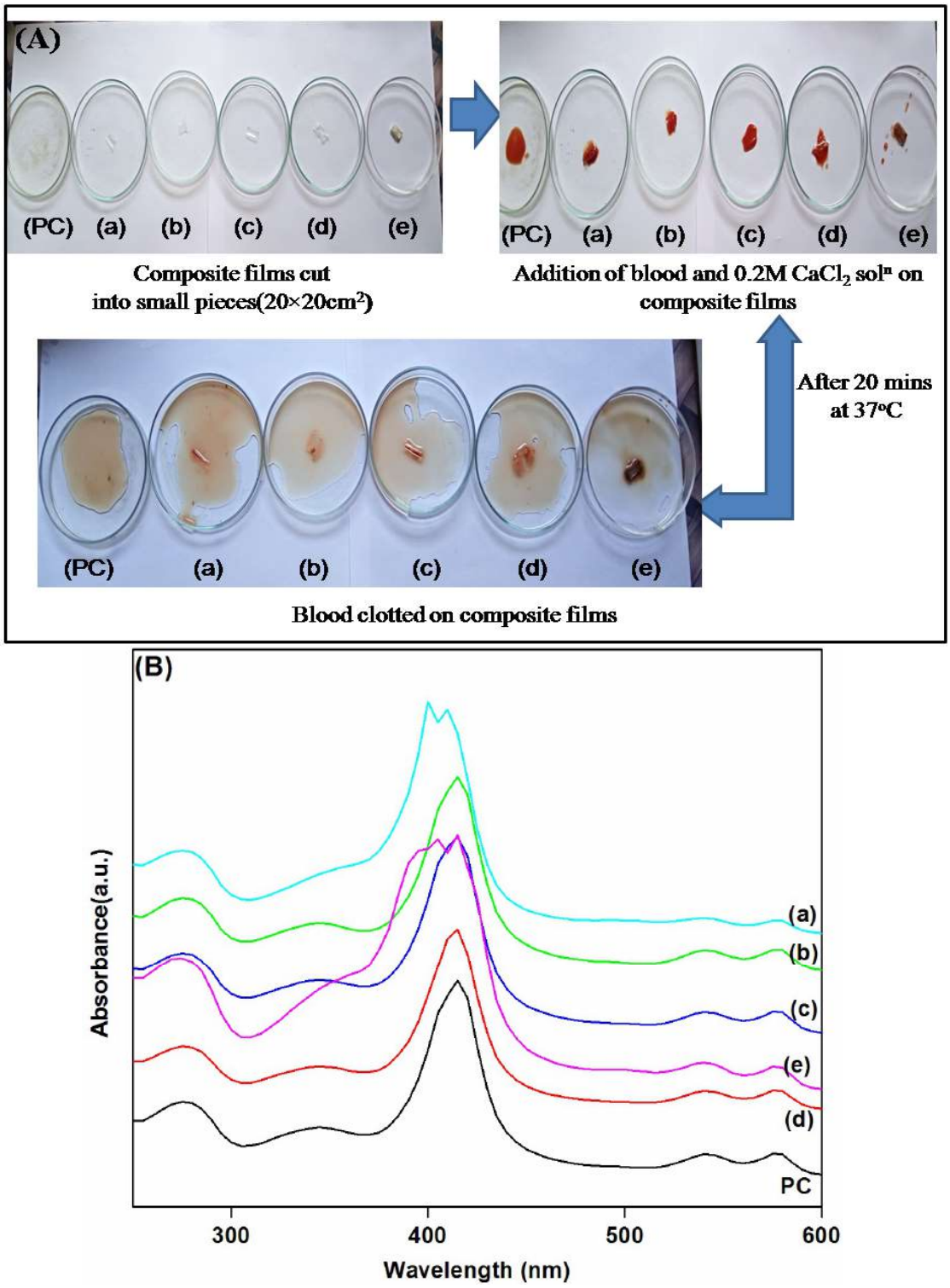

Figure 6.6 (**A)** Blood clotting abilities and **(B)** absorbance at wavelength 540 nm of **(a)** SF-PVA, **(b)** 0.2 wt % **(c)** 0.5 wt %, **(d)** 1 wt % hybrid chitosan-ZnO NPs coated SF-PVA composite films **(e)** Sterizone dressing, and (PC-Positive Control)

Blood clotting property of SF-PVA composite film is improved with the help of hybrid chitosan-ZnO NPs. In this study blood clotting ability of SF-PVA composite film is enhanced by the surface coating of hybrid chitosan-ZnO NPs. The mechanism of blood clotting shows that the chitosan and ZnO NPs denatured the anticoagulant proteins and affects the intrinsic pathway of blood coagulation by producing a short clotting time.

6.3.3 Cell viability study

6.3.3.1 Selection of cell type

The toxicity of nanomaterials is based on the organ and the type of cell lines, which is owing to the difference in cell physiology (e.g. epithelial or lymphoid), the proliferation of the cell, membrane characteristics and phagocyte characteristics among different cell types [18]. The important factor in cytotoxicity assay is the selection of suitable cell lines. In addition, it is also needed to give priority to the importance of optimizing the numbers and conditions of cells. In order to the exact effects of nanomaterials on the cells of interest, the cytotoxicity assay must include cells that represent the exposure route and organs targeted by NPs. Among the commonly used cell lines, fibroblast cells are conducive for the trial. In addition, cancer cells are also a better choice than normal cells owing enhanced rate of growth, metabolic activity and easy to use [19].

In the present study, L929 mouse fibroblast cell lines have selected for confirmation of biocompatibility study of the prepared SF-PVA, ZnO NPs embedded SF-PVA and hybrid chitosan-ZnO NPs coated SF-PVA composite films. The cell lines are commonly used to study the biocompatibility of materials.

6.3.3.2 Selection of Cytotoxicity assay

There are different assays can be employed to study the toxicity of nanomaterials on cell cultures. There are lactate dehydrogenase (LDH), leakage, 3-(4, 5-dimethylthiazol-2-yl) 2, 5-diphen-yltetrazolium bromide (MTT) assay, Dye exclusion assay (Trypan blue) including recognition of cytokine/ chemokine production etc [20]. Choice of accurate toxicity assay is a key to the accurate

assessment of nanomaterials toxicity. The NPs can absorb dyes, be redox active and it is significant that the cytotoxicity study is suitable. Among different assays, MTT assay is commonly used and easy to use.

Therefore, in the present investigation, the cytotoxicity has been evaluated by means of MTT assay to minimize the errors and to obtain the quality data. The assay is simple cheap and easy to evaluate.

6.3.3.3 MTT assay of SF-PVA and SF-PVA/ZnO NPs composite films

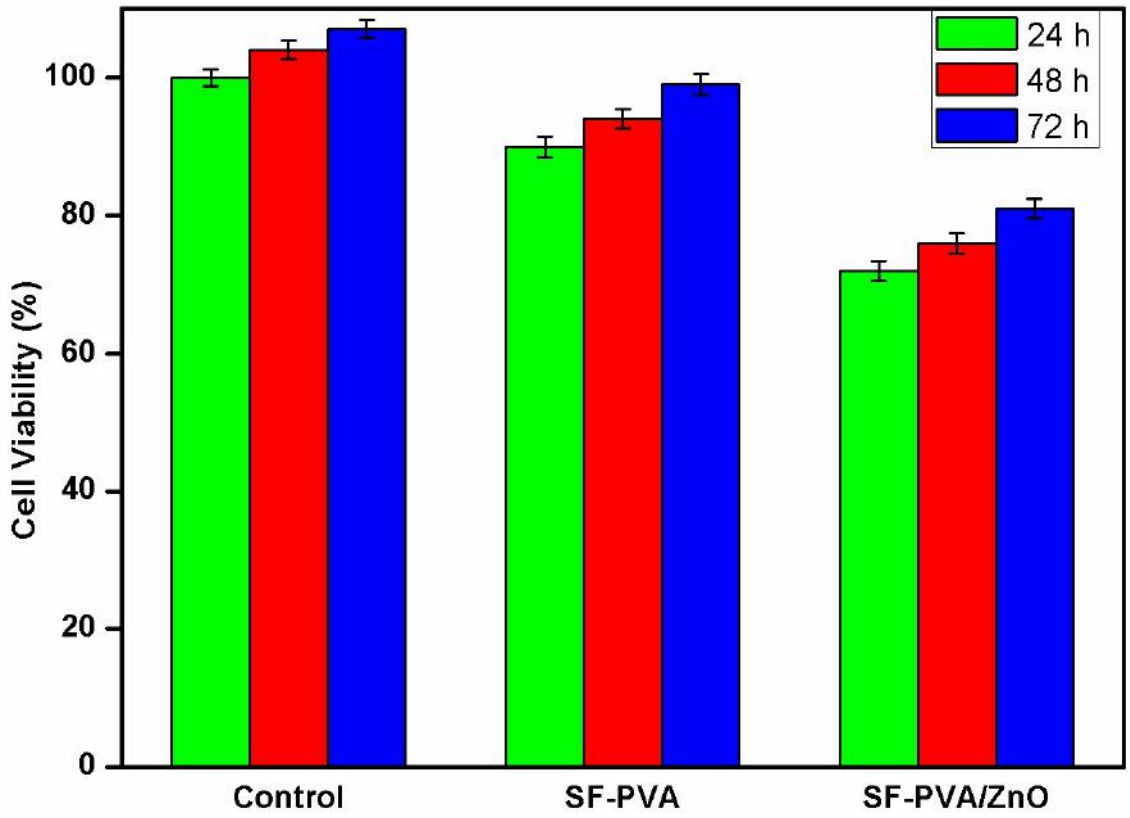

Figure 6.7 Cytotoxicity of SF-PVA and SF-PVA/ZnO composite films.

The perfect wound dressing should nontoxic and biocompatible. The cytotoxicity of prepared SF-PVA and SF-PVA/ZnO composite films under in-vitro conditions in L929 cell lines are examined in terms of their viabilities using the MTT assay in figure 6.7. Without composite films are taken as the control. It is commented that the cell viability of SF-PVA/ZnO composite films slightly increased after 48 h and after 72 h than 24 h of incubation time. Cell viability of

SF-PVA composite films is 100 % for 24 h and 105 % for 48 h and 107 % for 72 h of incubation time. However, the cell viability of SF-PVA/ZnO composite films is 72 % for 24 h and 76 % for 48 h and 81 % for 72 h of incubation time. From these results, it can be concluded that the prepared composite films are nontoxic in nature.

6.3.3.4 MTT assay of hybrid chitosan-ZnO NPs coated SF-PVA composite films

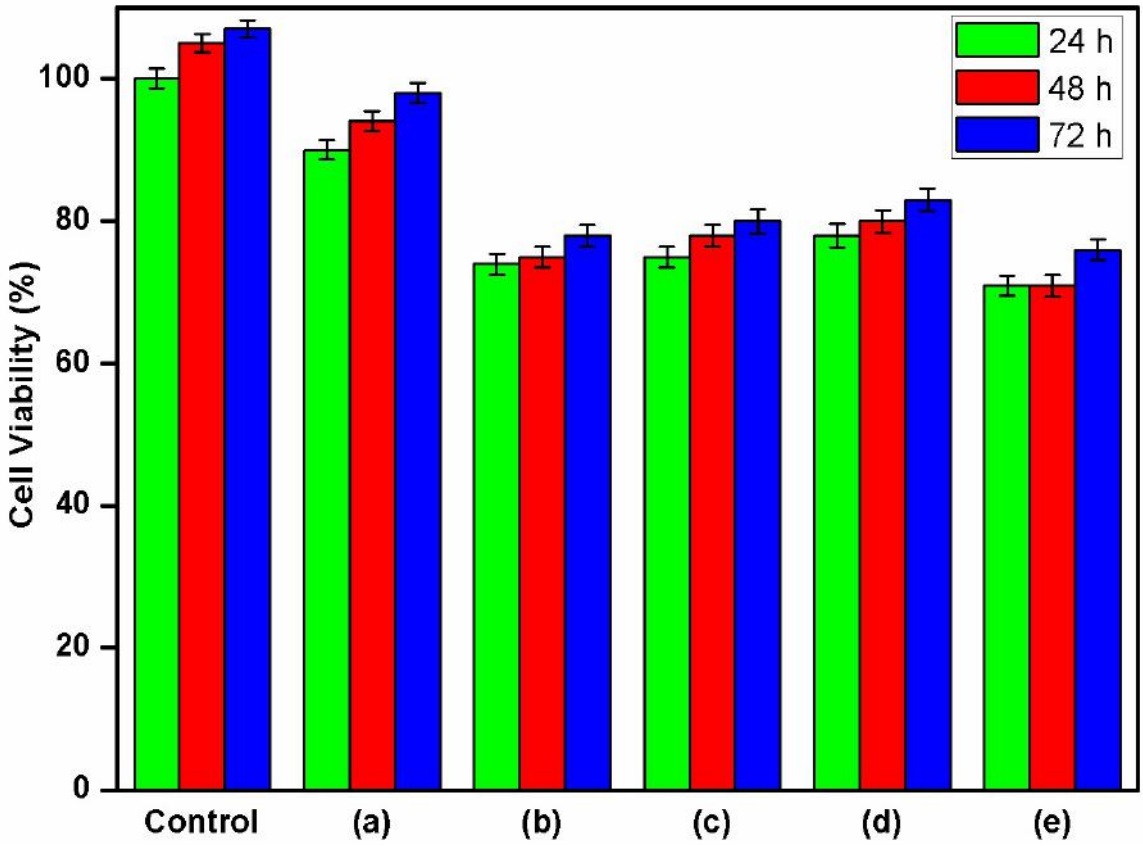

Figure 6.8 Cell viability of **(a)** SF-PVA, **(b)** 0.2 wt %, **(c)** 0.5 wt %, **(d)** 1 wt % hybrid chitosan-ZnO NPs coated SF-PVA composite films and **(e)** Sterizone dressing.

The cell viability studies of uncoated and coated composite films are shown in figure 6.8. Cell viability study is done using L929 mouse fibroblast cells by using MTT assay. The results obtained that the uncoated SF-PVA composite film is nontoxic to the L929 cells, which is similar to control. It is observed that the cell

viability of the 0.2 wt % hybrid chitosan-ZnO NPs coated composite film is 73 % for 24 h, 75 % for 48 h and 78 % for 72 h of incubation time. The 0.5 wt % hybrid chitosan-ZnO NPs coated composite film is 75 % for 24 h, 78 % for 48 h and 80 % for 72 h of incubation time. In addition, the 1 wt % hybrid chitosan-ZnO NPs coated composite film is 78 % for 24 h, 80 % for 48 h and 83 % for 72 h of incubation time. We have observed the cell viability slightly increased from the coating of a higher concentration of hybrid chitosan-ZnO NPs on SF-PVA composite film. The Sterizone dressing shows cell viability of 71 % for 24 h, 74 % for 48 h and 76 % for 72 h of incubation time. It might be concluded that the cell viability of hybrid chitosan-ZnO NPs coated SF-PVA composite films is higher than Sterizone dressing and nontoxic to fibroblast cells.

6.3.3.5 Mechanism of cytotoxicity of composite films

The properties of metal oxide materials especially nanosize make them desirable for nano-bio applications, but it also leads them to have some disadvantages like nanosize related toxicity [21]. Nanocomposite films receive the nanosized particles and the use of these NPs is very important to investigate their potential toxic effects. The toxicity of NPs on human and environment is a topic that has received increasing interest. There are different mechanisms can cause NPs toxicity. Nanotoxicity of ZnO NPs related to the following mechanisms [22],

- NPs release of the corresponding toxic ions.
- NPs produced excess reactive oxygen species.
- NPs toxicity will base on the physic-chemical characteristics of the NPs corresponding to size, shape, surface charge, chemical stability of the core legends etc.

ZnO NPs released toxic ions such as Zn^{+} ions. These ions form the acidic condition, which damage the cytoskeleton of the cell. Reactive oxygen species include superoxide anion (O_2^-), hydrogen peroxide (H_2O_2), hydrogen radical (HO•) and singlet oxygen ($^1O_2$), these are more reactive compared to oxygen (O_2) itself. This ROS production causes big cellular damage through induction of genotoxicity, inflammation, and disruption of biomolecules like DNA, proteins

and lipids [23]. This process causes the apoptosis and damages the cells. Physico-chemical characteristics of the NPs involve the toxicity of NPs. It includes the size, shape and surface charge of NPs. The size of the NPs decreases with an increase in the surface area and permits a greater potential of its atoms or molecules to be displayed either on the surface or the interior of the materials [24]. Surfaces of NPs should also be created to minimize protein adsorption leading to a well controlled and reproducible protein corona of certain composition and thickness. The size of NPs has also involved the toxicity of NPs. The spherical shaped NPs are suitable for endocytosis than the rod-shaped or fiber-like NPs. The surface charge of NPs promotes the adsorption of ions and biomolecules, which may change organism or cellular responses toward particles. As compared to anionic particles, cationic particles have been stable and exert the greatest cytotoxic effects [25].

Toxic effects of NPs can be controlled by mixing the ZnO NPs with other biocompatible and biodegradable materials [26]. Therefore, in the second part of the present work we have used the chitosan for controlling the toxic effects of ZnO NPs. Chitosan is the biocompatible, biodegradable and nontoxic in nature. Due to its good properties, chitosan is broadly applicable for nano-bio applications [27]. Therefore here, the hybrid chitosan-ZnO NPs are synthesized and coated on SF-PVA composite films. The results showed that the prepared composite films have nontoxic effect of L929 mouse fibroblast cell line compared to Sterizone dressing.

6.4 Conclusions

This chapter provides the protocol to study biocompatibility of SF-PVA, ZnO NPs embedded SF-PVA and hybrid chitosan-ZnO NPs coated SF-PVA composite films. The biocompatibility study is done by using the hemocompatibility, blood clotting ability and cytocompatibility of prepared composite films. The hemocompatibility study of all the composite films shows the good hemocompatibility to the RBCs compared to control Sterizone dressing which can be acceptable for biomedical applications, especially for wound dressings. The blood clotting ability study of composite films is done by using blood clotting assay. Blood clotting ability of SF-PVA composite film is enhanced

by integrating the ZnO NPs and coating of hybrid chitosan-ZnO NPs on SF-PVA composite films. The cytocompatibility study is done by studying MTT assay on L929 mouse fibroblast cell line. A change of the percent cell viability is demonstrated by using MTT assay which is attributed to differences in their mechanism and physical nature of the cells. The MTT assay is found that the cell viability of ZnO NPs embedded SF-PVA composite films slightly decreases compared to control SF-PVA composite film. In addition, the cytocompatibility study of hybrid chitosan-ZnO NPs coated SF-PVA composite films show the cell viability slightly decreases with increase in the concentration of hybrid chitosan-ZnO NPs. From all observations of biocompatibility studies, it is concluded that ZnO NPs embedded SF-PVA composite film and hybrid chitosan-ZnO NPs coated SF-PVA composite films are biocompatible and can be used for wound dressing application.

References

1. P. Sudha, K. Sangeetha, A. Kumari, E. Radha, N. Vanisri, S. Aisverya, S. Anil Fundam Mater Poly 2018, 217-247.
2. F. Khan, M. Tanaka, Inter Int J Mol Sci, 2018, 19, 17.
3. S. Prabhu, E. K. Poulose Inter nano letters, 2012, 2, 32.
4. M. Bernard, E. Jubeli, M. D. Pungente, N. Yagoubi, Bioma Sci, 2018, 6, 2025-53.
5. X. Liu, D. P. Rodeheaver, J. C. White, A. M. Wright, L. M. Walker, F. Zhang, and S. Shannon, Regul Toxicol Pharmacol , 2018, 97, 24-32.
6. S. Chatterjee, R. Kumari, S. Nimesh, Adv Nano Delivery Thera Nuc Aci, 2017, 187-201.
7. B. Houyvet, Y. Bouchon-Navaro, C. Bouchon, D. Goux, B. Bernay, E. Corre, C. Zatylny-Gaudin, Fish Shellfish Immunol, 2018, 72, 318-324.
8. M. Mehrabani, R. Karimian, R. Rakhshaei, F. Pakdel, H. Eslami, V. Fakhrzadeh, M. Rahimi, R. Salehi H. Kafil, Int J Biol Macromol, 2018, 116, 966–976.
9. M. Ganjali, S. Asl, M. Alizadeh, M. Shahlaei, A. Jam, J Int Thin Films Low Dime Sys, 2018, 1, 57-64.
10. S. Gnanavel, S. Ponnusamy, L. Mohan, Biocatal Agric Biotechnol, 2018, 15, 364-369.
11. M. Zamani, K. Rostamizadeh, H. Manjili, H. Danafar, Eur Polym J, 2018, 1, 260-70.
12. E. Babu, A. Subastri, A. Suyavaran, K. Premkumar, V. Sujatha, B. Aristatile, G. Alshammari, V. Dharuman, C. Thirunavukkarasu Sci Rep 2017, 7, 4203.
13. A. Ilinskaya, M. Dobrovolskaia, Nanomedicine, 2013, 8, 969-81.
14. M. Elahi, G. Guan L. Wang, Rev Adv Mater Sci, 2014, 38, 148-159.
15. M. Elahi, G. Guan, L. Wang, M. W. King, Jour of App Poly Sci, 2014 15, 131, 40772.
16. F. Seib, M. Herklotz, K. Burke, M. Maitz, C. Werner, D. Kaplan, Biomaterials, 2014, 35, 83-91.

17. A. Sasidharan, P. Chandran N. Monteiro-Riviere, ACS Biomater Sci Eng, 2016, 2, 1608–1618.
18. A. Sukhanova, S. Bozrova, P. Sokolov, M. Berestovoy, A. Karaulov, I. Nabiev, Nanoscale Res Lett, 2018, 13, 44.
19. C. Riebeling, J. P. Piret, B. Trouiller, I. Nelissen, C. Saout, O. Toussaint, and A. Haase, NanoImpact, 2018, 10, 1-10.
20. A. Clippinger, D. Allen, H. Behrsing, P. Hinderliter, R. Landsiedel, E. Reinke, V. Stone, Appl In Vitro Toxicol, 2018, 4, 82-88.
21. A. Jain, S. Ranjan, N. Dasgupta, C. Ramalingam, Crit Rev Food Sci Nutr, 2018, 58, 297-317.
22. R. Sinha, R. Karan, A. Sinha, S. Khare, Bioresour Technol, 2011, 102, 1516-1520.
23. O. Choi, Z. Hu, Environ Sci Technol 2008, 42, 4583-4588.
24. E. Roduner, Chem Soc Rev, 2006, 35, 583-592.
25. S. Sharifi, S. Behzadi, S. Laurent, M. Forrest, P. Stroeve, M. Mahmoudi Chem Soc Rev, 2012, 41, 2323-2343.
26. Z. Li, R. Yang, M. Yu, F. Bai, C. Li, Z. Wang, J Phys Chem C, 2008, 112, 20114-20117.
27. J. Edson, D. Ingato, S. Wu, B. Lee, Y. Kwon, Biomacromolecules, 2018, 19, 1508-1516.

CHAPTER 7

Antibacterial Study of SF based Composite Films

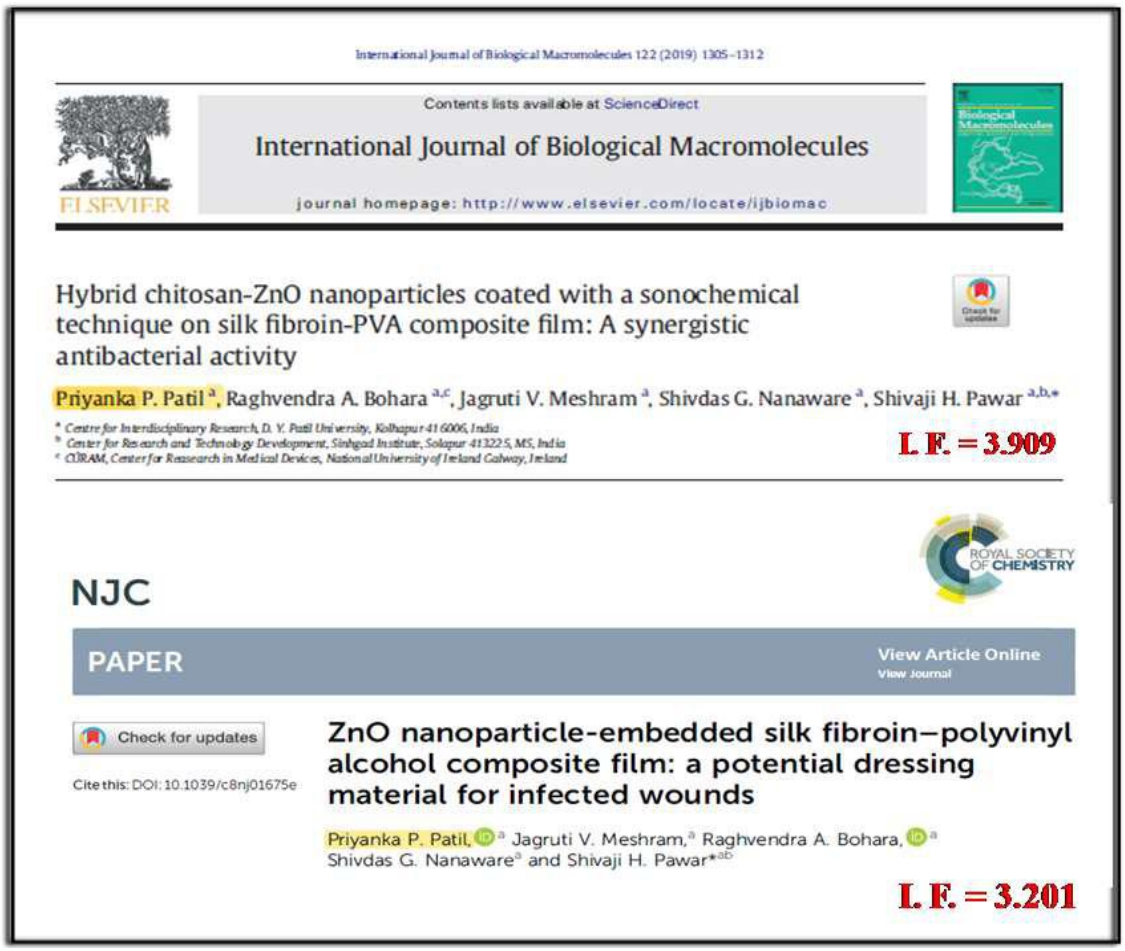

International Journal of Biological Macromolecules 122 (2019) 1305–1312

Contents lists available at ScienceDirect

International Journal of Biological Macromolecules

journal homepage: http://www.elsevier.com/locate/ijbiomac

Hybrid chitosan-ZnO nanoparticles coated with a sonochemical technique on silk fibroin-PVA composite film: A synergistic antibacterial activity

Priyanka P. Patil [a], Raghvendra A. Bohara [a,c], Jagruti V. Meshram [a], Shivdas G. Nanaware [a], Shivaji H. Pawar [a,b,*]

[a] Centre for Interdisciplinary Research, D. Y. Patil University, Kolhapur 416006, India
[b] Center for Research and Technology Development, Sinhgad Institute, Solapur 413255, MS, India
[c] CURAM, Center for Research in Medical Devices, National University of Ireland Galway, Ireland

I. F. = 3.909

NJC

PAPER

View Article Online
View Journal

Check for updates

Cite this: DOI: 10.1039/c8nj01675e

ZnO nanoparticle-embedded silk fibroin–polyvinyl alcohol composite film: a potential dressing material for infected wounds

Priyanka P. Patil, [a] Jagruti V. Meshram, [a] Raghvendra A. Bohara, [a] Shivdas G. Nanaware [a] and Shivaji H. Pawar*[ab]

I. F. = 3.201

7.1 Introduction

Skin and soft tissue infections (SSTIs) are the most common types of infections and they affect approximately 14 million people every year in the United States [1]. Depending on the etiology and severity of the microbial invasion, SSTIs can range from minor superficial to life-threatening infections. In the initial stage of the infectious process, gram-positive organisms such as *S. aureus* and *S. pyogenes* are the dominant organisms involved, while gram-negative organisms like *E. coli* and *P. aeruginosa* are only found in later stages of the process, i.e. when a chronic wound is developed [2, 3]. In a healthy human being, infection is avoided, by activating the immune system for abolishing the invading pathogens [4]. However, if the immune system is not able to remove the pathogen, infection occurs and causes the physiological damage such as (deterioration of granulation tissue, growth factors, and extracellular matrix components) thus compromising the normal wound healing process [5]. Therefore, it is fundamental to develop wound dressings that can prevent bacteria penetration into the wound or avoid microorganism's growth. Inorganic NPs have attracted important interest because of their highly active antimicrobial action [6]. Among different inorganic NPs ZnO NPs are increasingly important and it has been integrated with wound dressing materials due to their excellent antibacterial activity [7, 8].

Until now, ZnO NPs have been widely applicable for killing of bacterial cells. To increase the antibacterial resistance requires the development of new antibacterial agents. Although, different designed ZnO NPs have been used that is capping and mixing the other antibacterial agents, without disturbing its original properties [9]. This may be achieved for rise in the bacteria killing ability of ZnO NPs. Chitosan would show excellent antibacterial activities and it shows synergistic antibacterial activity. According to the previous reports the bacteria killing ability of ZnO NPs was enhanced by capping and mixing of the other antibacterial agent like chitosan [10, 11].

In this chapter, the antimicrobial activity of prepared composite films of SF-PVA, ZnO NPs embedded SF-PVA and hybrid chitosan-ZnO NPs coated SF-PVA composite films on various microbial strains have been studied in details,

which may be used as effective candidate for further application in wound dressings.

7.2 Experimental

7.2.1 ZnO NPs as antimicrobial agent

The rapid growth of nanotechnology inspires the significant interest of development of NPs, which shows antibacterial effects. Metal oxide NPs such as ZnO NPs are increasingly important and considered as reinforcing filler for polymer matrix [12]. ZnO NPs have properties of biocompatible, excellent antibacterial and currently used in cosmetic materials. The decontamination action of ZnO NPs has been widely examined with various pathogenic and non pathogenic microorganisms. Antibacterial properties of ZnO NPs exhibited owing to enhanced specific surface area and smaller particle size. There are various factors affected the decontamination activity of ZnO NPs. These factors are UV illumination, shape and size of particles, concentration, surface modifications, surface faults, and the minimum inhibitory concentration (MIC) of NPs [13]. There are several reported have been studied for the antimicrobial tests of ZnO NPs. The spherical shaped NPs noticed high bacteria killing ability against the pathogenic bacteria [14]. Thus, ZnO NPs doped materials exhibited considerably high antibacterial property towards *S. aureus* than *E. coli* and *P. aeruginosa* bacteria [15]. ZnO NPs have mostly used in antibacterial coatings for food packaging and wound dressing applications. Bacterial infection generally exposed on the surfaces of wound, this issue controlled the growth of microorganisms by using ZnO NPs based antibacterial surfaces of composite films [16].

7.2.2 Hybrid Chitosan-ZnO NPs as antimicrobial agent

There are several reports indicates the antibacterial action of ZnO NPs. Therefore, the formation of novel antibacterial agents is a great demand in biomedical applications [17]. Generally, the researchers are focused on the development of hybrid NPs because of its synergistic antibacterial properties. There are many researches are synthesized hybrid chitosan-ZnO NPs for

antibacterial purposes. Hybrid Chitosan-ZnO NPs demonstrated synergistic antibacterial action against bacteria. Hybrid chitosan-ZnO NPs was used as an antibacterial coating of cotton textiles, food packaging and wound dressings [18, 19]. Hybrid chitosan-ZnO NPs showed enhanced antibacterial properties against *B. subtilis, E. coli* and *S. aureus* bacteria. The antibacterial study of hybrid chitosan-ZnO NPs results obtained the ZOI is higher in *E. coli* bacteria than *S. aureus* and *P. mirabilis* bacteria. Moreover, the ZOI was increased with increasing the concentration of hybrid chitosan-ZnO NPs.

7.2.3 Materials and Reagent

The collected glassware for the experiment was cleaned with distilled water and autoclaved at 121º C for 20 min prior to use. The five types of bacteria like Gram-positive *S. aureus*, Gram-negative *E. coli*, *P. aeruginosa*, *P. mirabilis*, and *S. pyogenes* were selected for the antibacterial study. *S. aureus*, *E. coli*, *P. aeruginosa, P. mirabilis*, and *S. pyogenes* were collected from the National Collection of Industrial Microorganisms (NCIM), National Chemical Laboratory (NCL) in Pune, India. Nutrient media was supplied from himedia laboratories.

7.2.4 Bacteria sample preparation

The bacterial culture was maintained on the surface of sterile nutrient agar slants at refrigerator. The nutrient agar media composition used for the growth of bacterial cells is mentioned below. Firstly the nutrient medium was prepared and sterilization process was done in an autoclave at 121 °C for 20 min. After, the medium slants were prepared and bacterial culture suspension streaked on the surface of nutrient medium. The cultures of microorganisms were grown at 37 °C for 24 h.

Nutrient broth composition

- Peptone (1g),
- Beef extract (1g),
- Sodium chloride (0.5g),
- Double D/W (100 mL),

- pH after sterilization (7.3).

The optical density (O.D.) of this bacterial culture was adjusted to having a concentration of approximately 1 x 10^7 CFU/mL [20].

7.2.5 Determination of antibacterial activity by disc diffusion assay

The disc diffusion method was used to study the antimicrobial activities of SF-PVA, ZnO NPs embedded SF-PVA and hybrid chitosan-ZnO NPs coated SF-PVA composite films. [21]. A typical procedure was as follows: Bacterial cultures were grown overnight on nutrient agar medium. 100 μL of cultured bacterial cell suspension was spread over the agar plate using glass spreader. The discs of coated and uncoated composite films were first soaked into double distilled water for 1 h prior to a test. Discs of composite films were placed on the surfaces of agar plates. The plates were refrigerated at 10 °C for 10 min to diffuse the sample in the media. Then the plates were incubated at 37 °C for 24 h for the growth of microorganisms. After 24 h of incubation, plates were observed for ZOI (Zone of Inhibition). The ZOI was measured for each sample in mm.

7.2.6 Determination of minimum inhibition concentration (MIC) of NPs

MIC of NPs is the ability of NPs for the inhibition of microorganism's growth at lowest concentration. The most frequently used methods for determination of MIC of NPs are agar dilution or tube dilution and broth microdilution methods. In these methods, the serial dilutions are prepared by using the NPs in bacterial growth medium. Thereafter, test organisms are mixed to the test tubes containing the dilutions of the NPs and tubes incubated for growth. Further, calculate the MIC value. This method is a standard assay procedure for determination of MIC of NPs. The MIC is essential in diagnostic laboratories for confirmation of resistance of bacteria to an antibacterial agent. Moreover, it is used to detect the activity of newer antimicrobial agents [22].

7.2.7 Determination of the growth curve of bacteria cells

Growth curves were examined by bacterial culture exposed to ZnO NPs and hybrid chitosan-ZnO NPs, nutrient agar broth with MIC concentration of ZnO NPs (*E. coli*: 100 µg/mL, *S. aureus*: 50 µg/mL, P. mirabilis: 100 µg/mL), and hybrid chitosan-ZnO NPs (*E. coli*: 50 µg/mL, *S. aureus*: 25 µg/mL, *P. mirabilis*: 50 µg/mL) was used. The bacterial cell concentration was 10^6 CFU/ml. Bacterial culture flasks were incubated in a shaking incubator at 150 RPM at 37 ºC. The bacterial cell growth was examined for every 2 h under UV-vis spectrophotometer at 600 nm wavelength [23].

7.3 Results and discussion

7.3.1 Determination of antibacterial activity study of SF-PVA and SF-PVA/ZnO NPs composite films

Antibacterial studies of prepared composite films were studied using the disc diffusion method, which showed in figure 7.2. The bacterial cultures of *S. aureus*, *E. coli*, *P. aeruginosa*, *P. mirabilis* and *S. pyogenes* were used as model gram-positive and gram-negative organisms respectively. It is very essential to examine the bactericidal effect against these microorganisms. The test specimens are SF-PVA and SF-PVA/ZnO composite films which were sterilized for 2 h using UV light. SF-PVA/ZnO composites produced clear ZOI on nutrient agar plates inoculated with *S. aureus, E. coli, P. aeruginosa*, *P. mirabilis* and *S. pyogenes* bacteria.

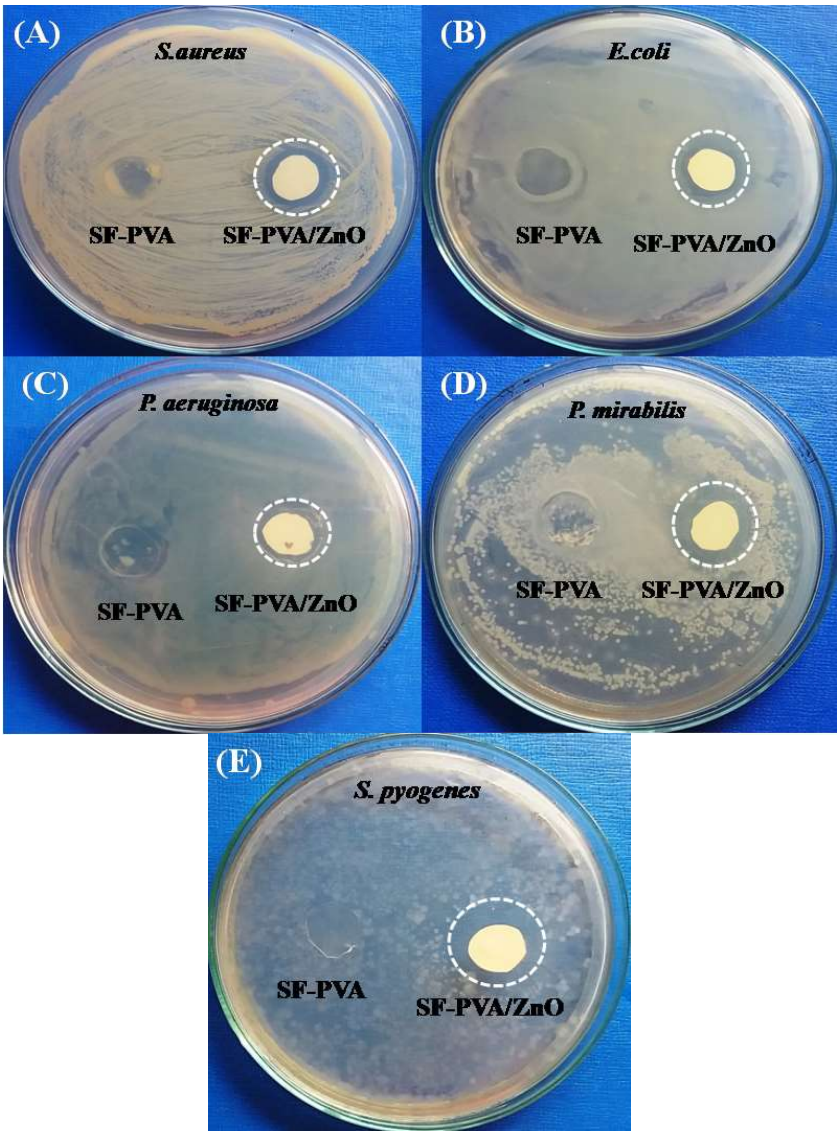

Figure 7.1 antibacterial activities of SF-PVA and SF-PVA/ZnO composite films against **(A)** *S. aureus* **(B)** *E.coli,* **(C)** *P. aeruginosa,* **(D)** *P. mirabilis* and **(E)** *S. pyogenes* microorganisms

The diameter of ZOI around each well is represented in figure 7.1. The diameter of ZOI of SF-PVA/ZnO is 3 mm in *S. aureus*, 2 mm in *E.coli,* 3 mm in *P. aeruginosa,* 3 mm in *P. mirabilis* and 3 mm against *S. pyogenes* as calculated. The ZOI of SF-PVA/ZnO is the reason of influence of ZnO NPs in the composite films. Reported literature study indicated that the ZOI increased with increasing ZnO NPs content of composite films and also observed that the inhibition zone for

S. aureus, P. aeruginosa, P. mirabilis and *S. pyogenes* was greater than that of *E.coli* [24].

7.3.2 Determination of antibacterial activity study of chitosan-ZnO NPs coated SF-PVA Composite films

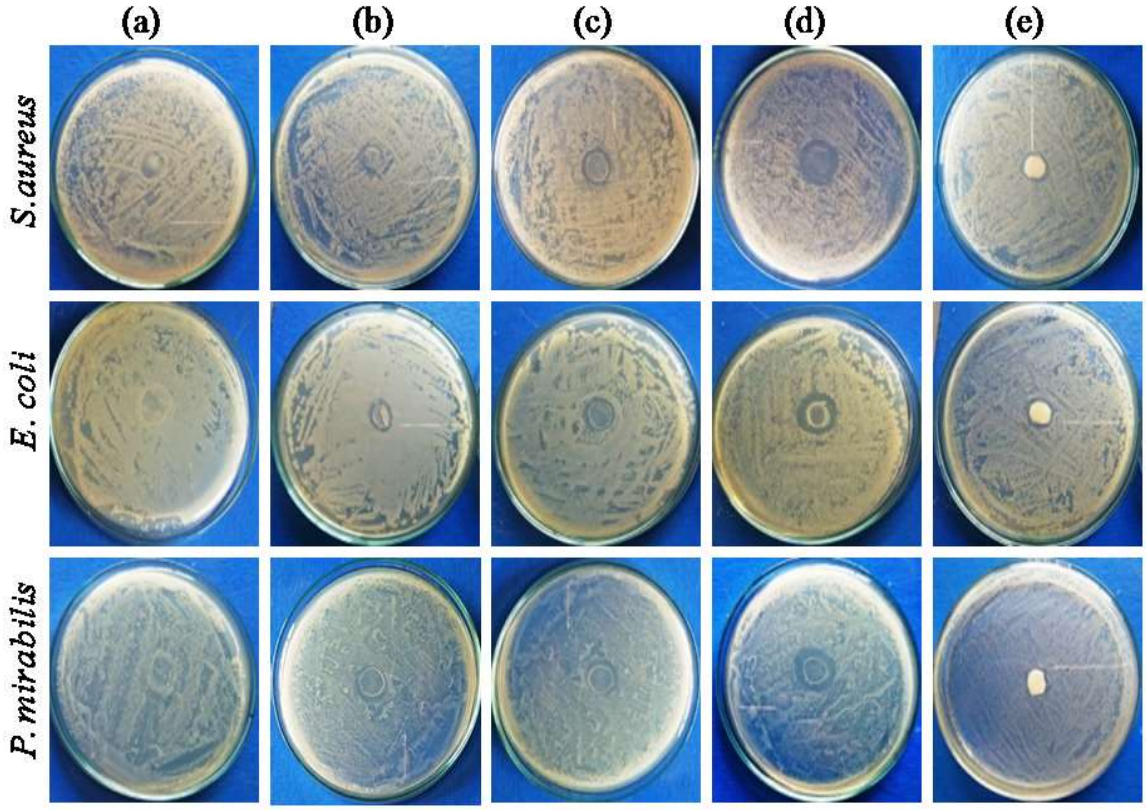

Figure 7.2 Antibacterial activities of **(a)** SF-PVA, **(b)** 0.2 wt %, **(c)** 0.5 wt %, **(d)** 1 wt % chitosan-ZnO NPs coated SF-PVA composite films and **(e)** Sterizone dressing.

The antibacterial assay of all the coated and uncoated composite films is presented in figure 7.2, which shows a higher ZOI against Gram-positive and Gram-negative bacteria when compared to the control SF-PVA composite film and Sterizone dressing. It can be seen that the inhibition zone of 0.2 wt % coating process shows the ZOI is 2 mm in *S. aureus*, 3 mm in *E.coli* and 2 mm in *P. mirabilis*. 0.5 wt % coating process observes the ZOI is 3 mm in *S. aureus*, 4 mm in *E.coli* and 3 mm in *P. mirabilis*. 1 wt % coating process shows the ZOI is 4 mm

in *S. aureus*, 5 mm in *E.coli* and 4 mm in *P. mirabilis* bacteria. Standard Sterizone dressing shows ZOI is 2 mm in *S. aureus*, 3 mm in *E.coli* and 2 mm in *P. mirabilis* bacteria. The obtained results can be concluded that the ZOI is higher in *E.coli* bacteria than *S. aureus* and *P. mirabilis* bacteria. The ZOI is increased with increasing the concentration of the chitosan-ZnO NPs on SF-PVA composite films. The obtained ZOI is due to the synergistic effect of chitosan and ZnO NPs.

7.3.3 Minimum inhibitory concentration (MIC) of ZnO NPs and hybrid chitosan-ZnO NPs

Table 7. 1 MIC of ZnO NPs and hybrid chitosan-ZnO NPs against *S. aureus*, *E. coli* and *P. mirabilis* bacteria

No.	Samples	*S. aureus*	*E. coli*	*P. mirabilis*
1.	ZnO NPs	50 µg/mL	100 µg/mL	100 µg/mL
2.	Hybrid chitosan-ZnO NPs	50 µg/mL	25 µg/mL	50 µg/mL

MIC of synthesized ZnO NPs and hybrid chitosan-ZnO NPs was determined by agar dilution method by using *E. coli*, *S. aureus* and *P. mirabilis* bacteria. Table 7.1 shows the MIC of ZnO NPs and hybrid chitosan-ZnO NPs against *E. coli*, *S. aureus* and *P. mirabilis*. It is found that the ZnO NPs are able to inhibit the bacterial growth at minimum concentration of 50 µg/mL against *S. aureus*, 100 µg/mL against *E. coli* and *P. mirabilis*. Hybrid chitosan-ZnO NPs are inhibited the bacterial growth at minimum concentration of 50 µg/mL against *S. aureus*, 25 µg/mL against *E. coli* and 50 µg/mL against *P. mirabilis* bacteria.

7.3.4 Determination of the growth curve of bacterial cells

Figure 7.3 (A), (B), (C) represents the growth curve of ZnO NPs, chitosan-ZnO NPs for *E. coli, S. aureus* and *P. mirabilis* bacterial cells, respectively. The obtained results indicate that the chitosan-ZnO NPs containing broth shows decreased bacterial cell growth than ZnO NPs. These results reveal that the effective bacteria killing ability of ZnO NPs and chitosan-ZnO NPs against bacteria. The absorbance of the sample increases with enhancing the bacterial cell growth. Hybrid chitosan-ZnO NPs depicts the lower absorbance that means bacterial cell growth is lower as compared to pure ZnO NPs. It shows improved diffusion into cell wall of bacteria, because presence of chitosan with ZnO NPs developing enhanced antibacterial activity. Hence, it is examined that the ZnO NPs, hybrid chitosan-ZnO NPs performs an essential role in antibacterial activity.

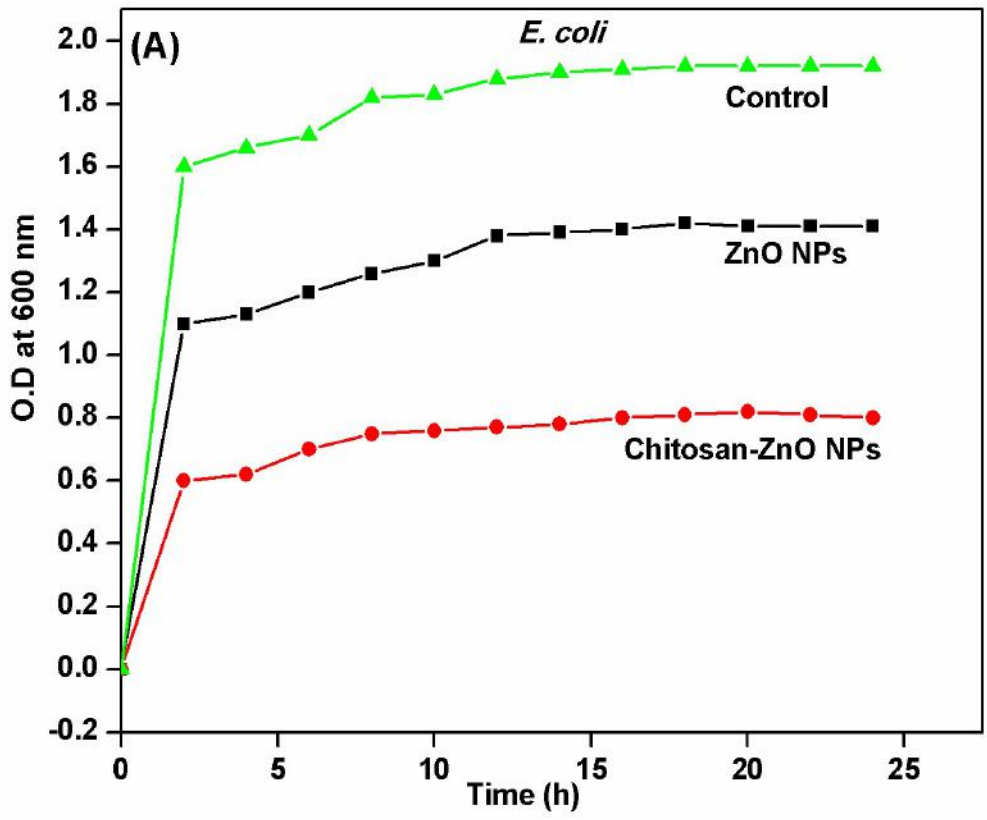

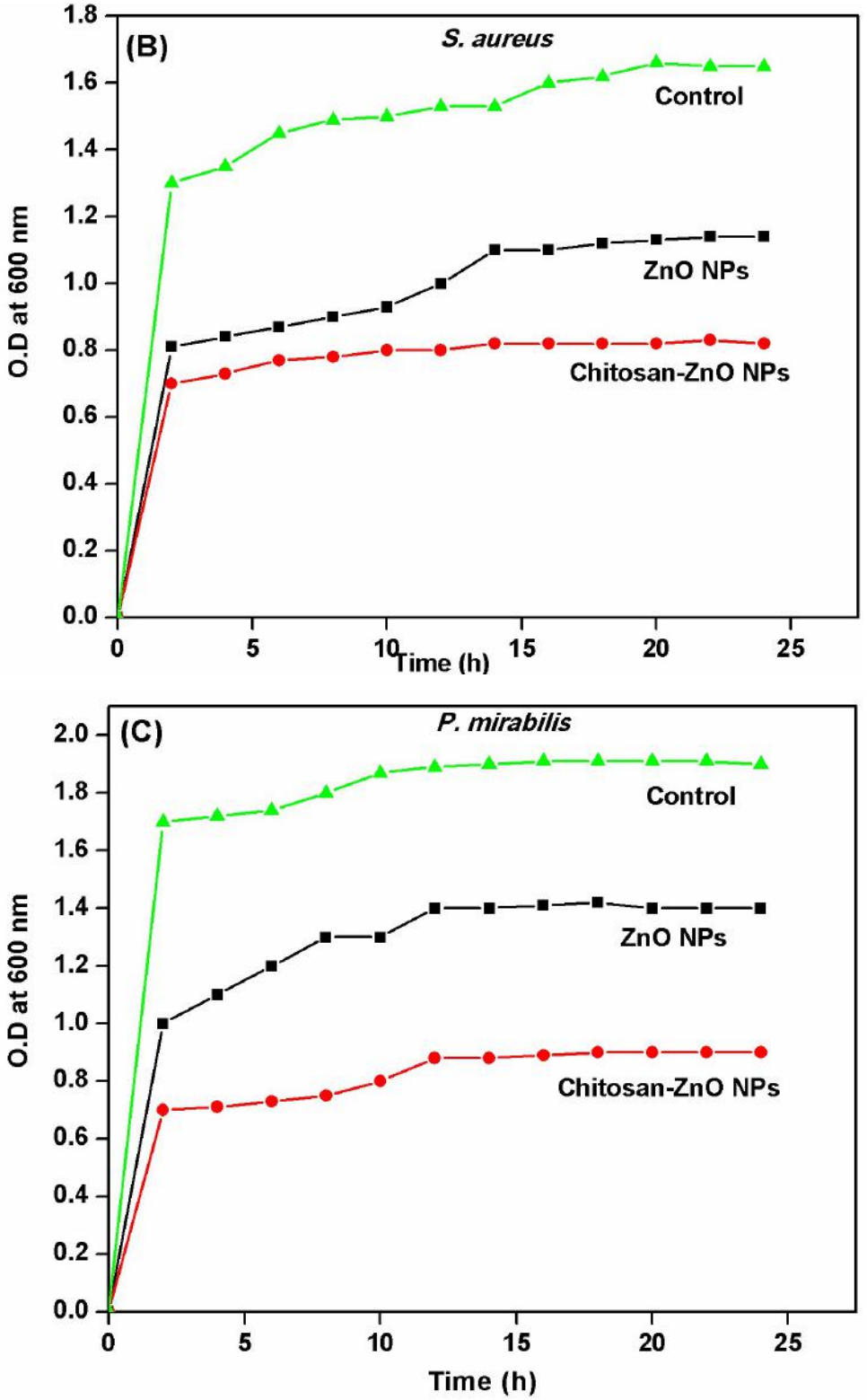

Figure 7.3 Growth curves of ZnO NPs, chitosan-ZnO NPs for **(A)** *E. coli*, **(B)** *S. aureus* and **(C)** *P. mirabilis* bacteria.

7.4 Mechanism of antibacterial activity of ZnO NPs and chitosan-ZnO NPs

Literature studies revealed that the ROS production as the major contribution responsible for ZnO NPs antibacterial activity. The schematic representation of antimicrobial property of ZnO NPs is shown in figure 7.4. ROS is derived from molecular oxygen. It is term for different reactive molecules and free radicals. ROS includes superoxide anion (O_2^-), hydrogen peroxide (H_2O_2), hydroxyl radicals (OH^-) and singlet oxygen ($^1O_2$). The antibacterial actions of ZnO NPs are enhanced by enhancing the production of ROS from ZnO NPs. ROS is damage the cellular biomolecules like DNA, lipids, and proteins. All this causes the apoptosis pathway and finally killing the bacterial cell. The mechanism of generation of ROS by ZnO NPs has the degradation of NPs and formation of ions, interaction of NPs with cellular organelles i.e. mitochondria, disrupting the electron transport chain and interaction of NPs with redox active protein i.e. NADPH oxidases etc.

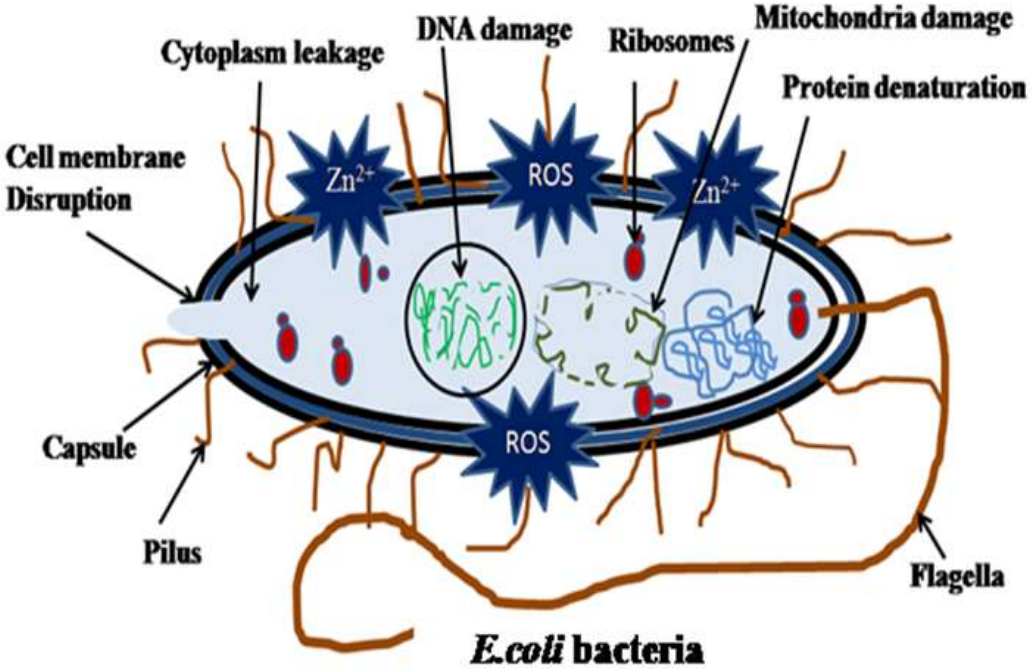

Figure 7.4 Schematic representation of mechanism of antibacterial activity of ZnO NPs.

The antibacterial activity can be enhanced due to the mechanism that is zinc ion release mechanism. When ZnO NPs (Eg = 3.37 eV) are under light irradiation, result in electron-hole pairs. This hole (h+) reacts with OH− on the surface of ZnO NPs, generating, and perhydroxyl radicals (HO_2•). These free radicals damage the cells of bacteria as a result of decomposition and complete destruction of microorganisms [25, 26].

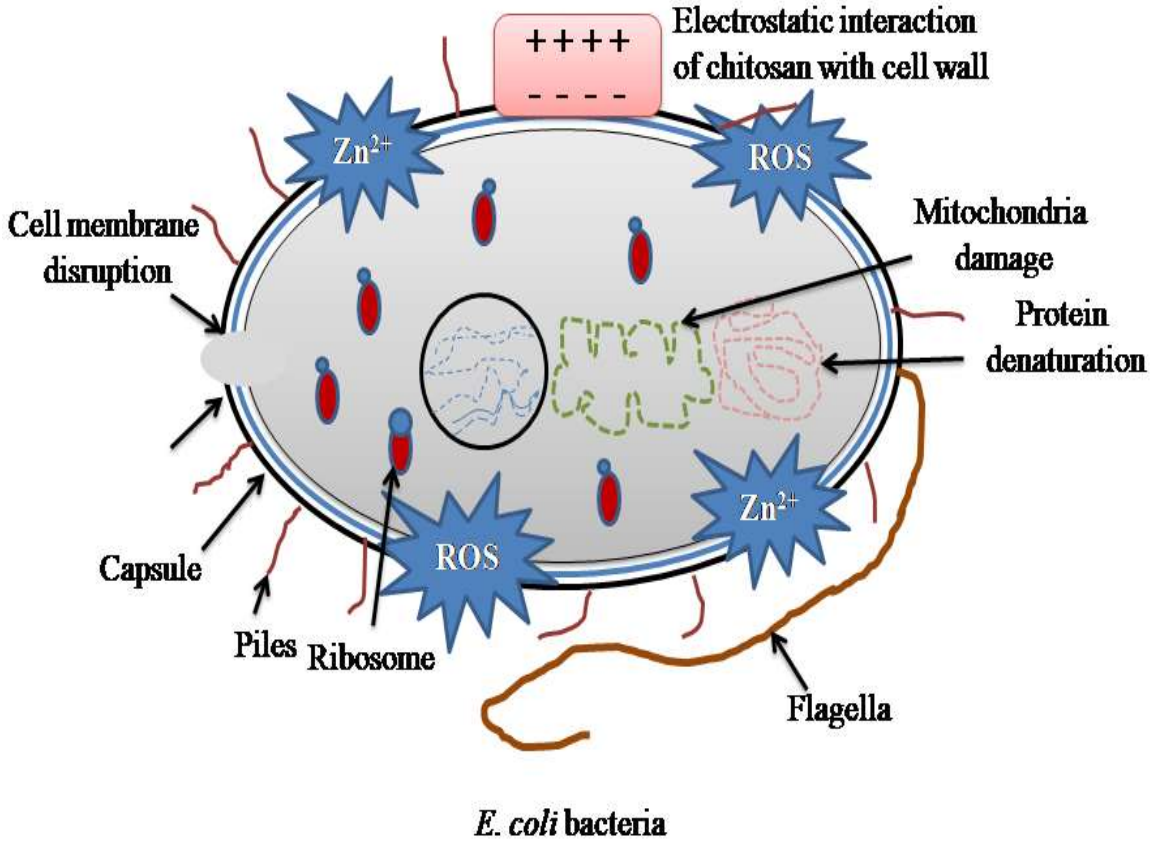

Figure 7.4 Schematic representation of mechanism of antibacterial activity of hybrid chitosan-ZnO NPs.

Combination of chitosan and ZnO NPs showed dual antibacterial properties due to reported study indicated that these two components are antibacterial agents. The mechanism of antibacterial activity of chitosan observed in several reported studies. Figure 7.5 shows the schematic representation of antimicrobial activity of hybrid chitosan-ZnO NPs. Firstly, the antibacterial activity of chitosan is due to its

positively charged amino groups, which can form electrostatic interactions with an anionic group of the microbial cell surface, inducing changes in permeability, metabolic disturbances and finally death [27, 28]. Secondly, the inhibition of the microbial growth was due to the chelation of nutrients, essential metal. In addition the surface of cell is creating a polymer matrix because of chitosan shows oxygen barrier capacity. These can restrict the growth of aerobic microorganisms. Additionally, the mechanism of bacteria killing ability of ZnO NPs explained on ROS and zinc ions [26].

7.5 Different factors affecting the antibacterial activity of ZnO NPs

There are different factors affected the antibacterial action of ZnO NPs such as size, shape, concentration, surface area, and synthesis process of NPs [25]. ZnO NPs exhibited attractive antibacterial activities could be a good choice of researchers and it applied in different areas like pharmaceuticals, food packaging, cosmetics, and wound healing and dressing applications [29]. This antibacterial action showed because the enhanced particular surface area as the smaller particle size leading to enhance particle surface activity. The size of NPs plays an essential and most important role of the antibacterial activity of ZnO NPs. It is investigated that smaller sized ZnO NPs showed higher antibacterial activity due to the smaller sized particles easily enter through the cell membrane of bacteria and damage the bacterial cell [30]. Reported study observed that the bacteria killing ability of ZnO NPs were studied against *S. aureus* and *E. coli* bacteria. The reported study concluded that the antimicrobial ability increased with decreasing the size of NPs. Another study indicated the smaller sized NPs observed best antibacterial activity under visible light [31].

Another important part is the bacterial killing action of ZnO NPs based on the shape of the particle. The shape of NPs is rods, spherical, tubes, wires, needles and ring like. Other shapes are spirals, disks, flowers, boxes, drums like. It is examined that the spherical shaped morphology of NPs showed higher antibacterial activity than other shaped NPs [30]. In another study nanowire shaped NPs revealed higher bacteria killing ability against *E. coli* bacteria [32].

Furthermore, the antibacterial property of ZnO NPs is based on the surface area and concentration of NPs. It is concluded that the more concentration and big surface area of NPs observed higher antibacterial activity. The antibacterial action was increased with increasing the concentration of NPs and modifying the surface area of NPs, due to ZnO NPs generates H_2O_2. This depends on the concentration and surface area of NPs [33]. The researchers found that the antibacterial activity also based on the synthesis process of NPs [15]. The synthesis methods of NPs are chemical precipitation, hydrothermal, sol-gel, simple thermal, combustion, polymerized complex method and vapour-liquid-solid technique. These Physico-chemical methods were used for synthesis of ZnO NPs. During these techniques the hydrothermal and chemical precipitation methods used to control the size of NPs and enhancing the antibacterial activity of NPs [34]. Other factors such as solvent type, precursor, temperature and pH, temperature are also played a significant role enhancing the antibacterial activity of ZnO NPs [30].

7.6 Different factors affecting the antibacterial activity of hybrid chitosan-ZnO NPs

Hybrid chitosan-ZnO NPs showed dual antibacterial activity against NPs. This hybrid coating is widely used to coat as an antibacterial coatings on cotton, paper and polymer matrices for antibacterial, food packaging and other biomedical applications. Antibacterial effect of hybrid chitosan-ZnO NPs has been investigated in many different studies and showed these hybrid NPs are best antibacterial agents [35]. There are various factors affected the antibacterial activity of hybrid chitosan-ZnO NPs. These factors are molecular weight of chitosan during synthesis of hybrid NPs, effects of pH, temperature and concentration [36]. Molecular weight of chitosan used in synthesis process plays a very essential role for antibacterial activities against pathogenic bacteria. The molecular weights of chitosan are classified into three groups, high and low molecular weight and oligochitosan. According to the reports it is indicated that the low molecular weight chitosan easily enter by microbial cell membrane and disturb the microbial cell whereas the high molecular weight chitosan cannot pass

easily through the microbial cell. Thus, it is very important to use low molecular weight chitosan for synthesis of hybrid chitosan-ZnO NPs [37]. It is reported that the low molecular weight chitosan coated composite films have higher antibacterial activity than high molecular weight chitosan coated films.

Additionally, decontamination activity of hybrid chitosan-ZnO NPs also based on the pH, temperature and concentration of NPs. According to the literature it is concluded that the low pH, low temperature and higher concentration of NPs enhanced the antibacterial effect against bacteria [9].

7.7 Conclusions

The present study evaluated the antibacterial activity of SF-PVA, SF-PVA/ZnO NPs and hybrid chitosan-ZnO NPs coated SF-PVA composite films. The antibacterial activity of ZnO NPs embedded SF-PVA composite films shows to inhibit the growth of Gram-positive as well as Gram-negative bacteria. Additionally, it shows higher inhibition zone against *S. aureus, P. aeruginosa, P. mirabilis* and *S. pyogenes* as compared to that for *E. coli* bacteria. Hybrid chitosan-ZnO NPs coated SF-PVA composite films represent the higher ZOI against Gram-positive and Gram-negative bacteria when compared to control SF-PVA composite film and Sterizone dressing. The obtained ZOI is due to the synergistic effects of chitosan and ZnO NPs. The obtained results depicted that the ZOI of all the chitosan-ZnO NPs coated SF-PVA composite films have higher than SF-PVA, SF-PVA/ZnO NPs composite film and Sterizone dressing. The ZOI is increased with increase in the concentration of the hybrid chitosan-ZnO NPs on SF-PVA composite film. ZnO NPs inhibited the growth of microorganisms of minimum concentration of 50 µg/mL against *S. aureus*, 100 µg/mL against *E. coli* and *P. mirabilis* and hybrid chitosan-ZnO NPs inhibited the growth of microorganisms of minimum concentration of 50 µg/mL against *S. aureus*, 25 µg/mL against *E. coli* and 50 µg/mL against *P. mirabilis* bacteria. Based on theses we can conclude that the composite films of SF-PVA/ZnO NPs and hybrid chitosan-ZnO NPs coated SF-PVA composite films show antibacterial activity. Among all composite films, 1 wt % coated composite film is examined higher antibacterial activity than other

composite films. Therefore, the obtained results indicated that hybrid chitosan-ZnO NPs coated SF-PVA composite film is promising candidates for antibacterial wound dressing applications.

References

1. A. Hersh, H. Chambers, J. Maselli, R. Gonzales, Arch Intern Med, 2008, 168, 1585-1591.
2. A. Surahio, A. Talpur, A. Memon, A. Junejo, A. Laghari, Professional Med J, 2017, 24, 57-63.
3. N. Kassam, D. Damian, D. Kajeguka, B. Nyombi, G. Kibiki, BMC Res Notes, 2017, 10, 757(1-6).
4. P. Vonaesch, M. Anderson, P. Sansonetti, FEMS Microbiol Rev 2018, 42, 273-292.
5. S. Ghatak, V. Hascall, R. Rodriguez, R. Markwald, S. Misra, Wound Healing, 2017, 195-209.
6. S. Sahoo, R. Misra, S. Parveen, Nanomedicine Cancer 2017, 73-124.
7. P. Patil, J. Meshram, R. Bohara, S. Nanaware, S. Pawar, New J Chem, 2018, 42, 14620-14629.
8. Z. Lu, J. Gao, Q. He, J. Wu, D. Liang, H. Yang, R. Chen, Carbohydr Polym, 2017, 156, 460-469.
9. V. Bui, D. Park, Y. C. Lee, Polymers, 2017, 9, 21(1-24).
10. R. Ahmed, M. Tariq, I. Ali, R. Asghar, P. Khanam, R. Augustine, A. Hasan, Int J Biol Macromol, 2018, 120, 385-393.
11. M. Khorasani, A. Joorabloo, A. Moghaddam, H. Shamsi, Z. Moghadam, Int J Biol Macromol, 2018, 114, 1203-1215.
12. P. Espitia, N. Soares, J. dos Reis Coimbra, N. de Andrade, R. Cruz, E. Medeiros, Food Bioprocess Tech, 2012, 5, 1447-1464.
13. A. Sirelkhatim, S. Mahmud, A. Seeni, N. Kaus, L. Ann, S. Bakhori, H. Hasan D. Mohamad, Nano-Micro Lett, 2015, 7, 219-242.
14. Y. Xie, Y. He, P. Irwin, T. Jin, X. Shi, Appl Environ Microbiol, 2011, 77, 2325-2331.
15. S. Dizaj, F. Lotfipour, M. Barzegar-Jalali, M. Zarrintan, K. Adibkia, Mater Sci Eng C, 2014, 44, 278-284.
16. V. Schwartz, F. Thetiot, S. Ritz, S. Pütz, L. Choritz, A. Lappas, R. Forch, K.

Landfester, U. Jonas, Adv Funct Mater, 2012, 22, 2376-2386.

17. Y. Chen, W. Tse, L. Chen, J. Zhang, Nanoscale Res Lett, 2015, 10.
18. M. Busila, V. Musat, T. Textor, B. Mahltig, RSC Adv, 2015, 5, 21562-21571.
19. M. AbdElhady, Int. J Carbohyd Chem, Article ID 840591, 2012, 1-6.
20. W. Diao, Q. Hu, H. Zhang, J. Xu, Food Control, 2014, 35, 109-116.
21. M. Balouiri, M. Sadiki, S. Ibnsouda, J Pharmaceut Anal, 2016, 6, 71-79.
22. H. Gunes, D. Gulen, R. Mutlu, A. Gumus, T. Tas, A. Topkaya, Toxicol Ind Health, 2016, 32, 246-250.
23. R. Maier, I. Pepper, Environmental Microbiology, 3rd Edition, 2015, 37-56.
24. R. Kumar, A. Umar, G. Kumar, H. Nalwa, Ceram Int, 2017, 43, 3940-3961.
25. K. Gold, B. Slay, M. Knackstedt, A. Gaharwar, Adv Therap, 2018, 1, 1700033 (1 – 15).
26. D. Chauhan, C. Gopal, D. Kumar, N. Mahato, M. Quraishi, M. Cho, Mater Discovery, 2018, 1, 19-25.
27. T. Wu, J. Huang, Y. Jiang, Y. Hu, X. Ye, D. Liu, J. Chen, Food Chem, 2018, 240, 361-369.
28. J. Li, Y. Wu, L. Zhao, Carbohydr Polym, 2016, 148, 200-205.
29. H. Mirzaei, M. Darroudi, Ceram Int, 2017, 43, 907-914.
30. L. Wang, C. Hu, L. Shao, Int J Nanomedicine, 2017, 12, 1227- 1249.
31. H. Yang, Q. Zhang, Y. Chen, Y. Huang, F. Yang, Z. Lu, Carbohydr Polym, 2018, 201, 162-171.
32. J. Wu, L. Tsay, Nanotechnology, 2015, 26, 395704 (1-10).
33. V. Lakshmi Prasanna, R. Vijayaraghavan, Langmuir, 2015, 31, 9155-9162.
34. M. Gharibshahian, M. Nourbakhsh, O. Mirzaee, J Solgel Sci Technol, 2018, 85, 684-692.
35. P. Petkova, A. Francesko, M. Fernandes, E. Mendoza, I. Perelshtein, A. Gedanken, T. Tzanov, ACS Appl Mater Interfaces, 2014, 6, 1164-1172.
36. N. Yusof, N. Zain, N. Pauzi, Int J Biol Macromol, 2018, 124, 1132-1136.
37. R. Goy, S. Morais, O. B. Rev. Bras, Farmacogn, 2016, 26, 122-127.

CHAPTER 8

Evaluation of SF based composite films for their wound dressing application

8.1 Introduction

Recently, researchers have been focused on the development of newer dressing materials for infected wound management due to wound infection causes pus formation and delay the wound healing. This issue can be controlled by using the wound dressings with antibacterial activity. In this regard, the materials like hydrogels, nanofibrous matrices, scaffolds, and composite films have been utilized widely for antibacterial wound dressings [1]. These dressing materials are designed from natural and synthetic polymers like chitosan, alginate, hyaluronic acid, collagen, gelatin, polyurethane (PU), polyethyleneimine (PEI), poly (L-lactic-co-glycolic acid) (PLGA), poly (lactic acid) (PLA), poly (vinyl alcohol) (PVA) etc [2, 3]. Most of the dressing materials prepared from the above materials are lacking one or the other factors like lower mechanical properties, insufficient blood clotting ability, lower swelling capacity, and inadequate antibacterial activity [4, 5]. Therefore, it is necessary to evaluate the potential of materials for antibacterial wound dressings.

Hence, the present chapter mainly focused on a comparative study between the prepared composite films of SF-PVA, SF-PVA/ZnO NPs and hybrid chitosan-ZnO NPs coated SF-PVA composite films. The potential of the prepared composite film for wound dressing application has been determined regarding its biological properties, physical properties, and environmental (biodegradable) property. Biological properties include the antibacterial activity and biocompatibility study. Antibacterial activity study of composite films was done by using wound infection causing microorganisms. The comparative study of antibacterial activity of composite films will help to confirm which composite film is better for controlling the high level of infection within the wound area. Biocompatibility study consists of cell viability, hemocompatibility and blood clotting ability. This will help to assume that how biological compatible of composite films. Further, physical properties include the swelling study and mechanical property. The comparative study of physical properties will evaluate the capacity of pus absorption and flexibility of composite films.

8.2 Experimental results and comparative studies of SF-PVA, SF-PVA/ZnO NPs and hybrid chitosan-ZnO NPs coated SF-PVA composite films

8.2.1 Comparative study of biological properties of SF-PVA, SF-PVA/ZnO NPs, and hybrid chitosan-ZnO NPs coated SF-PVA composite films

8.2.1.1 Antibacterial Activity

The evaluation of the antibacterial activity of composite films plays a significant role in wound dressing materials for controlling the infections within the wound area [6]. The wound infection-causing microorganisms are gram positive and gram negative bacteria such as *S. aureus*, *S. pyogenes*, *P. aeruginosa*, *E. coli* and *P. mirabilis* bacteria etc. In the present study, the antibacterial activity of composite films and synthesized NPs have been carried out and the results revealed that ZnO NPs embedded SF-PVA composite film showed excellent antibacterial property against wound infection associated bacteria. The diameter of ZOI of ZnO NPs embedded SF-PVA composite film observed 3 mm in *S. aureus*, 2 mm in *E. coli*, 3 mm in *P. aeruginosa*, 3 mm in *P. mirabilis* and 3 mm in *S. pyogenes* bacteria. The ZOI increased with increase in the concentration of ZnO NPs into SF-PVA composite film. The antibacterial activity of hybrid chitosan-ZnO NPs coated composite films were determined by using the three different bacteria which was *S. aureus*, *E. coli, P. mirabilis*. The obtained results were observed that the ZOI of 0.2 wt % coated composite film showed 2 mm in *S. aureus*, 3 mm in *E. coli* and 2 mm in *P. mirabilis* bacteria. The 0.5 wt % coated composite films observed the ZOI is 3 mm in *S. aureus*, 4 mm in *E. coli* and 3 mm in *P. mirabilis* bacteria. The 1 wt % coated composite films showed the ZOI was 4 mm in *S. aureus*, 5 mm in *E. coli* and 4 mm in *P. mirabilis* bacteria. The inhibition zone was increased with increase in the concentration of hybrid chitosan-ZnO NPs due to the synergistic antibacterial effect of chitosan and ZnO NPs. The market wound dressing material examined the ZOI was 2 mm in *S. aureus*, 3 mm in *E. coli* and 2 mm in *P. mirabilis* bacteria. The obtained results concluded that the 1 wt % of hybrid chitosan-ZnO NPs coated SF-PVA composite film has higher ZOI compared to other coated composite films and market Sterizone dressings.

The MIC of ZnO NPs was determined by broth dilution method. The obtained results found that the ZnO NPs were able to inhibit the growth of microorganisms at a minimum concentration of 50 µg/mL against *S. aureus*, 100 µg/mL against *E. coli* and *P. mirabilis* bacteria. The MIC of hybrid chitosan-ZnO NPs was 50 µg/mL against *S. aureus*, 25 µg/mL against *E. coli* and 50 µg/mL against *P. mirabilis* bacteria. Growth curves of ZnO NPs and hybrid chitosan-ZnO NPs were determined by using the *S. aureus*, *E. coli* and *P. mirabilis* bacteria. The results concluded that the hybrid chitosan-ZnO NPs containing broth showed decreased bacterial cell growth compared to ZnO NPs. The absorbance of the sample increased with an increase in bacterial cell growth. Hybrid chitosan-ZnO NPs were showed lower absorbance i.e. bacterial cell growth was lower than ZnO NPs. Hence the antibacterial activity of SF-PVA composite films represented by incorporation of ZnO NPs and coated surface of composite films with hybrid chitosan-ZnO NPs. All the antibacterial results concluded that the hybrid chitosan-ZnO NPs revealed higher antibacterial activity compared to pure ZnO NPs. Therefore, the hybrid chitosan-ZnO NPs plays a significant role in controlling the infections surrounding the wound area.

8.2.1.2 Biocompatibility study

The successful wound dressing applications of composite films are possible after confirming their biocompatibility study [7]. Herein, biocompatibility study includes the cell viability, hemocompatibility and blood clotting ability of prepared composite films.

The toxicity study of composite materials were studied by using well known MTT assay method using cell lines i.e. L929 mouse fibroblast cells. The ideal properties of best wound dressings are nontoxic and biocompatible [8]. The cell viability of SF-PVA composite film observed 100 % at 24 h, 105 % at 48 h and 107 % at 72 h of incubation time whereas, the cell viability of ZnO NPs embedded SF-PVA composite film showed 72 % at 24 h, 76 % at 48 h and 81 % at 72 h of incubation. The cell viability of all the hybrid chitosan-ZnO NPs coated

composite films have 75-85 % at 24 h, 48 h and 72 h of incubation time, higher to the Sterizone dressing it showed the cell viability 70-80 % at 24 h, 48 h and 72 h of incubation time. All the cell viability data revealed that the prepared composite films have nontoxic to cells. The reduced cell viability at 24 h, because the interaction of ZnO NPs and hybrid chitosan-ZnO NPs with the cells. Further, after 24 h of incubation the remaining cells began to multiply and the cell viability was increased after 48 h and 72 h of incubation time. Cell viability study also suggested that there was slightly increasing the cell viability of hybrid chitosan-ZnO NPs coated SF-PVA composite films than ZnO NPs embedded SF-PVA composite film and Sterizone dressings.

The SF-PVA composite film showed the hemolysis was 2.1 % and 2 % for 2 h and 20 h of incubation respectively while the ZnO NPs embedded SF-PVA composite film showed the hemolysis was 3.4 % at 2 h and 2.7 % for 20 h. The hemolysis percentage of SF-PVA and ZnO NPs embedded SF-PVA composite film showed below 5 %, which indicated that both the composite films have slightly hemolytic material. The hemolysis for 0.2 wt % hybrid chitosan-ZnO NPs coated SF-PVA composite film was found to be 2 % at 2 h and 1.8 % for 20 h of incubation, 0.5 wt % coated composite film was found to be hemolysis about 1.7 wt % for 2 h and 1.6 % for 20 h of incubation. The 1 wt % coated composite film showed hemolysis was about 1.5 % for 2 h and 1.3 % for 20 h of incubation while the Sterizone dressing showed the hemolysis about 1.8 % for 2 h and 1.6 % for 20 h of incubation time. Finally, results concluded that all hybrid NPs coated composite films as well as Sterizone dressing, have nonhemolytic materials. Hybrid chitosan-ZnO NPs coated composite films have hemocompatible to blood. Table 8.1 shows the comparative study of biological properties of SF-PVA, SF-PVA/ZnO NPs and hybrid Chitosan-ZnO NPs coated SF-PVA composite films.

Table 8.1: Comparative study of biological properties of SF-PVA, SF-PVA/ZnO NPs and hybrid Chitosan-ZnO NPs coated SF-PVA composite films.

Sr. No.	Biological Properties	SF-PVA Composite film	SF-PVA/ZnO NPs composite film	Hybrid Chitosan-ZnO NPs coated SF-PVA composite films			Sterizone dressing
				0.2 wt %	0.5 wt %	1 wt %	
1.	Antibacterial Activity						
	S. aureus	-	3 mm	2 mm	3 mm	4 mm	2 mm
	E. coli	-	2 mm	3 mm	4 mm	5 mm	3 mm
	P. aeruginosa	-	3 mm	-	-	-	-
	P. mirabilis	-	3 mm	2 mm	3 mm	4 mm	2 mm
	S. pyogenes	-	3 mm	-	-	-	-
2.	Biocompatibility						
	Cell Viability						
	24 h	100 %	72 %	73 %	75 %	78 %	71 %
	48 h	105 %	76 %	75 %	78 %	80 %	74 %
	72 h	107 %	81 %	78 %	80 %	83 %	76 %
	Hemolysis						
	2 h	2.1 %	3.4 %	2 %	1.7 %	1.5 %	1.8 %
	20 h	2 %	2.7 %	1.8 %	1.6 %	1.3 %	1.6 %

Blood clotting ability of prepared composite films was done by using blood clotting assay. Blood clotting ability of ZnO NPs embedded SF-PVA composite film was higher as compared to SF-PVA composite film due to the ZnO NPs are hemostatic in nature. The hybrid chitosan-ZnO NPs coated composite films showed higher blood clotting ability than SF-PVA composite film. The control SF-PVA composite film showed poor blood clotting ability, its clotting ability has

enhanced by embedding ZnO NPs into it and clotting the surface with hybrid chitosan-ZnO NPs due to both the material chitosan and ZnO NPs are hemostatic in nature. Hybrid chitosan-ZnO NPs can form a complex with fibrin protein in blood plasma.

8.2.2 Comparative study of physical properties of SF-PVA composite film, SF-PVA/ZnO NPs composite film, and chitosan-ZnO NPs coated SF-PVA composite films

8.2.2.1 Swelling study

The swelling property with high water uptake capacity has been shown to enhance the high wound exudates absorption capacity of dressing bandages, preventing infections and accelerating wound healing. High water uptake capacity maintains a moist environment in the wound area. Further, it prevents the dehydration of the tissue as well as latter cell death. It helps to remove the dead cells and promotes the angiogenesis process. Angiogenesis is the process of formation of new blood vessels [9]. Researchers have also reported that low levels of water uptake capacity of dressing material perform a significant role in delaying the wound healing process if these dressings are employed [10]. According to the obtained results of SF-PVA and ZnO NPs embedded SF-PVA composite films have showed the swelling ratio of 25-30 %. Addition of ZnO NPs to SF-PVA matrix were slightly reduced the swelling ratio due to SF and PVA both materials are more hydrophilic nature than ZnO NPs. This is due to the interactions between SF-PVA and ZnO NPs. The swelling ratio of both the composite films was increased after 7 days of incubations than 1 day. Hybrid chitosan-ZnO NPs coated composite films represented higher swelling capacity than control SF-PVA and market Sterizone dressings. The concentration of 1 wt % hybrid NPs coated composite film showed higher swelling ratio than other less concentration of coated composite films. The swelling ratio of the coated composite film has a lower capacity than ZnO NPs embedded SF-PVA composite films due to the concentration of SF-PVA was different. The ZnO NPs embedded SF-PVA

composite film has a concentration of SF-PVA wt. ratio 1:4. The hybrid NPs coated composite films have the concentration of SF-PVA wt. ratio 1:1. The swelling ratio also depends on the concentration of PVA. It also performs a significant role in enhancing the swelling ratio of composite films. The obtained swelling ratio similar to reported β-chitin hydrogel/nano ZnO composite bandage and chitin hydrogel/nano-ZnO composite bandage, which was in the range of 12-18 % and 16-18 % respectively [11, 12]. Therefore, the swelling study of composite films could be concluded that the prepared composite films were applicable for absorbing large volume of wound exudates. The composite films then started to slightly degrade after 21 days.

Swelling ratio is depending on the porosity of composite films due to higher porosity of materials absorb large amount of wound exudates within the wound area. Herein, the porosity of composite films has been carried out by BET analysis method. It explores in detail about the diameter and volume of pores. BET is a physical gas adsorption method. It is a standard method for determination of surface area and porosity of materials [13]. The SF-PVA composite film showed the pore diameter was 1.64 nm and the ZnO NPs incorporated SF-PVA composite film showed the pore diameter was 1.57 nm. Addition of ZnO NPs into SF-PVA composite film was slightly decreased the pore diameter due to interaction of ZnO NPs and SF-PVA matrix. The porosity of hybrid chitosan-ZnO NPs coated SF-PVA composite films were investigated by the BET analysis. The porosity of hybrid chitosan-ZnO NPs were observed due to the coating of hybrid NPs on the surface of SF-PVA composite film. Hence, the surface areas of coated composite films were also carried out by BET analysis. The composite film of 0.2 wt % coated composite film showed the surface area of 12.75 m^2/g, 0.5 wt % coated composite film showed the surface area 19.28 m^2/g and 1 wt % coated composite film noticed the specific surface area was about 41.39 m^2/g. The market Sterizone dressing revealed the surface area was about 18.14 m^2/g. According to the present results, the specific surface area of hybrid NPs coated composite films has higher than Sterizone dressing. The pore distribution analysis showed the mesopores

ranging from 2 to 24 nm. All these data concluded that the porosity of hybrid chitosan-ZnO NPs coated composite films have higher than control SF-PVA composite films. Higher diameter and volume of pores of composite materials are necessary for cell growth, migration and cell attachment. Moreover, it also required for distribution of oxygen, nutrients and medium from the wound surface [11].

8.2.2.2 Mechanical Property

The best wound dressings should have sufficient flexibility and mechanical strength, which can be suitable for specific areas particularly close to the joints. Therefore, the sufficient tensile strength and flexibility of dressing materials are necessary for the development of novel dressing materials. The mechanical property of SF-PVA and ZnO NPs embedded SF-PVA composite films determined by the universal testing machine. The tensile strength of SF-PVA composite film was about 3.125 MPa and % elongation was about 178 %. The ZnO NPs embedded SF-PVA composite film showed a tensile strength was about 3.791 MPa and % elongation about 207 %. After incorporation of ZnO NPs into SF-PVA composite film, the tensile strength and % elongation was increased. The 0.2 wt % hybrid chitosan-ZnO NPs coated composite film showed the tensile strength of 9 MPa and percent elongation of 133 %, 0.5 wt % hybrid NPs coated composite film showed the tensile strength of 9.4 MPa and % elongation of about 124 % and 1 wt % coated film revealed the tensile strength was 10.6 MPa and percent elongation of 106 %. The obtained data concluded that the coating of higher concentration of hybrid chitosan-ZnO NPs indicated that enhanced the tensile strength and reduced the percent elongation of composite films. All these results examined that hybrid chitosan-ZnO NPs coated composite films showed better mechanical property than control SF-PVA and ZnO NPs embedded SF-PVA composite films.

Previous study have been reported that the tensile strength of chitin hydrogel/ nano ZnO composite bandage showed in the range of 0.015 MPa to 0.022 MPa and % elongation was in the range of 40-50 %, the tensile strength of

β-chitin hydrogel/ nano ZnO composite material showed in the rage of 0.05 MPa and % elongation was 50 % and the tensile strength of chitosan hydrogel/ nano ZnO composite bandage represented 0.15 MPa and % elongation was in the range of 40-50 % [12, 11, 14]. The commercially available Kaltostat dressing indicated that tensile strength was 0.9 MPa and Resolut LT dressing noted tensile strength of about 1.7 MPa [15]. All these reported dressing materials examined that it showed excellent mechanical properties for wound dressing application. The obtained tensile strength and percent elongation of 1 wt % coated chitosan-ZnO NPs composite film exhibited higher than other reported composites, control SF-PVA and ZnO NPs embedded SF-PVA composite films. Therefore, it could be demonstrated that the obtained tensile strength and percent elongation of chitosan-ZnO NPs coated SF-PVA composite film showed excellent mechanical property for wound dressing application.

8.2.3 Comparative study of Environmental (Biodegradable) property of SF-PVA, SF-PVA/ZnO NPs and hybrid chitosan-ZnO NPs coated SF-PVA composite films

The determination of the biodegradability study of materials plays an ideal role in the environmental field [16]. Biodegradation study of all the composite films was evaluated by immersing composite films into the PBS medium of pH 7.5 containing lysozyme enzyme. The biodegradation nature of composite films would be very helpful to attain better wound healing process. The biodegradation rate of SF-PVA composite film showed the 50-65 % after 21 days and the ZnO NPs embedded SF-PVA composite film showed the 30-40 % after 21 days. The degradation rate was decreased by addition of ZnO NPs into it. The degradation rate of 0.2 wt % coated composite film observed 35-45 % after 21 days, 0.5 wt % coated composite films showed the degradation rate 30-40 % and 1 wt % coated composite film showed the degradation rate 40-50 % after 21 days. The Sterizone dressing has degradation capacity about 35-40 % after 21 days. The results concluded that the degradation rate of hybrid chitosan-ZnO NPs coated composite

films have higher than Sterizone dressing and ZnO NPs embedded SF-PVA composite films. The obtained results of degradation study are higher than reported chitosan hydrogel/ nano ZnO composite bandage. The chitosan/nano ZnO composite bandage showed the degradation rate of within 1 week was between 5 % -15 %, 20 % -35 % after 2 weeks and 25 % -35 % after 3 weeks [14]. The biodegradation of composite films was due to the mechanism of lysozyme. It separates the glycosidic linkage between monomers. The degradation compounds of SF are amino acids which are glycine and alanine. These are important for angiogenesis process. The degradation compounds of chitosan are D-glucosamine and glycosaminoglycans. These compounds are present in human body which are nontoxic to cells and used for process of wound healing. [17]. Table 8.2 shows the comparative study of physical and environmental (biodegradable) properties of SF-PVA, SF-PVA/ZnO NPs and hybrid Chitosan-ZnO NPs coated SF-PVA composite films.

Table 8.2: Comparative study of physical and environmental (biodegradable) properties of SF-PVA, SF-PVA/ZnO NPs and hybrid Chitosan-ZnO NPs coated SF-PVA composite films.

Sr. No.	Physical Properties	SF-PVA composite film	SF-PVA/ZnO NPs composite film	Hybrid Chitosan-ZnO NPs coated SF-PVA composite films			Sterizone dressing
				0.2 wt %	0.5 wt %	1 wt %	
1.	Swelling ratio	25-30 %	25-30 %	10-15 %	10-15%	15-20%	15-20%
	Porosity	1.65 nm	1.57 nm	2 nm	4 nm	6 nm	4 nm
2.	Mechanical property						
	Tensile strength	3.125 MPa	3.791 MPa	9 MPa	9.4 MPa	10.6 MPa	-
	% elongation	178 %	207 %	133 %	124 %	106 %	-
	Environmental (Biodegradable Property)	50-65 %	30-40 %	35-45 %	30-40 %	40-50 %	35-40 %

8.3 Role of ZnO NPs and hybrid chitosan-ZnO NPs in composite films

In our present study, we have formulated wound dressings of SF-PVA/ZnO NPs and SF-PVA, with and without NPs composite films respectively and the results of these composite films reported in chapter 4 and 5. The important wound dressing properties are biological and physical. The most important biological property is antibacterial activity. The bacteria-killing ability of inorganic NPs is stronger and suitable for controlling the infections within the area of the wound. NPs embedded composite film of SF-PVA/ZnO showed higher antibacterial activity than without NPs composite film. Similarly, NPs coated composite films exhibited higher antibacterial activity than SF-PVA composite film and Sterizone dressings. Sterizone is an Ag NPs based commercial dressing material commonly used as an antibacterial wound dressing. The antibacterial ability was observed because of the presence of ZnO NPs in film.

The obtained results indicated that the antibacterial activity of composite films increased by increasing the concentration of NPs. The similar report observed in the literature, Kumar *et al*. synthesized ZnO NPs embedded chitosan hydrogel for wound dressing application [14]. The antibacterial activity of composite bandages showed more of higher concentration of ZnO NPs embedded chitosan bandages than a lower concentration of ZnO NPs embedded chitosan bandages. One of the reported studies indicated that the antibacterial activity increased due to the addition of a higher concentration of chitosan modified ZnO NPs in the polymer matrix. The bacterial killing ability revealed due to only ZnO NPs and modified chitosan-ZnO NPs. The bacteria-killing mechanism is the ZnO NPs released Zn^{+} ions and production of ROS. The Zn^{+} ions and ROS binds on the negative surface of the bacterial membrane and cause the cell wall leakage, protein, nucleus denaturation, mitochondria damage and death of bacterial cell [18]. Hybrid chitosan-ZnO NPs showed synergistic action of antimicrobial because both chitosan and ZnO NPs have antibacterial activity. The mechanism of antibacterial activity of chitosan is the positively charged amino groups. These

amino groups form the electrostatic interaction of negatively charged bacterial cells and cause the damage of bacterial cells [19].

Another important property of wound dressing materials is biocompatibility. The cell viability of without NPs i.e. SF-PVA composite film exhibited higher than ZnO NPs embedded SF-PVA composite films. The slightly decreased cell viability of composite film observed due to the presence of ZnO NPs. These NPs released toxic ions and excess ROS production. Therefore, the decreasing in cell viability of composite films exhibited owing to the presence of ZnO NPs. This issue can be controlled by modifying the ZnO NPs with chitosan materials. Hence, the hybrid chitosan-ZnO NPs exhibited higher cell viability compared to the SF-PVA/ZnO NPs composite film and Sterizone dressing. Additionally, the cell viability results concluded that the cell viability of composite films increased after 72 h of incubation compared to 24 h of incubation time. The present results obtained due to the cells are multiplied after 24 h and 72 h of incubation time. Similar results observed in a reported bionanocomposite film based on chitosan modified ZnO NPs incorporated castor oil polymeric films and chitin hydrogel/ ZnO NPs composite bandage [15, 12]. Hence, the obtained results concluded that the cell viability of hybrid chitosan-ZnO NPs was higher than ZnO NPs embedded SF-PVA composite film and Sterizone dressing. Similarly, the hemocompatibility and blood clotting ability of hybrid chitosan-ZnO NPs coated SF-PVA composite films was enhanced than without NPs, SF-PVA composite film and ZnO NPs embedded SF-PVA composite film. The hemocompatibility and blood clotting ability was slightly enhanced due to the ZnO NPs and chitosan are hemostatic in nature, it forms complex with fibrin protein present in blood plasma. Additionally, cationic nature of chitosan interacts with negatively charged blood cells [20].

The absorption capacity of prepared composite films is important for best wound dressing materials. The absorption capacity was estimated by determining the swelling ratio composite films. The swelling ratio of ZnO NPs embedded SF-

PVA composite film was slightly decreased compared to SF-PVA composite film. This is due to the interaction of ZnO NPs to the polymer matrix. SF and PVA both materials are hydrophilic in nature. The obtained results matched with reported ZnO NPs embedded chitosan hydrogel composite bandages [14]. If the inorganic NPs were added to the hydrophilic polymer matrix, its hydrophilicity slightly decreased because of the interactions of these materials. The swelling ratio of SF-PVA composite film was increased by the coating of hybrid chitosan-ZnO NPs. Chitosan is hydrophilic in nature.

Mechanical strength and flexibility of composite materials are important in wound dressing materials. The mechanical property of ZnO NPs embedded SF-PVA composite film showed enhanced compared to SF-PVA composite film. Similarly, the mechanical property of hybrid chitosan-ZnO NPs coated composite films enhanced compared to SF-PVA composite film. The mechanical strength enhanced due to the embedded and coated NPs. The tensile strength of hybrid chitosan-ZnO NPs coated SF-PVA composite films increased due to the interaction of H-bonding of OH group of SF-PVA and NH_2 group of hybrid chitosan-ZnO NPs [15]. The mechanical property of composite films is higher than Sterizone dressing.

8.4 Conclusions

Wound contamination is one of the most common difficulties in a chronic wound. The development of new antibacterial agents is an important and significant role to reduce the infections within the wound area. From the examined data, it is clear that ZnO NPs embedded SF-PVA composite films show antibacterial activity, but comparative study the hybrid chitosan-ZnO NPs coated SF-PVA composite film shows a higher zone of inhibition against wound infection-causing microorganisms than SF-PVA, SF-PVA/ZnO NPs composite films, and market Sterizone dressing. This characteristic property is useful for prevention of microbial infections within the area of the wound. The ZnO NPs embedded SF-PVA composite film indicates nontoxicity, good hemocompatibility, and faster blood clotting ability. Further, it also shows higher tensile strength and percent elongation, appropriate swelling capacity, higher porosity and biodegradability. The hybrid chitosan-ZnO NPs coated composite films shows synergistic antibacterial activity, nontoxicity excellent hemocompatibility and faster blood clotting ability. The coated composite films also reveal higher swelling behavior, high tensile strength and percent elongation, and good biodegradability than Sterizone dressing. A comparative study indicates that the ZnO NPs embedded SF-PVA composite film should be used as a potential material for dressings but the hybrid chitosan-ZnO NPs coated SF-PVA composite films have excellent composite materials for wound dressing application. Hence, the present investigation suggested that 1 wt % hybrid chitosan-ZnO NPs coated composite films could be employed as a best antibacterial wound dressing materials.

References

1. M. Berthet, Y. Gauthier, C. Lacroix, B. Verrier, C. Monge, Trends Biotechnol, 2017, 35, 770-784.
2. G. Mogoşanu, A. Grumezescu, Int J Pharm, 2014, 463, 127-136.
3. Y. Pilehvar-Soltanahmadi, M. Dadashpour, A. Mohajeri, A. Fattahi, R. Sheervalilou, N. Zarghami, Mini-Rev Med Chem, 2018, 18, 414-427.
4. V. Jayarama Reddy, S. Radhakrishnan, R. Ravichandran, S. Mukherjee, R. Balamurugan,S. Sundarrajan, S. Ramakrishna, Wound Repair Regen, 2013, 21, 1-6.
5. Y. Zhou, D. Yang, X. Chen, Q. Xu, F. Lu, J. Nie, Biomacromolecules, 2008, 9, 349−354.
6. A. Khalid, R. Khan, M. Ul-Islam, T. Khan, F. Wahid, Carbohyd Polym, 2017, 164, 214-221.
7. M. Summa, D. Russo, L. Penna, N. Margaroli, I. Bayer, T. Bandiera, A. Athanassiou, R. Bertorelli, Eur J Pharm Biopharm, 2018, 122, 17-24.
8. S. Banerjee, B. Bagchi, S. Bhandary, A. Kool, N. Hoque, P. Biswas, K. Pal, P. Thakur, K. Das, P. Karmakar, S. Das, Colloids Surf B Biointerfaces, 2018, 171, 300-307.
9. A. Ajovalasit, M. Caccami, S. Amendola, M. Sabatino, G. Alotta, M. Zingales, D. Giacomazza, C. Occhiuzzi, G. Marrocco, C. Dispenza, Eur Polym J, 2018, 106, 214-222.
10. S. Li, L. Li, C. Guo, H. Qin, X. Yu, Int J Biol Macromol, 2017, 104, 969-978.
11. P. Sudheesh Kumar, V. Lakshmanan, M. Raj, R. Biswas, T. Hiroshi, S. Nair, R. jayakumar, Pharm Res, 2013, 30, 523-537.
12. P. Sudheesh Kumar, V. Lakshmanan, R. Biswas, S. Nair, R. Jayakumar, J Biomed Nanotechnol, 2012, 8, 891-900.
13. V. Stytsenko, D. Melnikov, O. Tkachenko, E. Saveleva, A. Semenov, L. Kustov, Russ J Phys Chem A, 2018, 92, 862-869.

14. P. Sudheesh Kumar, V. Lakshmanan, R. Biswas, T. Anilkumar, C. Ramya, P. Reshmi, A. Unnikrishnan, S. Nair, R. Jayakumar, ACS Appl Mater Interfaces, 2012, 4, 2618-2629.
14. A. Diez-Pascual A. Diez-Vicente, Biomacromolecules, 2015, 16, 2631-2644.
16. S. Ahmed, S. Ikram, Achiev Life sci, 2016, 10, 27-37.
17. M. Mehrabani, R. Karimian, R. Rakhshaei, F. Pakdel, H. Eslami, V. Fakhrzadeh, M. Rahimi, R. Salehi, H. Kafil, , Int J Biol Macromol, 2018, 116, 966-976.
18. W. Jiang, H. Mashayekhi, B. Xing, Environ Pollut, 2009, 157, 1619-1625.
19. I. Perelshtein, E. Ruderman, N. Perkas, T. Tzanov, J. Beddow,E. Joyce, T. Mason, M. Blanes, K. Molla , A. Patlolla, A. Frenkel, J Mater Chem B, 2013, 1, 1968-1976.
20. Z. Lu, J. Gao, Q. He, J. Wu, D. Liang, H. Yang, R. Chen, Carbohyd Polym 2017, 156, 460-469.

CHAPTER 9

Summery and Conclusions

9.1 Introduction

Wound infection is a serious problem and the status of WHO indicates that nearly 14 million people every year suffer from infected or chronic wounds worldwide. Wound infection-causing microorganisms are gram-positive *S. aureus* and *S. pyogenes* while gram-negative microorganisms are *E. coli* and *P. aeruginosa*. Gram-positive organisms are found in the initial stage of the infectious process and gram-negative organisms are found in later stages of process i.e. when a chronic wound is developed. In a healthy human being, if the immune system is not able to remove the infections, these pathogens occur and cause the physiological damage.

Hence, the present thesis focused on the synthesis of novel composite films for wound dressing applications. SF, PVA, ZnO NPs and hybrid chitosan-ZnO NPs are used for the synthesis of novel composite films. SF is obtained from the *Bombyx mori* silk cocoons. Due to its wide availability, biocompatibility, biodegradability, water absorption capacity, SF has been used in wound dressings in combination with PVA. It is one of the best polymers which has been studied to improve the mechanical properties and to promote cell growth, but without incorporation of an antibacterial agent, SF and PVA are incapable to produce the antibacterial effects. Therefore, in these studies, antibacterial agents such as ZnO NPs and hybrid chitosan-ZnO NPs are employed for the formation of composite films. Firstly, the ZnO NPs are embedded into SF-PVA composite film and in secondly, the hybrid chitosan-ZnO NPs are coated on the surface of SF-PVA composite films. The prepared composite films are subjected for mechanical study, swelling, porosity, biocompatibility, biodegradability, and antibacterial study. Finally, these composite films are evaluated for the potential for wound dressing applications.

9.2 Competent component of the thesis

The aim of the present thesis is to produce antibacterial composite films depending on SF, PVA and ZnO NPs. SF protein is a class of organic material which is widely applicable for biomedical applications such as wound dressings.

An SF microsphere is synthesized by chemical desolvation method. After purification, SF microspheres are selected for a potential for preparation of composite film. The properties of PVA are of water-soluble, film-forming ability, and it improves the mechanical properties by a combination of SF and PVA. The antibacterial properties are a prime important factor in the field of wound management. Over the last few decades, the preparation of antibacterial wound dressings based on ZnO NPs with polymers has become an important area of research. ZnO NPs are well significant interest due to its good tissue adhesive property, high ability and shows antibacterial activity. Hybrid chitosan-ZnO NPs shows very good properties of biocompatibility, biodegradability, nontoxicity, moisture retentive ability, and synergistic antibacterial activity etc. Hence, this hybrid NPs are widely suited in wound dressing applications.

The modified reflux method was used for the production of ZnO NPs. The advantage of this method is the smaller size of synthesized ZnO NPs as compared to precipitation method. The synthesis method is easy, higher purity and homogeneity at the molecular level. SF-PVA composite film was synthesized by mixing and casting method at room temperature. The concentration of blends of SF and PVA are of 1:4, and the blend solution was adjusted to a neutral value. The prepared SF-PVA composite film did not show antibacterial activity, so further modification is needed in order to have to show the antimicrobial action of composite films. Hence, the antimicrobial agents such as ZnO NPs were incorporated into SF-PVA composite films. These composite films examined qualitatively as well as quantitatively via physicochemical characterization method. Additionally, this technique provides basic information about the size and shape of NPs, molecular structure and surface morphology after the synthesis of NPs and composite films. The structural and spectroscopic characterizations of synthesized pure materials, as well as composite films, were done using XRD, UV-visible spectroscopy and FTIR techniques. The size of developed ZnO NPs was examined by TEM and DLS study. The sizes of the NPs obtained by ***TEM*** were in the range of ~***100*** nm and by ***DLS*** were in the range of ~***110 nm***. The UV-visible spectrum of ZnO NPs demonstrates a sharp peak at 370 nm, which

represented the ***monodispersed*** nature of ZnO NPs. The crystallite size and phase identification of prepared ZnO NPs and composite films were examined by XRD analysis. The average crystallite size of NPs acquired by reflux method is in the range of ***~13 nm***. The molecular structure of pure materials and composite films were determined by FTIR spectroscopy. UV-visible spectra of SF-PVA and ZnO NPs embedded SF-PVA composite films showed an absorption peak at 290 nm which is the small traces of tyrosine present in the SF. The absorption peak of 365 nm is the ZnO NPs. This absorption peak showed a blue shift for the ZnO NPs embedded SF-PVA composite film than pure ZnO NPs. ***All these XRD, FTIR and UV-visible spectroscopy results suggest that ZnO NPs are embedded into SF-PVA composite film.*** The surface morphology and ZnO NPs distributions into SF-PVA composite film were examined by FE-SEM analysis. ***The results indicated that the pure SF is porous in structure, pure PVA exhibited a uniform platform and pure ZnO NPs are spherical in shape.*** SF-PVA composite films also porous in structure and the ZnO NPs were inserted into the pores that were formed by the SF-PVA composite film. The ZnO NPs embedded SF-PVA composite film showed a rough structure compared to SF-PVA composite film. These results concluded that the ZnO NPs uniformly distributed in the SF-PVA composite film. DSC thermal analysis of composite films was studied and it showed that the exothermic peaks of ZnO NPs embedded SF-PVA composite film at 226 ºC and 318 ºC. These peaks showed due to the crystallization of SF, PVA, and ZnO NPs during heating. The exothermic peak is broadening at 318 ºC, which confirmed that ZnO NPs embedded into the SF-PVA composite film.

The successful dressing applications of composite films are possible after confirming their biological study. The biological characterization study was done by using antibacterial activity, in vitro cytotoxicity, hemocompatibility and blood clotting ability. Antibacterial study of composite films was done by a disc diffusion process using wound infection associated with bacteria such as *S. aureus*, *E. coli*, *P. aeruginosa, P. mirabilis,* and *S. pyogenes* bacteria. The results concluded that the SF-PVA did not show ZOI against bacteria, while in the ZnO NPs embedded SF-PVA composite film observed higher inhibition zone against *S.*

aureus, *P. aeruginosa*, *P. mirabilis* and *S. pyogenes* than *E. coli* bacteria. ***Minimum inhibition concentrations of ZnO NPs have obtained 50 µg/mL, against S. aureus, 100 µg/mL against E. coli, and P. mirabilis bacteria***. The ZOI is due to the presence of ZnO NPs into SF-PVA composite film. The obtained ZOI enhanced by enhancing the concentrations of ZnO NPs. The cell viability study of composite films is done by using well-known MTT assay method on cell line i.e. L929 mouse fibroblast cell lines. The cell viability of SF-PVA composite film was obtained 90 % for 24 h, 94 % for 8 % and 99 % for 72 h of incubation. The cell viability of ZnO NPs embedded SF-PVA composite film showed 72 % for 24 h, 76 % for 48h, and 81 % for 72 h of incubation. For wound dressing applications hemocompatibility and blood clotting ability study are essential for applying these materials for *in vivo* applications. ***The results suggested that the prepared composite films showed good haemocompatibility as well as faster blood clotting ability.***

The next characteristic study of composite films is swelling behavior of composite films. It has been seen that the ZnO NPs embedded SF-PVA composite films are 25-30 % swelling ability and it can be increased after 7 days of incubation and decreased after 14 days of incubation than those obtained for 1day incubation. ***The results of swelling behavior study concluded that the ZnO NPs embedded SF-PVA composite film could absorb a large volume of liquids in which it was immersed, and there was no change in the dressing up to 1 week.*** The tensile strength and % elongation study of prepared composite films are very important in wound dressing applications due to it showed the flexibility of materials. ***The tensile strength of ZnO NPs embedded SF-PVA composite film shows about 3.125 MPa and % elongation was about 178 %. It was concluded that the obtained tensile strength and percent elongation were sufficient for wound dressing applications.*** The biodegradation study of the composite film showed that the SF-PVA composite film has 50-55% of degradation after 7 days, 55-60% degradation after 14 days and 60-65% degradation after 21 days. The ZnO NPs embedded composite film shows the degradation 30-35% after 7 days, 14

days and 35-40% degradation rate after 21 days. The degradation rate decreased after incorporation of ZnO NPs into SF-PVA composite film.

The next part of the thesis is the synthesis of hybrid chitosan-ZnO NPs and its coating on the surface of SF-PVA composite film by using sonochemical coating technique. It is well known that the combination of chitosan and ZnO NPs enhances flexibility, antibacterial activity, and biocompatibility by modifying the surface with biocompatible materials. Surface modification of SF-PVA composite films are done by using the sonochemical method, it is also called as ultrasound irradiation technique. This method prevents the aggregation of NPs due to the application of high-intensity ultrasound and the obtained coatings are uniformly deposited on the surface of SF-PVA composite films. The role of coated hybrid NPs on structural and morphological properties was studied. The hybrid NPs were synthesized by blending of chitosan and ZnO NPs at a concentration of 1:1 ratio. During the process of synthesis of composite films, the coating concentrations of hybrid NPs were varied, which was 0.2 wt %, 0.5 wt % and 1 wt % for 30 min. The particle size and surface morphology of synthesized hybrid NPs were determined by SEM and TEM analysis. ***The SEM analysis observed that the particle size of synthesized hybrid NPs was ~ 168 nm and in the TEM analysis it was observed ~ 150-160 nm.*** The structural and spectroscopic study of coated and uncoated composite films was done by using XRD, FTIR analysis. The surface morphology and elemental analysis of synthesized surface coated composite films were done by using SEM and EDX analysis. The results suggested that the obtained chitosan-ZnO NPs are combined together and coated on the surface of SF-PVA composite films. The coated composite films show the slight aggregation of hybrid NPs on SF-PVA composite film. The surface area and porosity study of coated composite films were examined by BET analysis. The market Sterizone dressing was used for comparative study. The 0.2 wt % hybrid NPs coated SF-PVA composite film shows the specific surface area is about 12.75 m^2/g, 0.5 wt% coated film shows 19.28 m^2/g, 1 wt % coated film shows the specific surface area about 41.39 m^2/g and Sterizone dressing shows the specific surface area is about 18.14 m^2/g. ***The results concluded that all the coated composite films show a***

high specific surface area than Sterizone dressing. This coated surface area can give uniform antibacterial activity as well as reduce infections within the wound area. The pore size distribution shows the mesopores distribution from 2 to 24 nm. The antibacterial study of coated composite films concluded that the ZOI is higher in E. coli bacteria than S. aureus and P. mirabilis bacteria. ***The ZOI increased with increase in the concentration of hybrid chitosan-ZnO NPs. The increased ZOI is due to the synergistic effect of hybrid chitosan and ZnO NPs.*** The ideal wound dressing must be nontoxic and biocompatible in nature. The cell viability study of coated, uncoated composite films and Sterizone dressing were done by using L929 mouse fibroblast cell lines. ***The results suggest that the cell viability of all the coated composite films have 70-83% at 24 h, 48 h and 72 h of incubation time. It was higher to Sterizone dressing.*** The swelling and mechanical study of all the coated and uncoated composite films concluded that it was increased with increase in the concentration of hybrid NPs. The biodegradation study of all the coated composite films showed that the degradation rate was higher than Sterizone dressing. From all these observations, it is concluded that ZnO NPs embedded SF-PVA and hybrid chitosan-ZnO NPs coated SF-PVA composite films can be used as wound dressing applications.

9.3. Summary of thesis

The present thesis is divided into 9 chapters. The brief summary of each chapter is mentioned below.

Chapter 1 introduces all the necessary part in brief like wound dressings, classification of wound dressings, wound healing process, the necessity of wound dressings, requirements of wound dressings, biomaterials for dressings, and use of SF and PVA for wound dressings.

Chapter 2 includes the theoretical background regarding nanotechnology and wound dressings. Nanotechnology is best advancing field for fabrication of novel dressing materials. Nanotechnology and SF based dressings gained a lot of interest for development of dressing materials due to their ability to be manipulated upon wound dressing applications. There are different derivatives of SF such as

scaffolds, hydrogels, sponges, microparticles, NPs, and composite films. All these derivatives are innovative materials, based on the nanotechnology and used as a promising candidate for wound dressing materials.

Chapter 3 focuses on characterization techniques for wound dressing materials. The characterization techniques used to analyze physical, chemical, mechanical, swelling capability, porosity, and biological properties are discussed.

Chapter 4 deals with the synthesis of pure materials of SF, PVA by desolvation method and ZnO NPs by modified reflux method. The composite films of SF-PVA and ZnO NPs embedded SF-PVA are formulated by casting method at room temperature. It covers the physical, chemical, and biological studies of pure materials of SF, PVA and ZnO NPs and composite films.

C***hapter 5*** focuses on the synthesis of hybrid chitosan-ZnO NPs by desolvation method. The synthesized hybrid NPs coated on the surface of SF-PVA composite films with different concentrations by the sonochemical coating technique. This chapter covers the brief study on the hybrid chitosan-ZnO NPs coated SF-PVA composite films. It includes physical, chemical, mechanical, porosity, and biological study.

Chapter 6 deals with the brief of biocompatibility study of prepared composite films of SF-PVA, ZnO NPs embedded SF-PVA and hybrid chitosan-ZnO NPs coated SF-PVA composite films. It includes the hemocompatibility, blood clotting study, cytotoxicity study using L929 mouse fibroblast cell lines.

Chapter 7 focuses on the antibacterial study of synthesized NPs and prepared composite films of SF-PVA, ZnO NPs embedded SF-PVA and hybrid chitosan-ZnO NPs coated SF-PVA composite films. All the antibacterial experiments were done by using wound infection associated microorganisms like *S. aureus*, *E. coli*, *P. aeruginosa*, *P. mirabilis,* and *S. pyogenes*.

Chapter 8 deals with the comparative study of biological, physical and environmental (biodegradable) properties of prepared composite films of SF-PVA, ZnO NPs embedded SF-PVA, and hybrid chitosan-ZnO NPs coated SF-PVA composite films for wound dressing applications.

Chapter 9 deals with the summary and conclusions of the thesis.

9.4. Major conclusions

- The SF microspheres are successfully synthesized by chemical desolvation process and the ZnO NPs have been synthesized by modified reflux method having crystallite size to be ~ 13 nm.
- SF-PVA and ZnO NPs embedded SF-PVA composite films were successfully prepared by casting method at room temperature.
- Morphological and DSC thermal analysis confirmed that the ZnO NPs were embedded in the SF-PVA composite film.
- The *In vitro* cytotoxicity studies confirmed that the nontoxic nature of the prepared ZnO NPs embedded SF-PVA composite film using L929 mouse fibroblast cell line by MTT assay.
- Biodegradation study of ZnO NPs embedded SF-PVA composite film showed that the 30-35 % of degradation rate after 7 days and 14 days and 35-40 % degradation after 21 days. The degradation rate of composite films increased with increasing the time duration.
- The hybrid chitosan-ZnO NPs have successfully synthesized by mixing and casting method and surface coated hybrid chitosan-ZnO NPs on SF-PVA composite films of different concentrations of NPs have been successfully prepared by a sonochemical coating process.
- BET analysis confirmed the surface coated composite films have a high specific surface area and mesopores distributions on SF-PVA composite films.
- The swelling study of hybrid chitosan-ZnO NPs coated SF-PVA composite films suggest that the coated composite films have better exudates uptake capacity of up to 1 week, there is no change of dressing up to 1 week.
- The mechanical study of coated composite films examined that the coating of 1 wt % concentration of hybrid chitosan-ZnO NPs was highest tensile strength and % elongation than other less concentration of hybrid NPs.
- *The In vitro* antibacterial study of all the coated composite films showed a higher zone of inhibition against Gram-positive and Gram-negative bacteria, when compared to control SF-PVA composite film and market

Sterizone dressing. The obtained enhanced antibacterial activity of coated composite films due to the synergistic effect of hybrid chitosan and ZnO NPs.

- *In vitro* cell viability study of coated composite films suggested that the all the coated composite films having 70-83 % cell viability, higher to the market Sterizone dressing.
- Biodegradability study of hybrid chitosan-ZnO NPs coated composite films having higher degradation rate than Sterizone dressing.
- The enhancement of antibacterial activity, biodegradability, biocompatibility, nontoxicity, appropriate swelling ability and porosity of ZnO NPs embedded SF-PVA composite films and hybrid chitosan-ZnO NPs coated SF-PVA composite films suggested that it could be employed as an antibacterial wound dressing applications.
- The comparative study suggested that the 1 wt % hybrid chitosan-ZnO NPs coated SF-PVA composite film fulfilled all the requisites to be used for wound dressing applications. Therefore, hybrid chitosan-ZnO NPs coated SF-PVA composite could be excellent material for antibacterial wound dressings.

9.5 Future scope of the thesis

In future, prepared composite films will be the best challenge to carry out *in-vivo* experiments on an animal study. Therefore, the prepared antibacterial composite films can be significantly utilized for industrial and commercial purposes.

Curriculum Vitae

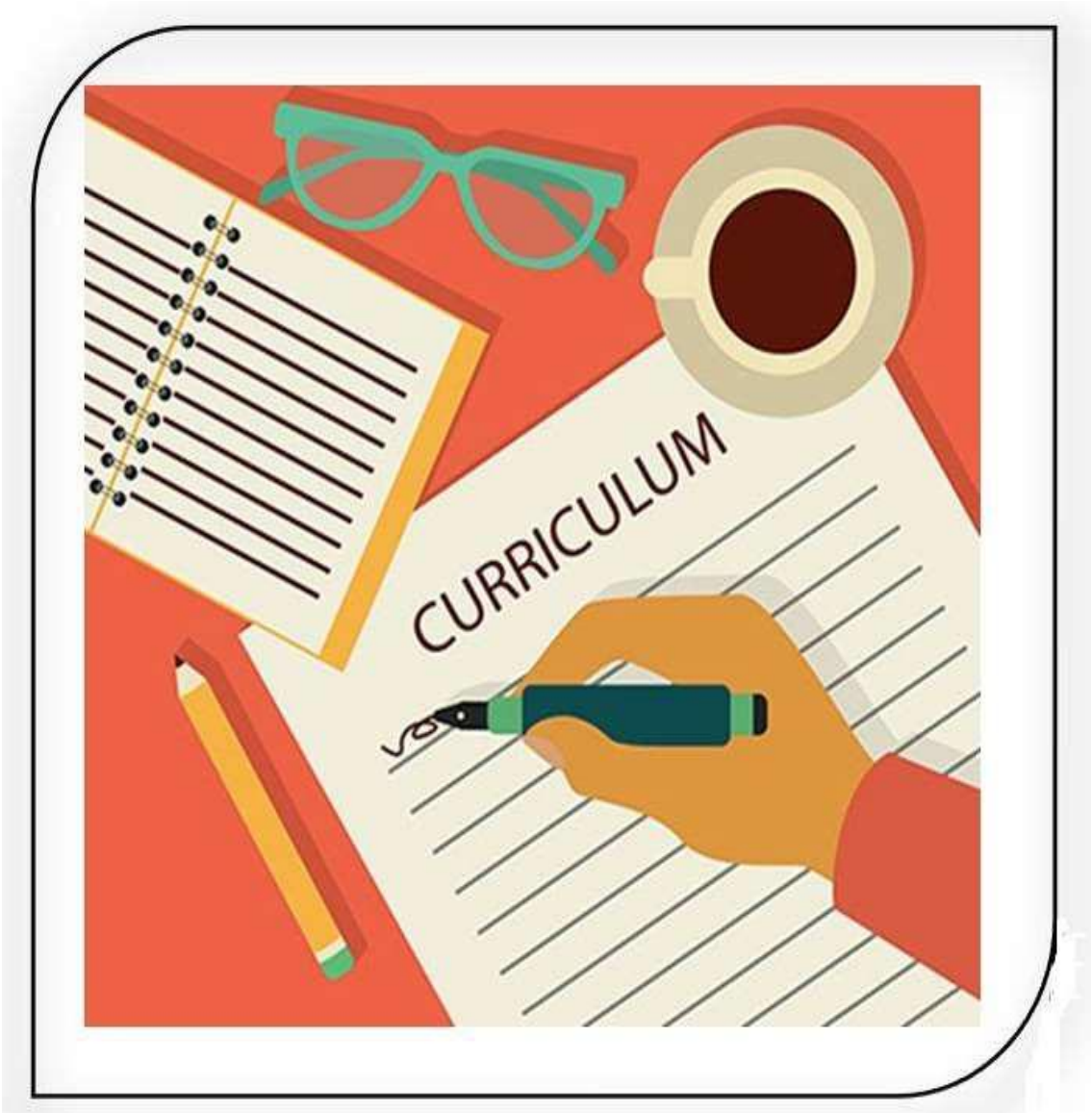

Ms. Priyanka Popat Patil

Research Scholar,

Centre for Interdisciplinary Research,

D. Y. Patil Education Society,

Kolhapur-416006,

E-mail: pps1402@gmail.com,

Date of birth: 28th September 1987,

Permanent address: A/P- Koregaon, Tal- Karad,

Dist- Satara-415110 (MS) India

Contact Number: +91 7043490108, +91 8007542045

ACADEMIC PROFILE

Ph. D. in Biotechnology,

Submitted thesis on March 2019

Centre for Interdisciplinary Research,

D. Y. Patil Education Society, Kolhapur-416006 (M.S.) India

Title of thesis:

"Studies on Preparation and Characterization of Silk Fibroin/PVA/ZnO NPs Composites for Wound Dressing Application"

M. Sc. In Biotechnology, 2009

Krishna Institute of Medical Science University Karad, Maharashtra- 415 110, India

First class (Specialization- Biotechnology)

B. Sc. In Zoology, 2007

Shivaji University Kolhapur, Maharashtra-416006, India

First class (Specialization- Zoology)

Date of registration: 26th November, 2012 at D. Y. Patil Education Society, Kolhapur.

EXPERIMENTAL KNOWLEDGE

I have an expertise in the synthesis of natural polymer composites, metal oxide nanoparticles and its functionalization by using different polymers, non-polymers and Fluorescent materials. I have also learned different methods of synthesis of nanocomposite materials. I have used different methods for preparation, which are high thermal decomposition technique, polyol method, combustion and Co-Precipitation for synthesis of metal oxide nanoparticles.

INSTRUMENTS HANDLED

- X-ray Diffractometer (XRD),
- PSS-Zeta potential and Particle size analyser,
- Scanning/Transmission electron microscope (SEM/TEM),
- Fourier transform infrared (FTIR), UV-Vis spectrophotometer, High resolution transmission electron microscopy (HR-TEM), and
- Field emission scanning electron microscopy (FE-SEM).

AWARDS AND PRIZES

- Best teacher award in 2014, College of Mahatma Phule arts, commerce and science college Panvel, Maharashtra.

- **2nd prize winner in innovation and healthcare category, Start-up India Maharashtra Yatra, 2018.**

RESEARCH EXPERIENCE

Ph. D. Thesis entitled **"Studies on Preparation and Characterization of Silk Fibroin/PVA/ZnO NPs Composites for Wound Dressing Application"** under the supervision of **Prof. (Dr.) S. G. Nanaware and Prof. (Dr.) S. H. Pawar**, Center for

Interdisciplinary Research, D. Y. Patil Education Society, Kolhapur-416006, India **(2012-2019)**.

TEACHING EXPERIENCE

Five years teaching experience, working as teaching assistance for B. Sc Biotechnology in Yashwantrao Chavan College of Science Karad and Mahatma Phule Arts, Commerce and Science College, Panvel. **(2009-2014)**.

LIST OF PUBLICATIONS

1. **Priyanka P. Patil,** Jagruti V. Meshram, Raghvendra A. Bohara, Shivdas G. Nanaware, and Shivaji H. Pawar. "ZnO nanoparticles-embedded silk fibroin–polyvinyl alcohol composite film: a potential dressing material for infected wounds." ***New Journal of Chemistry***, *42* (17), pp.14620-14629. **(I. F. = 3. 2).**

2. **Priyanka P. Patil**., Raghvendra A. Bohara, Jagruti V. Meshram, Shivdas G. Nanaware, and Shivaji H. Pawar. "Hybrid chitosan-ZnO nanoparticles coated with a sonochemical technique on silk fibroin-PVA composite film: A synergistic antibacterial activity." ***International journal of biological macromolecules***, *122*, pp.1305-1312 **(I. F. = 3. 9)**.

3. **Priyanka P. Patil**, S. H. Pawar, Overview of recent developments of wound dressing materials, ***Journal of frontiers in interdisciplinary research and technology development***, volume 1, issue 1, 2018.

4. Research article/Book Chapter entitled, “Synthesis and Characterization of Silk Fibroin Microspheres and Nanospheres for Biomedical Application” published in ***Innovative Technologies for rural developments (A compendium of CRTD events),*** Publishers Savitribai Phule shikshan Prasarak Mandal, Sinhgad Institutes, Solapur.

COMMUNICATED

1. **Priyanka P. Patil**, S. H. Pawar, Silk Fibroin and its Derivatives for Ideal Wound Dressings, submitted to analytical methods, **RSC publication**.

2. **Priyanka P. Patil**, S. G. Nanaware, S. H. Pawar, ZnO NPs based PVA-Silk Fibroin nanocomposite film shows significantly enhanced thermal stability and antibacterial activity" submitted to Composite interfaces, **Taylor and Francis Publication**.

PAPERS PRESENTED INTERNATIONAL / NATIONAL CONFERENCES / WORKSHOP / SYMPOSIUM

1. **Paper presented on A Multi Mega Event (ITRDC-2017)** organized by Center For Research and Technology Development (CRTD) Sinhgad Institutes, Solapur-413255 (MS) India in Collaboration with Bhabha Atomic Research Center, Mumbai and Indian Medical Association, Solapur 18th to 20th Feb. 2017.

2. **Paper presented in Third International Conference** on Nanomaterials: Synthesis Characterization and Applications held at Mahatma Gandhi University, Kottayam, Kerala, India Gdansk University of Technology Chemical Faculty Dept. Of Polymer Technology, Gdansk, Poland, and Beijing University of Chemical Technology, Bei San Huan East Road 15#, Chaoyang District, Beijing, China during 11, 12, and 13 may 2018.

3. **Presented research idea in Start-up India Maharashtra, Yatra 2018.**

CONFERENCES / WORKSHOPS / SEMINARS

1. **Poster presentation** on International Conference on Nanotechnology Addressing the Convergence of Materials Science, Biotechnology and Medical

Science held on Nov. 9-11, 2017 organized by Center for Interdisciplinary Research D. Y. Patil Education Society, Kolhapur.

2. **Oral presentation** on Dnyanshodh held on 28th Feb. 2018, organized by D. Y. Patil Education Society, Kolhapur.

3. **Poster Presentation** on National Conference on Emerging Trend in Nanomaterials and Their Applications, on 2nd and 3rd June, 2017 organized by department of medical physics, Center for Interdisciplinary research D. Y. Patil University, Kolhapur.

4. **Attended International Workshop on** Ph. D. Program for Medical Innovations, on 16th and 17th Feb. 2014, organized by D. Y. Patil University, Kolhapur.

5. **Attended National Seminar** on Biotechnology for Sustainable Growth and Development Organized by department of Biotechnology, Changu Kana Thakur Arts, Commerce and Science College New Panvel on 3rd and 4th Jan. 2014

6. **Attended National Seminar** on Impact of global climate change on Environment and ecological conservation, organized by Department of Zoology and Biotechnology, Mahatma Phule Arts, Science and Commerce College Panvel on 18th Jan. 2014.

COMPUTER LITERACY

Basic knowledge of operating systems, Windows 98, Windows 7, Windows XP, MS-CIT.

DECLARATION

I hereby declare that the above particulars are true and correct to the best of my knowledge.

Date: 30/03/2019

Place: Kolhapur

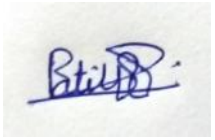

Priyanka Popat Patil